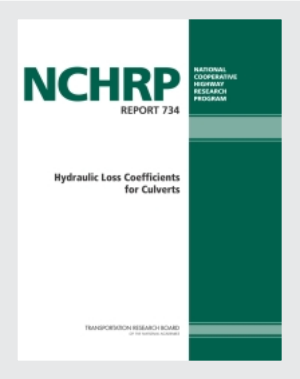

Hydraulic Loss Coefficients for Culverts

DETAILS

113 pages | 8.5 x 11 | PAPERBACK
ISBN 978-0-309-25867-8 | DOI 10.17226/22673

AUTHORS

Tullis, Blake P.

NATIONAL COOPERATIVE HIGHWAY RESEARCH PROGRAM

NCHRP REPORT 734

Hydraulic Loss Coefficients for Culverts

Blake P. Tullis
UTAH STATE UNIVERSITY
Logan, UT

Subscriber Categories
Hydraulics and Hydrology

Research sponsored by the American Association of State Highway and Transportation Officials
in cooperation with the Federal Highway Administration

TRANSPORTATION RESEARCH BOARD

WASHINGTON, D.C.
2012
www.TRB.org

NATIONAL COOPERATIVE HIGHWAY RESEARCH PROGRAM

Systematic, well-designed research provides the most effective approach to the solution of many problems facing highway administrators and engineers. Often, highway problems are of local interest and can best be studied by highway departments individually or in cooperation with their state universities and others. However, the accelerating growth of highway transportation develops increasingly complex problems of wide interest to highway authorities. These problems are best studied through a coordinated program of cooperative research.

In recognition of these needs, the highway administrators of the American Association of State Highway and Transportation Officials initiated in 1962 an objective national highway research program employing modern scientific techniques. This program is supported on a continuing basis by funds from participating member states of the Association and it receives the full cooperation and support of the Federal Highway Administration, United States Department of Transportation.

The Transportation Research Board of the National Academies was requested by the Association to administer the research program because of the Board's recognized objectivity and understanding of modern research practices. The Board is uniquely suited for this purpose as it maintains an extensive committee structure from which authorities on any highway transportation subject may be drawn; it possesses avenues of communications and cooperation with federal, state and local governmental agencies, universities, and industry; its relationship to the National Research Council is an insurance of objectivity; it maintains a full-time research correlation staff of specialists in highway transportation matters to bring the findings of research directly to those who are in a position to use them.

The program is developed on the basis of research needs identified by chief administrators of the highway and transportation departments and by committees of AASHTO. Each year, specific areas of research needs to be included in the program are proposed to the National Research Council and the Board by the American Association of State Highway and Transportation Officials. Research projects to fulfill these needs are defined by the Board, and qualified research agencies are selected from those that have submitted proposals. Administration and surveillance of research contracts are the responsibilities of the National Research Council and the Transportation Research Board.

The needs for highway research are many, and the National Cooperative Highway Research Program can make significant contributions to the solution of highway transportation problems of mutual concern to many responsible groups. The program, however, is intended to complement rather than to substitute for or duplicate other highway research programs.

NCHRP REPORT 734

Project 15-24
ISSN 0077-5614
ISBN 978-0-309-25867-8
Library of Congress Control Number 2012952178

COPYRIGHT INFORMATION

NOTICE

The project that is the subject of this report was a part of the National Cooperative Highway Research Program, conducted by the Transportation Research Board with the approval of the Governing Board of the National Research Council.

The members of the technical panel selected to monitor this project and to review this report were chosen for their special competencies and with regard for appropriate balance. The report was reviewed by the technical panel and accepted for publication according to procedures established and overseen by the Transportation Research Board and approved by the Governing Board of the National Research Council.

The opinions and conclusions expressed or implied in this report are those of the researchers who performed the research and are not necessarily those of the Transportation Research Board, the National Research Council, or the program sponsors.

The Transportation Research Board of the National Academies, the National Research Council, and the sponsors of the National Cooperative Highway Research Program do not endorse products or manufacturers. Trade or manufacturers' names appear herein solely because they are considered essential to the object of the report.

Published reports of the

NATIONAL COOPERATIVE HIGHWAY RESEARCH PROGRAM

are available from:

Transportation Research Board
Business Office
500 Fifth Street, NW
Washington, DC 20001

and can be ordered through the Internet at:

http://www.national-academies.org/trb/bookstore

Printed in the United States of America

THE NATIONAL ACADEMIES

Advisers to the Nation on Science, Engineering, and Medicine

The **National Academy of Sciences** is a private, nonprofit, self-perpetuating society of distinguished scholars engaged in scientific and engineering research, dedicated to the furtherance of science and technology and to their use for the general welfare. On the authority of the charter granted to it by the Congress in 1863, the Academy has a mandate that requires it to advise the federal government on scientific and technical matters. Dr. Ralph J. Cicerone is president of the National Academy of Sciences.

The **National Academy of Engineering** was established in 1964, under the charter of the National Academy of Sciences, as a parallel organization of outstanding engineers. It is autonomous in its administration and in the selection of its members, sharing with the National Academy of Sciences the responsibility for advising the federal government. The National Academy of Engineering also sponsors engineering programs aimed at meeting national needs, encourages education and research, and recognizes the superior achievements of engineers. Dr. Charles M. Vest is president of the National Academy of Engineering.

The **Institute of Medicine** was established in 1970 by the National Academy of Sciences to secure the services of eminent members of appropriate professions in the examination of policy matters pertaining to the health of the public. The Institute acts under the responsibility given to the National Academy of Sciences by its congressional charter to be an adviser to the federal government and, on its own initiative, to identify issues of medical care, research, and education. Dr. Harvey V. Fineberg is president of the Institute of Medicine.

The **National Research Council** was organized by the National Academy of Sciences in 1916 to associate the broad community of science and technology with the Academy's purposes of furthering knowledge and advising the federal government. Functioning in accordance with general policies determined by the Academy, the Council has become the principal operating agency of both the National Academy of Sciences and the National Academy of Engineering in providing services to the government, the public, and the scientific and engineering communities. The Council is administered jointly by both Academies and the Institute of Medicine. Dr. Ralph J. Cicerone and Dr. Charles M. Vest are chair and vice chair, respectively, of the National Research Council.

The **Transportation Research Board** is one of six major divisions of the National Research Council. The mission of the Transportation Research Board is to provide leadership in transportation innovation and progress through research and information exchange, conducted within a setting that is objective, interdisciplinary, and multimodal. The Board's varied activities annually engage about 7,000 engineers, scientists, and other transportation researchers and practitioners from the public and private sectors and academia, all of whom contribute their expertise in the public interest. The program is supported by state transportation departments, federal agencies including the component administrations of the U.S. Department of Transportation, and other organizations and individuals interested in the development of transportation. **www.TRB.org**

www.national-academies.org

COOPERATIVE RESEARCH PROGRAMS

AUTHOR ACKNOWLEDGMENTS

The research project herein was performed under NCHRP Project 15-24 by the Utah Water Research Laboratory, Department of Civil and Environmental Engineering, at Utah State University (USU). USU was the contractor and fiscal administrator for this study.

Dr. Blake P. Tullis, Associate Professor of Civil and Environmental Engineering at USU, was the Project Director and Principal Investigator. Other research participants and authors include Tyler G. Allen, Ph.D. candidate at USU; Gary M. Haderlie, MS student at USU; Derek S. Anderson, MS student at USU; S. Collin Robinson, MS student at USU; Dale Lentz, MS student at USU; and Steven L. Barfuss, Assistant Research Professor at USU. The work was done under the general supervision of Dr. Blake P. Tullis.

FOREWORD

By David A. Reynaud
Staff Officer
Transportation Research Board

Traditional culvert applications were designed by determining the minimum culvert size that will pass the specified design flood. In recent years, culvert performance objectives and designs have been expanded to include other considerations such as improving fish and/or terrestrial animal passage and rehabilitating old, deteriorated culverts. This project evaluated culvert geometries associated with these new applications to develop the hydraulic relationships, including loss coefficients. The report will be of interest to hydraulic engineers and environmental staff.

Culverts are designed and constructed to be hydraulically efficient, such that they are able to pass flood flows without overtopping the road embankment. Flow passing through a culvert typically experiences an increase in velocity, relative to the approach channel flow, due to reductions in cross-sectional flow area. Increased flow velocity can cause additional outlet erosion as well as be a problem for many types of migratory species. In addition to migratory species, resident fish such as juvenile salmon can also be affected by culverts. Juvenile salmon move up and down streams as population pressures and food sources change. If high velocities in culverts provide barriers to this movement, food sources and population may be limited. Other fish species may have requirements similar to those of juvenile salmon or may require upstream movement for spawning.

Research in the area of culvert hydraulics has centered on concrete box culverts and circular corrugated metal pipe culverts. The hydraulic analyses of these culvert types have been well defined for conventional installations, but not for environmentally sensitive and nontraditional culverts. It is desirable to design and construct some culvert crossings to minimize their impact on the natural environment. Culverts are now being designed to maintain natural velocities and minimize turbulence to allow migratory species to pass through the culvert barrel. Such designs may add baffles on the invert, bury the culvert invert, or use bottomless culverts to provide for a natural stream invert. Other designs use larger and wider culverts to reduce the amount of contraction and acceleration.

In order to design these culverts that minimize impacts to the natural stream environment, designers need the associated hydraulic equations and loss coefficients to be evaluated and made more accurate. In NCHRP Project 15-24, Utah State University conducted physical, numerical, and computer modeling to refine existing hydraulic relationships and develop new ones for analysis and design of culverts for conventional and nontraditional, environmentally sensitive installations.

CONTENTS

Note: Many of the photographs, figures, and tables in this report have been converted from color to grayscale for printing. The electronic version of the report (posted on the Web at www.trb.org) retains the color versions.

CHAPTER 1

Introduction

1.1 Project Introduction

Traditionally, culvert head-discharge relationships are determined using empirical data published in design manuals such as the Federal Highway Administration's *Hydraulic Design of Highway Culverts* (Normann et al., 2001), referred to in this report and in practice as *HDS-5.* Common culvert shapes used in practice include circular, elliptical, pipe arch, and box culverts. Historically, the determination of appropriate culvert size was based primarily on economic considerations (i.e., the appropriate size was the smallest culvert that would pass the required design discharge without exceeding the minimum allowable freeboard on the upstream side of the road crossing). More recently, however, the function of some culverts has been expanded to include aquatic and terrestrial animal passage.

Fish passage culverts typically consist of an oversized circular or elliptical culvert (oversized relative to what would be required to meet the head-discharge requirements) that is partially buried in the streambed. These culverts are referred to as buried-invert or embedded culverts. The percent of invert burial can vary from zero to ~50% of the culvert height.

Culvert head-discharge relationships are determined by balancing the culvert energy loss with the available differential driving head across the culvert (outlet control) or by the shape of the culvert inlet and upstream driving head (inlet control). Typical culvert energy losses are associated with entrance loss, exit or outlet loss, and friction losses. Culvert design manuals, like *HDS-5,* provide entrance loss coefficient (k_e) data (outlet control) and empirical coefficients and exponents for inlet control head-discharge relationships. In general, however, similar culvert hydraulic performance data are not available for buried-invert culvert geometries. The aim of this study (NCHRP Project 15-24) has been to develop a better understanding of embedded culvert hydraulics and to provide culvert design and analysis tools to engineers and to evaluate, among other things, the hydraulic characteristics of fish passage culverts. Chapter 2 reports the findings specific to the buried-invert culvert hydraulics.

The hydraulics of slip-lined culverts is addressed in Chapter 3. As a result of an aging transportation infrastructure, many culverts are near the end of their useful service life. In many cases, it is more economical to rehabilitate an existing or host culvert than to replace it. Inserting a smaller-diameter liner pipe inside the host culvert, a process referred to as slip lining, is a common culvert rehabilitation technique. Relative to the host culvert head-discharge characteristics, the head-discharge characteristics of the slip-lined culvert will be influenced by the reduction in cross-sectional area associated with the liner; the decrease in hydraulic roughness of the liner wall (slip liners are often solid-wall high density polyethylene) relative to the host culverts, which often have profiled pipe walls (e.g., corrugated metal pipe); and the geometry of the end treatment resulting from the slip-lining process. This study evaluated the head-discharge characteristics of projecting and tapered slip-lined culvert end treatments where the liner pipe projected 0.17 and 0.34 pipe diameters (D) upstream from the projecting end of the host culvert. The results of the slip-lined culvert study are presented in Chapter 3.

For the case where a culvert or pipe discharges into a downstream reservoir where the reservoir velocity is essentially zero, the exit loss is equal to the velocity head in the pipe. When the culvert discharges into a downstream channel that has a similar alignment to the culvert, the exit loss has traditionally been estimated to be the difference in velocity head [$\Delta V^2/(2g)$] between the culvert and discharge channel. In the case of short, mild, or zero-slope culverts, however, sometimes the calculated exit loss represents a significant percentage of the total system energy loss. Another objective of this study was to evaluate the nature of culvert exit loss and compare experimental exit loss data with the predictive relationships for accuracy. The results of the exit loss study are presented in Chapter 4.

In many wide-channel road-crossing applications, particularly when the channel slope is mild and/or the road embankment height is limited, multibarrel culverts are required. The majority of the culvert design data, such as data in *HDS-5,* is specific to single-barrel tests, and in general, is applied to multibarrel culvert design using the principle of superposition. In other words, the discharge capacity of a single-barrel culvert is determined for a specific design head and the culvert design flow is divided by the single-barrel discharge capacity to determine the number of culverts needed. Culvert entrance loss (outlet control) and the inlet control head-discharge relationships are influenced by the amount of flow contraction that occurs at the culvert inlet. The supposition is that the hydraulic capacity of a single culvert barrel may change when additional barrels are installed adjacent to it due to the change in the nature of the flow contraction. Another objective of this study was to evaluate the behavior of multibarrel culverts, relative to the single-barrel superposition assumption. The results of the multibarrel culvert study are presented in Chapter 5.

A major factor affecting head-discharge relationships in culverts and open channels is the flow resistance or friction loss associated with shear stresses that develop near the flow boundaries. Friction loss is typically accounted for by applying one-dimensional flow resistance relationships like the Darcy-Weisbach or Manning equations with empirically determined flow resistance coefficients (f and n, respectively). The flow resistance coefficients can vary with the relative roughness of the channel or pipe boundary, the Reynolds number (*Re,* discharge and viscous effects), and the cross-sectional shape of the channel flow area.

When sediment is deposited in the bottom of a culvert, whether through sediment transport processes or intentionally (embedded culvert design), the cross-sectional shape of the culvert can change relative to traditional culvert pipe shapes (e.g., circular or elliptical), which may affect the flow resistance characteristics of the culvert. It is likely to be more significant, however, that the hydraulic roughness of the wetted perimeter along the flow boundary of the flow cross-section is not constant and represents a condition referred to as "composite" roughness. One-dimensional hydraulics may not be able to account for the potentially multidimensional nature of flow resistance in composite roughness channels or culverts. As part of this study, boundary roughness materials of differing hydraulic roughness were tested in a rectangular channel for both uniform roughness and composite roughness configurations. The experimental results were compared with 16 composite roughness predictive relationships for Manning's *n.* The results of the composite roughness study are presented in Chapter 6.

Historically, the culvert hydraulics experimental databases have consisted of data collected using laboratory-scale culverts with $D \leq 6$ to 8 in. To investigate potential size-scale effects in culvert hydraulics, entrance loss tests were conducted using 12- and 24-in. diameter circular culverts. The results of the size-scale testing are presented in Chapter 2.

The data for NCHRP Project 15-24 were generated using experimental data collected in the hydraulics laboratory of the Utah Water Research Laboratory at Utah State University. A variety of different test facilities were utilized, including a 6-ft-deep by 8-ft-wide by 300-ft-long channel, a 3-ft-deep by 4-ft-wide by 48-ft-long tilting, rectangular flume, and an elevated head box and tail box between which culverts were installed for testing.

The following is a list of published peer-reviewed journal and conference papers that related to this project: Allen (2012), Tullis and Anderson (2010), Tullis et al. (2008), Haderlie and Tullis (2008), Haderlie (2007), Anderson (2006), Anderson and Tullis (2006), Robinson (2005), Robinson and Tullis (2005), and Tullis et al. (2005).

1.2 Culvert Hydraulics

Consistent with traditional culvert hydraulics, buried-invert culverts can operate under either inlet or outlet flow control. Under outlet control, culverts may flow full or partially full over a portion or the entire length of the culvert. For outlet control, the culvert discharge is determined by balancing the energy loss through the culvert with the energy available. Culvert energy losses include entrance loss, barrel friction loss, exit loss, and any other minor losses. The entrance loss, which is specific to the culvert inlet geometry, is typically expressed as a loss coefficient, k_e, multiplied by the culvert velocity head (Equation 1-1).

$$H_e = k_e \frac{V^2}{2g} \tag{1-1}$$

In Equation 1-1, H_e is the head loss associated with the culvert entrance flow condition (ft), V is the average flow velocity in the culvert (ft/s), and g is the gravitational acceleration constant (ft/s^2).

Robinson (2005) showed experimentally that the entrance loss coefficients for a buried-invert elliptical culvert were independent of viscous or Reynolds number (*Re*) effects, where $Re = V4R_h/\nu$ and R_h is the hydraulic radius (flow area divided by the wetted perimeter). Based on the fact that field-scale *Re* values are typically larger than lab-scale *Re* values and that the influence of viscosity tends to diminish with increasing *Re,* viscous or *Re* effects on culvert entrance loss coefficients are likely to be insignificant and were not considered in this study.

Under inlet control, culvert discharge capacity is a function of the available upstream energy, the culvert inlet geometry, and a critical flow section that forms just downstream of the

inlet. The inlet control culvert flow capacity is typically quantified using empirical, quasi-dimensionless, head-discharge relationships such as those published in *HDS-5*. Different relationships are used for submerged (headwater above the crown of the culvert inlet) and unsubmerged (headwater below the crown of the culvert inlet) culvert inlet conditions. *HDS-5* recommends Equations 1-2 and 1-3, referred to as Form 1 and 2, respectively, for unsubmerged inlet flows and Equation 1-4 for submerged inlet flow conditions.

Unsubmerged Form 1

$$\frac{Hw_i}{D} = \frac{H_c}{D} + K\left[\frac{K_u Q}{AD^{0.5}}\right]^M - 0.5S_o \tag{1-2}$$

Unsubmerged Form 2

$$\frac{Hw_i}{D} = K\left[\frac{K_u Q}{AD^{0.5}}\right]^M \tag{1-3}$$

Submerged

$$\frac{Hw_i}{D} = c\left[\frac{K_u Q}{AD^{0.5}}\right]^2 + Y - 0.5S_o \tag{1-4}$$

For Equations 1-2 through 1-4: Hw_i is the headwater depth (piezometric head) measured relative to the culvert invert or streambed elevation at the inlet for buried-invert culverts (ft), D is the interior height (streambed to pipe crown) of the culvert barrel (ft), H_c is the total head at critical depth (ft), Q is the flow rate (ft^3/s), A is the full cross-sectional area of the culvert barrel (ft^2), S_o is the culvert barrel slope (ft/ft), K_u is 1.0 (K_u = 1.811 SI units), and K, M, c, and Y are all empirical constants unique to a particular culvert installation. For a mitered inlet end treatment, S_o is multiplied by a constant of +0.7 instead of –0.5 in Equations 1-2 and 1-4.

Outlet Control Testing

To determine entrance loss coefficients, the culvert must be flowing under outlet control, which corresponds to subcritical flow conditions in the culvert. Outlet control is achieved by installing the test culverts at a slope that is less than the critical slope (critical slope is discharge specific). For all outlet control culvert tests, the test culverts were installed in as horizontal a position as possible (i.e., zero slope) to ensure subcritical culvert flow and outlet control conditions. The culverts discharged into a tail box. A stop log assembly in the tail box was used in many cases to artificially control the tailwater depth, forcing the culvert to flow under outlet control.

The entrance loss (H_e) for each test condition was determined as follows. The culvert entrance loss is equal to the difference between the total head in the head box and the representative, one-dimensional total head value in the culvert at the inlet. The total head in the head box was determined by measuring the piezometric head in the head box at a location where the velocity head was negligible. The head box pressure tap location is shown in Figure 2-7. The total head inside the culvert inlet was determined by projecting the total head determined at pressure tap locations distributed along the length of the culvert invert (see Figure 2-7) back to the culvert inlet by either adding back the calculated friction loss for full-pipe flow conditions or by using gradually varied flow computational techniques for open channel culvert flow conditions. The resulting calculated upstream total head values for each of the pressure taps were averaged to give an average total head at the inlet. After the entrance loss (H_e) was calculated, the entrance loss coefficient was calculated using Equation 1-1 with the average culvert velocity as the representative velocity term.

Using buried-invert culverts with a smooth uniform material on all flow boundaries made it possible to estimate friction losses for full-culvert flows by applying standard closed-conduit friction loss relationships and friction factors. It was also possible to calculate gradually varied flow profiles for free-surface culvert flows. Culvert entrance loss was assumed to be primarily a function of the inlet geometry of the culvert, not the roughness of the culvert material. Using smooth steel plate also facilitated accurate piezometric head measurements inside the pipe. With a smooth wall boundary, the pressure taps were oriented normal to the streamlines in the culvert. No localized turbulence regions were generated by a boundary profile as would exist with a corrugated pipe wall, for example. If streambed materials had been used for the culvert invert, it would have been difficult to account for friction loss and gradually varied flow profile variations associated with the composite hydraulic roughness flow boundary.

Due to the irregular flow cross-section, four times the hydraulic radius was used as the representative pipe diameter in the friction relationships, as suggested by Flammer et al. (1986). The Froude number (Fr) was monitored for free-surface culvert flow conditions to verify that subcritical flow ($Fr < 1.0$) existed in the culvert barrel, an indicator of outlet control. The material roughness height for the steel test culverts was assumed to be 0.0018 in. (Flammer et al., 1986).

Inlet Control Testing

Inlet control conditions were achieved by installing the test culverts at a slope greater than the critical slope. In addition, Equations 1-2 and 1-4 suggest that culvert inlet control head-discharge relationships are slope-dependent. Based on inlet control testing of buried-invert culverts, Robinson (2005)

concluded that for culverts with slopes ≤ 3%, the effect of slope on the inlet control discharge rate was negligible. Additionally, it is worth noting that the magnitude of the slope term in Equations 1-2 and 1-4 will be quite small for slopes on the order of 3%. As a result, the buried-invert culvert inlet control flow tests for this study were conducted at a uniform slope (approximately 3%).

In order to ensure inlet control conditions in the test culverts, the Froude number corresponding to the average flow depth and velocity through the culvert was calculated to verify supercritical flow ($Fr > 1.0$). For inlet control flow conditions, the empirical constants for Equations 1-2 through 1-4 were determined for the appropriate inlet conditions (i.e., submerged or unsubmerged) as follows. For each test culvert and end treatment tested, upstream total head (Hw) and discharge (Q) data were collected for both submerged and unsubmerged inlet conditions as well as ponded and channelized approach flow conditions. The total head in the head box was determined using the pressure tap in the head box for outlet control as explained previously. Note that the piezometric head (Hw_i) in Equations 1-2 through 1-4 was replaced by the total upstream head (Hw), as Hw is the more appropriate head term when comparing the variation in culvert inlet performance between ponded and channelized approach flow conditions. For ponded upstream conditions, Hw and Hw_i were equivalent.

Once the Hw and Q data were collected for each test culvert, end treatment, and flow condition (i.e., submerged and unsubmerged inlet and ponded and channelized approaches), the data were plotted according to quasi-dimensionless relationships corresponding to Equations 1-2 through 1-4. Regression analysis was used to determine the corresponding inlet control head-discharge relation constants, K, M, c, and Y, which were unique for each culvert geometry tested.

1.3 Report Layout Summary

The various topics associated with this project are discussed separately in individual report chapters. The chapters are as follows:

- Chapter 2: Buried-Invert or Embedded Culverts
- Chapter 3: Slip-Lined Culverts
- Chapter 4: Culvert Exit Loss
- Chapter 5: Inlet Control Hydraulics of Multiple Circular Culverts
- Chapter 6: The Behavior of Hydraulic Roughness Coefficients in Open Channel Flow
- Chapter 7: Open Channel Flow Resistance: the Hydraulic Radius Dependence of Manning's Equation and Manning's n
- Chapter 8: Open Channel Flow Resistance: Composite Roughness

A summary is presented in each chapter. Tabular experimental data related to Chapters 2, 3, and 5 are presented in the report appendices.

CHAPTER 2

Buried-Invert or Embedded Culverts

2.1 Summary

Concerns about roadway crossings for fish, debris, and terrestrial animals have promoted the development of alternative designs for culverts that are larger than traditional culverts, use buried-invert (embedded) circular or elliptical barrel shapes or bottomless arches, and often span the existing bank-full channel or feature a simulated streambed. Matching the culvert streambed (material composition and slope) with the adjacent upstream and downstream channel reaches allows the culvert streambed to aggregate and erode at natural rates, greatly reducing the potential for artificial fish passage barriers to form, such as perched outlets, as often occurs with traditional culverts.

In current practice, entrance loss coefficients and inlet control head-discharge relationships for buried-invert culverts designed for fish passage applications are either ignored or approximated using traditional culvert design data due to a lack of data specific to these alternative culvert geometries. In this study, experimental methods were used to determine entrance loss coefficients and inlet control head-discharge relationships for circular culverts with 20%, 40%, and 50% invert burial depths and an elliptical culvert with a 50% invert burial depth.

In general, the entrance loss coefficients for buried-invert culverts were higher than entrance loss coefficients for traditional culverts of the same cross-sectional shape without invert burial. The influence of approach flow conditions (ponded or channelized) on entrance loss coefficients and inlet control head-discharge relationships is also reported. This chapter outlines the experimental methods used to determine entrance loss coefficients and inlet control head-discharge regression constants relative to these alternative culvert geometries and presents the data relevant to the hydraulic design and evaluation of these culverts.

2.2 Introduction

Due to increased concern about the environmental impact of traditional culvert designs, more environmentally sensitive culvert designs are now being implemented in the field. Traditionally, the smallest culvert capable of passing a design flood was installed in order to minimize costs. Issues associated primarily with debris and fish passage through culverts, however, have promoted the implementation of larger culverts and alternative culvert barrel geometries.

These larger culverts, which in some cases span the entire streambed width, are typically installed so that the pipe invert is located below the natural streambed grade. Substrate is placed inside the culvert up to the level of the natural streambed grade and arranged in such a way as to simulate a streambed throughout the culvert. Additionally, the culverts are generally sized and the substrate placed so that little or no discontinuity exists between the simulated streambed in the culvert and the adjacent upstream and downstream reaches. These culverts are commonly referred to as buried-invert or embedded culverts. Similar fish passage culvert environments are also created using bottomless culverts, such as pipe arches. The results of this study are applicable to both buried-invert and bottomless culverts. Examples of buried-invert culverts with a simulated streambed are shown in Figure 2-1.

One advantage of buried-invert fish passage culverts over traditional culvert designs is the elimination of high flow velocities in the culvert at shallow flow depths due to the increase in culvert flow area. Another advantage of buried-invert culverts is that the simulated streambed can aggregate and erode streambed materials similarly to the natural streambed, thus maintaining a more natural system.

Many aspects of buried-invert fish passage culvert designs are primarily influenced by fish passage considerations, such as the composition of the simulated streambed. Structural capacity, hydraulic requirements, and public safety are also

Figure 2-1. Examples of buried-invert culverts for fish passage.

important to consider in decisions regarding culvert size, pipe material, and culvert end treatments for buried-invert culvert designs. A review of publications related to the hydraulics of buried-invert culverts for fish passage produced a significant amount of information; very little information was found regarding buried-invert culvert hydraulics (i.e., entrance loss coefficients and inlet control head-discharge relationships).

Two documents summarized a variety of design procedures for buried-invert culverts (Bates et al., 2003 and Jordan and Carlson, 1987). Because the design of buried-invert culverts for fish passage is a relatively new process, Bates et al. (2003) recommended that current design methods be implemented conservatively until the hydraulics of buried-invert culverts are more completely understood. Bates et al. (2003) also suggested that it is imperative that the discharge capacity of buried-invert culverts be evaluated. No procedure or data for doing so, however, were discussed in the document. Jordan and Carlson (1987) produced a discharge coefficient for a buried-invert culvert with a square-edged vertical headwall end treatment. Their design procedure was not consistent with current FHWA's culvert design method, published in a report entitled *Hydraulic Design of Highway Culverts* (Normann et al., 2001), referred to here and in practice as *HDS-5*. Jordan and Carlson (1987) suggested that further research is necessary to determine the discharge coefficients of other frequently used buried-invert culvert inlet geometries.

In current practice, there is some uncertainty in determining the head-discharge relationships for buried-invert culverts due to a lack of hydraulic data specific to buried-invert culvert geometries (e.g., entrance loss coefficients, verified friction loss predictive methods for composite hydraulic roughness culvert flow, and inlet flow control head-discharge relationships). At present, head-discharge relationships for buried-invert culverts are either not determined or are approximated using traditional culvert design data such as the data presented in *HDS-5*. The objective of this part of NCHRP Project 15-24 was specifically to investigate the hydraulics of buried-invert culverts, including the experimental determination of buried-invert entrance loss coefficients and inlet control head-discharge relationships for a variety of traditional culvert end treatments. Due to the wide range of design possibilities for buried-invert culverts, a variety of buried-invert culvert end treatments were evaluated to determine their influence on buried-culvert inlet control head-discharge relationships or outlet control energy loss characteristics.

2.3 Research Objectives

The objectives of this research included determining the entrance loss coefficient, k_e, and the inlet control head-discharge relationships for circular culverts with invert burial depths of 20%, 40%, and 50% and an elliptical culvert with a 50% invert burial depth. All buried-invert culverts were tested with four different end treatments: (1) thin-wall projecting, (2) mitered flush to 1.5:1.0 (horizontal to vertical) fill slope, (3) square-edged inlet with vertical headwall, and (4) 45° beveled entrance with vertical headwall, the bevel extending 1 in. vertically for every 24 inches of horizontal culvert span. The four end treatments tested are illustrated in Figures 2-2 and 2-3.

Each end treatment was tested with two different approach flow conditions—ponded and channelized. The ponded approach represented a reservoir condition with negligible velocities everywhere except near the culvert inlet. Significantly higher approach velocities developed when two parallel guide

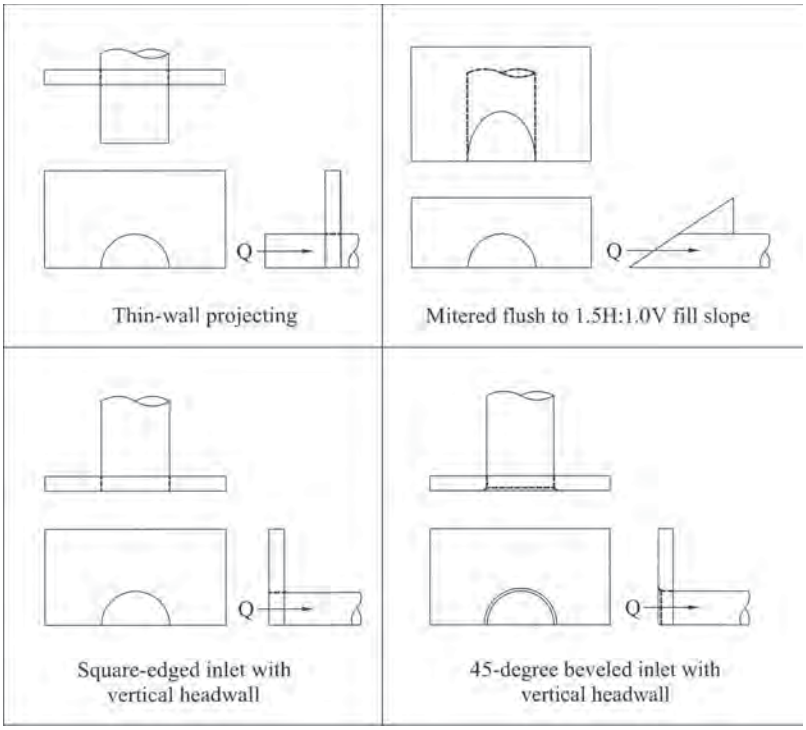

Figure 2-2. Buried-invert culvert inlet end treatments using a circular culvert with a 50% invert burial.

walls were installed, one on each side of the culvert inlet, creating the channelized approach with a ratio of channel width to culvert horizontal span of 2. The wing walls were approximately four times the culvert span in length. Figure 2-4 illustrates ponded and channelized approach conditions.

To make an accurate comparison between channelized and ponded approach flow conditions, it was determined that the total upstream head (*Hw*) would be a more appropriate term for quantifying inlet control head-discharge relationships than the piezometric head (Hw_i). Consequently, for both approach flow conditions, the upstream head was measured in a location with negligible velocity head (i.e., $Hw_i = Hw$). By doing so, the upstream head term in Equations 1-2 through 1-4, Hw_i, was replaced by the total head term, *Hw*. For the channelized approach flow conditions, some energy loss occurs between the reservoir and the culvert inlet due to flow contraction at the channel inlet and friction loss. *Hw* at the culvert inlet was approximated by subtracting the friction loss (Manning's n = 0.009 assumed) and a contraction loss at the channel entrance (entrance loss coefficient = 0.36 assumed) from the total head measured at the reservoir pressure tap.

As the data from this lab-scale culvert study will likely be applied to larger, field-scale buried-invert culverts, another research objective was to gain some understanding regarding the dependence of entrance loss coefficients on culvert diameter (size-scale effects). Entrance loss testing was conducted using 12-in. [inside diameter (I.D.) = 11.75 in.] and 24-in. diameter (I.D. = 23.45 in.) traditional circular culverts with square-edged inlet with headwall end treatments as shown in Figure 2-5. The entrance loss coefficients were determined for each culvert tested with submerged and unsubmerged ponded inlet conditions.

2.4 Experimental Method

A detailed discussion of the testing procedures associated with the determination of k_e for outlet control and the empirical constants associated with the head-discharge relationships (Equations 1-2 through 1-4) for inlet control is presented in Chapter 1. Commercially available circular PVC pipe with the dimensions shown in Table 2-1 were used for the entrance loss coefficient size-scale testing. The buried-invert culverts were fabricated using smooth steel plate for the culvert wall and the flat invert that represented the simulated streambed. The circular culverts with 20%, 40%, and 50% invert burial depths had an inside diameter or horizontal dimension (D_h) of approximately 18 inches with the vertical rise (D) dimension varying with burial depth. The dimensions of the elliptical culvert were D_h = 25 inches and a vertical span of 17 inches; D = 8.5 inches with the 50% invert burial geometry. The aspect ratio of the elliptical culvert was based on dimensions of commercially available culverts.

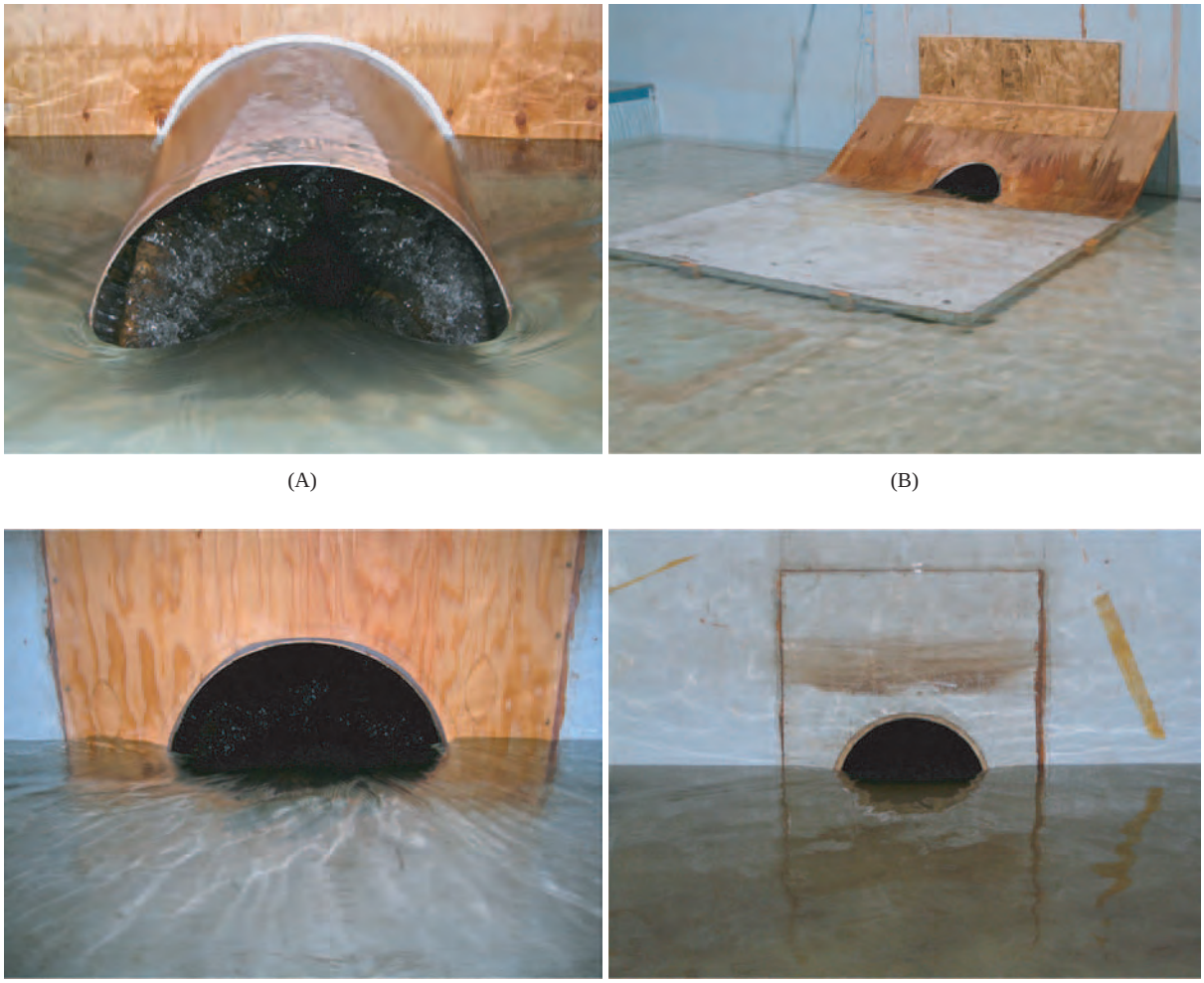

(A) (B)

(C) (D)

Figure 2-3. Buried-invert culvert end treatments evaluated: (A) thin-wall projecting, (B) mitered flush to 1.5:1 (horizontal to vertical) fill slope, (C) square-edged inlet with vertical headwall, and (D) 45° beveled inlet with vertical headwall.

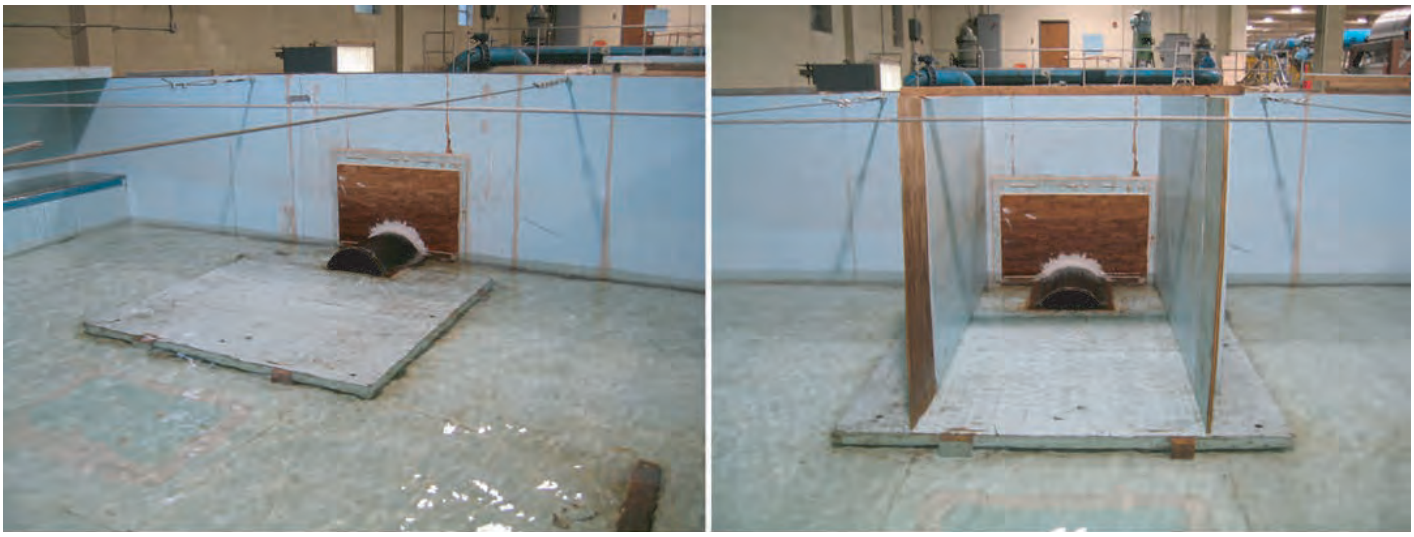

(Ponded) (Channelized)

Figure 2-4. Culvert approach flow test conditions.

12-in. circular culvert

24-in. circular culvert

Figure 2-5. Overview of entrance loss size-scale testing.

Each buried-invert culvert had a wall thickness of 0.125 in., was approximately 20 ft long, and was supported continuously along the flat invert by two parallel, 4-in. square steel box beams that ran the length of the culvert. The culverts were also supported with vertical columns at regular intervals to minimize culvert deflection (maintain a constant slope) during testing. A schematic of the cross-sectional geometry for each buried-invert test culvert is provided in Figure 2-6. The buried-invert culvert cross-sections illustrated in Figure 2-6 were uniform over the entire length of each test culvert.

Water was supplied to the test culverts via a head box, which measured 24 ft long by 22 ft wide by 5 ft deep. Water was supplied to the head box via 20-in. and/or 8-in. supply lines, both containing calibrated orifice flow meters. A schematic of the culvert test facility is shown in Figure 2-7, and a photo overview is provided in Figure 2-8. The location of the

Table 2-1. Test culvert geometries.

Dimension	Circular culverts			Elliptical culvert
	20% buried invert	40% buried invert	50% buried invert	50% buried invert
D (in)	14.57	11.02	9.05	8.66
D_h (in)	18.11	18.11	18.11	25.20
L (ft)	20	20	20	20

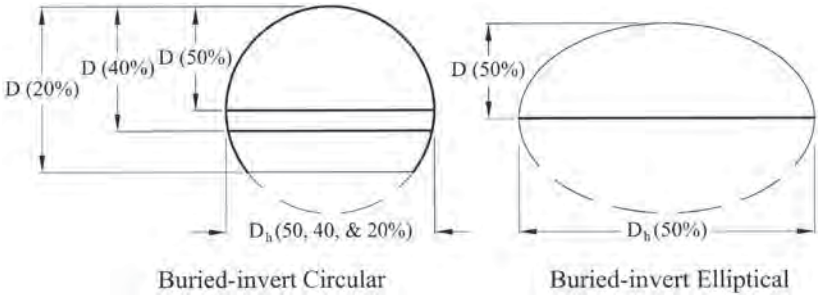

Figure 2-6. Buried-invert test culvert cross-sectional geometries.

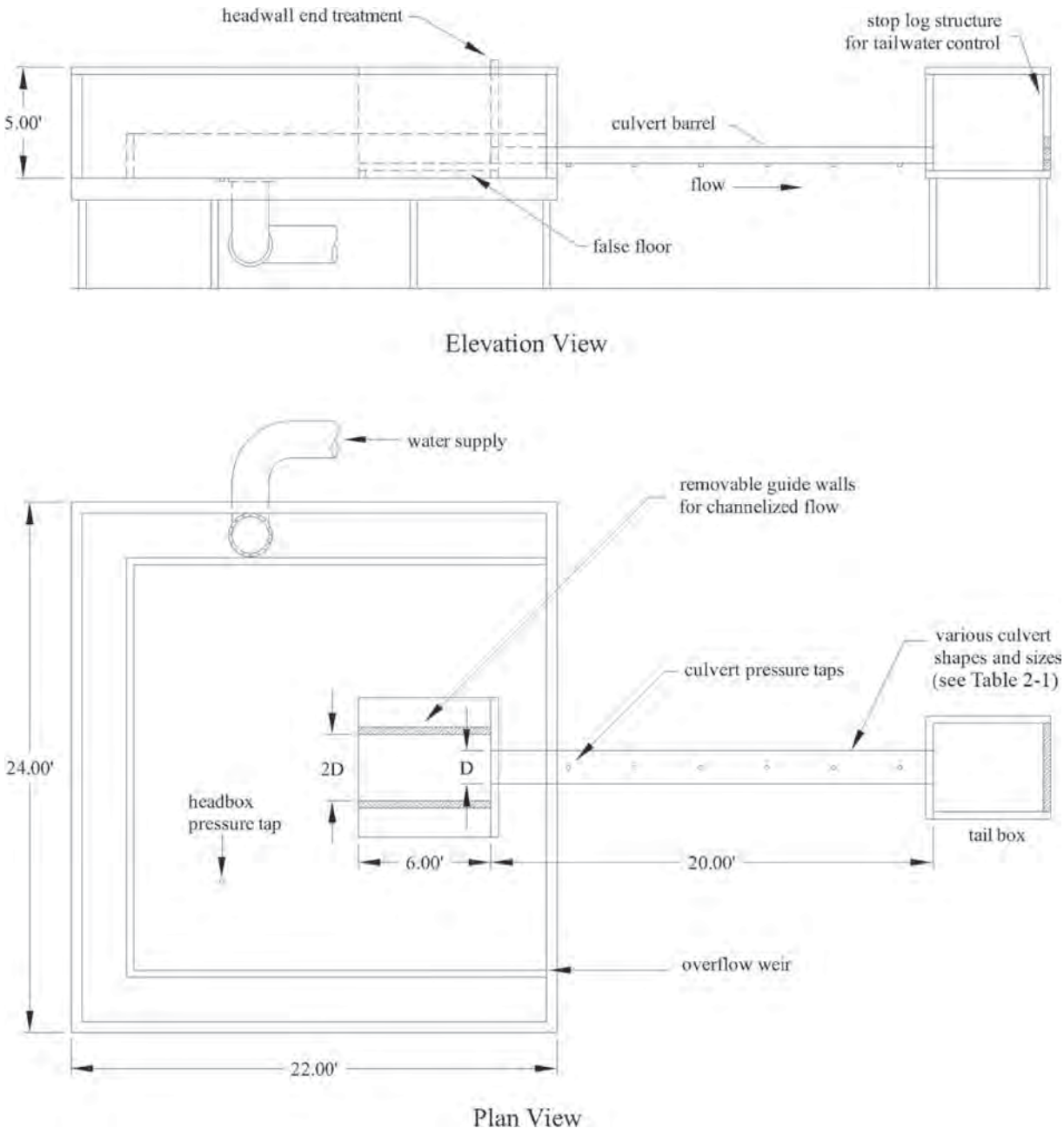

Figure 2-7. Culvert test facility.

Figure 2-8. Culvert test setup.

pressure tap that was used to measure *Hw* in the upstream reservoir is identified in Figure 2-7.

The entrance loss coefficient, k_e, and the inlet control regression constants, *K, M, c,* and *Y,* were determined for both submerged and unsubmerged inlet conditions. The entrance loss coefficient data are presented as a function of (*Hw/D*), where *Hw* represents total upstream head and *D* is the buried-invert culvert vertical height (streambed to pipe crown).

2.5 Experimental Results

Outlet Control

The results of the size-scale effects testing for the circular culverts with square-edged inlets and a vertical head wall are shown in Figure 2-9, where the entrance loss coefficient, k_e, is plotted as a function of *Hw/D.* At *Hw/D* values greater than 1.0, the 24-in. diameter circular culvert yielded an average entrance loss coefficient of 0.515, while the 12-in. diameter circular culvert produced an average entrance loss coefficient of 0.511. The average value of experimental uncertainty for the size-scale entrance loss testing was approximately 1.5%. The fact that the 12- and 24-in. diameter tests produced essentially the same entrance loss coefficient and that the experimental loss coefficient was consistent with the typical published k_e value for square-edged inlets with headwall end treatment ($k_e = 0.5$) suggests that there were no biases in the entrance loss coefficient experimental data associated with culvert size. Based on this result, it is also assumed that the buried-invert culvert hydraulic performance data from this study may be applied to larger field-scale culverts.

The entrance loss coefficient data for the circular culvert with 20%, 40%, and 50% invert burial and the elliptical culvert with 50% invert burial are shown in Figures 2-10 through 2-13. The entrance loss coefficient, k_e, is plotted as a function of *Hw/D* and classified by end treatment and approach flow condition (ponded or channelized). For each of the four end treatments tested [thin-wall projecting, mitered flush to 1.5:1.0 (horizontal to vertical) fill slope, square-edged inlet with vertical headwall, and 45° beveled inlet with vertical headwall], the entrance loss coefficient varied significantly with *Hw/D* for *Hw/D* values less than 1.0 to 1.5. Above that range, k_e remained relatively constant. For all end treatments tested, channelized approach flow had no appreciable effect on the entrance loss coefficients, with the exception of the thin-wall projecting end treatment. For the thin-wall projecting inlet, the channelized approach condition was more efficient (smaller k_e value) than the ponded approach condition. The increase in efficiency for the thin-wall projecting channelized approach flow condition was likely due in part to a decrease in the amount of flow contraction at the inlet relative to the ponded condition.

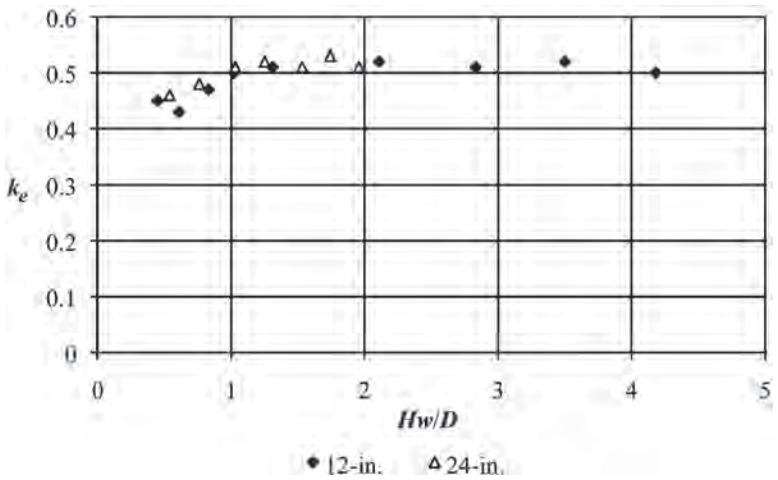

Figure 2-9. Size-scale effect entrance loss coefficients for traditional circular culverts (square edged with vertical headwall and ponded approach flow).

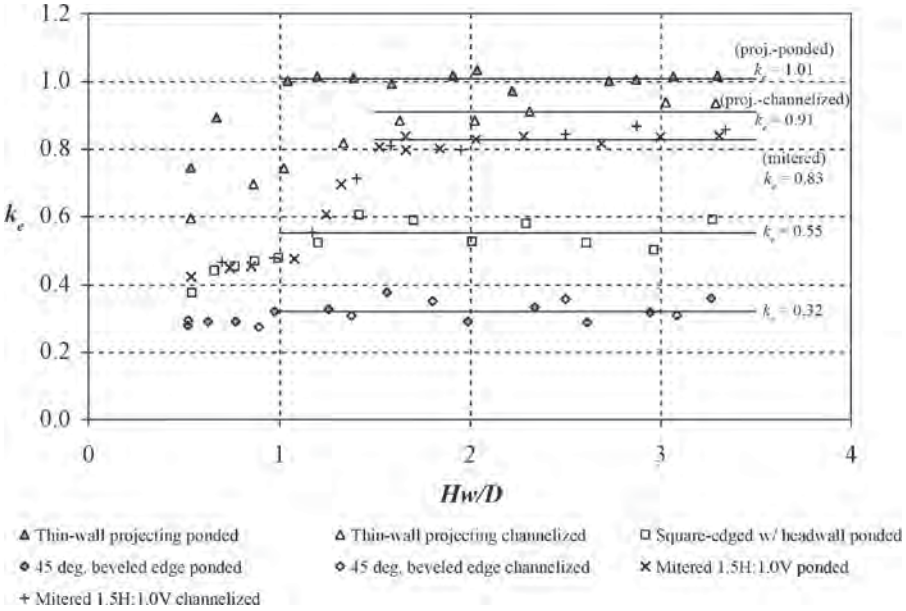

Figure 2-10. Circular culvert, 20% buried invert, entrance loss coefficient data.

Table 2-2 summarizes the average k_e values for each end treatment for the buried-invert circular and elliptical test culverts. As a comparison, Table 2-3 presents the entrance loss coefficient values reported in *HDS-5* for traditional circular culverts with end treatments similar to those evaluated in this study. The entrance loss coefficients for all the buried-invert culvert geometries and various end treatments were larger (more head loss) than the entrance loss coefficients for traditional circular culverts with the same or similar end treatments. The k_e values for the circular culvert with 20%, 40%, and 50% invert burial depths and the elliptical culvert with 50% invert burial depth were relatively uniform for a given end treatment. Consequently, a single representative or average k_e value is presented in Table 2-4 for each end treatment tested. The average experimental uncertainty of 1.8% associated with the data and the even larger uncertainty associated with predicting culvert velocities in the field are such that the scatter in the k_e data relative to the average values associated with the various buried-invert culvert barrel geometries is considered negligible.

Inlet Control

Inlet control head-discharge relationships were created for unsubmerged and submerged inlet conditions (i.e., 0.3 <

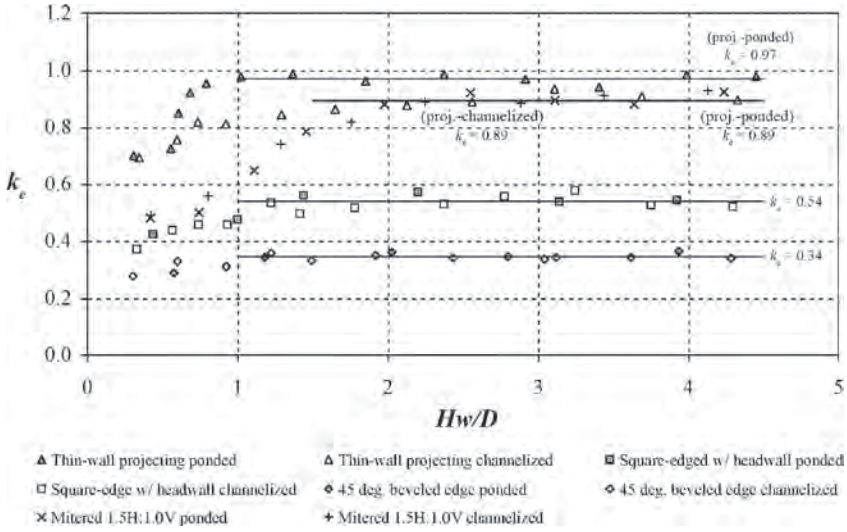

Figure 2-11. Circular culvert, 40% buried invert, entrance loss coefficient data.

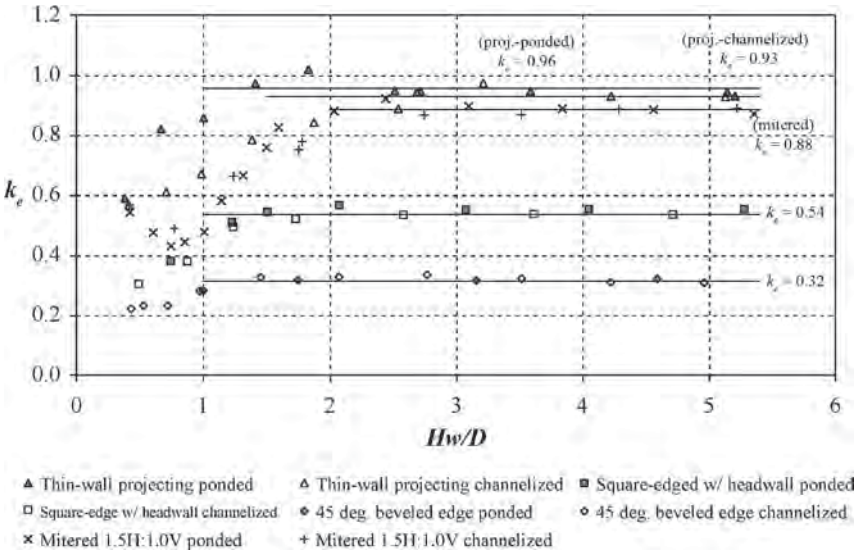

Figure 2-12. Circular culvert, 50% buried invert, entrance loss coefficient data.

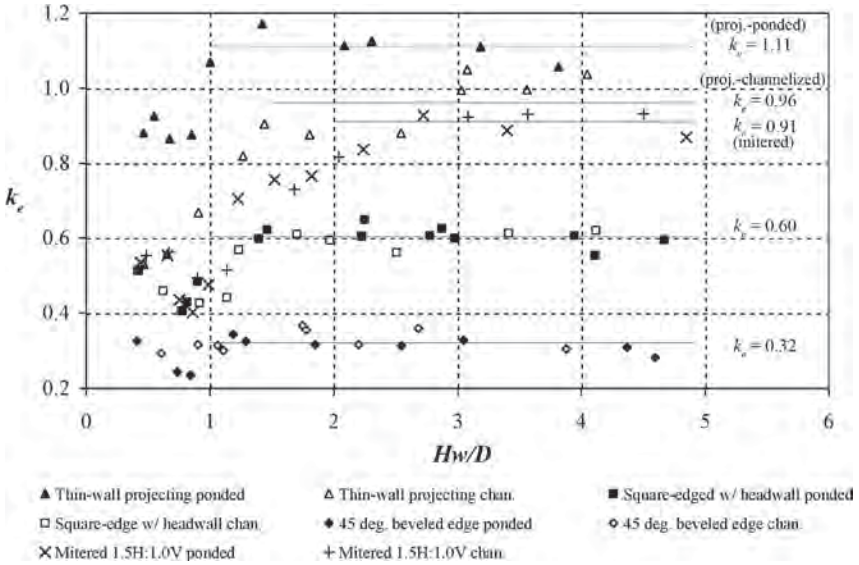

Figure 2-13. Elliptical culvert, 50% buried invert, entrance loss coefficient data.

Table 2-2. Average buried-invert culvert entrance loss coefficients.

Culvert end treatment	Average k_e (± extreme % deviation from average)			
	20% circular	40% circular	50% circular	50% elliptical
Thin-wall projecting (ponded)	1.01 (±3.5%)	0.97 (±3.2%)	0.96 (±6.6%)	1.11 (±9.8%)
Thin-wall projecting (channelized)	0.91 (±3.1%)	0.89 (±4.4%)	0.93 (±4.6%)	0.96 (±9.1%)
Mitered to 1.5H:1.0V w/ vertical headwall	0.83 (±4.9%)	0.89 (±3.1%)	0.88 (±4.1%)	0.91 (±4.6%)
Square-edged inlet w/ vertical headwall	0.55 (±9.7%)	0.54 (±8.0%)	0.54 (±5.6%)	0.60 (±7.2%)
45° beveled inlet w/ vertical headwall	0.32 (±11%)	0.34 (±5.7%)	0.32 (±4.3%)	0.32 (±14.1%)

Table 2-3. Circular culvert entrance loss coefficients from HDS-5 (Normann et al., 2001).

Circular culvert inlet end treatment	k_e
Projecting from fill slope	0.9
Mitered to fill slope	0.7
Square-edged with headwall	0.5
45° beveled edge with headwall	0.2

Table 2-4. Recommended buried-invert culvert entrance loss coefficients.

Culvert inlet end treatment	k_e
Projecting (circular)	1.00
Projecting (elliptical)	1.10
Mitered to fill slope (circular)	0.90
Square-edged with headwall (circular)	0.55
Square-edged with headwall (elliptical)	0.60
45° beveled edge with headwall	0.35

Hw/D < 5.0) for each of the four end treatments for the circular culverts with 20%, 40%, and 50% invert burial depths and the elliptical culvert with 50% invert burial depth. Figures 2-14 through 2-17 present inlet control quasi-dimensionless relationships in Equation 1-3 (Form 2) for the four culverts tested and the various end treatments, approach flow conditions, and inlet submergence conditions.

Regression of the unsubmerged data in Figures 2-14 through 2-17 produced the empirical constants *K, M, c,* and *Y* associated with Equations 1-2 through 1-4. The inlet control regression constants generated for buried-invert culverts are shown in Table 2-5 and are classified by culvert geometry, inlet end treatment, approach flow condition, and inlet submergence condition. For comparative purposes, Table 2-6 includes inlet control regression constants for traditional circular culverts with end treatments similar to those of the buried-invert culverts tested in the current study. These regression constants for Equations 1-2, 1-3, and 1-4 are published in *HDS-5* (Normann et al., 2001). Experimental uncertainty for the generation of inlet control head-discharge relationships for this study was < 1%.

Channelized approach flow had a significant effect on the head-discharge relationship for the thin-wall projecting end treatment. The channelized approach flow had a higher discharge for a given *Hw* than the ponded condition. Consequently, separate regression constants were derived for

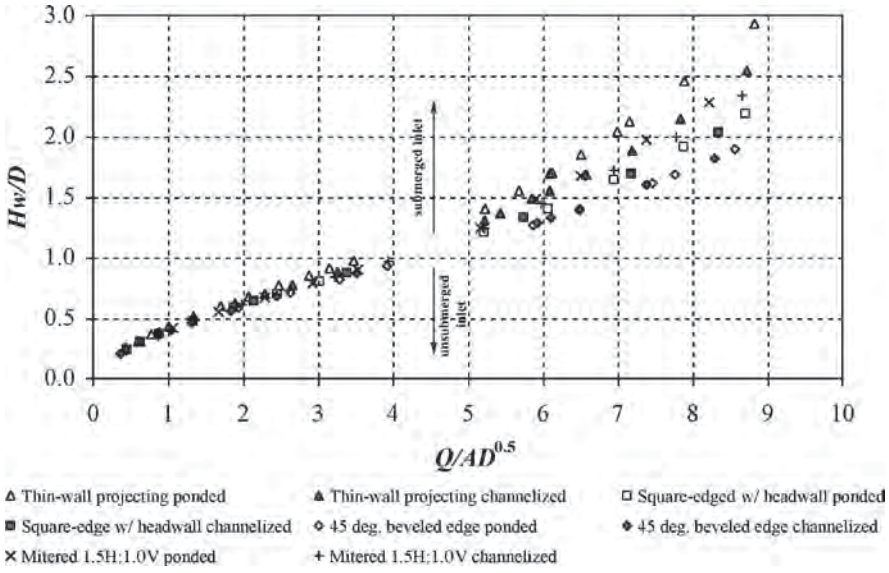

Figure 2-14. Circular culvert, 20% buried invert, inlet control Form 2 (Equation 1-3) data.

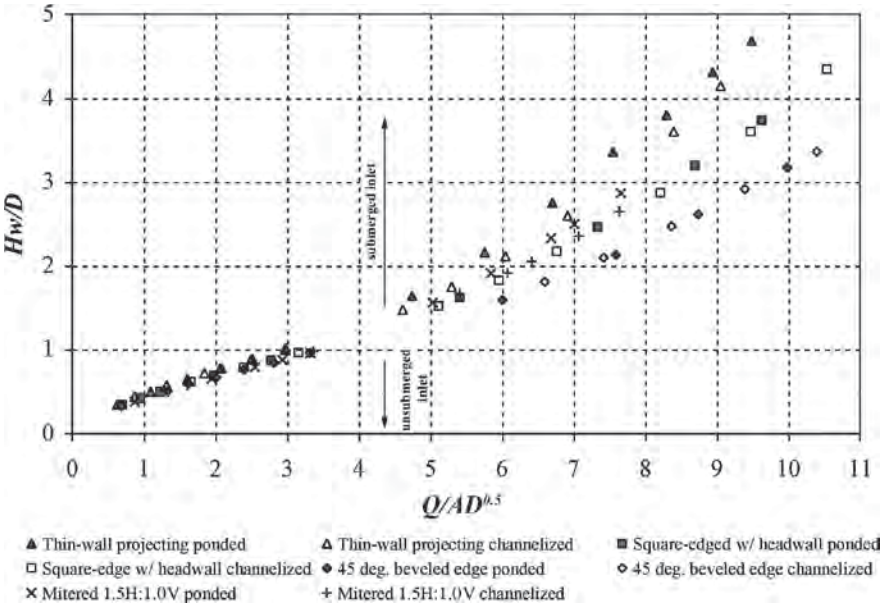

Figure 2-15. Circular culvert, 40% buried invert, inlet control Form 2 (Equation 1-3) data.

each approach flow condition for the thin-wall projecting end treatment. Regression constants for the square-edged inlet with vertical headwall, 45° beveled inlet with vertical headwall, and mitered flush to 1.5 horizontal to 1.0 vertical fill slope end treatments were developed by combining both the ponded and channelized data since channelization had a minimal effect on the inlet efficiency. This suggests that the inlet geometry has a much greater effect on the inlet efficiency than the reduction of flow contraction due to channelization for the square-edged, 45° beveled, and mitered inlet end treatments. Tabular support data for the Chapter 2 experimental results are included in Appendices A and B.

2.6 Conclusions

Prior to this study, entrance loss coefficients and inlet control head-discharge relationships for buried-invert culverts were either ignored or approximated using traditional circular culvert data because of the lack of data specific to buried-invert culvert geometries. The entrance loss coefficient data and

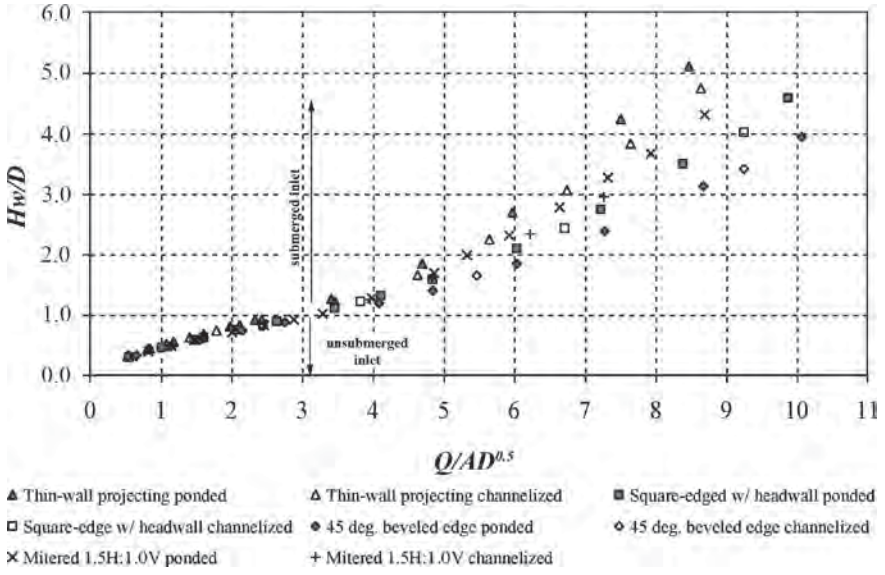

Figure 2-16. Circular culvert, 50% buried invert, inlet control Form 2 (Equation 1-3) data.

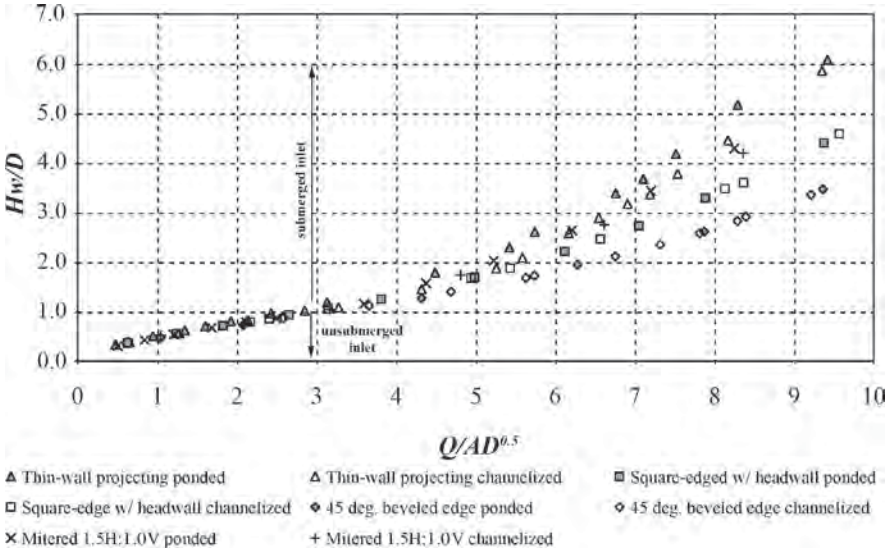

Figure 2-17. Elliptical culvert, 50% buried invert, inlet control Form 2 (Equation 1-3) data.

Table 2-5. Buried-invert culvert inlet control regression constants.

Culvert type	Unsubmerged				Submerged	
	Form 1		Form 2			
	K	*M*	*K*	*M*	*c*	*Y*
20% Buried invert circular						
Projecting end, ponded	0.0860	0.58	0.4293	0.64	0.0303	0.58
Projecting end, channelized	0.0737	0.45	0.4175	0.62	0.0250	0.63
Square headwall	0.0566	0.44	0.4001	0.63	0.0198	0.69
45° Beveled end	0.0292	0.57	0.3869	0.63	0.0161	0.73
Mitered end, 1.5H:1.0V	0.0431	0.58	0.4002	0.63	0.0235	0.61
40% Buried invert circular						
Projecting end, ponded	0.0840	0.76	0.4706	0.69	0.0453	0.69
Projecting end, channelized	0.0927	0.59	0.4789	0.66	0.0441	0.52
Square headwall	0.0490	0.71	0.4354	0.68	0.0332	0.67
45° Beveled end	0.0358	0.62	0.4223	0.67	0.0245	0.75
Mitered end, 1.5H:1.0V	0.0317	0.77	0.4185	0.68	0.0363	0.65
50% Buried invert circular						
Projecting end, ponded	0.1057	0.69	0.4955	0.71	0.0606	0.54
Projecting end, channelized	0.1055	0.59	0.4955	0.69	0.0570	0.48
Square headwall	0.0595	0.59	0.0595	0.59	0.0402	0.65
45° Beveled end	0.0464	0.46	0.4364	0.69	0.0324	0.67
Mitered end, 1.5H:1.0V	0.0351	0.59	0.4419	0.68	0.0504	0.44
50% Buried invert elliptical						
Projecting end, ponded	0.1231	0.51	0.5261	0.65	0.0643	0.50
Projecting end, channelized	0.0928	0.54	0.4937	0.67	0.0649	0.12
Square headwall	0.0819	0.45	0.4867	0.66	0.0431	0.61
45° Beveled end	0.0551	0.52	0.4663	0.63	0.0318	0.68
Mitered to slope	0.0599	0.60	0.482	0.67	0.0541	0.50

Table 2-6. HDS-5 traditional circular culvert inlet control regression constants (Normann et al., 2001).

Test Culvert & End Treatment	Unsubmerged				Submerged	
	Form 1		Form 2			
	K	*M*	*K*	*M*	*c*	*Y*
HDS-5 Circular CMP						
Projecting	0.0340	1.50	–	–	0.0553	0.54
Mitered to slope	0.021	1.33	–	–	0.0463	0.75
Square headwall	0.0078	2.0	–	–	0.0379	0.69
HDS-5 Circular						
Beveled ring, 45° bevels	0.0018	2.50	–	–	0.0300	0.74
Smooth tapered inlet throat	–	–	0.534	0.555	0.0196	0.90
Rough tapered inlet throat	–	–	0.519	0.640	0.0210	0.90

the inlet control head-discharge design curves determined in this study will assist in evaluating the hydraulic capacity of buried-invert culverts.

Based on the experimental results of the entrance loss coefficient data and inlet control head-discharge data for the 20%, 40%, and 50% buried-invert circular culverts and the 50% buried-invert elliptical culvert with four different end treatments, the following conclusions are made:

1. Buried-invert culvert entrance loss coefficients, k_e, are higher than entrance loss coefficients for traditional circular culverts with the same or similar end treatments. Buried-invert circular and elliptical culverts with the 45° beveled with vertical headwall end treatment produced k_e values 65% higher, on average, than the traditional circular culverts with the same end treatment. The buried-invert circular culvert with the thin-walled projecting end treatment produced k_e values, on average, that were 9% larger than the traditional circular culvert with the same end treatment. Traditional culvert (invert not buried) k_e data for this study were based on values published in *HDS-5.*
2. For square-edged with headwall and thin-wall projecting inlets, the shape of the culvert (20%, 40%, and 50% buried-invert circular or 50% buried-invert elliptical) had no significant effect on k_e. The elliptical buried-invert culvert with mitered flush to 1.5:1.0 (horizontal to vertical) fill slope and the 45° beveled inlet with vertical headwall end treatments produced larger k_e values than for the circular buried-invert culverts.
3. Under unsubmerged inlet conditions, k_e for buried-invert culverts varies significantly with *Hw/D.* This may be due in part to variations in flow contraction at the culvert inlet with *Hw/D.* For a submerged inlet, k_e is relatively independent of *Hw/D* (k_e = constant) and is higher than the unsubmerged inlet values. The submerged k_e values are listed in Table 2-4 and are recommended for use in design, as they constitute a more conservative value.
4. With the exception of the thin-wall projecting end treatments, a channelized approach flow with a channel to culvert width ratio of 2 had no significant effect on k_e or on the inlet control head-discharge relationships for buried-invert circular and elliptical culverts when using total upstream head rather than piezometric head. The channelized approach was slightly more efficient than the ponded approach for the thin-wall projecting inlet for both inlet and outlet flow control. For all buried-invert culvert geometries and end treatments tested, the Form 2 equation (Equation 1-3) matched the experimental data more closely than the Form 1 equation (Equation 1-2) for unsubmerged inlet control flow conditions.

CHAPTER 3

Slip-Lined Culverts

3.1 Summary

Culvert rehabilitation, in many cases, represents a cost-effective alternative to culvert replacement. Slip lining old culverts with new liner pipe represents a culvert rehabilitation practice that is becoming more and more common. A relined culvert must be able to pass the design flood while meeting the necessary embankment freeboard condition. The discharge capacity of a slip-lined culvert is influenced by the geometry of the inlet end treatment. For inlet control, the culvert head-discharge relationship is a unique function of the culvert inlet geometry and driving head, which must be determined experimentally. For outlet control, the head-discharge relationship is determined by balancing the energy loss through the culvert (entrance, friction, exit, and other minor losses) and the available driving head, with the coefficient for entrance loss being determined experimentally. A number of factors, including reduced inlet flow area, the liner pipe wall roughness, and the inlet end treatment, influence the relined culvert discharge capacity relative to the original culvert.

Four different slip-lined culvert inlet end treatments associated with a thin-wall projecting host pipe were evaluated experimentally. Inlet control head-discharge relationship and outlet control entrance loss coefficient trends were evaluated as a function of liner projection distance and liner-to-host pipe transition detail (sudden or tapered). The test results showed that the entrance loss coefficient (k_e) for the projecting slip liner was independent of the projection distance for projection distances of 0.17D and 0.34D; k_e values for the projecting slip-lined culvert were slightly smaller (more efficient) than the traditional thin-wall projecting k_e values published in design manuals. The inlet control head-discharge relationships were independent of projection distance and were consistent with the performance of traditional thin-wall projecting culverts operating under inlet control. Tapered grout transitions between the host and liner pipe were found to reduce k_e due to a reduction in entrance flow contraction.

3.2 Introduction

Many existing culverts have reached or will soon reach the end of their useful service life. When a culvert is in need of repair, replacement methods can be very costly and may not be feasible due to budgetary or environmental constraints (Maine DOT, 2004). Culvert rehabilitation, when applicable, can become a significant resource and time saving tool. Slip lining is a common rehabilitation technique where a new culvert, often a smooth-walled pipe, is placed inside an existing or host culvert (Plastics Pipe Institute, 1993). An example of a slip-lined culvert is illustrated in Figure 3-1.

In order to minimize the reduction in cross-sectional area, the slip liner typically matches the host culvert shape and has the largest available diameter that can be slipped inside the existing culvert (Ballinger and Drake, 1995b). The invert of the slip liner is placed directly on top of the invert of the existing culvert, and the space between the slip liner and the host culvert is grouted. Typically, the slip liner is extended a short distance (≥ 6 in.) beyond the existing culvert at each end to allow for expansion and contraction, as well as for installation purposes.

A review of publications related to the hydraulics of slip-lined culverts produced very little information regarding the effects that slip lining may have on the hydraulic parameters of a culvert inlet (i.e., entrance loss coefficients and inlet control head-discharge relationships). The Plastics Pipe Institute (1993) showed how the hydraulic capacity of a slip-lined culvert may be affected because of a difference in pipe wall roughness between the existing culvert and the slip liner; however, no information was given regarding the impact of the inlet geometry on the hydraulic capacity of slip-lined culverts. Ballinger and Drake (1995a) recognized that the hydraulic capacity of a culvert may be influenced by the inlet geometry and that the flow capacity (for a given upstream head) can either increase or decrease as a result of the slip-lining procedure, but they did not produce any experimental

Figure 3-1. Example of a slip-lined culvert.

data to show how the change in inlet geometry might affect the hydraulic capacity of a slip-lined culvert.

Following the literature review, it was apparent that there is a need to quantify the hydraulic parameters (i.e., entrance loss coefficients and inlet control head-discharge relationships) of slip-lined culvert inlets since the hydraulic capacity of such culverts is typically approximated with traditional culvert design data such as the data published in FHWA's *Hydraulic Design of Highway Culverts* (Normann et al., 2001), referred to here and in practice as *HDS-5*. The generation of data specific to slip-lined culvert inlet geometries is important in the derivation of the abovementioned design parameters so that design engineers can accurately predict the hydraulic capacity of slip-lined culvert configurations.

3.3 Research Objectives

The objective of this research was to determine the effect of several projecting end-treatment geometries specific to segmental-pipe slip lining on k_e and on the inlet control head-discharge relationship. Two typical end treatments were constructed, and the slip liner was extended two distances from the existing culvert end for each end treatment.

The first type of slip-lined culvert end treatment was created by installing a projecting liner inside a larger host pipe and grouting the annular space between the two pipes with a vertical grout face at the end of the host pipe (see Figure 3-2). The second type of slip-lined culvert end treatment also featured a projecting slip liner upstream of the host culvert; however, the grout was tapered and extended from the end of the host culvert to the end of the slip liner (see Figure 3-2).

The projecting distance between the outside culvert and the slip liner was tested at 2 and 4 in. (0.17D and 0.34 D, respectively) to investigate the influence of projection distance on

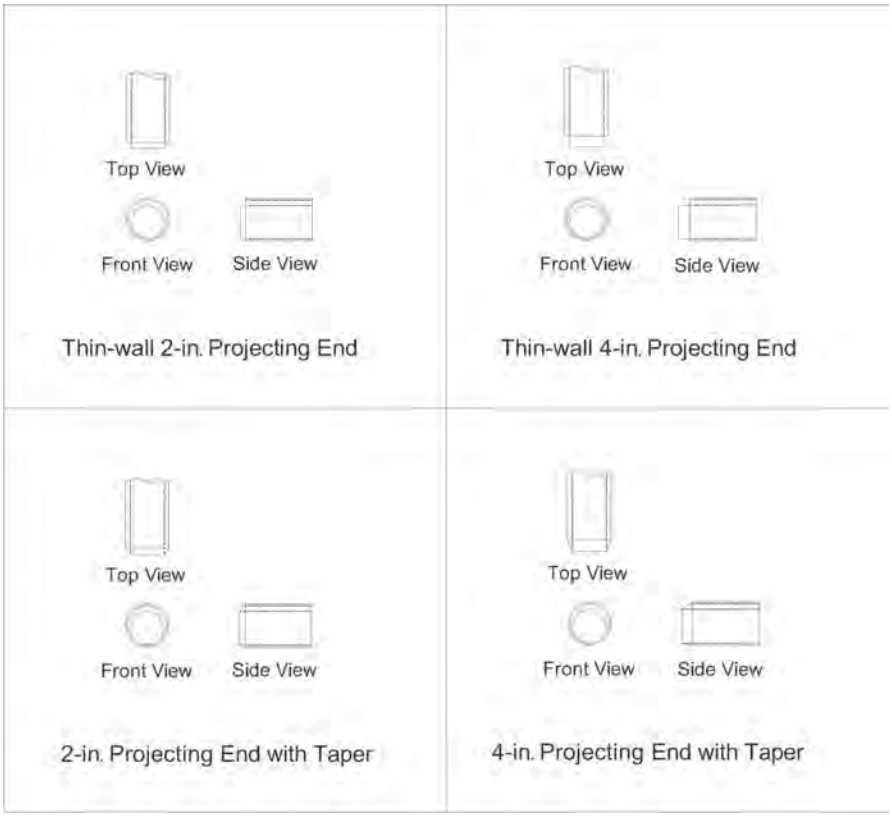

Figure 3-2. Slip-lined culvert inlet end treatments.

Figure 3-3. Ponded approach flow condition.

inlet performance. For the tapered end treatment, the angle of the tapered grout at the crown of the pipe ranged from 34° to 53° depending on the projecting distance of the slip liner from the outside culvert. The culvert used as the slip liner was also tested alone (no host culvert) as a traditional projecting inlet in order to investigate the difference between traditional projecting end treatments and slip-lined projecting end treatments. Examples of the end treatments tested are demonstrated in Figure 3-2.

Each end treatment was tested with a ponded approach flow condition. The ponded approach represented a reservoir condition with negligible velocities everywhere except near the culvert inlet. Figure 3-3 illustrates a ponded approach condition. With velocity head equal to zero, the piezometric head equals the total head. Consequently, the flow depth, or piezometric head term (Hw_i), in Equations 1-2 through 1-4 was replaced with total head (Hw) for analysis of the inlet control flow data. Hw represents a more appropriate upstream head parameter, particularly when the approach velocity head is significant (i.e., a channelized approach flow condition).

Each end treatment was tested over a range of headwater depths for both submerged and unsubmerged inlet conditions. Corresponding values of k_e (outlet control) and K, M, c, and Y (inlet control) were determined. The upstream energy or headwater levels were measured in terms of the dimensionless headwater over diameter (Hw/D), where D is the total vertical rise of the slip-liner culvert inlet. The submerged case was created when the upstream headwater fully inundated the culvert inlet, typically at an Hw/D value of 1.2 or greater.

3.4 Experimental Method—Outlet Control Testing

A detailed discussion of the testing procedures associated with the determination of k_e for outlet control and the empirical constants associated with the head-discharge relationships (Equations 1-2 through 1-4) for inlet control is presented in Chapter 1. A 20-ft long, 12-in. diameter, commercially available PVC pipe with an 11.75-in. inside diameter (I.D.) and a 0.25-in. wall thickness was used as the slip liner for all slip-lined culvert testing. The host culvert had an I.D. of approximately 14 in. and a wall thickness of 0.625 in. This test setup represented an inside diameter reduction of approximately 20%.

Water was supplied to the test culverts via a head box, which measured 24 ft long by 22 ft wide by 5 ft deep. Water was supplied to the head box via a 20-in. supply line and/or 8-in. supply line, both containing calibrated orifice plate flow meters. A schematic of the culvert test facility is shown in Figure 3-4, and a photo of the culvert test setup is shown in Figure 3-5.

To determine entrance loss coefficients, the culvert must be flowing under outlet control, which corresponds to subcritical flow conditions in the culvert. Outlet control is achieved by installing the test culvert at a slope less than the critical slope for a given discharge. For all outlet control culvert tests, the test culvert was installed in as horizontal a position as possible (i.e., $S_o = 0$) to ensure subcritical culvert flow and outlet control conditions.

The culvert entrance head loss (H_e) is the difference between the total head in the head box and the representative one-dimensional total head value in the culvert at the inlet and was evaluated for each test condition as follows. The total head in the head box was determined by measuring the piezometric head in the head box, relative to the invert of

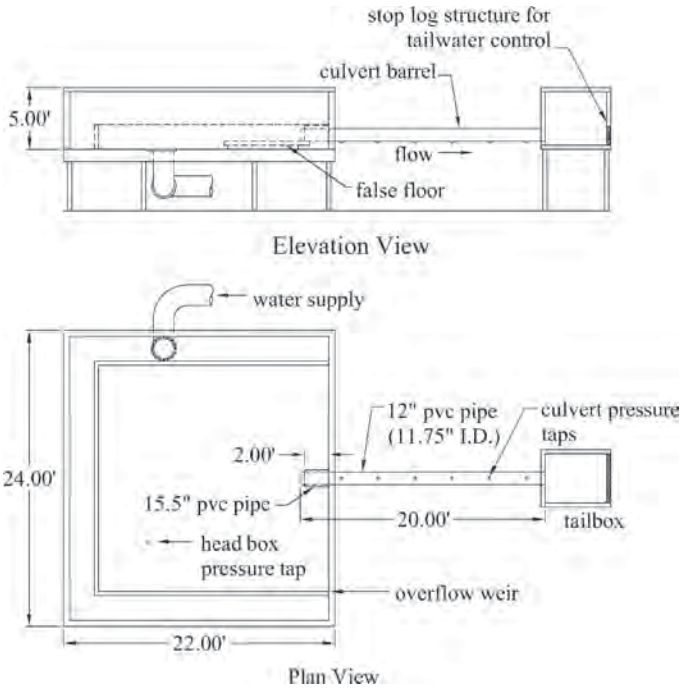

Figure 3-4. Testing facility at the Utah Water Research Laboratory.

Figure 3-5. Overview photo of the culvert test setup.

the culvert inlet, at a location where the velocity head was negligible. The head box pressure tap location is shown in Figure 3-4. The total head inside the culvert inlet was found by projecting the total head determined at pressure tap locations distributed along the length of the culvert invert back to the culvert inlet by either adding back the calculated friction loss (full-pipe flow) or by using gradually varied flow computational techniques (open channel culvert flow). The resulting calculated culvert inlet total head values for each of the pressure taps were averaged to give an average total head at the inlet. After determining H_e, the k_e was calculated using Equation 1-1.

Using slip liners with a smooth pipe wall made it possible to determine friction losses for full-culvert flows by applying standard closed-conduit friction loss relationships and friction factors and to calculate gradually varied flow profiles for free-surface culvert flows. It was assumed that culvert entrance loss is primarily a function of the inlet geometry of the culvert, not the roughness of the culvert material. With a smooth wall boundary, the pressure taps were oriented normal to the streamlines in the culvert, which facilitated accurate piezometric head measurements inside the pipe. There were no localized turbulence regions generated by a boundary profile as would exist with a corrugated pipe wall, for example.

The Froude number was monitored for free-surface culvert flow conditions to verify that subcritical flow ($Fr < 1.0$) existed in the culvert barrel, an indicator of outlet control. The material roughness height for the PVC test culvert was assumed to be 0.00006 in. (Flammer et al., 1986).

3.5 Experimental Results

Outlet Control

The k_e test results for the slip-lined circular culverts are shown in Figure 3-6, where k_e is plotted as a function of *Hw/D* and classified by end treatment and inlet submergence condition. From the end treatment specific data plotted in Figure 3-6 (thin-wall 2-in. projecting, thin-wall 4-in. projecting, 2-in. projecting with taper, 4-in. projecting with taper),

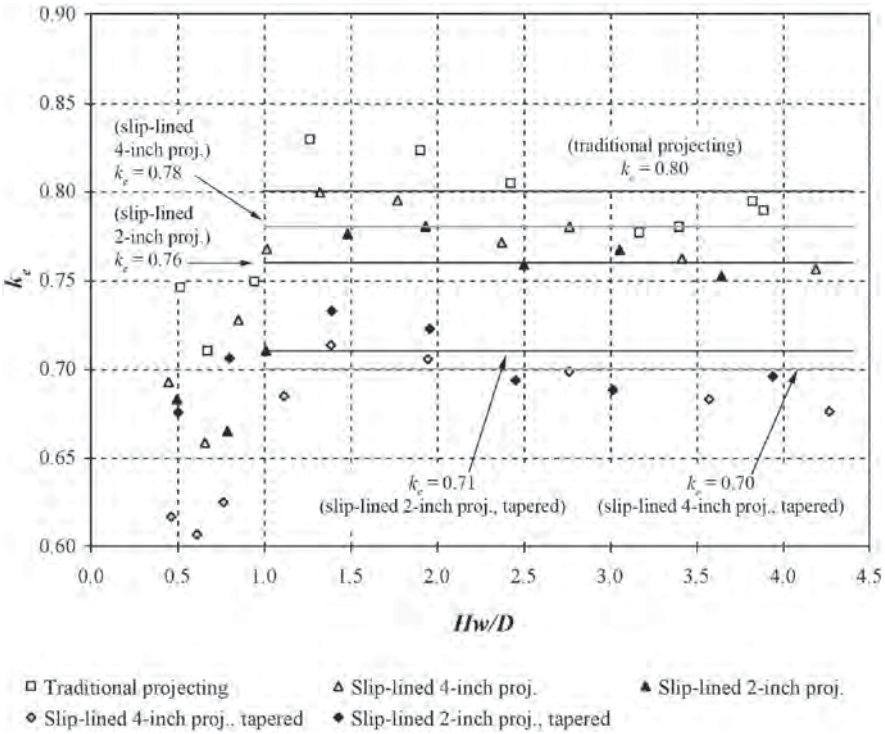

Figure 3-6. Slip-lined culvert entrance loss coefficients.

Table 3-1. Slip-lined culvert entrance loss coefficients.

Test culvert inlet end treatment	Unsubmerged	Submerged		
	k_e	mean k_e	Hw/D	± extreme deviation from mean
Traditional projecting	see Figure 3-6	0.80	>1.0	± 3.7%
Slip-lined, 2-in. projecting	see Figure 3-6	0.76	>1.0	± 2.6%
Slip-lined, 4-in. projecting	see Figure 3-6	0.78	>1.0	± 3.0%
Slip-lined, 2-in. projecting, tapered	see Figure 3-6	0.71	>1.0	± 3.2%
Slip-lined, 2-in. projecting, tapered	see Figure 3-6	0.70	>1.0	± 3.4%

it was discovered that at $Hw/D > 1.0$, k_e tends to decrease in value with increasing Hw/D until the coefficient eventually levels off to a constant value. This trend may be a phenomenon associated with the projecting end treatment. For Hw/D values less than 1.0, the entrance loss coefficients varied significantly with headwater elevation.

The average k_e for the traditional thin-wall projecting end treatment (without slip-lining) was 0.80 (see Figure 3-6), which is consistent with values reported by Tullis (1989). In comparison, the slip-lined end treatments were only slightly more efficient hydraulically. The slight increase in efficiency is due to the suppression of flow contraction at the inlet, especially in the case of the projecting end treatment with tapered grout. Also, it can be noted that, relative to the two projecting distances tested [2 in. (0.17D) and 4 in. (0.34D)], the projecting distance of the slip liner from the existing culvert had little influence on k_e. For example, k_e equals 0.71 for the tapered mortar end treatment projecting 2 in.; k_e equals 0.70 for the tapered mortar end treatment projecting 4 in. The thin-wall projecting inlet slip-liner condition (no tapered mortar) yielded an average k_e of 0.77, which was only slightly more efficient than the traditional projecting inlet, suggesting that slip lining a culvert without tapering the grout has little effect on k_e. Table 3-1 summarizes the average slip-lined culvert k_e values obtained for each end treatment tested. The average experimental uncertainty associated with the slip-lined culvert data was 1.5%.

Inlet Control

Inlet control head-discharge relationships were created for unsubmerged and submerged inlet conditions (i.e., $0.3 < Hw/D < 4.0$) for each of the four end treatments. Figure 3-7 presents inlet control data for each slip-lined culvert end treatment plotted as a function of the Form 2 quasi-dimensionless relationship.

Under inlet control conditions, the traditional thin-wall projecting end treatment and the slip-lined projecting end treatment [2 in. (0.17D) and 4 in. (0.3D)] produced nearly identical results at the same flow rates. The slip-lined projecting with taper end treatment did, however, exhibit an increase in efficiency compared to the traditional thin-wall projecting end treatment due to the reduction of flow contraction. A regression of the inlet control data was performed to produce design coefficients for use in Equations 1-2 through 1-4; the results are presented in Table 3-2.

Tabular support data for the Chapter 3 experimental results are included in Appendices C and D.

3.6 Conclusions

Based on the experimental determination of entrance loss coefficients and inlet control head-discharge relationships for slip-lined culverts, the following conclusions were made:

1. Relative to the two projecting distances tested [2 in. (.017D) and 4 in. (0.34D)] for slip-lined culverts, there are no significant effects associated with the inlet hydraulics of the culvert unless the grout is tapered down from the existing culvert inlet to the inlet of the projecting slip liner. The increase in inlet efficiency that is observed over the range of tapered projections tested is due to the reduction of flow contraction at the inlet. The fact that the inlet hydraulics of the liner were independent of the projecting distance from the host culvert is not necessarily a general conclusion. As the projection distance increases, k_e should approach the value of the traditional projecting inlet k_e value (~0.8). There was approximately a 2.5% difference in k_e between the slip-lined 2- and 4-in. thin-wall projecting end treatments.
2. For the tapered projecting end treatment, the projection length and the corresponding angle of the taper at the pipe crown, which ranged from 34° to 53°, did not influence

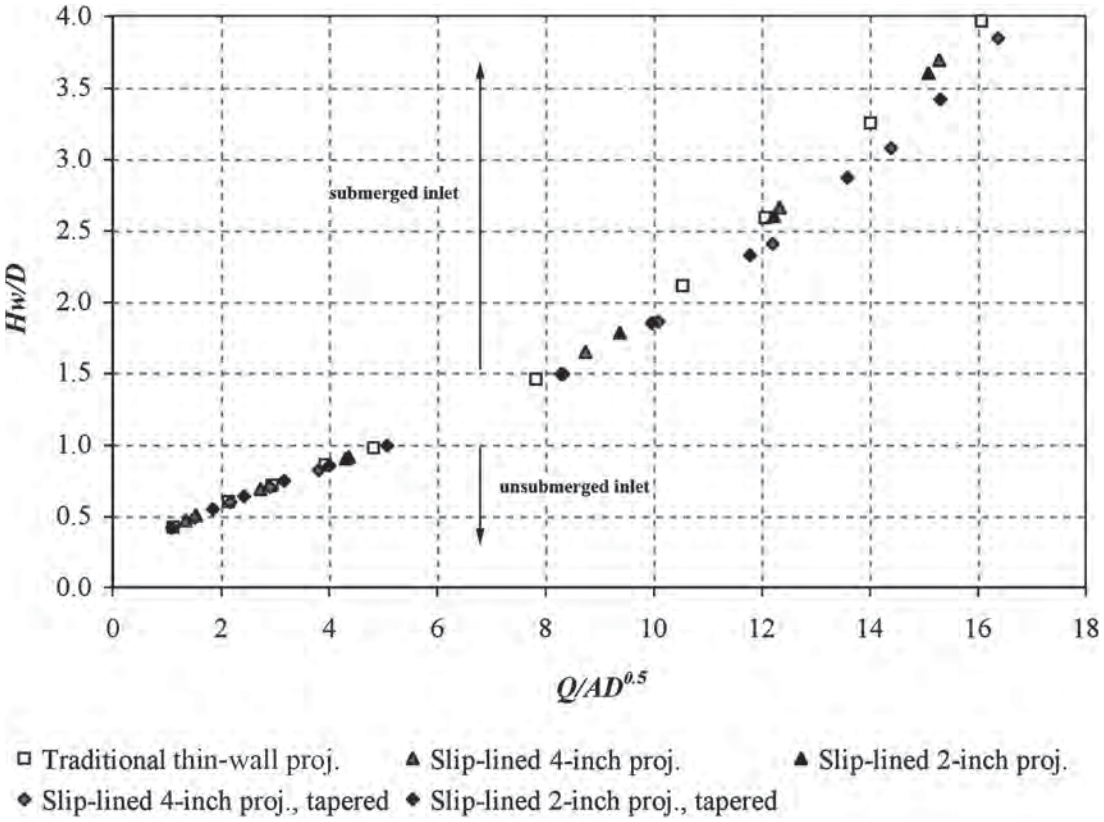

Figure 3-7. Traditional and slip-lined culvert inlet control quasi-dimensionless (Form 2) performance.

the degree of flow contraction significantly enough to increase the inlet efficiency under inlet control testing, or significantly affect k_e under outlet control testing.

3. The slip-lined projecting end treatment with tapered grout was more efficient than the slip-lined thin-wall projecting inlet. Under outlet control testing, the tapered projecting inlet produced values of k_e on average 9% lower than those for the slip-lined thin-wall projecting inlet, and 13% lower than the traditional thin-wall projecting inlet.
4. Under inlet control, there is no appreciable difference between the head-discharge relationships for the traditional thin-wall projecting inlet and the slip-lined thin-wall projecting inlet. When the inlet control data for the traditional thin-wall projecting inlet and the slip-lined

Table 3-2. Slip-lined culvert inlet control regression constants.

Test Culvert Inlet End Treatment	Unsubmerged				Submerged	
	Form 1		Form 2			
	K	*M*	*K*	*M*	*c*	*Y*
Traditional projecting	0.0946	0.60	0.5812	0.58	0.0513	0.69
Slip-lined, 2-in. projecting	0.0971	0.55	0.5830	0.57	0.0520	0.64
Slip-lined, 4-in. projecting	0.0945	0.54	0.5808	0.57	0.0520	0.66
Slip-lined, 2-in. projecting, tapered	0.0908	0.54	0.5772	0.57	0.0467	0.69
Slip-lined, 2-in. projecting, tapered	0.0841	0.52	0.5697	0.56	0.0473	0.65

thin-wall projecting inlet [2 in. (.017*D*) and 4 in. (0.34*D*)] are combined for regression analysis, an R^2 value of 0.999 is obtained for both the unsubmerged Form 2 data fit (Equation 1-3) and the submerged data fit (Equation 1-4).

5. For a long slip-lined culvert (outlet control), where the energy loss is dominated by friction, the hydraulic benefit gained by using a mortar-tapered projecting end treatment over a thin-wall projecting end treatment would likely be minimal. For shorter outlet control culverts or inlet control culverts, however, enhancing the inlet geometry may have a measurable influence on the hydraulic capacity of the culvert, and therefore tapering the grout is recommended. The durability of the tapered grout with respect to thermal expansion/contraction of liner pipe and/or freeze/thaw effects was not evaluated in this study.

Based on the research completed, the effects of slip lining on the inlet capacity of a projecting culvert are minimal when flowing under both outlet control and inlet control conditions. Although the inlet geometry may be improved to increase the inlet efficiency, more significant factors related to the hydraulic capacity of a slip-lined culvert are the diameter and hydraulic roughness of the slip liner.

CHAPTER 4

Culvert Exit Loss

4.1 Summary

The methodology for estimating culvert exit loss as presented in FHWA's *HDS-5* (Normann et al., 2001), which is based on conservation of energy principles, is reviewed and evaluated. An improved method that considers both conservation of energy and momentum principles is suggested, which is useful for culverts with channelized outlets for both submerged and unsubmerged outlet conditions. The expression utilized, although originally developed for sudden expansions in pressurized pipes, is shown through laboratory experiments to be valid for sudden-expansion (projecting) culvert outlets. A comparison of the experimental data to the traditional exit loss methods and the improved method is made. The derivation of the improved method is reviewed and a design example provided. For short culverts where friction or other energy loss components are relatively small, a more accurate prediction of exit energy loss may impact culvert design.

4.2 Introduction

FHWA's *HDS-5* (Normann et al., 2001) and the U.S. Army Corps of Engineers' *River Analysis System Hydraulic Reference Manual* (*HEC-RAS*) (Brunner, 2002) both recommend using the difference in culvert and downstream channel flow velocity heads to calculate culvert exit loss. The following is a paraphrase of the discussion in *HDS-5* regarding exit loss:

> Outlet control culvert flow capacity is calculated based on a conservation of energy approach. The total energy differential, or driving head required to pass a given flow rate through a culvert barrel, is equivalent to the summation of the total energy loss, comprised of entrance loss, friction loss through the barrel, exit loss, and any other minor losses that may be applicable to the particular installation. Exit loss is expressed as the change in velocity head at the outlet of the culvert barrel. For a culvert with a sudden expansion, the exit loss is

$$H_o = k_o\left(\frac{V_p^2 - V_{ch}^2}{2g}\right) \tag{4-1}$$

where H_o is exit loss expressed in units of length; V_p and V_{ch} are the pipe velocity and channel flow velocity downstream of the culvert exit, respectively; g is the gravitational acceleration constant; and the exit loss coefficient k_o is typically equal to 1.0. This equation may overestimate exit loss and a coefficient of less than 1.0 may be appropriate, according to the *Hydraulic Engineering Circular No. 14* (Thompson and Kilgore, 2006), referred to as *HEC-14* which provides empirically determined coefficients for five uniquely proportioned outlet geometries. The downstream channel velocity is often assumed to be small and is neglected, in which case the exit loss is equal to the velocity head in the barrel per Equation 4-2:

$$H_o = k_o\left(\frac{V_p^2}{2g}\right) \tag{4-2}$$

Equations 4-1 and 4-2 likely overestimate exit loss because they do not account for a conversion of a portion of the kinetic energy in the pipe to potential energy in the channel, a phenomenon observable in laboratory tests and likely in the field as well. In many cases, a small hydraulic jump with three-dimensional velocity components develops at the surface near the culvert exit, suggesting that momentum principles may also be important in describing exit loss. Experimental exit loss data collected as part of this study indicate that with k_o = 1.0, Equation 4-1 overestimates the actual exit loss by as much as 143% for the conditions tested. Neglecting the downstream channel velocity head in the exit loss calculation (Equation 4-2) and assuming k_o = 1.0 results in a larger overestimation of the exit loss, up to 187%.

The Borda-Carnot loss is an expression for head loss at sudden expansions in pressurized pipes, derived using both energy and momentum principles (Vennard, 1940). It is hypothesized that this expression may accurately characterize

head loss at culvert outlets with projecting, sudden expansions for pressurized and free-surface culvert flow and for submerged and unsubmerged outlet conditions.

4.3 Borda-Carnot Derivation

The derivation of the Borda-Carnot energy loss equation assumes steady, incompressible, turbulent flow with no change in elevation, no appreciable friction loss, and no external forces acting on the control volume besides hydrostatic pressure forces (Vennard, 1940). A control volume schematic to accompany the derivation is provided in Figure 4-1, with upstream and downstream locations labeled 1 and 2, respectively; Location 1 is at the culvert outlet and Location 2 is located in the discharge channel a short distance downstream. The projecting culvert boundary condition is not included in this derivation. The derivation stems from one-dimensional momentum and one-dimensional energy equations.

Momentum

Assuming the flow area at Location 1 to be the cross-sectional flow area of the culvert exit (A_1) and the hydrostatic pressure at Location 1 to be acting on the channel cross-sectional flow area (A_2), the one-dimensional momentum equation, relative to the primary flow direction (x), can be expressed as

$$\sum F_x = P_1A_2 - P_2A_2 = \rho V_2\left(V_2A_2\right) - \rho V_1\left(V_1A_1\right) \tag{4-3}$$

where P is the hydrostatic pressure, A is the cross-sectional flow area, ρ is the fluid density, V is the mean flow velocity, and the subscripts 1 and 2 correspond to the upstream and downstream boundaries of the control volume, as illustrated in Figure 4-1. Substituting γ/g (fluid specific weight/gravitational acceleration constant) for ρ and V_2A_2 for V_1A_1 (continuity) and rearranging terms yields

$$\frac{P_1 - P_2}{\gamma} = \frac{V_2^2 - V_1V_2}{g} \tag{4-4}$$

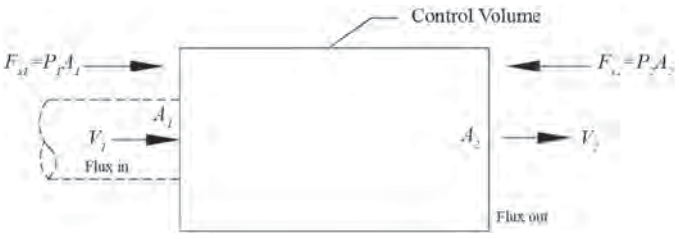

Figure 4-1. Control volume for momentum and energy analysis.

Energy

Along the centerline of the control volume between Locations 1 and 2 in Figure 4-1, the applicable terms from the one-dimensional Bernoulli Energy Equation are presented in Equation 4-5:

$$\frac{V_1^2}{2g} + \frac{P_1}{\gamma} = \frac{V_2^2}{2g} + \frac{P_2}{\gamma} + H_o \tag{4-5}$$

Isolating the $(P_1 - P_2)/\gamma$ terms in Equation 4-5 and substituting this expression into Equation 4-4 yields the following relationship:

$$H_o = \frac{\left(V_1 - V_2\right)^2}{2g} \tag{4-6}$$

Designating V_1 as the pipe velocity (V_p) and V_2 as the downstream channel flow velocity (V_{ch}) and adding the loss coefficient k_o yields the following equation, referred to here as the Borda-Carnot loss for sudden expansions:

$$H_o = k_o\frac{\left(V_p - V_{ch}\right)^2}{2g} \tag{4-7}$$

Note that the numerator in Equation 4-7 is the square of the velocity difference, whereas the numerator in Equation 4-1 is the difference in the squared velocities. Assuming $k_o = 1.0$ in Equation 4-7 and replacing V_{ch} with V_pA_p/A_{ch} (continuity) results in the following alternate form of the Borda-Carnot loss expression, as presented by Streeter and Wylie (1979):

$$H_o = k_o\frac{V_p^2}{2g}, \quad \text{where} \quad k_o = \left(1 - \frac{A_p}{A_{ch}}\right)^2 \tag{4-8}$$

Equations 4-2 and 4-8 are identical with the exception of the way k_o is defined. Equation 4-8 suggests that based on energy and momentum considerations, the exit loss is proportional to the pipe velocity head, with a k_o that varies with flow conditions. Although this expression is not new, its application to culvert exit loss is new.

Montes (1998) compared the experimentally determined open channel flow sudden-expansion exit loss results reported by Hinds (1928) and Mathaei and Lewin (1932) to values predicted by Equation 4-3. Mathaei and Lewin (1932) reported a Borda-Carnot loss coefficient (k_o) of approximately 1.0. This result is consistent with pressurized pipe applications. Hinds (1928) and Formica (1955) reported k_o values closer to 0.8.

The objective of this study was to experimentally determine the exit loss for a variety of culvert sizes and flow conditions, including pressurized culvert flow and free-surface culvert flow for submerged and unsubmerged outlet conditions. The test culvert sizes ranged from 12 to 60 in. in diameter. All culvert exit loss tests were conducted in a laboratory flume as

(12-inch diameter pipe exit loss test) (60-inch diameter pipe exit loss test)

Figure 4-2. Overview photos of exit loss testing.

shown in Figure 4-2. By varying the culvert size, the influence of the culvert-to-downstream channel flow area ratio on the exit loss was evaluated at the projecting, sudden-expansion outlet. The experimental exit loss data were compared with the predicted results from the two exit loss expressions from *HDS-5* (Equations 4-1 and 4-2) and the Borda-Carnot loss expression (Equations 4-7 and 4-8).

4.4 Experimental Results

Five exit loss experiments were conducted featuring four different circular pipe sizes ranging from 2 to 60 in. in diameter. Three of the five tests featured free-surface flow in the pipe and an unsubmerged outlet. The other two test conditions featured pressurized pipe flow and a submerged outlet. Each culvert or pipe was installed in a flume that was 8 ft wide by 6 ft deep by 500 ft long with a rectangular cross-section. Each test pipe length was a minimum of 10 pipe diameters from the upstream laboratory supply pipe to the pipe exit. The test pipe diameters, the pipe diameter-to-exit-channel-width ratio, and the tailwater conditions are summarized in Table 4-1. The specific range of test pipe sizes was selected to provide a wide range of expansion ratios (A_p/A_{ch}), approximately 0.02 to 0.39.

Due to momentum effects under free discharge conditions, the tailwater elevation was higher than the water level in the pipe. As a result, each test pipe was chained to the flume floor to keep the pipe from floating due to buoyant forces. Due to the magnitude of the buoyant forces, however, no submerged outlet tests were conducted with the two largest test pipe sizes, as the pipes could not be kept from floating. The 24-in. diameter pipe was the only pipe tested under both pressurized and free-surface flow conditions.

Water was supplied to the test pipes via a 20-in. diameter supply line instrumented with a calibrated ASME flow tube, traceable to the National Institute of Standards and Technology (NIST) by weight, for flow rate quantification. A sluice gate near the downstream end of the channel was used to control tailwater elevation, ensuring outlet flow control in the test pipe. All test pipes were installed with a slope of zero (horizontal). All pipes had projecting ends, some of which were flanged (standard 150-lb flanges). No improved end treatments were tested. Figure 4-2 shows photos of two exit loss tests, and Figure 4-3 shows a schematic overview of the test setup.

The total energy in the pipe was determined two diameters upstream of the outlet in order to ensure hydrostatic pressure conditions at the measurement point. The total energy in the pipe was determined as follows: a pressure tap, installed

Table 4-1. Exit loss test configurations.

Test	Nominal pipe diameter	Actual pipe inside diameter	Pipe diameter over channel width	Tailwater condition at pipe exit
12-S	12 in.	12 in.	0.17	Submerged
24-S	24 in.	23.25 in.	0.32	Submerged
24-U	24 in.	23.25 in.	0.32	Unsubmerged
48-U	48 in.	47.25 in.	0.66	Unsubmerged
60-U	60 in.	59.25 in.	0.82	Unsubmerged

in the invert of each test pipe approximately two pipe diameters upstream of the outlet, was connected to a stilling well for measuring piezometric head at the outlet. The velocity head at the measurement location was calculated based on the calculated flow depth, calculated flow rate, and flow cross-sectional area and added to the piezometric head to get total energy values. The total energy at the pipe outlet was determined by subtracting the amount of energy lost due to friction between the pressure tap in the pipe and the pipe outlet. The friction loss was estimated using the Darcy-Weisbach Equation and friction factors as determined by the Swamee-Jain Equation (Crowe et al., 2001) using a pipe wall roughness, k_s, of 0.00016 ft (steel pipe).

Surveying equipment was used to determine the channel invert profile and pipe invert elevation at the outlet. The total energy was determined in the channel (downstream of the jet expansion) at 50-ft intervals using the piezometric head measured using stilling wells connected through the channel sidewall and the calculated velocity head at each location.

The energy differential between the pipe and channel flows at the outlet represents the exit loss. It was not possible to determine a representative one-dimensional total energy value in the channel at the outlet based on direct measurements due to the turbulent, three-dimensional flow characteristics at the outlet. A representative total energy value in the channel at the outlet was determined by projecting the total energy grade line, as determined by the downstream channel measurement location, back to the pipe outlet. This total energy value represents a theoretical water surface (with its corresponding average velocity and velocity head) consistent with a one-dimensional energy assumption. The channel friction factor for each run was determined using the Darcy-Weisbach Equation and the total energy data from the downstream channel measurement locations.

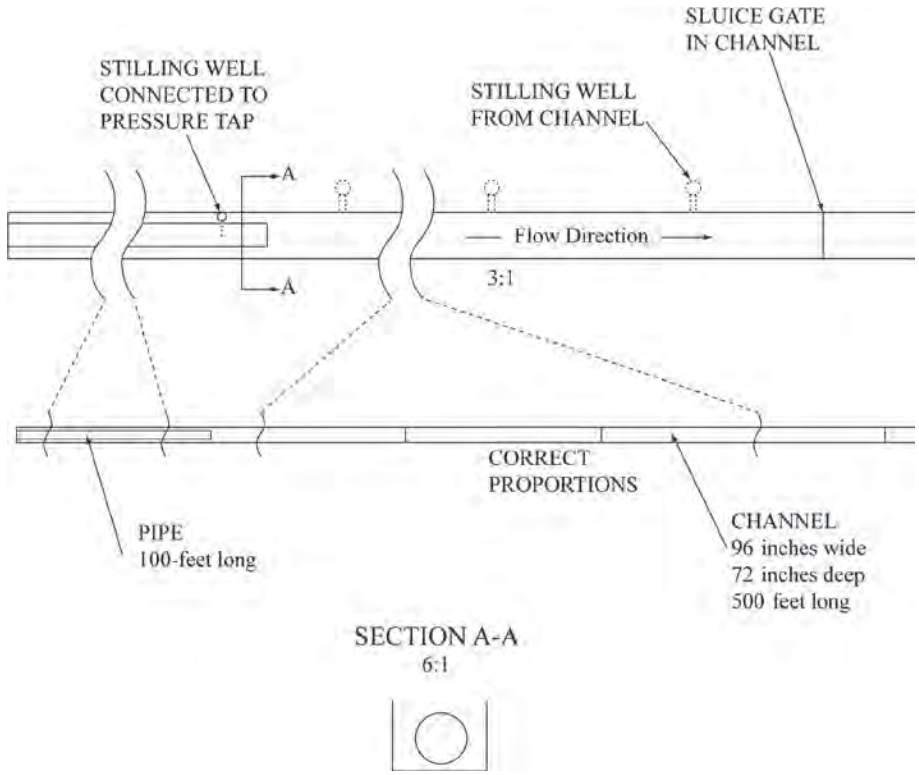

Figure 4-3. Plan view schematic of exit loss test setup.

Table 4-2. Experimental data from exit loss tests.

Run	Q [cfs]	Pipe Re	Pipe Fr	Δz [ft]	% Full-Pipe [%]	Tw/D	A_p/A_{ch}	H_o [ft]
12-S	7.06	722,450	–	2.51	100	1.99	0.0218	1.18
24-S	16.24	651,033	–	2.13	100	1.26	0.0808	0.420
24-U	13.07	827,299	0.97	2.13	69	0.75	0.0757	0.469
48-U	34.96	1,304,322	0.72	1.18	53	0.57	0.2413	0.259
60-U	62.15	2,104,402	0.52	0.728	64	0.68	0.3920	0.131

Table 4-2 summarizes exit losses observed and other information pertinent to the aforementioned experiments. Run numbers consist of the nominal pipe diameter in inches and a one-letter indicator of the outlet submergence condition: "U" for unsubmerged and "S" for submerged. The "Pipe *Re*" column contains pipe flow Reynolds number values, where four times the hydraulic radius was used to represent the characteristic length. The "Pipe *Fr*" column contains pipe flow Froude number values for the free-surface flow tests. All tests were conducted under outlet control as indicated by either a full-pipe or subcritical flow condition ($Fr < 1.0$). The "Δz" column contains the height of each pipe's invert above the channel invert. The "% Full pipe" column is the pipe flow depth divided by the inside pipe diameter and multiplied by 100. The pipe outlet submergence parameter, Tw/D, was calculated by dividing the channel tailwater depth (Tw), measured relative to the pipe exit invert, by the pipe inside diameter (D). The flow area expansion term, A_p/A_{ch}, is the ratio of the pipe and channel flow cross-sectional areas.

The exit loss coefficients corresponding to Equations 4-1, 4-2, 4-7, and 4-8 were calculated with H_o equal to the experimentally determined exit loss. The calculated k_o values corresponding to each predictive method are presented for each run in the "k_o Exp." columns in Table 4-3. The corresponding theoretical exit loss coefficient values, equal to 1.0 for Equations 4-1, 4-2, and 4-7 or calculated using Equations 4-7 and 4-8, are given in the "k_o Theor." columns. A comparison of the experimental and theoretical coefficient values for each method is also presented in Table 4-3 in terms of percent error. Dividing the difference between the experimental and theoretical coefficient values by the experimental value and multiplying the result by 100 determined the percent error reported in the "Error" columns.

General inspection of Table 4-3 reveals that discrepancies between experimental and theoretical coefficient values are significantly lower for the Borda-Carnot method (Equations 4-7 and 4-8) than the more traditional exit loss methods (Equations 4-1 and 4-2). The error percentages reported for Equations 4-7 and 4-8 are identical because they are different algebraic forms of the same expression. Because Equations 4-2 and 4-8 only differ by the theoretical discharge coefficient definition, the experimental coefficient values reported for Equations 4-2 and 4-8 are identical. According to a sensitivity analysis, the experimental uncertainty was approximately ±2.0%, which is consistent with the percent variation between the experimental and theoretical exit loss coefficients associated with the Borda-Carnot loss expression (Equations 4-7 and 4-8) in Table 4-3. The disparity between the experimental and theoretical exit loss coefficients for the more traditional methods (Equations 4-1 and 4-2) is larger than can be explained based solely on experimental uncertainty. Accordingly, the Borda-Carnot loss expression (Equations 4-7 and 4-8), applied to culvert exit loss at a projecting sudden expansion such as a projecting outlet, is significantly more accurate than the more traditional energy-based methods (Equations 4-1 and 4-2) when the theoretical discharge coefficients are used.

Table 4-3. Experimental and theoretical exit loss coefficient comparison.

	$H_o = k_o\left(\frac{V_p^2 - V_{ch}^2}{2g}\right)$			$H_o = k_o\left(\frac{V_p^2}{2g}\right)$			$H_o = k_o\left(\frac{V_p - V_{ch}}{2g}\right)^2$			$H_o = k_o\left(\frac{V_p^2}{2g}\right)$, $k_o = \left(1 - \frac{A_p}{A_{ch}}\right)^2$		
	Equation 4-1			Equation 4-2			Equation 4-7			Equation 4-8		
Run	K_o Exp.	K_o Theor.	Error [%]	K_o Exp.	K_o Theor.	Error [%]	K_o Exp.	K_o Theor.	Error [%]	K_o Exp.	K_o Theor.	Error [%]
12-S	0.93	1.0	7.3	0.93	1.0	7.3	0.97	1.0	2.7	0.93	0.96	2.7
24-S	0.88	1.0	13.9	0.87	1.0	14.6	1.03	1.0	3.1	0.87	0.85	3.1
24-U	0.84	1.0	18.9	0.84	1.0	19.6	0.98	1.0	2.2	0.84	0.85	2.2
48-U	0.63	1.0	60.0	0.60	1.0	69.9	1.02	1.0	2.2	0.60	0.58	2.2
60-U	0.41	1.0	143.1	0.35	1.0	187.3	0.94	1.0	6.2	0.35	0.37	6.2

4.5 Example of Application

The relative impact of using the Borda-Carnot approach (Equations 4-7 and 4-8) instead of the traditional methods (Equations 4-1 and 4-2) is illustrated by the following sample calculation. An 80-ft long, 48-in. diameter, circular corrugated metal culvert is installed under a road prism on grade in a trapezoidal channel 4 ft wide at the base, with a side slope of 0.5 horizontal to 1.0 vertical ($m = 0.5$) and a bed or channel slope (S_o) of 0.0008. The culvert has a square-edged inlet with a vertical headwall and a projecting outlet. The channel has a Mannings n value of 0.025. The design discharge is 90 cfs. The upstream depth is to be calculated in order to design a road prism of sufficient height to prevent overtopping.

The normal depth of 4.98 ft in the channel is calculated using Manning's Equation:

$$V = \frac{1}{n} R_h^{2/3} S_e^{1/2} \tag{4-9}$$

where n is the hydraulic roughness coefficient (Mannings n), R_h is the hydraulic radius (flow area divided by the wetted perimeter) at normal depth, and S_e is the slope of the total energy grade line, which equals the channel slope (S_o) at normal depth conditions. The Froude number, corresponding to normal depth, is 0.26 as calculated by Equation 4-10:

$$Fr = \frac{Q}{\sqrt{g \frac{A_c^3}{T}}} \tag{4-10}$$

In Equation 4-10, T is the width of the water surface in the channel perpendicular to the primary flow direction. A Froude number less than 1.0 indicates subcritical flow. Assuming no downstream tailwater control other than channel friction, the tailwater will be equal to the normal depth at the culvert outlet. As the normal depth is greater than the culvert rise (culvert diameter), the culvert will likely be flowing full (in the absence of any air vents) with both the inlet and outlet submerged (outlet control). Assuming an entrance loss coefficient, k_e, of 0.5 (square-edged inlet with headwall, Normann et al., 2001), a Mannings n of 0.02 for the culvert, and using the Borda-Carnot expression (Equation 4-8) to describe exit loss, the upstream flow depth is 6.43 ft. Using Equation 4-2 with $k_o = 1.0$, as suggested in *HDS-5,* results in an upstream depth of 6.93 ft, which exceeds the previously obtained value by 7.8% or 6 in. Although this exact difference is unique to these design parameters, it shows that improved accuracy in exit loss quantification can impact design.

It should be noted that these sample calculations are solely to illustrate application of the expressions recommended for adoption, and they do not demonstrate the complete design process as the scenario is evaluated under only one flow control regime. For a detailed treatment of the design process, see *HDS-5* (Normann et al., 2001).

4.6 Conclusions

Although originally developed for sudden expansions in pressurized pipes, the Borda-Carnot loss expression can be used to more accurately express energy losses at projecting sudden-expansion culvert outlets (and likely non-projecting sudden-expansion outlets), relative to energy-based traditional methods such as those described in *HDS-5HEC-14.* Exit loss is more accurately described by multiplying the pipe or culvert velocity head by an exit loss coefficient, k_o, defined as $k_o = (1 - A_p/A_{ch})^2$ (Equation 4-8) than by the traditional exit loss coefficient, defined as $k_o = 1.0$. This approach to exit loss quantification correlated well with laboratory tests for both pressurized and free-surface pipe flow for sudden-expansion projecting outlets, submerged or unsubmerged, where the downstream channel flow is supplied solely by the culvert discharge. The theoretical exit loss coefficient for traditional methods varied from the corresponding experimental exit loss coefficient by as much as 187%, while the same comparison for the Borda-Carnot loss expression had a maximum variation of 6.2%, with most data being better than approximately 3%. This improvement in accuracy may be particularly significant for culvert design where the culvert span is similar to the channel width, such as driveway cross drains along highly channelized ditches and fish passage culverts, which often have spans just larger than the bank-full channel width.

The results of this study show that when appropriately applied, the exit loss approach recommended in *HDS-5* is conservative in that it overestimates exit loss at outlets with channelized discharge channels. The degree of overestimation is relatively large in some cases. Future exit loss research should include additional tests with submerged outlets and channelized downstream flow; the number of submerged outlet test conditions was limited by the size of the test channel, pipe sizes, and buoyant forces, which caused the test pipe to float under submerged conditions. As the derivation of the Borda-Carnot expression is independent of pipe geometry, investigation of its applicability to other culvert shapes, such as buried-invert culverts and box culverts, might not be necessary; however, it may be valuable to evaluate this expression for culvert outlets with end treatments other than the projecting sudden-expansion outlet evaluated in this study.

CHAPTER 5

Inlet Control Hydraulics of Multiple Circular Culverts

5.1 Summary

In general, multibarrel culvert design is based on the assumption that the head-discharge relationships for the individual culvert barrels in a multibarrel culvert assembly are independent of the other culvert barrels and that the multibarrel culvert head-discharge relationship may be developed by multiplying the single culvert discharge by the number of barrels (assuming all culvert barrels are the same size, geometry, and material type and are installed at the same elevation and slope). This study evaluated that assumption for a variety of multibarrel culvert configurations (i.e., two- and three-culvert assemblies with various culvert spacings) and approach flow conditions. Single-barrel culvert performance data were also collected for comparison.

The results of the two-barrel multibarrel culvert tests showed that average individual-barrel flow rate for the multibarrel culvert (total flow rate divided by the number of barrels) was essentially the same as the single-barrel culvert performance for the same headwater and approach flow conditions. The three-barrel test results were similar with respect to matching the single-barrel performance except for tests where the approach flow was non-uniform. The average individual-barrel flow rate for the non-uniform inlet invert configuration was still within 3% of the single-barrel performance. For the non-uniform approach modeled, the single-barrel model accurately predicts the average barrel flow rate over most of the unsubmerged inlet range. For the near- and full-submergence inlet conditions, the non-uniform-approach three-barrel (uniform inlet invert elevation) condition produced an average barrel discharge 10% less than the single-barrel discharge. While the average individual-barrel flow rate in the multibarrel culvert assemblies correlated well with the single-barrel data, the measured individual-barrel flow rates varied by as much as ±7% of the flow predicted by the single-barrel model, a circumstance that may warrant consideration when considering fish passage and/or scour protection at the outlet.

5.2 Introduction

Culverts are the primary means for transporting water through road embankments, and the FHWA and others have published a significant amount of culvert design data. One of the most widely used culvert design documents is FHWA's *HDS-5* (Normann et al., 2001). This manual is based primarily on a number of tests conducted by John L. French (1955, 1956, 1957, 1961, 1966a, 1966b, 1967) for the National Bureau of Standards (now the National Institute of Standards and Technology, NIST) under the sponsorship of the Bureau of Public Roads (now FHWA). Several researchers before and after have both verified and expanded the dataset.

In the many years since French's work (French, 1955, 1956, 1957, 1961, 1966a, 1966b, 1967), most public agencies have designed culverts and multibarrel culverts according to *HDS-5.* While *HDS-5* was primarily developed for single-barrel culverts, designers have used the same procedures to design multibarrel culverts, treating each barrel in the multibarrel culvert assembly as a single, independent culvert and summing the individual flow capacities (superposition).

Multibarrel culverts are commonly used (instead of a single, larger culvert design) for wide, shallow channels or flood plains (relative to the road embankment height) and for channels where sediment transport and/or fish passage are a concern at low-flow conditions. Some common fish passage designs (Bates et al., 2003) exclude multibarrel culverts due to the general undersizing of the culvert relative to fish and habitat needs. To improve fish passage and sediment transport conditions through multibarrel culverts at low discharge conditions, one of the culvert barrels (typically the barrel nearest the center of the stream) is sometimes installed at a lower elevation than the other barrels, restricting low discharges to a single culvert barrel. Concentrating low discharges in a single culvert barrel increases flow depth, which aids fish passage, and flow velocity, which aids sediment transport.

Multibarrel culverts can be problematic in drainages that transport large debris elements (e.g., branches, trees, shopping carts, etc.) as the individual-barrel sizes may be too small to pass such debris during flood events. Some federal agencies, including the Federal Emergency Management Agency (FEMA), discourage the use of multibarrel culverts, perhaps in part because FEMA must deal with failed culverts that result primarily from extreme flow events that likely exceed the culvert design capacity. Mountainous states, such as Washington, highly discourage the use of multiple culverts because of potential debris problems.

An example of a multibarrel circular culvert is shown in Figure 5-1. The barrel spacings in Figure 5-1 are small enough that the amount of flow contraction experienced at the entrance of each barrel is likely influenced (reduced) by the presence of the adjacent barrels. As the amount of flow contraction at the culvert barrel inlet decreases, the flow capacity of the culvert should increase. This suggests that the performance of individual barrels in a multibarrel culvert assembly may vary relative to the performance of summed singe-barrel culverts.

A limited number of studies on circular, multibarrel culverts were found in the literature. Wargo and Weisman (2006) performed circular pipe tests comparing scour depths and culvert flow depths and their influence on fish passage. They speculated that backwater depths could potentially be less for multibarrel culverts than for single-barrel culverts, but their findings were not conclusive. Johnson and Brown (2000) tested multibarrel, circular culverts, but they focused mainly on stream impacts rather than head-discharge relationships.

Applying the *HDS-5* (Normann et al., 2001) single-barrel culvert data to multibarrel culvert design via superpositioning is likely to be a common practice (primarily due to a lack of other alternatives), but the accuracy of this approach has not been adequately verified. Jones et al. (2006) suggest that multibarrel box culverts behave similarly to single-barrel box culverts. Charbeneau et al. (2002, 2006) also reported similarities between single-barrel and multibarrel box-culvert performance data but suggest that *HDS-5* data (Normann et al., 2001) may over predict box-culvert spans by 17% for one design example. One limitation to the findings from these studies is that neither study reported directly measuring the individual-barrel flow rates.

Figure 5-1. Example of multibarrel culvert installation.

Based on their work with culverts on steep slopes, Korr and Clayton (1954) noted that the presence of intermittent vortices could cause the flow regime to fluctuate back and forth between open channel flow (inlet control) and full-pipe (outlet control), causing both the upstream head and discharge to fluctuate. French (1961) also noted these effects and artificially suppressed vortex activity for some laboratory tests. Blaisdell (1966) reported vortex-based flow regime instability for $1 < Hw/D < 3$. Similar flow regime fluctuations were noted in the current study.

French (1961) studied the effect of pipe wall thickness and determined that, for pipe wall thickness values less than 0.04D, flow contraction was initiated at and controlled by the outer edge of the culvert at the inlet; for wall thickness values greater than 0.04D, the inside edge was the control. The pipe used in the current study had a pipe wall thickness of 0.02D (8-in. PVC pipe).

5.3 Research Objectives

The objective of this study was to test the superposition-based multibarrel culvert design process by comparing single-barrel and multibarrel culvert hydraulic performance under various barrel layout and approach flow conditions. A culvert test facility was constructed at the Utah Water Research Laboratory (Utah State University), and inlet control culvert experimental data were collected for this purpose. The results of multibarrel culvert performance tests were compared with single-barrel experimental results as well as single-barrel data in *HDS-5* (Normann et al., 2001). Empirical coefficients are presented for use in the traditional inlet control head-discharge relationships presented in *HDS-5* (Equations 1-2 through 1-4). This research was limited to circular culverts operating under inlet control. All tests were conducted using square-edged, thin-wall, projecting, 8-in. PVC pipe.

In an effort to determine where multibarrel culverts are used in the United States, along with the extent to which designs featuring one culvert barrel installed lower than the other barrels are used, a survey of state departments of transportation (DOTs) was conducted with approximately half of the States responding. The survey results are shown in Table 5-1.

Table 5-1. State DOT multibarrel culvert use survey results (February 2007).

State	Multibarrel Culvert Use	Typical End Treatments	One Barrel w/ Lowered Invert
Alaska	circular & box	varies, headwall common	sometimes
Arkansas	circular & box	flared concrete section	typically not
California	circular & box	headwall/ flared end	not usually
Colorado	circular & box	headwall, no projecting	sometimes
Connecticut	not specified	headwall	yes (1 to 2 ft lower typical)
Georgia	circular & box	headwall w/ 45° wingwalls	not usually
Hawaii	circular	headwall w/ wingwalls	not usually
Idaho	circular	projecting	no
Indiana	uncommon	projecting if circular	–
Iowa	box normally	projecting common	no
Kentucky	circular	headwall	no, training wall used for low flows
Maine	circular (mostly) & box	projecting, mitered for D > 8 ft, few headwalls	yes (0.5 to 1.0 ft lower typical)
Maryland	circular typically	headwall, mitered, projecting	buried-invert (embedded) culverts typically used
Michigan	precast (box?)	–	yes (>1 lower typical)
Minnesota	circular & box	headwall	sometimes (box: 2 ft lower typical)
Missouri	box sometimes	–	yes (box: 1 ft lower typical)
Nebraska	circular & box (>20 ft)	headwalls for boxes	sometimes (box: 0.5 to 1 ft lower typical)
Nevada	yes	depends on situation	depends
New Mexico	yes	headwalls	not usually
North Dakota	pipes and box	headwall/flared	maybe about 1 ft lower.
Ohio	rarely used	–	–
South Carolina	pipes and box	Headwall	yes (1 ft lower typical)
Utah	circular & box	–	yes
Washington	no multibarrel culverts	–	–
Wyoming	?	Headwall and flared end sections	uncommon

5.4 Experimental Method

Test Facility

The culvert testing was conducted using a 24-ft-long by 22-ft-wide by 5-ft-deep reservoir head box (shown in Figure 5-2). Water was supplied through 4-, 8-, and 20-in. parallel supply lines with calibrated orifice plates in each line facilitating accurate flow measurement over a wide range of flow rates. The orifice plate calibrations are traceable to NIST by weight. The head box piezometer tap, used to determine *Hw,* was located in an area where the flow velocities were essentially zero, making the piezometric head equal to the total head. The head box pressure tap location is shown in Figure 5-2. Uniform approach flow into the reservoir and a relatively calm water surface were achieved by passing flow over a weir that spanned three sides of the reservoir.

Culvert Barrels

The test culverts were constructed of 8-in. diameter (I.D. = 7.8 in.) PVC pipe installed at a slope (S_o) of ~ 3% with square-edged, thin-wall, projecting end treatments. The parameters evaluated in this study that influence inlet

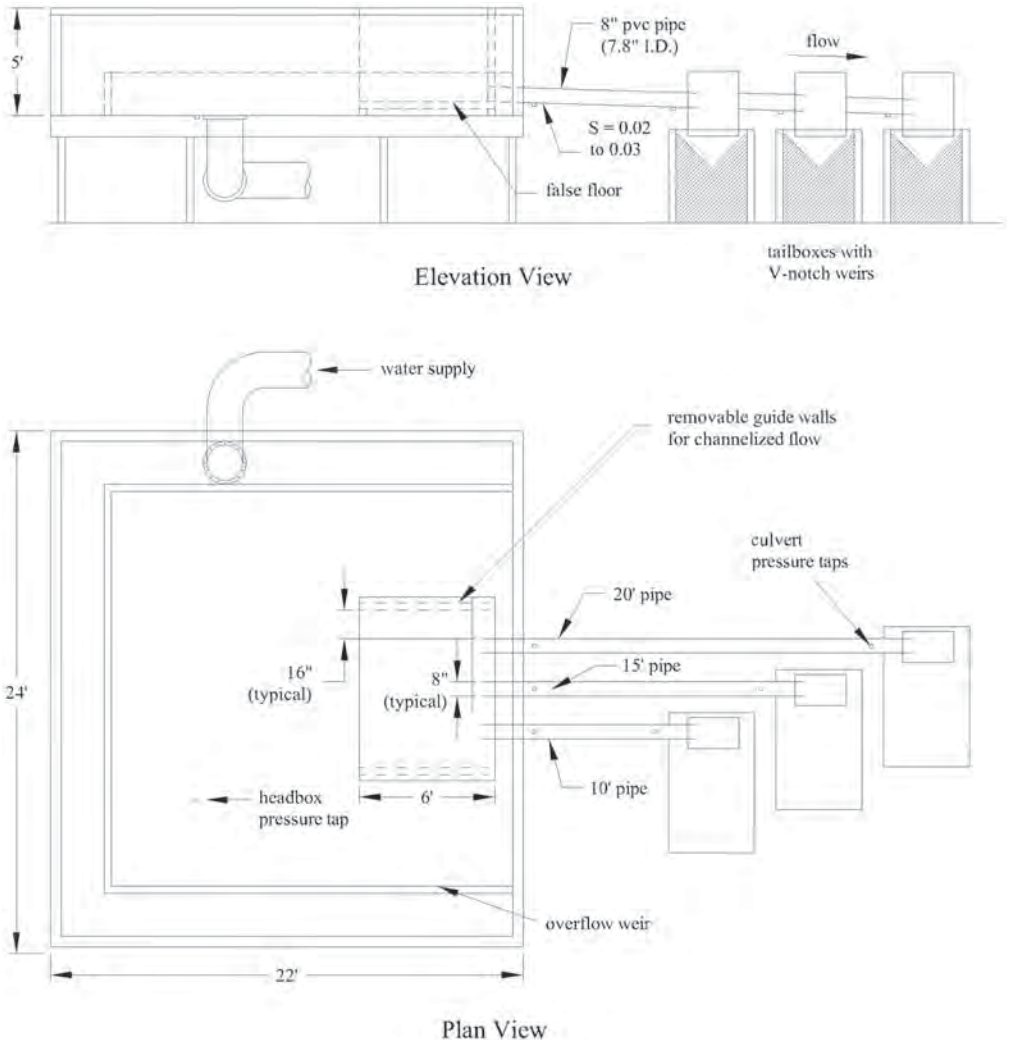

Figure 5-2. Overview of culvert testing facility.

control flow efficiency included the number of barrels (two or three), the barrel spacing (two or three barrel diameters), and the approach flow conditions. The barrel lengths were 10, 15, and 20 ft, as shown in Figure 5-2.

The projection distance of the barrels was typically 1.5 ft (2.25 pipe diameters) past the reservoir headwall, except for the skewed headwall configuration where the projection distance was about 0.5 ft (0.75 pipe diameters). Two pressure taps were installed in each culvert barrel invert approximately four pipe diameters downstream from the barrel inlet and upstream of the barrel outlet for determining culvert flow depth and velocity information at those locations. Barrel Froude numbers (Fr) were calculated to confirm supercritical flow and inlet control ($Fr > 1.0$). The inlet end of each culvert barrel rested on a false floor in the reservoir with the same slope as the culvert barrels (S_o). A uniform invert elevation was maintained for all barrels to ensure that each culvert barrel had a common Hw measurement reference. The barrels were supported at mid-span to minimize slope variations associated with culvert deflection. Longitudinal restraints were also used to keep the barrels in place.

The barrel inlet invert reference elevations were referenced on the piezometer as follows. A 4-in. diameter beaker, partially filled with water, was hydraulically connected to the piezometer tube via flexible tubing. The water surface in the beaker was placed at the same elevation as the barrel inlet and the piezometer reading noted. The 4-in. diameter beaker was used in an effort to minimize the surface tension effects in referencing the inlet invert elevation. Because all flow depth measurements determined using the piezometers were differential measurements (i.e., a reference piezometer reading was subtracted from the indicated piezometer reading), no correction for piezometer surface tension effects was required.

Outlet Structures

A primary objective of this study was to identify the variation in discharge between barrels in a multibarrel culvert assembly for various culvert configurations and approach flow conditions. To facilitate this objective, individual tail boxes were constructed for each culvert barrel. An elbow installed

Figure 5-3. V-notch weir/tail box assemblies.

on the downstream end of each culvert directed the flow into a drop structure, which was enclosed to contain splash and was vented to atmosphere. The water entered a tail box via a screen structure, which improved the flow uniformity. A calibrated-in-place V-notch weir was used to measure the discharge as it exited the tail box. Stilling wells hydraulically connected to the tail boxes were used to determine the water depth or head on each weir. An overview photo of the tail box/V-notch weir assemblies is shown in Figure 5-3.

The standard V-notch weir equation (Equation 5-1) was used for determining the discharge through each barrel/tail box assembly:

$$Q = \frac{8}{15}\sqrt{2g}C_d \tan\left(\frac{\theta}{2}\right)H^{2.5} \quad (5\text{-}1)$$

where

Q is the volumetric flow rate,
C_d is the discharge coefficient,
θ is the angle of the V-notch ($\theta = 90°$ in this study), and
H is the upstream flow depth measured relative to the invert of the V-notch.

The calibrated-in-place C_d values, which varied slightly with flow rate, correlated very well with published C_d values [e.g., 0.585 (Henderson, 1966)].

Data Collection

For each test condition, the following data were collected: flow rate into the head box (i.e., total multibarrel culvert flow rate), headwater depth, flow depth in each barrel (two locations), individual-barrel discharges, and any general observations such as vortex formation and persistence. Differential manometers were used in conjunction with the orifice flow meter to determine the flow rate into the head box. Piezometers were used to determine *Hw* and culvert barrel flow depths (y). The culvert invert elevation and invert of the barrels at the pressure tap locations reference elevations were identified on the appropriate piezometers to facilitate flow depth measurement. All tubing connected to pressure taps was thoroughly bled to expel air bubbles prior to collecting data.

In some cases, measuring the flow depth in the culvert is not entirely straightforward. Figure 5-4 shows the surface waves present inside the culvert for one test condition. When water surface fluctuations were present, a visual averaging of the piezometric reading on the piezometer was required. Water surface fluctuations were more prevalent for submerged inlet conditions.

Test Matrix

The various single-barrel and multibarrel culvert configurations tested are listed in Table 5-2. Culvert combinations

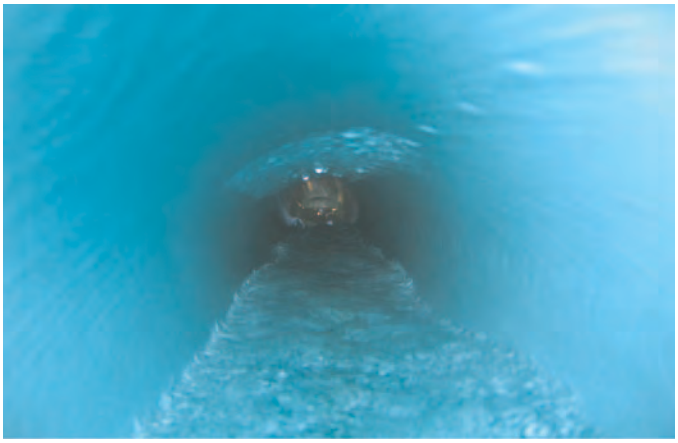

Figure 5-4. Example of surface waves inside the culvert.

Table 5-2. Single-barrel and multibarrel culvert test configurations.

Configuration No.	# of Culvert Barrels	Barrel Spacing Center-to-Center	Approach Flow Angle (degrees)	Upstream Channel Configuration	Depressed Culvert Invert Offset
1	1	–	0	Reservoir	0
2	2	1.5D	0	Reservoir	0
3	2	2D	0	Reservoir	0
4	2	3D	0	Reservoir	0
5	3	1.5D	0	Reservoir	0
6	3	2D	0	Reservoir	0
7	3	3D	0	Channeled	0
8	3	3D	40	Channeled	0
9	3	3D	0	Reservoir	0
10	3	3D	0	Non-uniform	0
11	1	2D	0	Trapezoid 2:1	0.5D
12	2	2D	0	Trapezoid 2:1	0.5D
13	3	2D	0	Trapezoid 2:1	0.5D
14	3	3D	0	Trapezoid 2:1	0.5D

tested included one, two, and three circular barrel culverts with various horizontal and vertical spacing distances and different approach conditions. A culvert barrel installed lower than the other barrels in a multibarrel culvert assembly is referred to in this study as a "depressed barrel" or "depressed culvert." For each test configuration shown in Table 5-2, data were collected for a range of flow rates and headwater values (submerged and unsubmerged inlet conditions). Sufficient time, sometimes up to 1 h, was allowed for each flow condition to reach steady state. Steady state conditions were confirmed by repeatedly measuring the *Hw* until changes were no longer observed. Test conditions were typically limited to $Hw/D < 3.5$.

Photographic overviews of the various barrel and approach flow configurations are shown in Figure 5-5 (A–H). Dimensional drawings of some of the test configurations are shown in Figures 5-6 (A–D). Removable end caps were used to seal the extra barrels during the one- and two-barrel test configurations. The influence of the non-flowing culverts on adjacent flowing culverts was assumed to be minimal.

5.5 Experimental Results

This section presents the experimental results for the single-barrel and multibarrel (two- and three-barrel) culvert tests. The single-barrel culvert data are used both as a baseline and to compare the performance of the individual barrels in the multibarrel assemblies. Observations of hydraulic phenomena that appeared to influence the culvert head-discharge relationships are also briefly discussed.

Figure 5-5(A). Two-barrel, 1.5D spacing with reservoir approach.

Figure 5-5(B). Three-barrel, 2D spacing with reservoir approach.

Figure 5-5(C). Three-barrel, 3D spacing with reservoir approach.

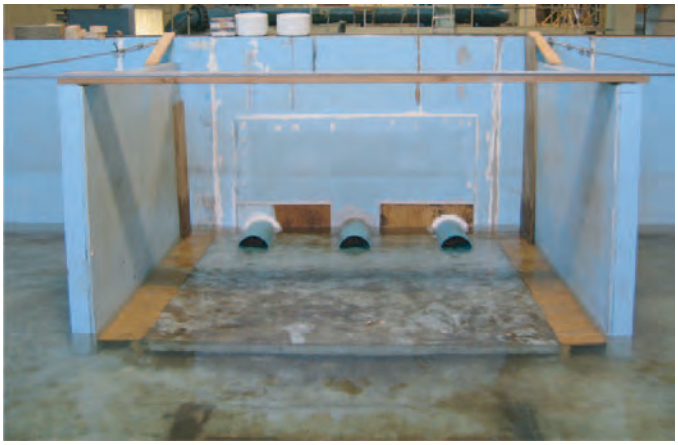

Figure 5-5(D). Three-barrel, 3D spacing with rectangular channel approach.

Figure 5-5(E). Three-barrel, skewed, 3D spacing with rectangular channel approach.

Figure 5-5(F). Three-barrel, 3D spacing with a non-uniform approach flow.

Figure 5-5(G). Three-barrel, 2D horizontal spacing, 0.5D depressed culvert with a trapezoidal channel approach.

Figure 5-5(H). Three-barrel, 3D horizontal spacing, 0.5D depressed culvert with a trapezoidal channel approach.

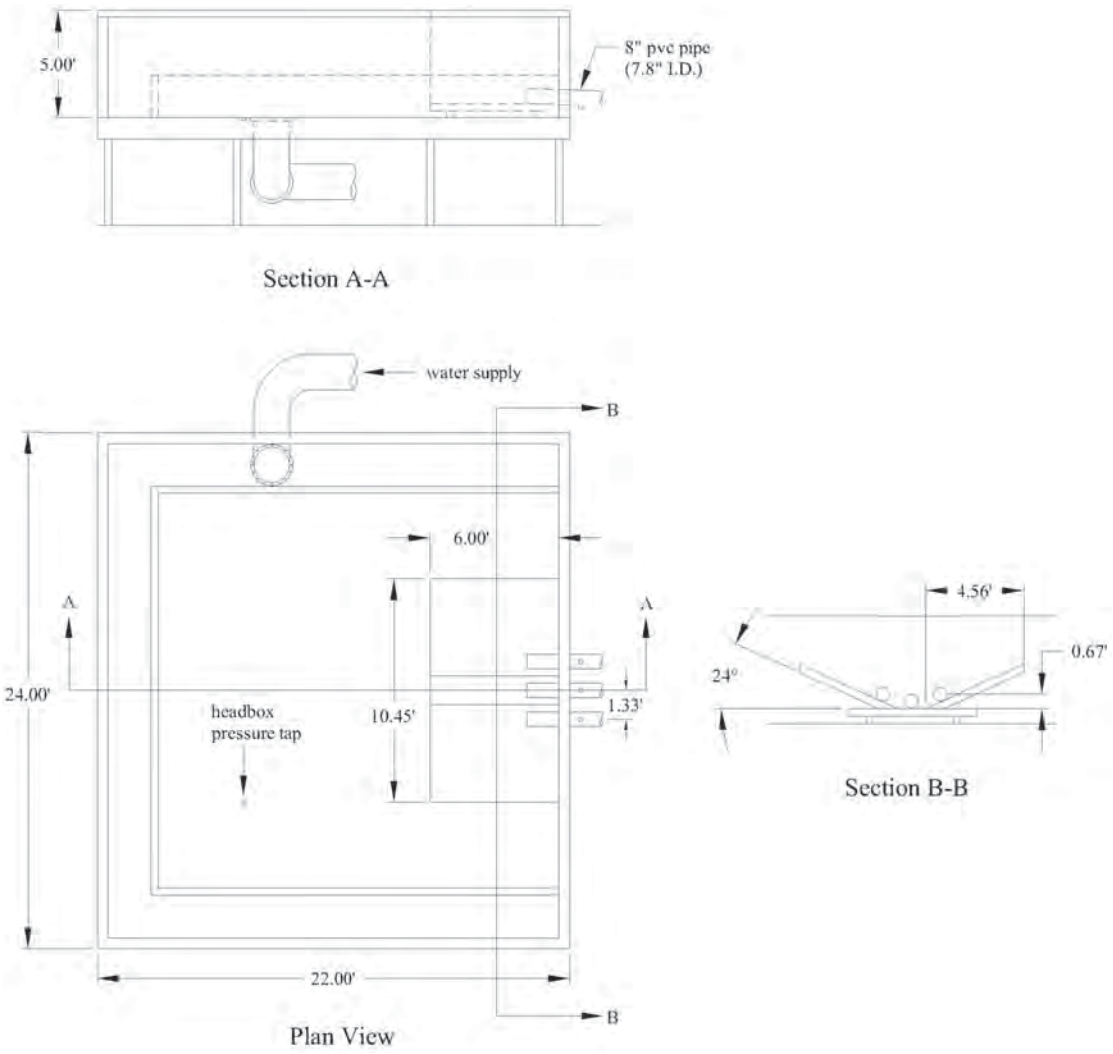

Figure 5-6(A). Multibarrel culvert configuration with 2D horizontal barrel spacing and a trapezoidal approach channel.

Observed Influences on Culvert Hydraulics

Vortex Activity

Water level fluctuations during "steady state" submerged inlet conditions were observed in the reservoir and V-notch weir head boxes and were tied to vortex activity at the culvert inlets. When aerated surface vortices or vortices that formed between barrel inlets (observed only with the 1.5D horizontal spacing culvert assemblies) were present, as shown in Figure 5-7, the culvert efficiencies reduced and the headwater depth increased. Once the vortices dissipated, the headwater depth decreased. The unsteady nature of vortex-induced reservoir level fluctuations was observable in the reservoir piezometer readings. Reservoir water levels were very stable for unsubmerged flow conditions and for the barrel inlets free of vortex activity. Previous studies (Blaisdell, 1966; French, 1955, 1956, 1957, 1961, 1966a, 1966b, 1967; Korr and Clayton, 1954; Schiller, 1956) have also reported that vortex activity played a role in the hydraulic efficiency of submerged inlet culvert hydraulics for ranges of *Hw/D* consistent with those evaluated in this study. In the present study, vortex activity was most noticeable for $1.0 < Hw/D < 3.0$ and for horizontal barrel spacings of 1.5D.

Inlet Flow Contraction

Figure 5-8 shows inlet flow conditions for the 1.5D horizontal culvert spacing (uniform inlet invert elevation) for an unsubmerged inlet and a nearly submerged inlet condition. Note the relatively large flow separation regions on the lateral side of the inlet for the outside barrels in the unsubmerged inlet condition; the flow separation regions for the center barrel are much less evident. The sizes of the separation regions for the transitional submergence case are similar in size but

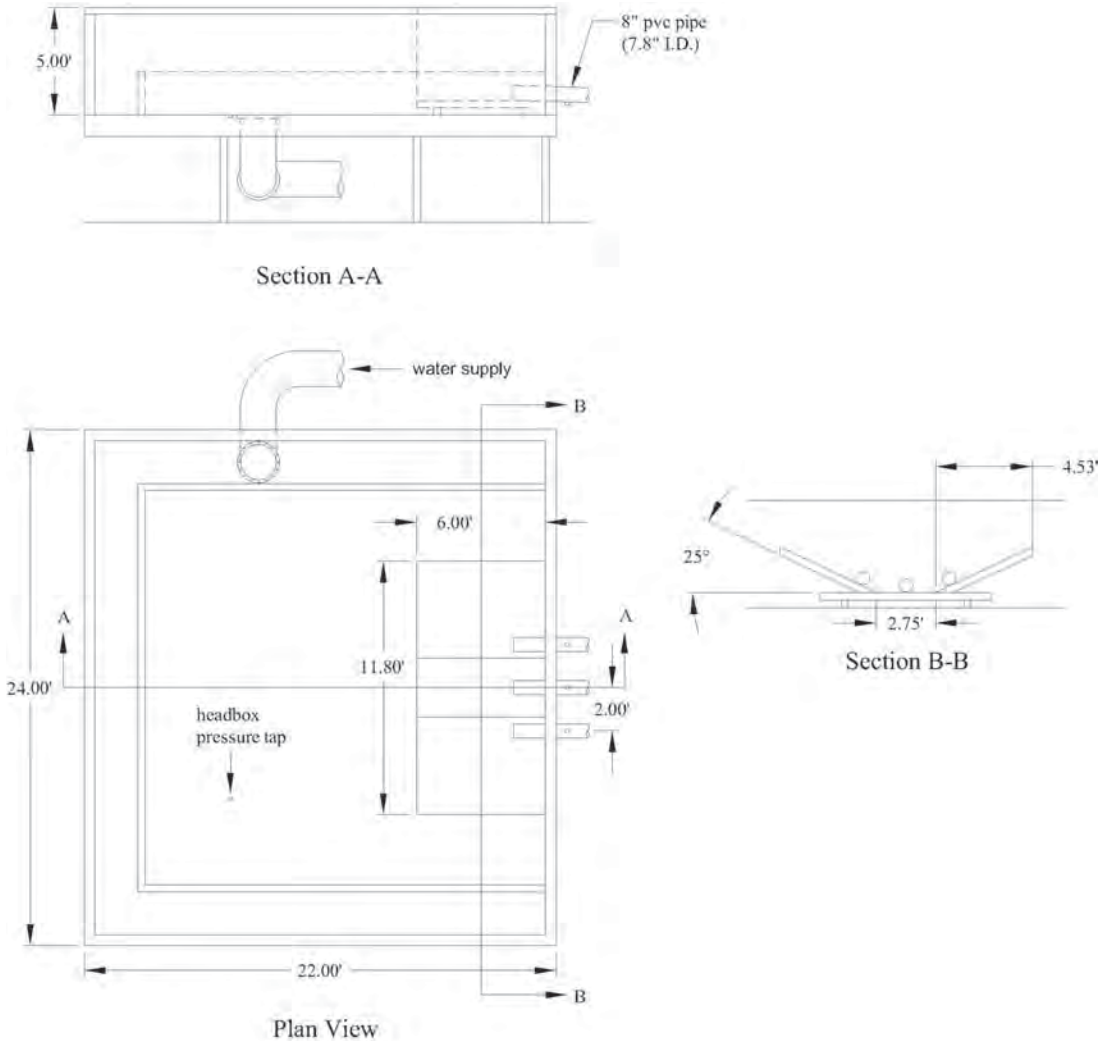

Figure 5-6(B). Multibarrel culvert configuration with 3D horizontal barrel spacing and a trapezoidal approach channel.

vary in location. Flow separation at multibarrel culvert inlets appears to be a contributing factor to the performance variations observed between single-barrel culvert and multibarrel culvert performance.

Single-Barrel Test Results

Figure 5-9 shows the experimental, quasi-dimensionless head-discharge data for a single-barrel PVC circular culvert with a thin-wall projecting end treatment and a reservoir approach. The single-barrel, thin-wall projecting, circular culvert data were collected for each barrel in the three-barrel 1.5D and 3D horizontal barrel spacing assemblies by placing sealed end caps on the inlets of the unused barrels. Figure 5-5(A) shows an example of a capped barrel inlet. The data for the six single-barrel test configurations are plotted as a single data set in Figure 5-9. The close agreement in the data in Figure 5-9 suggests that the geometry created by the presence of the capped barrels did not inhibit the single-barrel culvert flow performance. The "trend line" data represents the unsubmerged inlet control Form 2 (Equation 1-3) head-discharge relationship for $Hw/D < 1$ and the submerged inlet control head-discharge relationship (Equation 1-4) for $Hw/D > 1$ fit to the experimental data. Experimental and trend line data for a single-barrel PVC circular culvert with a trapezoidal approach channel are also presented in Figure 5-9. The single-barrel culvert with the channelized approach is slightly more efficient than the reservoir approach condition, likely due to a decrease in the inlet flow contraction. The corresponding *K, M, c,* and *Y* coefficients for the data in Figure 5-9 are presented in Table 5-3. The single-barrel data presented in Figure 5-9 were used as the baseline data for evaluating the individual-barrel performance of the multibarrel culvert test assemblies. Multibarrel culvert configurations with reservoir approach conditions were

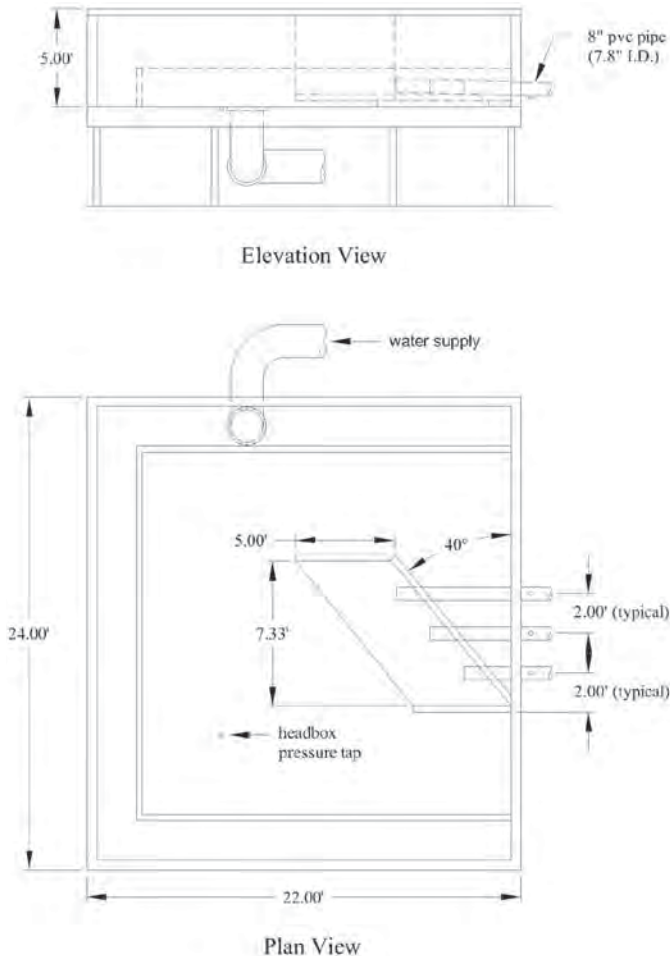

Figure 5-6(C). Multibarrel culvert configuration with 3D horizontal barrel spacing and a 40°, skewed, rectangular approach channel.

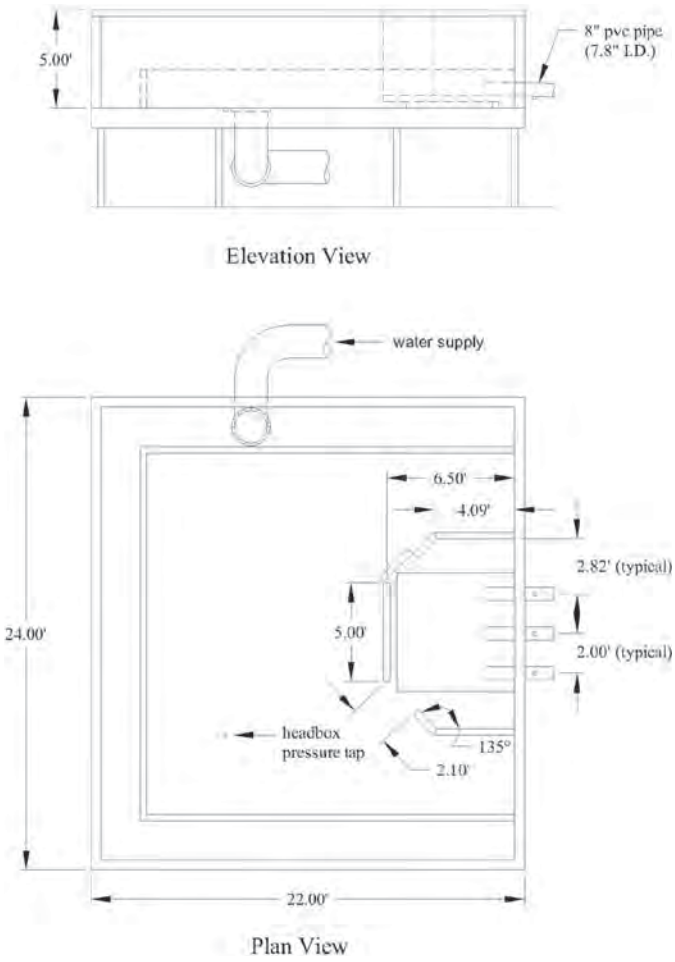

Figure 5-6(D). Multibarrel culvert configuration with 3D horizontal barrel spacing and a non-uniform approach flow channel.

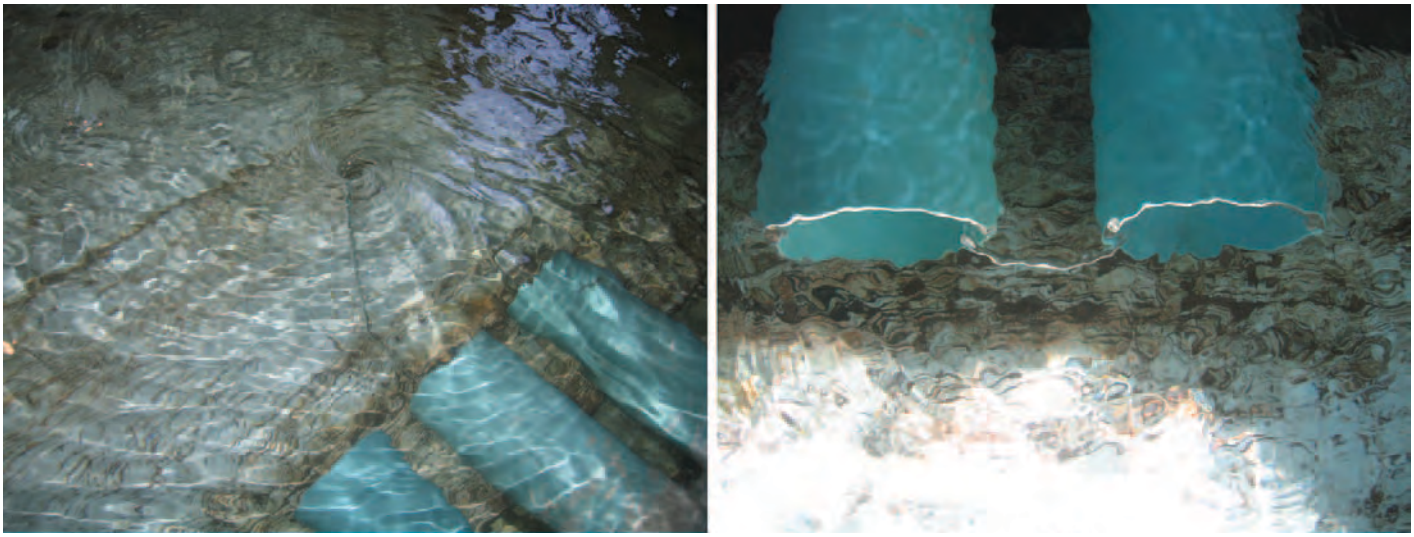

(A) (B)

Figure 5-7. Examples of an aerated surface vortex (A) and a submerged barrel-to-barrel vortex (B).

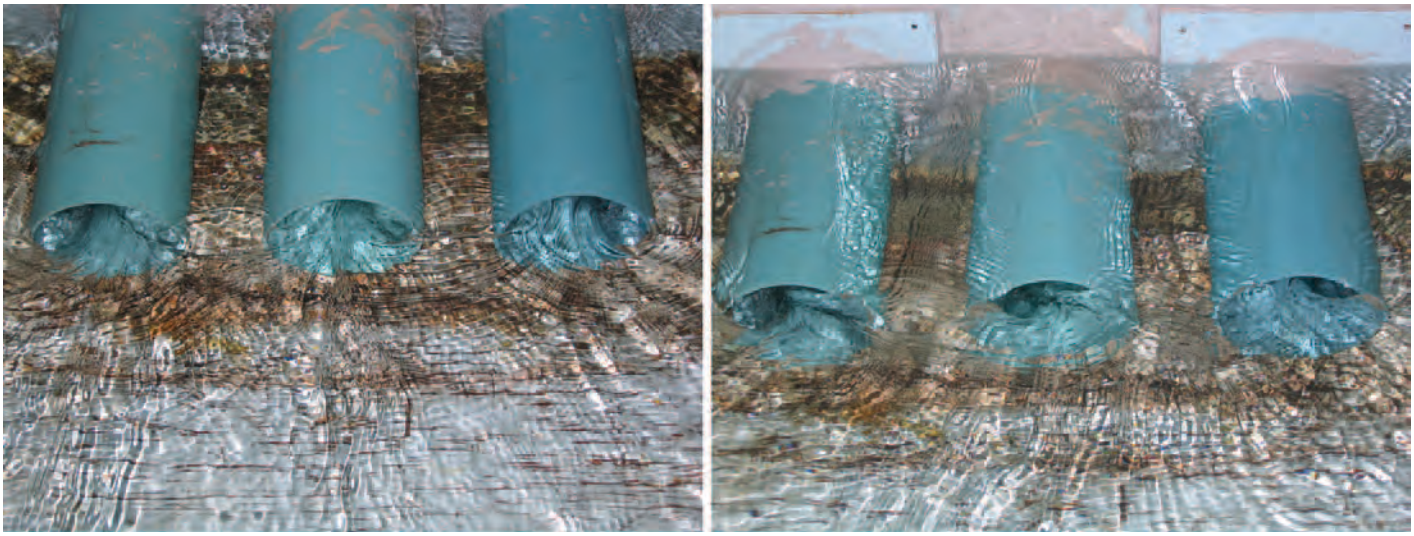

(A) (B)

Figure 5-8. Variations in flow contraction patterns between the middle and outside barrels for unsubmerged (A) and nearly submerged or transitional submergence inlet conditions (B).

compared with the single-barrel, reservoir approach data. Multi-barrel culvert configurations with channelized approaches (i.e., trapezoidal or rectangular) were compared with the single-barrel, trapezoidal channel approach data.

The inlet control, thin-wall projecting, corrugated metal pipe (CMP) head-discharge data with a reservoir approach condition, calculated using the coefficients published in *HDS-5,* are plotted in Figure 5-9. The thin-wall projecting CMP culvert data, which represents the most similar culvert/end treatment configuration in *HDS-5* to the single-barrel culverts tested in the current study, were included as a relative comparison and a quality-control check for the single-barrel data from this study. For $1 < Hw/D < 3.0$, the agreement is very good. Outside that range, the performance varies. At $Hw/D > 2.5$–3.0, the slightly thicker pipe wall of the non-corrugated PVC pipe inlet becomes slightly more efficient. The general agreement between the two data sets is a good indication that it is likely that there were no systemic biases associated with the experimental method of the

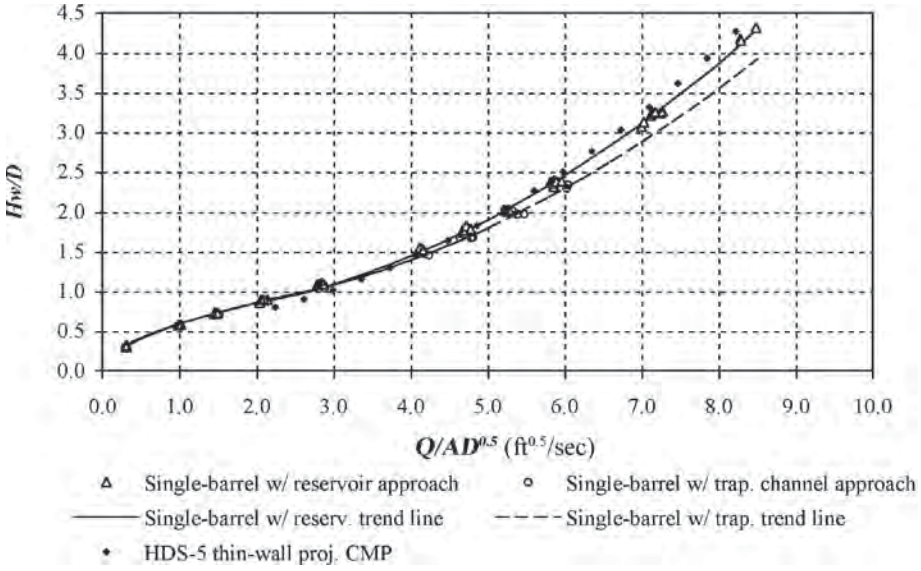

Figure 5-9. Single-barrel, inlet control, head-discharge data and trend lines based on testing all three barrels individually with 1.5D and 3D horizontal barrel spacing and a reservoir approach or a trapezoidal channel approach flow condition.

Table 5-3. Inlet control empirical coefficients for Equations 1-3 and 1-4.

Test No.	No. of barrels	Culvert Barrel center-to-center (*D*)	Headwall-to-approach flow (deg)	Upstream Approach Condition	Depressed middle-barrel vertical offset	Unsubmerged Form 1		Unsubmerged Form 2		Submerged	
						K	*M*	*K*	*M*	*c*	*Y*
1	1	–	0	Reservoir	0	0.0885	0.5370	0.5870	0.5490	0.0506	0.6500
2	2	1.5	0	Reservoir	0	0.0900	0.6123	0.5874	0.5621	0.0482	0.7257
3	2	2.0	0	Reservoir	0	0.0846	0.6117	0.5825	0.5609	0.0508	0.6483
4	2	3.0	0	Reservoir	0	0.0936	0.5412	0.5924	0.5498	0.0499	0.6767
5	3	1.5	0	Reservoir	0	0.0844	0.5341	0.5859	0.5224	0.0503	0.6609
6	3	2.0	0	Reservoir	0	0.0858	0.5570	0.5840	0.5545	0.0494	0.6603
7	3	3.0	0	Channeled	0	0.0631	0.5986	0.5587	0.5615	0.0417	0.6952
8	3	3.0	40	Channeled	0	0.0941	0.2396	0.5925	0.5072	0.0501	0.5677
9	3	3.0	0	Reservoir	0	0.0914	0.5497	0.5885	0.5525	0.0502	0.6532
10	3	3.0	0	Non-uniform	0	0.0899	0.6812	0.5874	0.5777	0.0443	0.7659
11	1	2.0	0	Trapezoidal 2:1	0.5	0.0744	0.7984	0.5715	0.5462	0.0486	0.6202
12	2	2.0	0	Trapezoidal 2:1	0.5	0.0944	0.2737	0.5937	0.5068	0.0472	0.6635
13	3	2.0	0	Trapezoidal 2:1	0.5	0.0992	0.2716	0.6002	0.5076	0.0418	0.7512
14	3	3.0	0	Trapezoidal 2:1	0.5	0.0998	0.3753	0.6004	0.5265	0.0423	0.7196

current study and that the use of the single-barrel experimental data set for comparison with the multibarrel culvert assemblies is representative of published single-barrel performance data.

Two-Barrel Test Results

The two-barrel culvert tests were conducted using the three-barrel installation with one of the outside barrels capped off, as shown in Figure 5-5(A). The two-barrel test configuration variations included the middle barrel with each outside barrel, 2D and 3D horizontal barrel spacings, reservoir and trapezoidal channel approach flow conditions, and a 0.5D depressed middle barrel culvert.

The experimental, two-barrel, quasi-dimensionless data for the different test conditions are plotted in Figures 5-10 through 5-13. As with the single-barrel data, the trend lines represent the average individual-barrel head-discharge relationship for the multibarrel culvert configurations using the Form 1 and Form 2 relationships (Equations 1-2 and 1-3) for unsubmerged inlet conditions ($Hw/D < 1.0$) and the submerged relationship

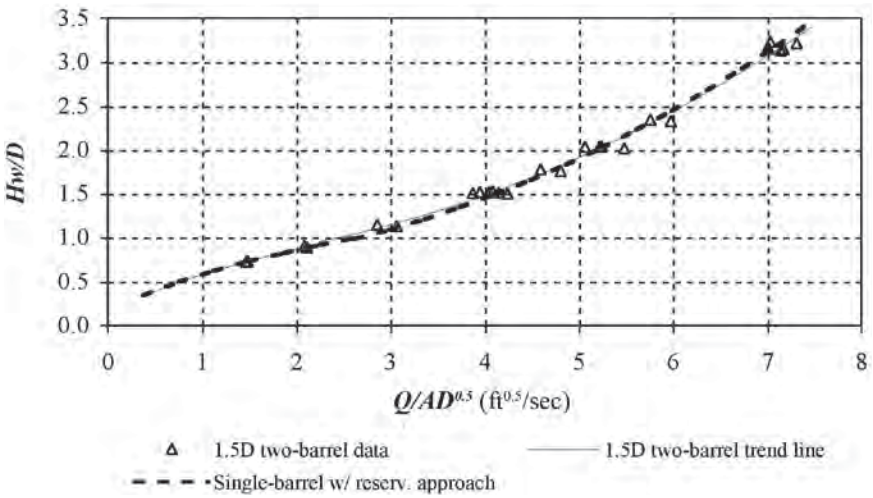

Figure 5-10. Experimental data for two-barrel, 1.5D horizontal spacing tests with common invert elevations and a reservoir approach flow condition.

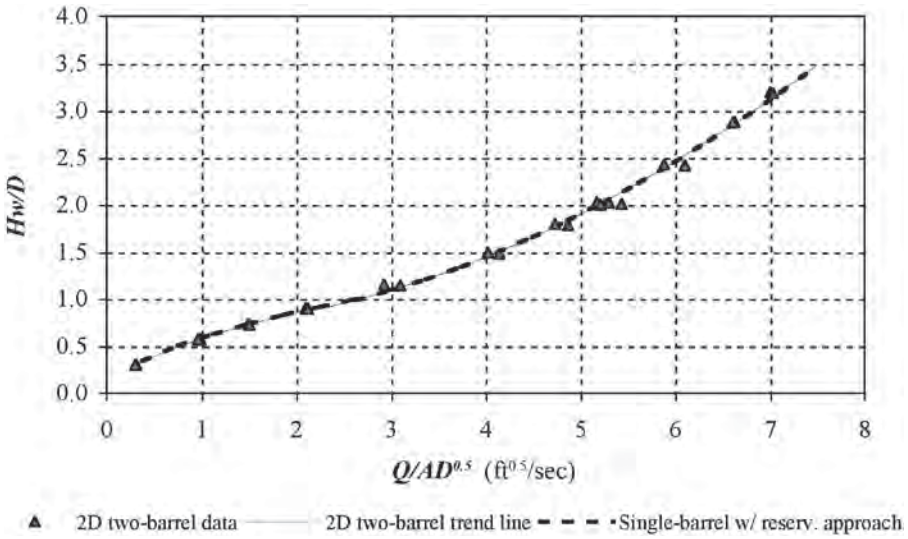

Figure 5-11. Experimental data for two-barrel, 2D horizontal spacing tests with common invert elevations and a reservoir approach flow condition.

(Equation 1-4) for $Hw/D > 1.0$. The single-barrel culvert data for the same approach flow condition [i.e., reservoir or channelized (trapezoidal channel)] are also plotted.

The data points in Figures 5-10 through 5-13 were not segregated with respect to the individual barrels or pairings due to poor readability (congested data points). In general, the trend lines for each of the two-barrel test configurations [i.e., 1.5D (Figure 5-10), 2D (Figure 5-11), and 3D (Figure 5-12) horizontal spacing with a reservoir approach and the 2D horizontal, 0.5D depressed barrel with trapezoidal channel approach (Figure 5-13)] correlate well with the single-barrel culvert trend lines. Note that the test data for the two-barrel 0.5D depressed barrel configuration shown in Figure 5-13 follow the same trend line, despite the offset in culvert inlet elevations. This correlation suggests that the practice of designing multibarrel culverts as multiples of single-barrel culverts (superposition) may be appropriate for determining multibarrel head-discharge relationships.

The individual two-barrel data points in Figure 5-10, however, show some variation from the trend line (±5%), suggesting that, while superposition may be a good predictor of the average performance, the variations in barrel flow rates and increases in velocities as the barrel spacing decreases may warrant additional consideration with respect to culvert outlet

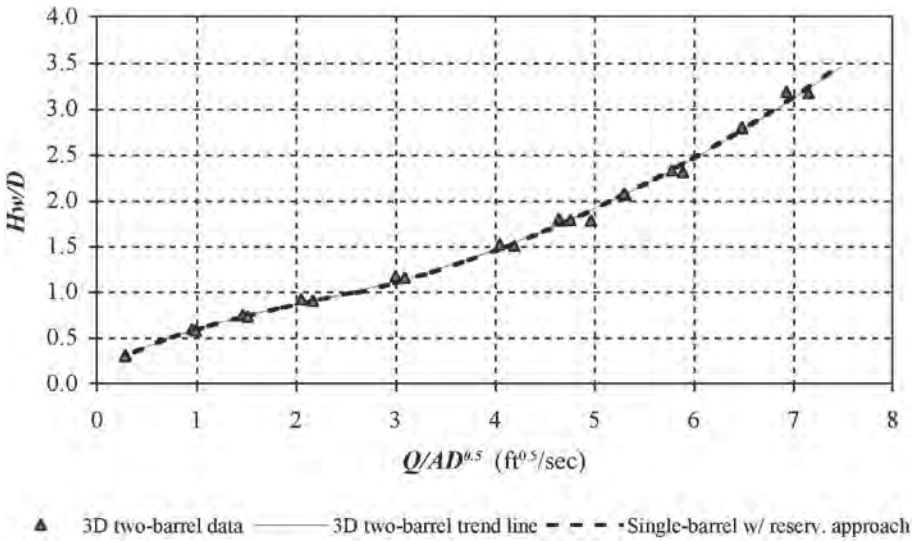

Figure 5-12. Experimental data for two-barrel, 3D horizontal spacing tests with common invert elevations and a reservoir approach flow condition.

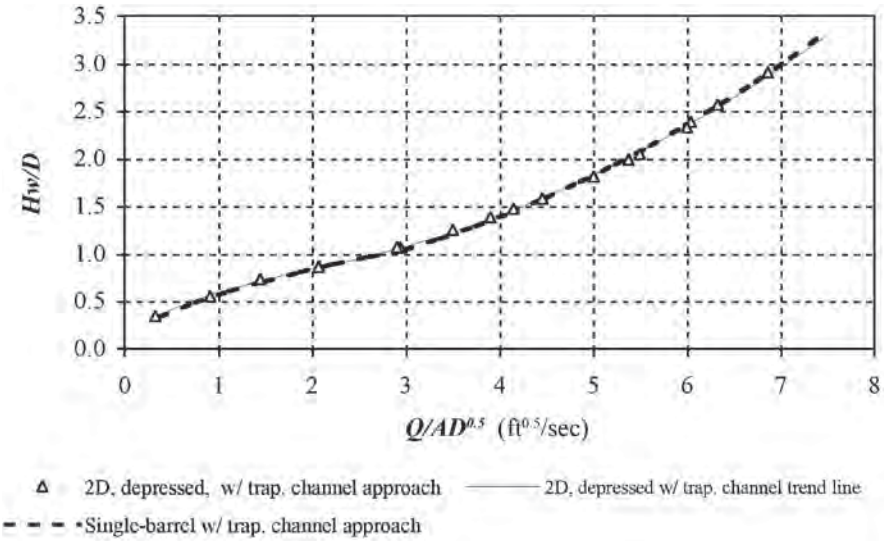

Figure 5-13. Experimental data for two-barrel, 2D horizontal spacing, 0.5D depressed-barrel tests and single-barrel with trapezoidal channel approach flow condition.

riprap protection and fish passage velocity requirements. The flow rate variations between individual barrels, corresponding to submerged inlet conditions, were usually attributable to sporadic surface or barrel-to-barrel vortex activity.

All of the data for the two-barrel culvert configurations tested and the single-barrel experimental reference data are plotted in Figure 5-14. The quasi-dimensionless head-discharge relationships appear to be influenced more by the approach flow condition than the specific two-barrel, multibarrel culvert configuration. Figure 5-14 shows that the single-barrel and multibarrel configurations tested with a trapezoidal approach channel were more efficient than those tested with a reservoir approach flow. All of the single-barrel and multibarrel culvert assemblies tested with the reservoir approach flow condition performed very similarly. The empirical coefficients, corresponding to Equations 1-3 and 1-4 (i.e., *K, M, c,* and *Y*), for all inlet control two-barrel multibarrel culvert configurations tested are presented in Table 5-3.

Three-Barrel Test Results

The two-barrel culvert test configurations were repeated for the three-barrel culvert tests (i.e., 1.5D, 2D, and 3D horizontal spacing with a reservoir approach and the 2D horizontal, 0.5D depressed middle barrel with a trapezoidal channel approach). Several additional 3D horizontal spacing (uni-

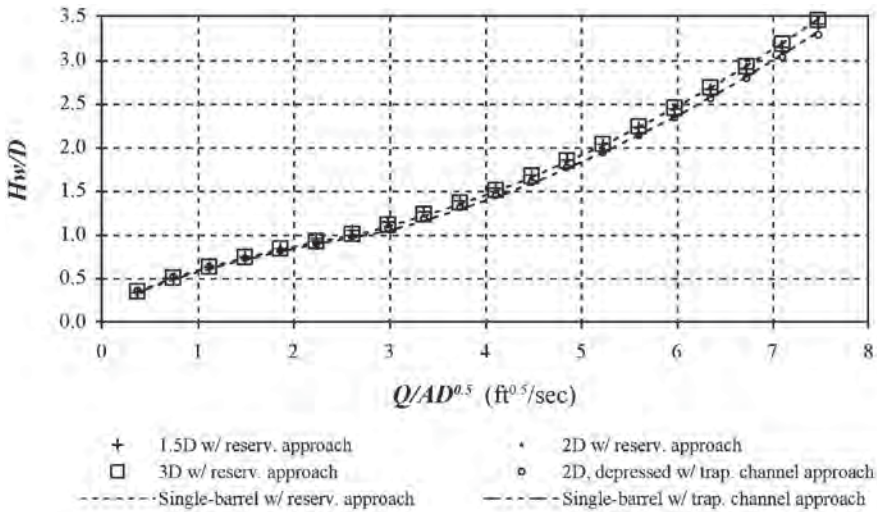

Figure 5-14. Trend line summary for all two-barrel culvert and single-barrel culvert configurations tested.

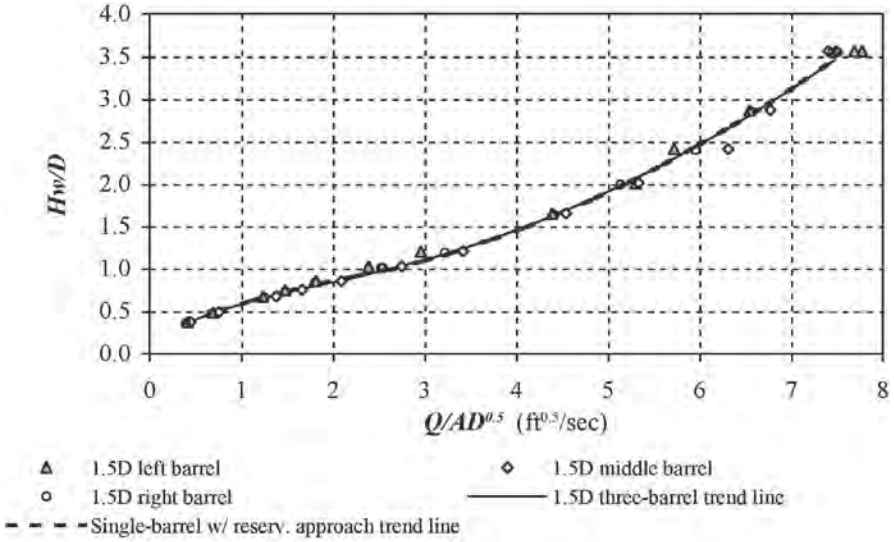

Figure 5-15. Experimental data for three-barrel, 1.5D horizontal spacing tests with common invert elevations and a reservoir approach flow condition.

form inlet invert elevation) configurations were also tested, including a rectangular channel approach; a skewed headwall with a rectangular channel approach; a 3D horizontal spacing, 0.5D depressed middle-barrel configuration; and a non-uniform approach flow condition.

The three-barrel experimental results are presented in Figures 5-15 through 5-22. In each plot, the individual-barrel data are presented along with a best-fit trend line [based on the Form 2 relationship (Equation 1-3) for unsubmerged and Equation 1-4 for submerged inlet conditions] and the single-barrel trend line for either the reservoir or trapezoidal channel approach flow condition for comparison. The barrels are identified as viewed from the upstream direction (i.e., left, middle, and right). Figures 5-15 through 5-22 indicate that, in general, the middle barrel is more efficient, likely due in part to the decrease in middle-barrel inlet flow contraction compared to the outside barrels. Despite the variation in the individual-barrel performances, the best-fit three-barrel trend lines generally correlate well with the single-barrel performance data.

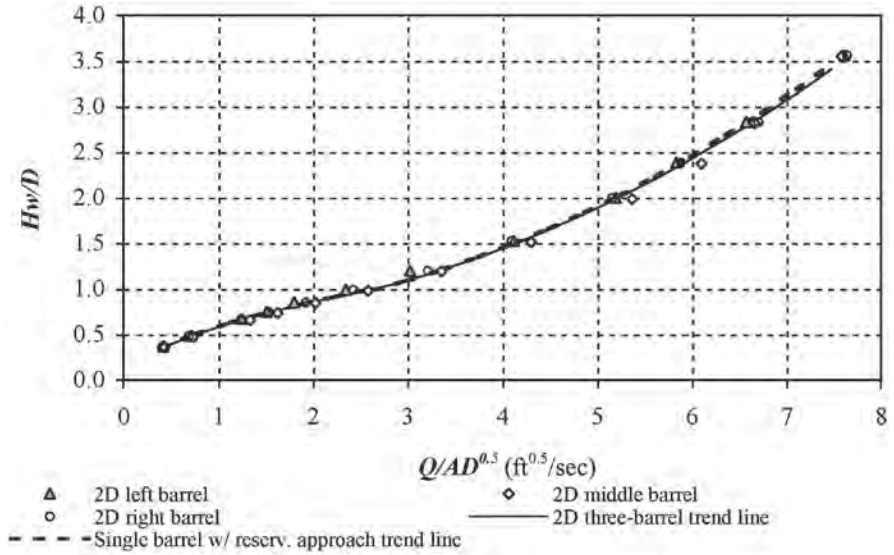

Figure 5-16. Experimental data for three-barrel, 2D horizontal spacing tests with common invert elevations and a reservoir approach flow condition.

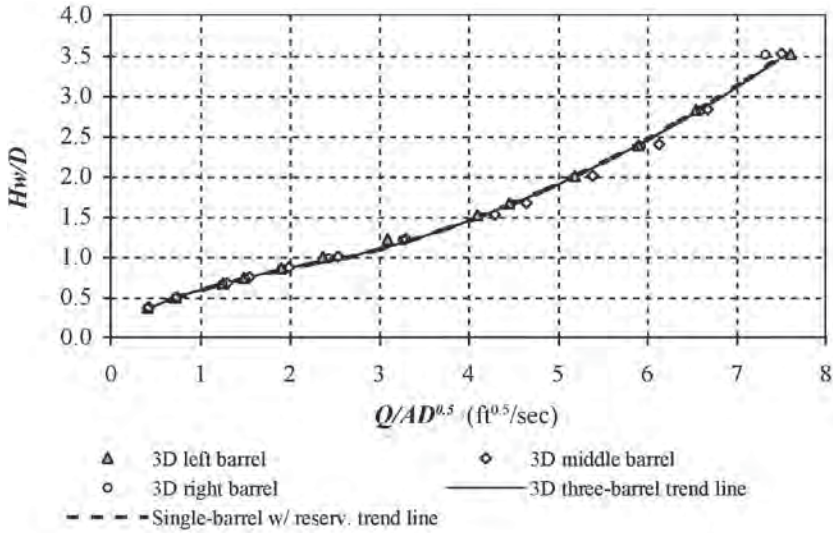

Figure 5-17. Experimental data for three-barrel, 3D horizontal spacing tests with common invert elevations and a reservoir approach flow condition.

In Figure 5-15, the data points for the 1.5D spacing show more scatter than the other test configurations. A repeat of the test, including setup and data collection, produced similar results. Closer inspection revealed an increase in surface and sub-surface (barrel-to-barrel) vortex activity for the 1.5D barrel spacing relative to the larger culvert spacing configurations. Barrel-to-barrel, sub-surface vortices were not observed for the 2D and 3D barrel spacing configurations. Intermittent surface vortices were observed for all barrel spacings, but in general, the duration of the individual surface vortices increased as the barrel spacing decreased.

The trend lines for the 3D three-barrel with a rectangular channel approach (Figure 5-18) and the skewed headwall with a rectangular channel approach (Figure 5-19) match the single-barrel trapezoid approach trend line reasonably well. Only part of the 3D three-barrel with a trapezoidal channel approach data are plotted in Figure 5-18. During data collection, it was noted that at the higher discharge/headwater conditions, the drop structures at the outlet ends of the culvert barrels were not sufficiently vented, which allowed sub-atmospheric pressure to develop and increase the discharge capacity of the multibarrel culvert assembly. This caused the experimental data and the

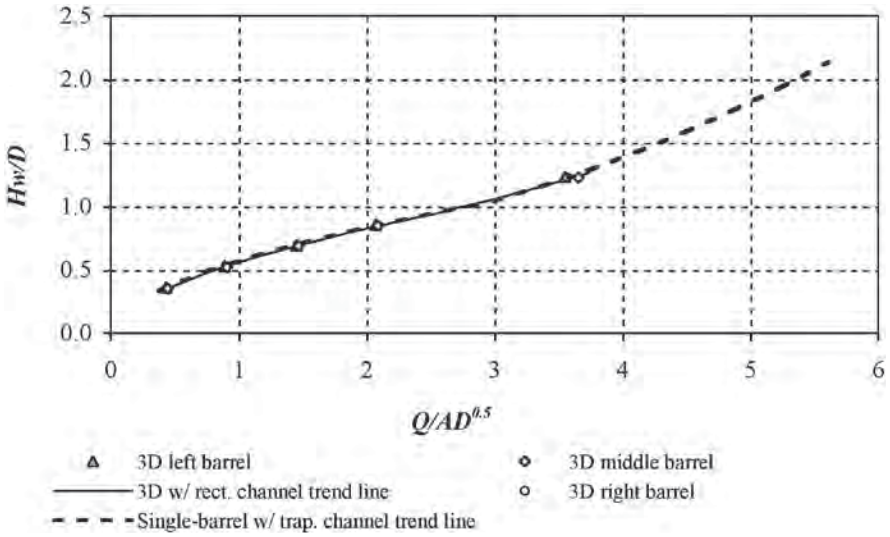

Figure 5-18. Experimental data for three-barrel, 3D horizontal spacing tests with common invert elevations and a rectangular channel approach flow condition.

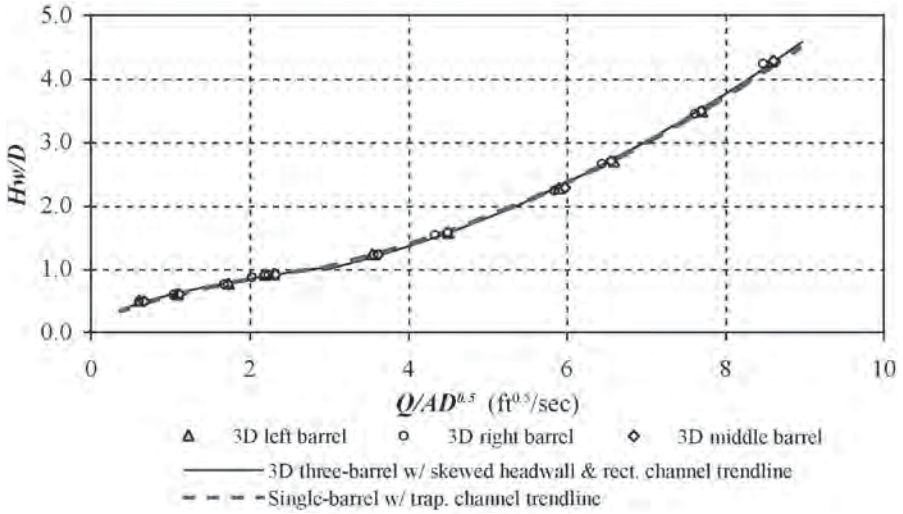

Figure 5-19. Experimental data for three-barrel, 3D horizontal spacing tests with common invert elevations, a skewed headwall, and a rectangular channel approach flow condition.

trend line to deviate from the single-barrel with a trapezoidal channel approach trend line. Following that test and prior to installing and testing the 3D, three-barrel skewed headwall with a rectangular channel approach, vent holes were added to the drop structures. Based on the good agreement between the three-barrel and single-barrel trend lines in Figure 5-19, it was assumed that the trend lines in Figure 5-18 would likely maintain their agreement at the higher *Hw/D* values with the vent holes and that the test did not warrant repeating.

Figure 5-20 shows the 3D three-barrel performance with a non-uniform approach condition. Admittedly, the specific non-uniform approach flow condition [shown in Figures 5-5(F) and 5-6(D)] was of arbitrary design and is not necessarily representative of other non-uniform approach flow conditions. This non-uniform approach flow configuration successfully created a notable disparity in discharge capacity between the more efficient middle barrel and the outside barrels. The non-uniform approach produced a larger deviation between the three-barrel and the single-barrel trend lines than any other configurations tested. The single-barrel trend line had a maximum under-prediction of the average three-barrel trend line (near $Hw/D = 1.0$) of approximately 10%.

Figures 5-21 and 5-22 present the three-barrel test results with a 0.5D depressed middle barrel and a trapezoidal

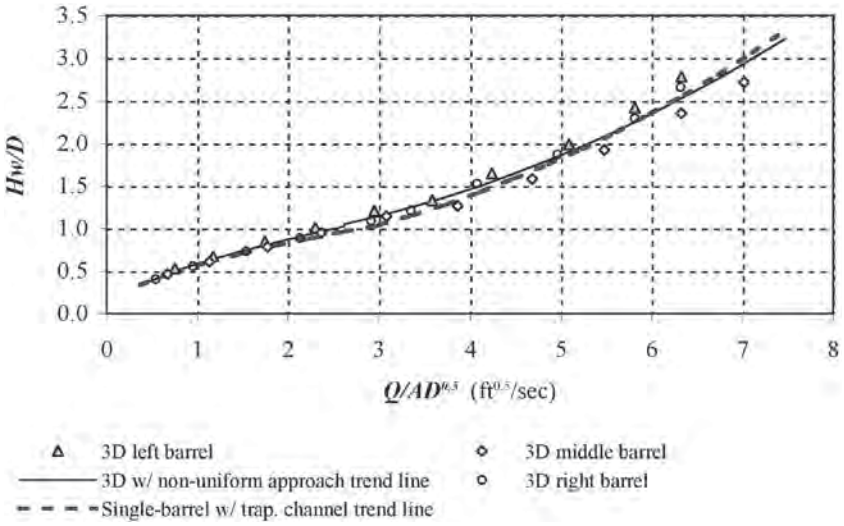

Figure 5-20. Experimental data for three-barrel, 3D horizontal spacing tests with common invert elevations and a non-uniform approach flow condition.

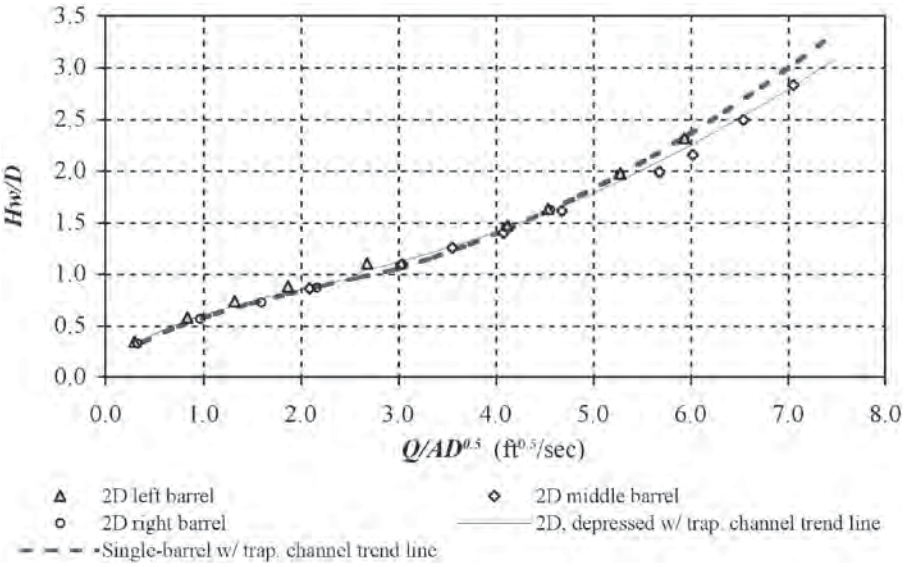

Figure 5-21. Experimental data for three-barrel, 2D horizontal spacing tests with a 0.5D depressed middle barrel and a trapezoidal channel approach flow condition.

channel approach. Note that for the individual test conditions, the middle-barrel data do not match up with the left- and right-barrel data (at common *Hw/D* values) because of the offset in barrel inlet inverts. The trend line for the unsubmerged and low submergence inlet flow regions matches the single-barrel flow curve fairly well. As the inlet submergence increased (*Hw/D* = 1.5 to 2.0 range), the discharge efficiency of the depressed middle barrel began to increase compared to the outside barrels and the single-barrel trend line. The single-barrel trend line in Figure 5-21 underestimates the average individual-barrel trend line for the three-barrel configuration by approximately 4% at higher *Hw/D* values. Due to the limited *Hw/D* data range in Figure 5-22, a similar comparison cannot be made; however, the data appear to have a similar trend to the data in Figure 5-21. These results suggest that single-barrel head-discharge relationships and super-

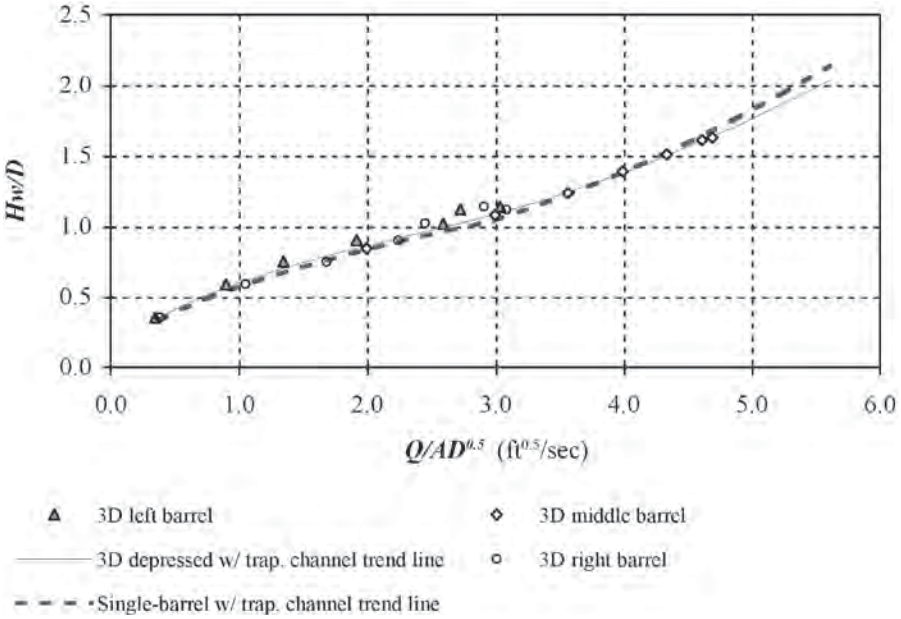

Figure 5-22. Experimental data for three-barrel, 3D horizontal spacing tests with a 0.5D depressed middle barrel and a trapezoidal channel approach flow condition.

position can be used to predict with reasonable accuracy total culvert discharge in the design of multibarrel culverts with a depressed middle barrel and a trapezoidal channel approach.

In summary, good correlation was observed between the single-barrel and the average individual-barrel head-discharge relationships for all three-barrel culvert test conditions, with the exception of the non-uniform approach flow condition, suggesting that superposition is a reasonable design method for estimating the total culvert discharge. The variation in individual culvert barrel discharges increased as the barrel spacing decreased (7% for 1.5D), or as the non-uniformity of the approach flow increased (10%). As was discussed for the two-barrel test results, when designing barrel-discharge-specific applications such as outlet energy dissipation, outlet riprap, or fish passage, the single-barrel superposition design method may produce non-conservative discharge predictions for the middle barrel. The empirical coefficients, corresponding to Equations 1-3 and 1-4 (i.e., *K, M, c,* and *Y*), for all inlet control three-barrel multibarrel culvert configurations tested are presented in Table 5-3.

Tabular support data for the Chapter 5 experimental results are included in Appendix E.

5.6 Conclusions

The objective of this study was to evaluate the inlet control head-discharge relationships (quasi-dimensionless) for a variety of multibarrel culvert configurations and compare the individual-barrel, the average-barrel, and the single-barrel head-discharge performances using experimental data collected using laboratory-scale (8-in.) culverts and a culvert testing facility. The comparisons were made in an effort to determine the appropriateness of the superposition approach to designing multibarrel culverts using single-barrel culvert design data, such as is presented in *HDS-5.* The empirical coefficients (i.e., *K, M, c,* and *Y*) corresponding to Equations 1-2 (unsubmerged inlet, Form 1 relationship), 1-3 (unsubmerged inlet, Form 2 relationship), and 1-4 (submerged inlet relationship) for all inlet control, multibarrel culvert configurations tested were also calculated and presented in Table 5-2. The results of this study are the basis of the following conclusions:

1. The single-barrel, thin-wall projecting PVC culvert head-discharge data developed in this study compared favorably with the thin-wall projecting CMP culvert performance calculated using *HDS-5* data, indicating that no significant systemic biases or quality-control issues were present in the current study.
2. The single-barrel, thin-wall projecting culvert head-discharge relationships varied with approach flow condition. The channelized approach flow associated with the upstream trapezoidal channel was more efficient than the reservoir approach flow condition, primarily due to a reduction in flow contraction entering the culvert barrel with the channelized approach flow.
3. The single-barrel head-discharge relationships (reservoir and trapezoidal channel approaches) correlated very well with the average-barrel head-discharge relationships for all two- and three-barrel multibarrel culvert configurations listed in Table 5-2. The three-barrel depressed culvert tests with 2D and 3D horizontal spacing and a 0.5D vertical offset of the middle barrel with a trapezoidal channel approach (Tests No. 13 and 14 in Table 5-3) and the three-barrel, non-uniform approach flow condition (Test No. 10 in Table 5-3) deviated the most from the single-barrel culvert performance. For $Hw/D > 3.0$, the single-barrel culvert relationship underestimated the average individual-barrel depressed culvert relationships by up to approximately 4% (for the range of experimental data). The single-barrel culvert relationship underestimated the average individual-barrel relationship for the 3D, three-barrel configuration with a non-uniform approach flow by as much as 10%.
4. Determining the total multibarrel culvert discharge using single-barrel design data and superposition is likely to be appropriate for most multibarrel culvert applications, with the exception of some non-uniform approach flow conditions, provided that representative single-barrel culvert design data are available (i.e., similar culvert type and approach flow condition).
5. For some test configurations, particularly the 1.5D and 2D horizontal spacing three-barrel culverts, the middle barrel had a higher discharge than the outside barrels by as much as 7% at common *Hw/D* values. Intermittent surface and sub-surface vortex activity, which was more prevalent for the 1.5D, two-, and three-barrel test configurations with a reservoir upstream approach, and flow contraction variations between the middle and outside barrels were contributing factors to the disparity between individual-barrel discharges. Individual-barrel discharge variations for the two-barrel tests were as high as ±5%.
6. The variation in the individual-barrel discharges for the two- and three-barrel multibarrel test configurations suggest that while superposition may be a good predictor of the overall culvert discharge, additional considerations may be warranted for applications such as energy dissipation and riprap protection at the individual-barrel outlets and fish passage velocity requirements.
7. Inclusion of the inlet control empirical coefficients presented in Table 5-3 for the single-barrel and multibarrel culvert configurations in culvert design manuals, such as *HDS-5,* would be beneficial to culvert designers.

CHAPTER 6

The Behavior of Hydraulic Roughness Coefficients in Open Channel Flow

6.1 Summary

Quantifying hydraulic roughness coefficients is commonly required in order to calculate flow rate in open channel and closed conduit applications. Much of the theory of resistance on open channel flow is derived from studies on pressurized circular pipe, which features the Darcy-Weisbach roughness coefficient, *f,* which is dependent upon *Re, R_h,* and/or *k.* Relative to full-pipe flow, however, the behavior of open channel flow resistance is more complicated because of the presence of a free surface and because the flow area does not remain constant.

A primary objective behind the development of Manning's Equation was to create a simple open channel flow equation with a roughness coefficient (*n*) that was solely dependent upon the boundary roughness characteristic (e.g., roughness height, *k*). Currently, hydraulic engineering handbooks publish singular representative *n* values (or a small range to account for variations in material surface finish) per boundary material type (e.g., concrete, cast iron, clay, etc.). More recent studies, however, have suggested that R_h, *k,* S_e, and *Fr* can influence *n.*

The behavior of *f* and *n* as a function of *Re,* R_h, *k,* S_e, and *Fr* for open channel flow was evaluated for four different boundary roughness materials, ranging from smooth to relatively rough, by conducting stage-discharge tests in a rectangular tilting flume. The test results showed that when plotting *f* or *n* versus *Re,* a family of curves resulted, with each curve corresponding to a specific channel slope (S_o). For a given S_o, both *f* and *n* decrease with increasing *Re.* The S_o-specific family of *f* curves converges to a bounding curve, unique to each boundary roughness material tested, with increasing *Re,* which represents a *quasi-smooth* flow boundary condition. For the *n* data, the *quasi-smooth* flow condition caused the *n* values to converge to a constant *n* value at larger *Re* values. A *quasi-smooth* flow boundary condition describes a condition where a boundary layer develops adjacent to the channel boundary that consists of a layer of flow eddies. The boundary layer thickness exceeds the material roughness height, reducing the influence of the boundary roughness elements of flow resistance.

With increasing R_h, *f* and *n* also decrease, with *n* eventually approaching a constant value. The constant *n* assumption (*n* is independent of *Re* and R_h) is most appropriate for smoother boundary materials or rough boundary materials where a *quasi-smooth* flow boundary condition exists. Where a *quasi-smooth* condition does not exist, the constant *n* assumption is less appropriate for rougher boundary roughness materials.

6.2 Introduction

Quantifying hydraulic roughness coefficients is commonly required for discharge calculations for both closed conduit and open channel flow applications. Common open channel discharge equations include the Darcy-Weisbach Equation, Equation 6-1, and Manning's Equation, Equation 6-2, which include the friction factor (*f*) and Manning's *n,* respectively, as hydraulic roughness coefficients.

$$V = \sqrt{\frac{8g}{f} R_h S_e} \tag{6-1}$$

$$V = \frac{K_n}{n} R_h^{2/3} S_e^{1/2} \tag{6-2}$$

In Equations 6-1 and 6-2, *V* is the mean velocity, *g* is acceleration due to gravity, K_n is 1.0 (International System of Units) and 1.486 (English System of Units), R_h is the hydraulic radius [the cross-sectional area (*A*) divided by the wetted perimeter (*P*), $R_h = D/4$ for a pipe of diameter *D*], and S_e is the energy grade line or friction slope. Under uniform flow conditions in open channel flow, S_e is equal to the channel slope (S_o).

Turbulence level and the relative roughness of the pipe or channel can influence the flow resistance or hydraulic roughness. Much of the current theory regarding resistance is based on knowledge gained from the study of commercial pipes flowing full. Turbulence effects are commonly quantified using f and its relationship with the Reynolds number (Re), where $Re = VD/v$ (v represents the fluid kinematic viscosity), and relative roughness, quantified as k/D, where k is a representative value for the boundary material roughness height. For open channel flow, these parameters are represented as $Re = V4R_h/v$, and R_h/k, referred to as relative submergence.

The behavior of the hydraulic roughness coefficients in open channel flow is not nearly as well understood as with full-pipe flow. Open channel flow resistance theory is commonly compared qualitatively with full-pipe flow resistance, but the complexities of flow resistance behavior associated with the free surface, variable flow area, and the wider variety of boundary roughness types found in open channel situations significantly complicate the behavior of f. Manning's n is often applied to open channel application because, according to Streeter and Wylie (1979), n is thought to be an absolute roughness coefficient, i.e., dependent upon surface roughness only. Representative Manning's n values for common channel lining materials are typically presented in hydraulic handbooks as singular values or as a high, average, and low value to account for surface finish variations. Streeter and Wylie (1979) also state that n actually depends upon the size and shape of the channel cross-section in some unknown manner. This dependency and others have been described by researchers with equations where $n = F(R_h, k, Fr,$ and $S_e)$ (Limerinos, 1970; Jarrett, 1984; Bathurst, 2002; Ugarte and Madrid, 1994). It is useful to know, however, that for many of the test conditions evaluated by Bathurst (2002), the height of the roughness elements making up the boundary exceeded the flow depth (y) (i.e., small R_h/k values) in some cases. Other research has suggested adjusting other open channel head-discharge relationship flow parameters in lieu of adjusting hydraulic roughness coefficients to better match physical conditions. For example, Christensen (1992) proposed an alternative definition of R_h based on the idea that the shear stress values are not constant along the wetted perimeter; Blench (1939) proposed a change to the exponent of the R_h term.

The current study presents similarities and differences between full-pipe flow and open channel flow resistance coefficients by evaluating the behavior of f and n with respect to Re, R_h, k, S_o, and Froude number (Fr). Special attention was given to the validity of the assumption of a constant n value and how it might relate to f. The analysis was based on open channel flow testing conducted in a rectangular tilting flume featuring boundary roughness materials ranging from smooth to relatively rough.

6.3 Background

Darcy-Weisbach *f*

The Darcy-Weisbach Equation (Equation 6-1) dates back to the mid 1800s (Rouse and Ince, 1957). Nikuradse (1933) performed tests on turbulent flow in artificially roughened pipes (pipes roughened with uniformly sized sand grains) flowing full to investigate the behavior of f. Nikuradse made two important conclusions. At low Re for pipe with relatively small sand grains (high R_h/k values), the values of f were similar to smooth pipe values [$f = F(Re)$ only and the flow condition is known as smooth turbulence or smooth-walled pipe flow]. At relatively low R_h/k values and high Re values, f is solely a function of R_h/k, and the flow condition is known as fully rough turbulence. A transitional turbulence Re range also exists where f is a function of both Re and R_h/k. Colebrook (1939), using commercial pipe data, developed an empirical equation that describes the dependencies of f on R_h/k and Re. From Colebrook's Equation, the Moody Diagram was developed, and it has become a common source for assigning a value to f for full-pipe flow under turbulent conditions.

Chow (1959) compiled data from various open channel flow tests performed in rough channels with turbulent flow. Some of the data compiled by Chow show that at relatively high Re, f becomes independent of Re and is solely dependent on R_h and k. Chow also observed, for some data, that f decreased with increasing Re, with the minimum f values bounded by an equation in the form of Equation 6-3, where f is a function of Re and the coefficients a and b are boundary roughness specific (k):

$$\frac{1}{\sqrt{f}} = a \log \frac{Re\sqrt{f}}{b} \tag{6-3}$$

In Equation 6-3, a and b are empirical coefficients specific for a given channel shape and boundary roughness. Prandtl developed an equation (commonly referred to as the Prandtl-von Kármán Equation) of the form of Equation 6-3, which reasonably describes f data for smooth-walled pipe, with a and b equal to 2 and 2.51, respectively (Crowe et. al, 2001). The open channel flow stage-discharge data presented by Chow (1959) suggest that a and b will vary with boundary roughness type, i.e., f values increase with increasing boundary roughness or increasing k values. Chow (1959) also suggests that when the behavior of f for a given boundary roughness material can be described by Equation 6-3 with a constant set of empirical coefficients (a and b), a *quasi-smooth* flow condition exists. The idea of a *quasi-smooth* boundary flow condition was introduced by Morris (1955) and describes a flow state where the areas between the roughness elements are filled with stable eddies, creating a pseudo wall flow boundary

similar to a smooth wall (See Figure 6-1). The results from this study confirm that Equation 6-3 is a relative limiting boundary to *f* and also show that this limiting boundary has relevance to the assumption of a constant *n*.

Manning's *n*

Equation 6-4 relates the Manning's *n* roughness coefficient and *f*.

$$\frac{V}{V^*} = \sqrt{\frac{8}{f}} = \frac{K_n R_h^{1/6}}{n\sqrt{g}} \tag{6-4}$$

In Equation 6-4, V^* is the shear velocity [$V^* = (gR_hS_e)^{1/2}$]. Manning (1889) developed Equation 6-2 with the expressed intent of providing a simplified open channel flow equation where, contrary to existing equations, the empirical coefficients (including the roughness coefficient) would remain constant for a given channel boundary type, independent of *Q* and R_h variations. Manning applied Equation 6-2 with river-reach-specific constant *n* values to more than 100 data points taken from various rivers and concluded that it was "sufficiently accurate."

Chow (1959) states that if the bed and banks of a channel are equal in roughness and the slope is uniform, then *n* is usually assumed to be constant for all flow depths (*y*). Chow (1959) presents Manning's *n* data (constant values) and photographs for a number of different channel types as a reference for designers. More recent studies, however, have shown that *n* is not necessarily a constant even under the conditions described by Chow (1959). A number of relationships have been developed based on the results of these studies in order to predict the behavior of *n.* For example, Limerinos (1970), Bray (1979), Griffiths (1981), and Bathurst (2002) have presented relationships suggesting that *n* is a function of R_h/k. Jarrett (1984) suggested that *n* is dependent upon S_e and R_h. Ugarte and Madrid (1994) proposed relationships for *n* involving R_h, *k*, S_e, and *Fr*. These relationships were developed based on studies where Manning's Equation was applied to a specific type of channel. The Limerinos, Bray, and Griffith relationships were developed for rivers with gravel beds; the Bathurst, Ugarte and Madrid, and Jarrett relationships were specific to "mountain streams" characterized as steep with relatively small R_h/k values. Yen (2002) maintains, however, that for a given boundary roughness, *n* should be relatively constant, independent of *Re,* and R_h, provided that the equivalent *f* value per Equation 6-4 is in the fully turbulent range [i.e., $f = F(R_h \text{ and } k)$].

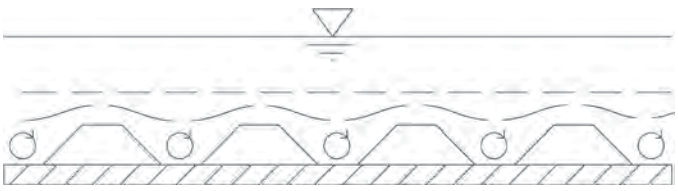

Figure 6-1. Illustration of the quasi-smooth flow boundary theory.

Froude Number Effects

Flow state is commonly characterized by the value of the Froude number (*Fr*) (see Equation 6-5), which represents the ratio of inertial to gravitational forces. In Equation 6-5, *T* is the channel top width. When $Fr < 1$, gravitational forces are dominant, flow velocities are low, and the flow condition is referred to as subcritical. When $Fr > 1$, the inertial forces are dominant, the velocity is high, and the flow condition is referred to as supercritical.

$$Fr = V\Big/\left(gA/T\right)^{1/2} \tag{6-5}$$

Chow (1959) states that when $Fr < 3$, the influence of *Fr* on open channel roughness coefficients is negligible. Chow concedes, however, that as more data become available, the influence of *Fr* on open channel roughness coefficients may need to be reconsidered. Ugarte and Madrid (1994) concluded that *n* has *Fr* dependencies; however, it is important to note that their study was generally limited to relatively small R_h/k values. Bathurst et al. (1981) also found that *Fr* was a factor in quantifying the *n;* however, instead of using the traditional *Fr* definition, R_h was substituted for A/T in Equation 6-5.

Objectives

The objectives of this study were to investigate the relationships of the roughness coefficients *f* and *n* with *Re,* R_h, *k,* and *Fr* in open channel flow in an effort to better understand the appropriateness of the constant *n* value assumption for a given boundary roughness. Comparisons are made for four different roughness materials ranging from smooth (acrylic sheeting) to relatively rough (block and trapezoidal corrugated roughness elements).

6.4 Experimental Method

The behavior of Manning's *n* for four different boundary roughness materials was investigated by conducting flow tests in a 4-ft-wide by 3-ft-deep by 48-ft-long, adjustable-slope, rectangular laboratory flume. The four channel boundary materials tested include acrylic sheeting (see Figure 6-2); a low-profile, commercially available expanded metal lath adhered to the acrylic walls and floor of the flume (see Figure 6-3); regularly spaced wooden blocks (see Figures 6-4 and 6-5); and

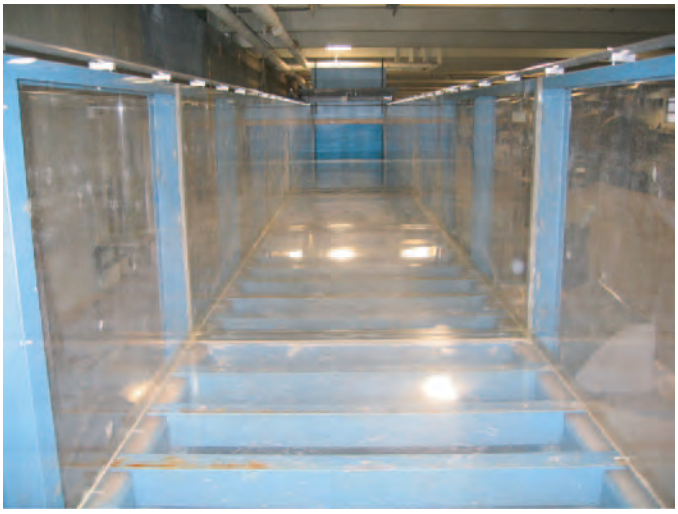

Figure 6-2. Acrylic boundary roughness material.

Figure 6-4. Block boundary roughness material.

trapezoidal corrugations oriented normal to the flow direction (see Figures 6-6 and 6-7). The wooden blocks, measuring 4 in. wide (normal to flow direction) by 3.5 in. long by 1.5 in. tall, with the top edges rounded (1-in. radius roundover), featured a painted exterior and were assembled in a closely spaced, uniform pattern. The wooden trapezoidal corrugation elements were 1.5 in. tall, had a top width of 1.5 in. and a base of 4.5 in., and were spaced 1.5 in. apart. The blocks and trapezoidal corrugation elements were attached to sheets of painted marine grade plywood, which were attached to the flume floor and walls.

Assigning a *k* value to various types of roughness material is not an exact process. For gravel-lined channels, the mean grain size diameter is often used. In this study, all roughness materials, save the acrylic sheeting, have more than one geometric dimension that influences the hydraulic roughness

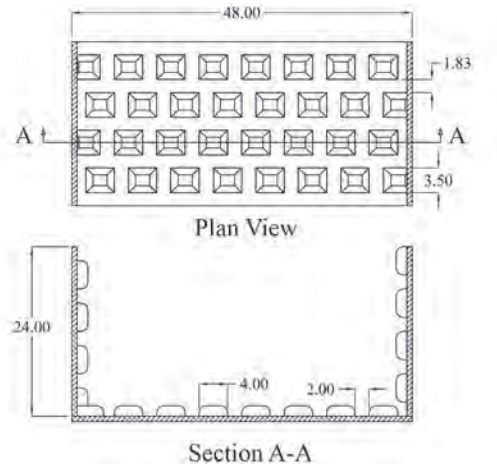

Figure 6-5. Schematic of block boundary roughness material (dimensions shown in inches).

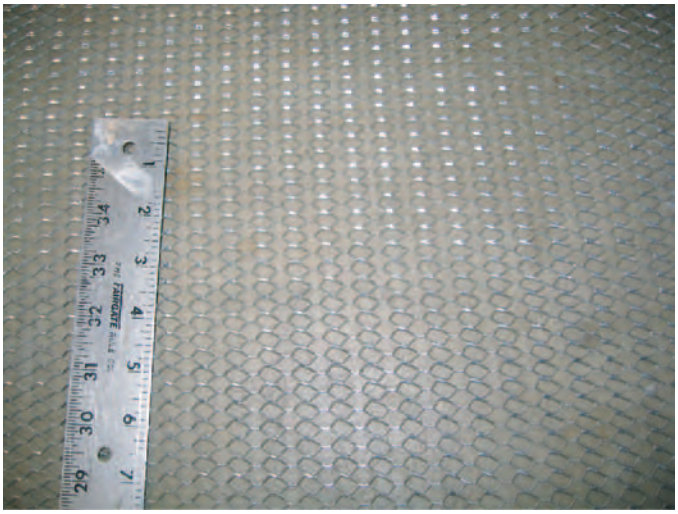

Figure 6-3. Metal lath boundary roughness material.

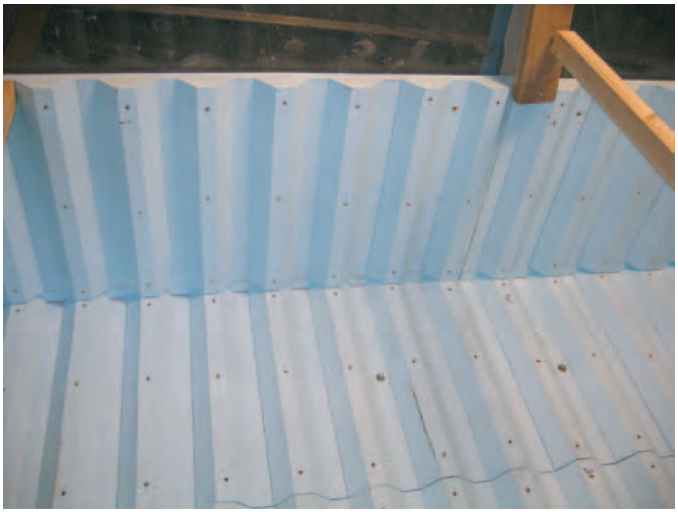

Figure 6-6. Trapezoidal corrugation boundary roughness material.

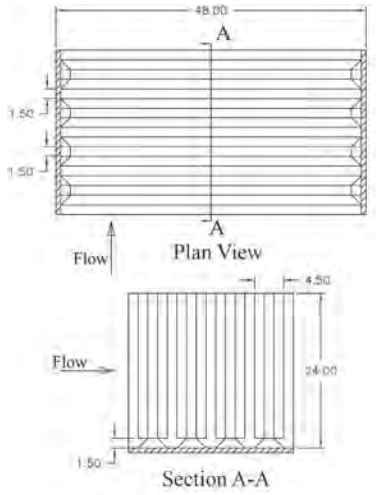

Figure 6-7. Schematic of trapezoidal corrugation boundary roughness material (dimensions shown in inches).

(e.g., the block height, width, length, and spacing). Chow (1959) explains that while k represents a measure of a boundary's roughness, it is an empirical parameter that doesn't necessarily correspond to a specific geometric dimension of the roughness element that can be measured using a linear scale and that k is influenced by many factors such as roughness element shape, orientation, and distribution. In this study, k was assumed to be equal to the physical height of the roughness elements, for lack of a more appropriate alternative. The acrylic sheeting k value was selected to be consistent with published values ($k = 0.00006$ in.).

Water was supplied to the flume from a reservoir located adjacent to the laboratory and was metered using calibrated orifice flow meters. Flow depths were measured using a precision point gage, readable to 0.008 in., attached to a movable carriage located above the flume.

Manning's n can be directly calculated via Equation 6-2 when uniform flow exists in the channel and y and Q are known. Due to the limited length of the laboratory flume, uniform flow depth could not be achieved for all test conditions. In laboratory practice, a tailgate is often used to help establish uniform depth in a flume by increasing the downstream flow depth and truncating part of the gradually varied flow (GVF) profile. According to Yen (2003), this method does not guarantee the presence of a uniform flow condition. In addition to a constant flow depth, the velocity distribution, pressure, and turbulence characteristics must also be uniform for uniform flow to exist. Yen (2003) states that even though a constant depth may be forced in a short channel with the use of a tailgate, the effects of the channel inlet and tailgate may affect the characteristics of the flow, resulting in a flow condition that is not "uniform." In the current study, all tests featured a free-overfall downstream boundary condition. For flow conditions that did not achieve normal depth naturally, Manning's n values were determined using a computational GVF profiling technique. For each steady state flow condition, the GVF profile was determined by measuring flow depths ($y_{measured}$) at 33 different locations along the length of the flume. The Manning's n coefficient was determined for each flow condition by adjusting the Manning's n value in a GVF computer program until the computed water surface profile best matched the measured profile. To determine the "best fit" of the data, a coefficient of determination (r^2), Equation 6-6, was maximized.

$$r^2 = 1 - \frac{\sum \left(y_{measured} - y_{calculated} \right)^2}{\sum \left(y_{measured} - y_{average} \right)^2} \tag{6-6}$$

In Equation 6-6, $y_{calculated}$ is the flow depth calculated by the GVF computer program and $y_{average}$ is the average of $y_{measured}$.

The data collection proceeded as follows. For each slope and discharge, the water surface was measured in relation to the flume floor at 2-ft intervals over the upstream half of the flume and at 1-ft intervals over the downstream half. Due to the nature of the block and trapezoidal corrugation roughness materials, no single channel invert datum was present. Consequently, a representative datum was determined by calculating the total volume of the roughness elements (blocks or trapezoidal corrugations) divided by the total flume floor area and adding the resulting height to the elevation of the plywood floor upon which the roughness elements were installed.

Using this GVF method, a separate Manning's n value was determined for each flow condition. Early in the data collection process, however, it became apparent that for the relatively rough boundary materials (blocks and trapezoidal corrugations), Manning's n exhibited variability with flow depth for a common flow rate. Figure 6-8, for example, shows Manning's n data for a number of flow conditions in the block-lined channel. With steeper channel slopes, where uniform flow conditions were more prevalent, n values were determined using the measured normal depth (y_n), Q, and Equation 6-2. For milder sloping channels, where uniform flow profiles were less common, n values were determined using the GVF profile method. A comparison of the block-lined Manning's n values determined using both techniques is presented in Figure 6-8, which plots n versus the average channel profile flow depth ($y_{average}$). The uniform flow depth data in Figure 6-8 show that for the block roughness, n varies ($0.087 \geq n \geq 0.038$) with changes in uniform flow depth ($0.13 \leq y \leq 0.9$). Analysis of various truncated sections of a single GVF profile, using the GVF n method, also produced different predictive values for n, suggesting that n is also variable with depth throughout a GVF profile. Based on the variable nature of n with flow depth in GVF profiles, it may be

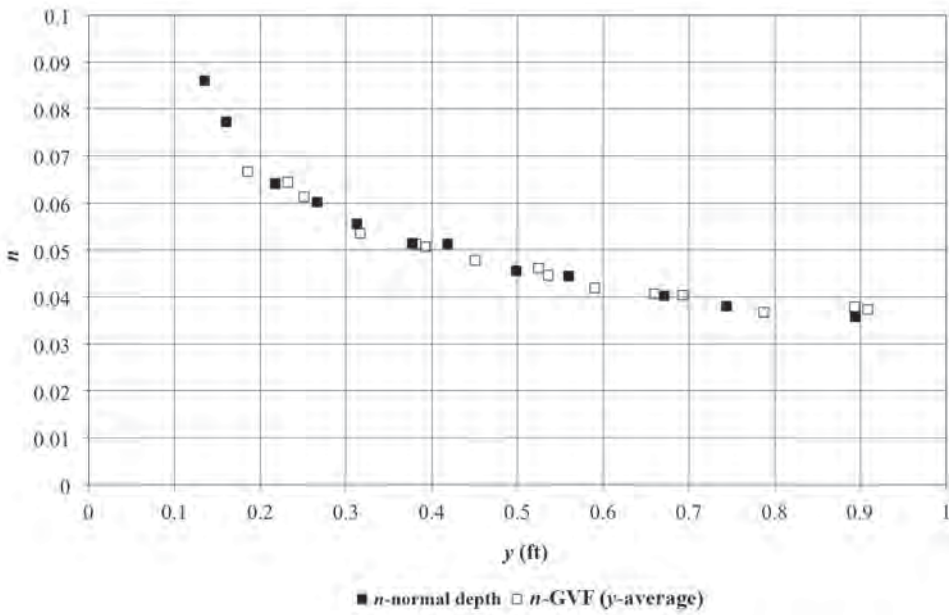

Figure 6-8. Comparison of Manning's* n *values determined using the uniform flow depth and the GVF technique (non-uniform flow conditions) versus $y_{average}$ of the measured water surface (data from block-lined channel).

expected that the predicted normal depths associated with the variable *n* values should also vary. Consequently, based on the good correlation between the uniform flow and GVF *n* data presented in Figure 6-8, $y_{average}$ was selected as the representative flow depth parameter for calculating R_h, *Re, V,* etc., rather than a predicted normal depth, for flow conditions where a uniform flow was not present.

Manning's *n* data for the acrylic boundary were collected at three different slopes (i.e., $S_o = 0.0002$, 0.0003, and 0.0022) with the number of flow conditions at each slope ranging from 6 to 17. The metal lath boundary was tested at four different slopes (i.e., $S_o = 0.0066$, 0.0118, 0.0179, and 0.022) with 4 to 29 flow conditions tested at each slope. The block and trapezoidal corrugation boundaries were each tested at five slopes (i.e., $S_o = 0.0004$, 0.0018, 0.0095, 0.0237, and 0.05) with seven different flow conditions per slope. The channel discharges ranged from 0.24 to 23 cfs.

6.5 Discussion and Analysis

f Relationships

Figure 6-9 plots the Darcy-Weisbach *f* versus *Re* data for each of the roughness materials in a uniformly lined channel. The data from the acrylic-lined channel generally follow the Prandtl-von Kármán smooth-wall pipe flow curve. Although they are not necessarily discernable in Figure 6-9 due to the scale of the y-axis, the acrylic experimental *f* values exceed the Prandtl-von Kármán curve values at higher *Re* values. At a given *Re* value, *f* increases with increasing boundary roughness (i.e., *f* of the blocks is greater than the metal lath, which is greater than the acrylic).

At first glance, there appears to be considerable scatter in the data for the two larger roughness materials (block and trapezoidal roughness materials) in Figure 6-9; however, a closer look reveals families of curves segregated by S_o. The data show that for a prismatic channel where S_o is held constant, *f* decreases as *Re* increases. For a constant *Re, f* increases with increasing S_o. As *Re* increases, the roughness-element-specific, slope-dependent family of curves converges to a single curve. There is no single *Re* value, however, at which the individual curves converge. The *Re* value at which a slope-specific curve converges to the bounding curve for an individual roughness material increases with increasing S_o.

The bounding curve to which the acrylic, metal lath, and trapezoidal corrugation data converge is consistent with Equation 6-3, which, as described by Chow (1959), becomes a limiting boundary to the decreasing effect of the boundary roughness on the total resistance to the flow. Figure 6-9 shows that the block slope-specific data curves do not fully converge to a single curve within the range of *Re* tested; however, the trend lines appear to be converging toward a single bounding curve with increasing *Re.* The convergence of the metal lath and the trapezoidal corrugation roughness data to a single bounding *f* versus *Re* curve indicates that the conditions in the channel have reached a *quasi-smooth* boundary flow condition consistent, in theory, with the illustration in Figure 6-1.

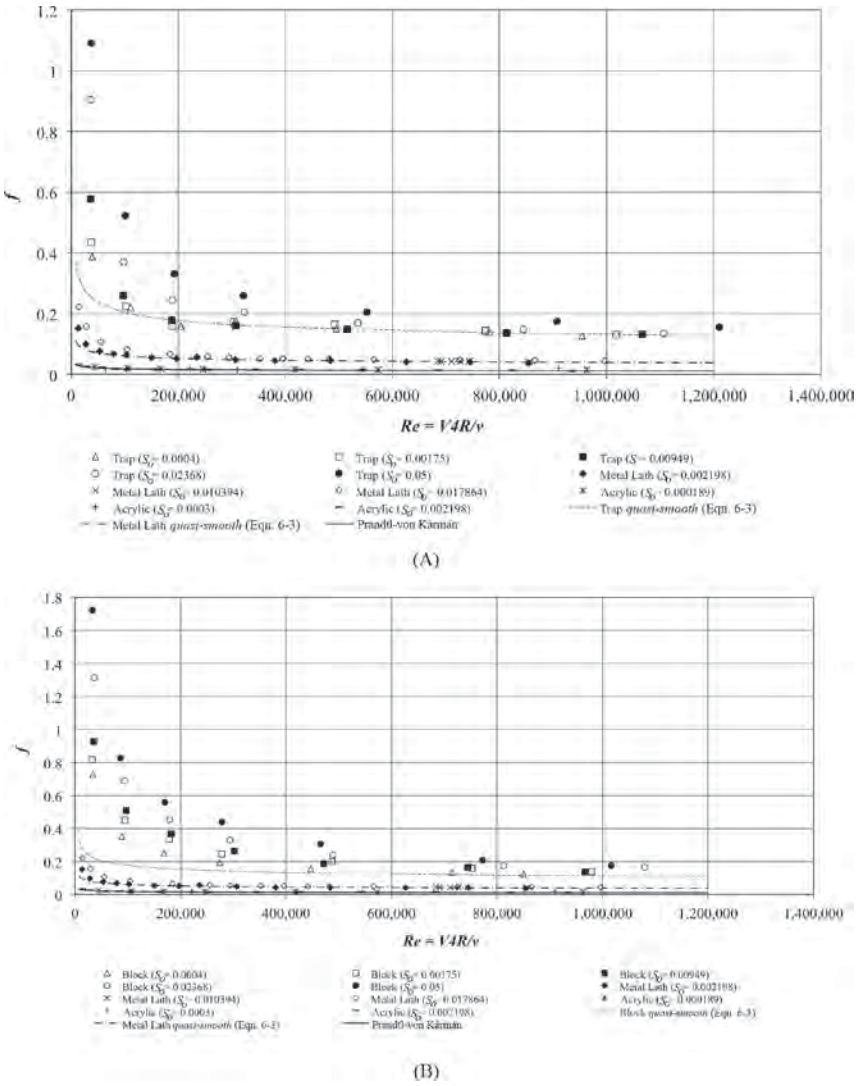

Figure 6-9. **f** ***versus*** **Re** ***data for acrylic, metal lath, trapezoidal corrugation (A), and block (B) roughness materials.***

n Relationships

If *n* were constant (as is often assumed) and solely dependent on *k,* four horizontal lines, one for each roughness material tested, should result when plotting *n* versus *Re.* The results in Figure 6-10 show relatively constant *n* values for the smooth acrylic data and over most of the *Re* data range for the metal lath. There is a small range of relatively small *Re* values over which *n* for the metal lath varies. For the two rougher materials (block and corrugation roughness), *n* varies significantly over the range of *Re* tested. The data for these roughness materials show trends similar to the *f* data presented in Figure 6-9: there is a family of curves segregated by S_o, *n* decreases with increasing *Re, n* increases with an increasing slope (at a constant *Re* value), and the S_o-specific curves converge as *Re* increases. An inspection of the data in Figures 6-9 and 6-10 reveals a subtle but important difference between the behavior of *n* and *f* with *Re.* In Figure 6-10, the slope-dependent Manning's *n* data curves converge to a constant (minimum) value as *Re* increases, indicating that *n* is solely dependent upon *k* at higher *Re* values. In contrast, the S_o-specific *f* curves in Figure 6-9 converge to a bounding curve in the form of Equation 6-3 as *Re* increases. Although the slopes of the bounding curves become relatively small at higher *Re* values, the bounding curves do not reach a zero slope, indicating that *f* remains a function of *Re* and *k* over the range of *Re* numbers tested.

The data in Figure 6-10 also suggest that the appropriateness of a constant *n* value assumption increases as the relative smoothness of the channel boundary increases. The *n* values for the acrylic and metal lath channels are constant over the majority of the *Re* range tested. As the relative roughness increases (e.g., the blocks and trapezoidal corrugations), the range of *Re* over which *n* is constant diminishes. Based on the data presented in Figure 6-10, the constant *n* assumption, commonly used when applying Manning's Equation (Equation 6-2), is appropriate for smooth-wall channel lining

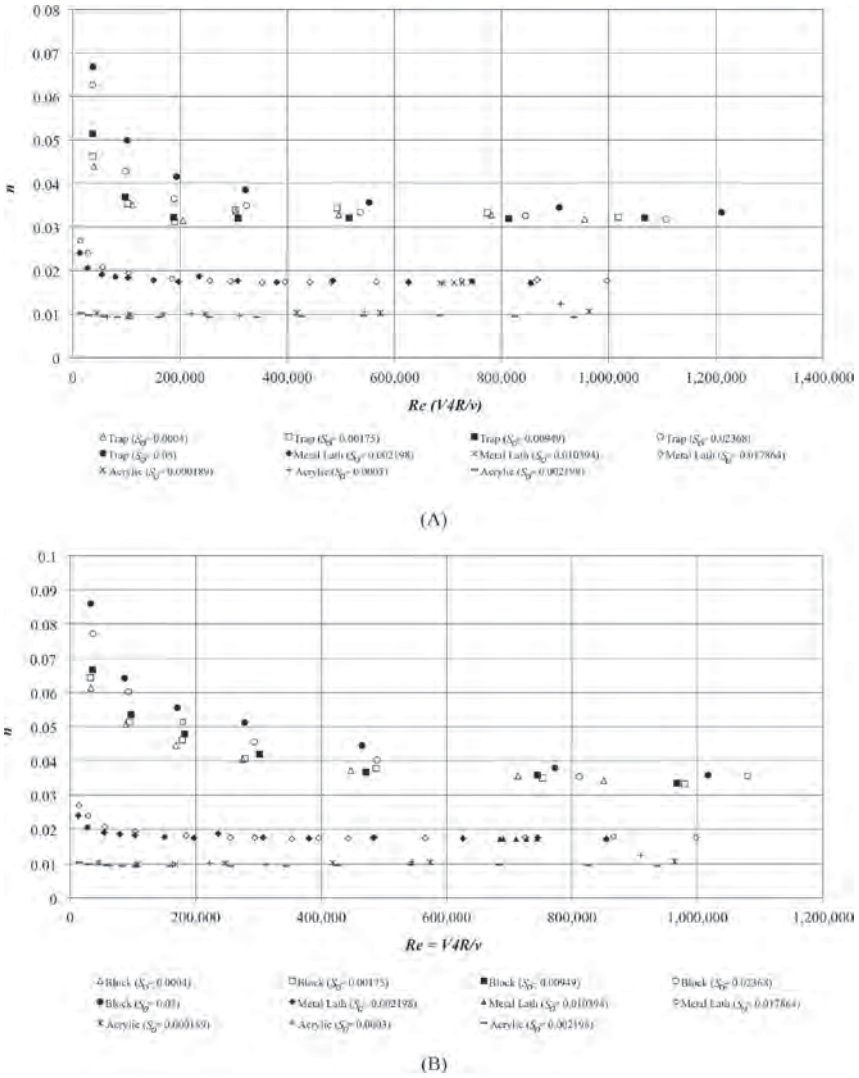

Figure 6-10. **n** ***versus*** **Re** ***data for acrylic, metal lath, trapezoidal corrugation (A), and block (B) roughness materials.***

materials (e.g., smooth acrylic sheeting) or for "rougher" boundary materials when a *quasi-smooth* boundary condition is present (e.g., metal lath and trapezoidal corrugation roughness material *n* versus *Re* data become constant). Under these conditions, *n* is a function of *k* and is no longer dependent on *Re, S_o*, or R_h/k.

The behavior the block roughness *n* data in Figure 6-10 is similar to that of the *f* data in that the *n* data do not fully converge to a constant value (a bounding curve for the *f* data) due to the limited range of experimental *Re* values. It is assumed, however, that similar to the trapezoidal corrugations, the block data will converge to a constant *n* value at higher *Re* values.

Figure 6-11 presents *n* versus R_h/k for the block and trapezoidal corrugations. The block data show a strong dependence on R_h/k (*n* decreases with increasing R_h/k) and are relatively independent of S_o, as the data essentially collapse to a single curve. The fact that the *n* versus R_h/k data are essentially independent of S_o means that for the rectangular flume used in this study *n* was solely a function of flow depth. This means that *n* will be the same for two different channel slopes, provided that flow depths are the same, independent of the differences in *Q, V,* and *Re* for the two slope conditions. As a result, when correlating *n* versus R_h/k, *n* is essentially independent of *V* and *Re.* The trapezoidal corrugation data in Figure 6-11 also show a strong dependence on R_h/k; however, a slight data segregation (family of curves) associated with S_o exists (more than with the block data).

The reason for the variation in the behavior of *n* versus R_h/k between the block and trapezoidal corrugation materials isn't clear, but the variation may be related to the nature of the flow paths near the boundaries. With the blocks, flow passes over and around the individual roughness elements. With the trapezoidal corrugations, the flow only passes over the roughness elements, making the velocity profile near the boundary primarily two dimensional rather than three dimensional like the blocks. The disparity between the S_o-specific *n* versus R_h/k

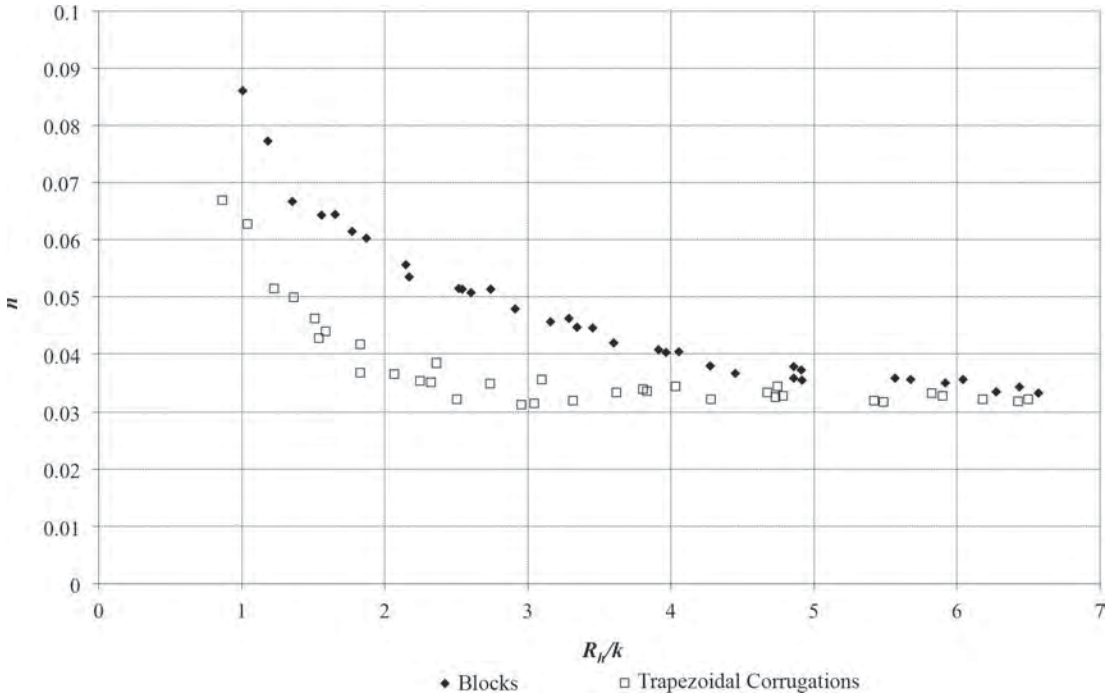

Figure 6-11. **n** ***versus*** **R_h/k** ***for block and trapezoidal corrugation roughness materials.***

curves in Figure 6-11, however, is significantly reduced relative to the *n* versus *Re* data in Figure 6-10.

It is also interesting to note that despite the fact that the block and trapezoidal corrugation roughness elements are the same height, the *n* versus R_h/k data trend differently in Figure 6-11. At smaller flow depths (e.g., $R_h/k = 1.0$), the flow resistance of the blocks is larger (larger *n*) than that of the trapezoidal corrugations. For the trapezoidal corrugations, *n* decreases more rapidly with increasing R_h/k than for the blocks, and the point at which *n* becomes constant occurs at a lower R_h/k value. This suggests that equating *k* to the height of the roughness element does not adequately characterize the influence of the roughness elements on flow resistance. Although perhaps not a general conclusion, it is interesting to note that the trapezoidal corrugations and the block, which were approximately the same height, both approach approximately the same constant *n* value at high R_h/k values (*n*~0.033). More research is recommended to investigate the characteristic differences between the flow resistance behavior of two-dimensional and three-dimensional boundary roughness element types.

With respect to the data presented in Figure 6-11, the *quasi-smooth* flow boundary condition occurs for rougher boundary materials when a sufficiently high R_h/k condition, referred to as relative submergence or the boundary roughness elements, is reached and *n* becomes constant. For R_h/k values below the *quasi-smooth* flow limit, the constant *n* assumption is not appropriate. According to the data presented in Figure 6-11, the level of relative submergence required to produce a *quasi-smooth* flow condition varies with the boundary roughness characteristics, which are partially described by *k* and R_h/k. Manning (1889) reported relatively constant *n* values for numerous river channel sections. The river channel sections most likely featured sufficiently high R_h/k values to validate a constant *n* assumption.

Subcritical versus Supercritical Flow

Nineteen of 35 data points taken from a metal-lath-lined flume featured supercritical flow conditions and were dispersed over the range of *Re* tested. Three of seven flow conditions corresponding to the steepest channel slope for the block and trapezoidal roughness produced supercritical flow. Although the data are not specifically identified as subcritical or supercritical flow in Figure 6-10, the consistent trends in the data sets indicate that *n* is relatively independent of *Fr* over the range of *Fr* values tested. For the entire data set (all four boundary roughness data sets) *Fr* ranged from 0.33 to ~1.54. These results concur with Chow (1959), who stated that for small *Fr* ($Fr < 3$), the effect of gravity on flow resistance is negligible.

6.6 Conclusions

Quantifying hydraulic roughness coefficients is commonly required to calculate flow rate in open channel and closed conduit applications. Much of the theory of resistance on open channel flow is derived from studies on pressurized circular pipes and features the Darcy-Weisbach roughness coefficient, *f,* and its relationship with *Re, R_h,* and *k.*

In developing Equation 6-2, Manning's (1889) primary objective was a simple open channel flow equation with a roughness coefficient (n) that was solely dependent upon k. Currently, hydraulic engineering handbooks publish singular representative n values (or a small range to account for variations in material surface finish) per boundary material type (e.g., concrete, cast iron, clay, etc.). Manning concluded that the constant n assumption was "sufficiently accurate" after applying Equation 6-2 to numerous data taken from rivers; however, later studies (Limerinos, 1970; Jarrett, 1984; Bathurst et al., 1981; Ugarte and Madrid, 1994) suggest that n can be influenced by R_h, k, S_e, and Fr.

The behavior of f and n as a function of Re, R_h, k, S_o (rather than S_e), and Fr in open channel flow was evaluated in a rectangular tilting flume for four different boundary roughness materials ranging from smooth to relatively rough. Based on the results of this study, the following is concluded:

1. In relation to Re, the f and n data from this study have similar characteristics to the data presented by Chow (1959). At a constant S_o, both f and n decrease with increasing Re. The Re-dependent f data were bound by a material-roughness-specific limiting curve consistent with Equation 6-3; the corresponding n data were bound by a limiting constant n value. Chow (1959) suggested that the f-data bounding curves are consistent with a smooth surface condition, analogous to the Prandtl-von Kármán smooth pipe wall boundary condition, or a *quasi-smooth* boundary flow condition, which describes a condition where the voids between boundary roughness elements are filled with stable eddies, reducing the influence of the boundary roughness elements on flow resistance. The constant n assumption is appropriate for smooth and *quasi-smooth* flow conditions. For rougher boundary materials, n can vary considerably for non-*quasi-smooth* flow conditions, which if not appropriately accounted for, could significantly increase the level of uncertainty associated with open channel flow stage-discharge calculations.
2. For a single boundary roughness material (characterized by k), flow resistance testing over a range of channel slopes produced a family of curves dependent on channel slope (S_o) (see Figures 6-9 and 6-10). The families of f and n data curves in Figures 6-9 and 6-10 do not necessarily confirm S_o as a significant parameter influencing flow resistance behavior; it is more likely that these families are an indicator that there are additional system parameters that influence open channel flow resistance that are not appropriately accounted for in an f or n versus Re analysis. The differences between the S_o-dependent curves for a single boundary roughness material increased as the material roughness height, k, increased (i.e., the metal lath family of curves is more closely spaced than the curves for the block or trapezoidal corrugation boundary materials in Figures 6-9 and 6-10). Figures 6-9 and 6-10 also show that f and n increase with increasing S_o for a given boundary roughness material.
3. Figure 6-11 shows that the S_o-dependent family of curves collapse relatively well to a single curve where n is plotted with respect to R_h/k, indicating that n is the same for two different channel slopes, provided that flow depths are the same. The S_o-dependent family of curves is also independent of the differences in Q, V, and Re for the two slope conditions. The trapezoidal corrugations show a greater scatter in the data than do the blocks when plotted with respect to R_h/k; however, the R_h/k relationship is a great improvement to the Re relationship in collapsing the data to a single curve. More research is needed to fully explain the scatter shown in the data.
4. According to Figures 6-10 and 6-11, the appropriateness of the constant Manning's n assumption or the existence of a *quasi-smooth* flow condition is dependent upon the boundary roughness and a specific value of R_h/k. There exists a minimum R_h/k value for each boundary roughness material tested above, which n is essentially constant. The constant n minimum values of R_h/k decrease as k decreases (as the boundary becomes more smooth). It is interesting to note that despite the fact that the trapezoidal corrugation and block elements had similar height dimensions (1.5 in.) used to quantify their k values, the constant n minimum R_h/k values differed appreciably (as shown in Figure 6-11). This suggests that simply using the vertical dimension or height of a boundary roughness element, particularly for relatively rough boundary materials, does not sufficiently characterize their equivalent roughness height (k). Height, width, length, spacing, uniformity, and surface texture, etc. will all influence the behavior of n with variations in R_h/k. It is also interesting to note that despite the fact that the block and trapezoidal corrugations reach the constant n condition at differing values of R_h/k, the block and trapezoidal corrugation boundary roughness materials converge to approximately the same constant n values.
5. Consistent with the findings of Chow (1959), n was found to be independent of Fr for $Fr < 3$ (all test data from this study were less than $Fr = 3$). Ugarte and Madrid (1994) reported that n was Fr dependent, but their test conditions were limited to relatively small values of R_h/k (large roughness elements and/or shallow flow depths) relative to the current study.

The appropriateness of assuming material-specific constant Manning's n values for all stage and discharge conditions is limited to smooth (physically smooth or *quasi-smooth*) boundary flow conditions. Additional research is needed to provide engineers with more comprehensive Manning's n data that better characterize the flow resistance behavior of common channel lining materials for design purposes.

CHAPTER 7

Open Channel Flow Resistance: the Hydraulic Radius Dependence of Manning's Equation and Manning's *n*

7.1 Summary

Manning's Equation, which is used to estimate the head-discharge relationships in open channel flow applications, states that the mean channel flow velocity is inversely proportional to the Manning's *n* hydraulic roughness coefficient and proportional to the hydraulic radius raised to an exponent (x') of ⅔ (i.e., $R_h^{2/3}$). *n* and x' represent empirical coefficients used to correlate Manning's Equation with experimental data. In developing Manning's Equation, Manning evaluated the stage-discharge characteristics of a range of boundary roughness materials ranging from smooth cement to course gravels and reported unique values of *n* and x' for each boundary type. The x' values ranged from approximately 0.65 (smoothest boundary tested) to 0.84 (roughest boundary tested). Manning chose $x' = ⅔$ as representative, compared it with field data, and suggested that it was sufficiently accurate. He also offered the caveat, however, that the use of Manning's Equation should be limited to cases where its accuracy has been validated.

Chapter 6 showed that Manning's *n* is not constant for all boundary materials and all stage-discharge conditions. This chapter evaluates the behavior of x' with respect to constant *n* assumptions for the four boundary roughness materials discussed in Chapter 6 (smooth acrylic sheeting, metal lath, trapezoidal corrugations, and blocks) and the boundary roughness materials analyzed by Manning (1889). Consistent with the results reported by Manning (1889), this study found that the $x' = ⅔$ assumption is appropriate for smooth boundaries (e.g., acrylic and pure cement) and for rougher boundary materials when a *quasi-smooth* boundary condition exists. The *quasi-smooth* boundary condition describes a condition where the voids between the boundary roughness elements are filled with stable eddies, which effectively reduces the influence of the boundary roughness elements on flow resistance. For rougher boundary materials not in the *quasi-smooth* boundary flow condition, applying the constant Manning's *n* assumption results in x' values in excess of ⅔. If the constant $x' = ⅔$ assumption is applied, then *n* must vary, as discussed in Chapter 6, in order to accurately predict the stage-discharge relationship using Manning's Equation.

7.2 Introduction

Uniform-flow head-discharge relationships for open channel applications correlate flow rate (Q) or mean channel velocity (V) to an energy gradient, taking into account the flow resistance associated with the channel cross-sectional shape and boundary roughness. Most open channel head-discharge or uniform-flow equations are in the form of Equation 7-1 (Chow, 1959).

$$V = CR_h^{x'} S_e^{y'} \tag{7-1}$$

In Equation 7-1, R_h is the hydraulic radius [the flow area (A) divided by the wetted perimeter (P)], S_e is the energy grade line or friction slope (equal to the channel slope S_o for uniform flow conditions), C is a flow resistance coefficient, and x' and y' are exponents. The Chezy Equation (Equation 7-2), Darcy-Weisbach Equation (Equation 7-3), and Manning Equation (Equation 7-4) represent three common open channel flow head-discharge relationships derived from Equation 7-1:

$$V = C_c \sqrt{R_h S_e} \tag{7-2}$$

$$V = \sqrt{\frac{8g}{f} R_h S_e} \tag{7-3}$$

$$V = \frac{K_n}{n} R_h^{2/3} S_e^{1/2} \tag{7-4}$$

In Equations 7-2 through 7-4, g is the acceleration due to gravity; $K_n = 1$ for International System of Units and $K_n =$

$3.281^{(1-x')}$ for English Standard Units; and C_c, f, and n are equation-specific hydraulic roughness coefficients. Equations 7-2 and 7-3 are equivalent, with the same x' and y' values and alternate definitions of the flow resistance coefficient, with the exception of the way the hydraulic roughness for flow resistance is quantified. Manning's Equation is different from the other two, with $x' = ⅔$ instead of ½. Manning (1889) made this change with the hope of developing a simplified open channel equation where the roughness coefficient (n) would be constant for a given channel lining material (i.e., independent of stage and discharge). Equation 7-4 is commonly applied in practice with the assumption that n remains constant for a given boundary roughness material.

Chow (1959) stated that if the boundary roughness in a channel is uniform (i.e., the roughness is the same for the entire wetted perimeter over the length of the channel section) and the slope of the channel bottom is also uniform, then there is a possibility that Manning's n could remain constant for all flow stages. More recently, Yen (2002) suggested that the constant n assumption is appropriate under certain conditions and makes Equation 7-4 more convenient to use than Equations 7-2 and 7-3. Data have also shown, however, that n is not always constant with stage and discharge (Bathurst et al., 1981; Jarrett, 1984; and Ugarte and Madrid, 1994). These studies were performed on "steep" mountain streams with relatively rough natural channel boundaries [in some cases, the height of the roughness elements exceeded the flow depth (y)]. The results of Bathurst et al. (1981), Jarrett (1984), and Ugarte and Madrid (1994) and the statements of Yen (2002) and Chow (1959) are all somewhat supported by the discussion in Chapter 6, which documents both variable and constant n flow regimes in a rectangular channel with a uniform roughness boundary.

In this chapter, the appropriateness of the constant n assumption, relative to the behavior of the other empirically determined fitting parameter in Manning's Equation, x', is evaluated by applying a similar analysis method to that used by Manning (1889) in the development of Equation 7-4 to the data sets used by Manning (1889) and the Manning's n data presented in Chapter 6 (acrylic, metal lath, trapezoidal corrugation, and the block channel boundary roughness materials).

7.3 Background

Chezy Equation and Darcy-Weisbach Equation

The Chezy Equation (Equation 7-2) was developed circa 1769 for uniform open channel flow. Two basic assumptions contributed to its derivation: (1) the force resisting the flow per unit area of the streambed is proportional to the square of the velocity and (2) the flow gravitational force is equal and opposite to the flow resistance force (Chow, 1959).

The Darcy-Weisbach Equation was developed for pressurized pipe flow via dimensional analysis. Values for f, which vary with k/D (k is defined as an equivalent roughness height and D is the pipe diameter) and Re, are presented for smooth-walled or non-profiled-wall pipe in the Moody Diagram, which can be found in most hydraulic handbooks. Chow (1959) stated that if S_e represents the head loss per unit length of pipe or channel and if D were replaced by $4R_h$, then Equation 7-3 could be applied to open channel flow. The relationship between C_c and f is shown in Equation 7-5:

$$C = C_c = \sqrt{\frac{8g}{f}} \tag{7-5}$$

Manning's Equation

Aware of the variable nature of hydraulic roughness coefficient behavior with most open channel flow equations, including Equations 7-2 and 7-3, Manning (1889) presented an alternate open channel flow head-discharge relationship (Equation 7-4) intended to produce constant hydraulic roughness coefficients for given channel boundary materials (i.e., the roughness coefficient is independent of flow conditions). Manning assumed this equation would take the form of Equation 7-1 with $y' = ½$ as shown in Equation 7-6.

$$V = CR_h^{x'}S_e^{1/2} \tag{7-6}$$

The empirical basis for Equation 7-4 came from experimental data published by Bazin (1865), who hydraulically tested four different flow boundary materials [pure cement and 2-to-1-ratio mixes of cement and fine sand, cement and small gravel (particle sizes ranging from 0.36 to 0.84 in.), and cement and large gravel (particle diameters ranged from 1.2 to 1.6 in.)]. After determining boundary-roughness-specific constant values for C in Equation 7-6, Manning reported that the boundary-roughness-specific average exponent x' values ranged from 0.6499 to 0.8395, with x' generally increasing with increasing boundary roughness. Manning assumed $x' = ⅔$ (a value most consistent with smoother boundary roughness materials) to be representative and considered the resulting equation, Equation 7-4, to be "sufficiently accurate" after applying the equation to numerous experiments. Recognizing the potential limitations of Equation 7-4, Manning (1889) suggested that due to its empirical nature the application of Equation 7-4 should be limited to situations where it has been tested and proven.

Equations for Variable Roughness Coefficients

Bathurst (2002) stated that some researchers have found success in using empirical formulas based on a power law relationship in the form of Equation 7-7 to describe hydraulic roughness coefficient variations:

$$\frac{V}{V^*} = a\left(\frac{R_h}{k}\right)^b \tag{7-7}$$

In Equation (7-7), V^* (shear velocity) = $(gR_hS_e)^{1/2}$, a and b are empirical coefficients, and k is the equivalent roughness height, which Chow (1959) suggests is not necessarily equal to the height or even the average height of the roughness elements. The effect of the roughness elements on the hydraulic roughness coefficient is characterized by k; however, it has limited physical meaning and its definition can vary by user. It is therefore another empirical coefficient, and its physical meaning depends on how it is defined for a particular equation. For example, in equations involving gravel beds, k is often defined as a representative D_r (the representative particle diameter of the channel boundary where r indicates the percentage of particles that are smaller than D_r). V/V^* is related to the standard hydraulic roughness coefficients as shown in Equation 7-8:

$$\frac{V}{V^*} = \sqrt{\frac{8}{f}} = \frac{C_c}{\sqrt{g}} = \frac{k_n R_h^{1/6}}{n\sqrt{g}} \tag{7-8}$$

Bray (1979) and Griffiths (1981) published power law relationships consistent with Equation 7-7 for rigid-boundary, gravel-bed rivers. Bathurst (2002) observed that, even though mountain streams may be characterized as gravel-bed rivers, these equations were relatively inaccurate when applied. Mountain streams are characterized by steep slopes and relatively low R_h/k values. According to Bathurst, one reason for these inaccuracies is that the relationships were developed by compiling data from many different river sites, fitting one curve to all the data, and then extrapolating these relationships to predict behaviors outside of the experimental data set. By gathering data for different flow conditions from the same river section and methodically grouping the data from similar sites, Bathurst (2002) showed that for the same type of channel (mountain streams), the data were best described by two significantly different relationships, suggesting that a and b are fairly site-specific parameters and are not solely dependent on a single channel type. Bathurst concluded that the differences between the coefficients in mountain streams were primarily related to variations in channel slope. Table 7-1 presents the coefficients for Equation 7-7 published in the referenced studies.

Table 7-1. Published coefficients for the power law equation (Equation 7-7).

Study	a	b	x'	k
Bray (1979)	5.03	0.268	0.768	D_{90}
Griffiths (1981)	3.54	0.287	0.787	D_{50}
Bathurst (2002)	3.84	0.547	1.047	D_{84}
Bathurst (2002)	3.10	0.93	1.430	D_{84}

If Equation 7-7 is simplified and solved for V, as shown in Equation 7-9, the equation takes on the form of Equation 7-6 ($x' = b + ½$ and $C = ag^{1/2}/k^b$), which suggests a constant exponent, x', and a constant roughness coefficient, C, for a given boundary roughness, provided that a and b are constant.

$$V = \left(\frac{a\sqrt{g}}{k^b}\right) R_h^{(1/2+b)} S_e^{1/2} \tag{7-9}$$

Applying the coefficients from Table 7-1 to Equation 7-9 shows that the $x' = ⅔$ assumption made by Manning (1889) is not necessarily "sufficiently accurate" for all open channel flow conditions since the value of x' can be boundary roughness specific, as illustrated by the data in Table 7-1. This study investigates the variation in x' related to different boundary roughness types in a laboratory setting, where parameters are more easily controlled, to gain a better understanding of the appropriateness of the constant n assumption applied to Manning's equation.

7.4 Experimental Method

The behavior of Manning's n for four different boundary roughness materials was investigated by conducting flow tests in a 4-ft-wide by 3-ft-deep by 48-ft-long adjustable-slope, rectangular laboratory flume. The four boundary roughness materials tested included acrylic sheeting (see Figure 6-2); a low-profile, commercially available, expanded metal lath adhered to the acrylic flume walls and floor (see Figure 6-3); regularly spaced wooden blocks (see Figures 6-4 and 6-5); and trapezoidal corrugations oriented normal to the flow direction (see Figures 6-6 and 6-7). The wooden blocks measured 4 in. wide (normal to flow direction) by 3.5 in. long by 1.5 in. tall and the top edges were rounded (1-in. radius round-over). The blocks featured a painted exterior and were assembled in a closely spaced, uniform pattern. The wooden trapezoidal corrugation elements were 1.5 in. tall, had a top width of 1.5 in., had a base width of 4.5 in., and were spaced 1.5 in. apart. The blocks and trapezoidal corrugation elements were attached to sheets of painted marine grade plywood that were attached to the flume floor and walls.

Water was supplied to the flume from a reservoir located adjacent to the laboratory and was metered using calibrated

orifice flow meters located in the supply piping. Flow depths were measured using a precision point gage, readable to 0.008 in., attached to a movable carriage located above the flume.

Manning's n can be directly calculated via Equation 7-4 when uniform flow exists in the channel and the flow depth (y) and flow rate (Q) are known. Due to the limited length of the laboratory flume, uniform flow depths could not be achieved for all test conditions. For non-uniform flow conditions, a gradually varied flow (GVF) profile analysis technique was used, as discussed in Section 6-4. Figure 6-8 shows a plot of the n data calculated using the uniform flow and the GVF methods versus y for the block boundary roughness. The plotted data show good agreement between the two methods.

The uniform flow data in Figure 6-8 show that, for the block roughness, n varies ($0.087 \geq n \geq 0.038$) with changes in uniform flow depth ($0.13 \leq y \leq 0.9$). Analysis of various truncated sections of a single GVF profile using the GVF n method also produced different predictive values for n, suggesting that n is also variable with depth (and velocity) throughout a GVF profile. Based on the variable nature of n with y in the GVF profiles, the predicted normal depths (y_n) associated with the variable n values would also vary. Consequently, based on the good correlation between the uniform flow and GVF n data presented in Figure 6-8, $y_{average}$, the average value of y in the measured GVF profile, was selected as the representative flow depth parameter in this analysis for calculating R_h, Re, V, etc. For flow conditions where uniform flow developed, $y_{average} = y_n$. The four boundary roughness materials were tested over a range of channel slopes and discharges.

7.5 Discussion and Results

For Manning's n coefficient to remain constant for a given channel lining material, independent of stage and discharge, the following two conditions must be met:

1. The mean flow velocity can be represented by an equation in the form of Equation 7-6.
2. x' will equal ⅔, independent of the channel lining material.

If these conditions are not met, then n must vary in order to match Equation 7-4 with the actual head-discharge relationship. Conditions 1 and 2 were tested by plotting $\log(V/S_e^{1/2})$ versus $\log(R_h)$ using data from Bazin (1865) and the current study. To satisfy Condition 1, the data should be well represented by a linear equation of the form of Equation 7-10. In Equation 7-10, C is equal to the y-intercept on the plot, and x' is the slope. The corresponding x' values are presented in Table 7-2.

$$\log\left(\frac{V}{S_e^{1/2}}\right) = C + x' \log\left(R_h\right) \tag{7-10}$$

The x' values corresponding to Bazin's data in Table 7-2 are consistent with those calculated and reported by Manning (1889) for the same data sets. The r^2 values [coefficient of determination applied to the linear relationship of $\log(V/S_e^{1/2})$ versus $\log(R_h)$] in Table 7-2, which are all ≈1.0, indicate that V is relatively well represented by Equation 7-6, and Condition 1 is satisfied.

However, according to the x' data presented in Table 7-2, which vary and are boundary roughness specific, Condition 2 is not met. The smoother roughness boundary x' values (e.g., pure cement, cement/sand mix, and acrylic) are approximately

Table 7-2. Optimal x' values.

Boundary Roughness Material	Description	x'	r^2
Bazin Study (1865)			
Pure Cement	Pure cement lining	0.676	0.998
Cement-Sand Mix	2/3 cement, 1/3 fine sand mix	0.684	0.994
Small Gravel	Diameters ranging from 0.36 in. to 0.84 in.	0.721	0.997
Large Gravel	Diameters ranging from 1.2 in. to 1.56 in.	0.822	0.999
Laths of Wood (Corrugations)	0.36 in. tall, 1.1 in. wide, spaced 1.92 in. apart, oriented normal to flume centerline	0.732	0.997
Current Study			
Acrylic	Acrylic lining of flume boundary (see Figure 6-2)	0.644	0.982
Metal Lath	Commercially available expanded metal lath with a thickness of 0.125 in. (see Figure 6-3)	0.795	0.989
Trapezoidal Corrugations	1.5 in. in height, top width of 1.5 in., and bottom width of 4.5.in., spaced 1.5 in. apart, oriented normal to flume centerline (see Figure 6-6)	0.968	0.968
Blocks	4.5 in. wide by 3.5 in. long by 1.5 in. tall, with the top edges rounded (1-in. radius round-over) (see Figure 6-4)	1.160	0.997

equal to the ⅔ value used by Manning (see Equation 7-4). For the rougher boundaries, x' varied significantly (up to 1.16 for the blocks). Figure 7-1 illustrates the relevance to the assumption of a constant roughness coefficient of the different x' values associated with Equation 7-6.

Figure 7-1 compares the roughness coefficients from three different versions of Equation 7-6: the Chezy Equation (Equation 7-2) or Darcy-Weisbach (Equation 7-3) Equation (where $x' = ½$), Manning's Equation (Equation 7-4) ($x' = ⅔$), and Equation 7-6 where x' is varied per Equation 7-10 in order to maintain a constant n value (n_{opt}). For convenience, the hydraulic roughness coefficient results in Figure 7-1 are all presented in terms of an equivalent n value (n_{eq}). This was done by replacing C in Equation 7-6 with K_n/n_{eq} and noting that $K_n = 3.281^{(1-x')}$ for the individual boundary roughness materials (i.e., x' varies with boundary roughness type).

Figure 7-1(A) presents n_{eq} versus R_h for the pure cement lining data reported by Bazin (1865). The data show a variable n_c; n and n_{opt} are relatively constant and equal. The constancy of n and n_{opt} is due to the fact that Conditions 1 and 2 are both satisfied. The Manning's n data for the acrylic and the cement-sand mixture boundary conditions (not presented) had similar x' values to the pure cement and behaved similarly.

Figures 7-1(B) and (C) present the data for the large gravel roughness (Bazin, 1865) and the block roughness, respectively. These figures show examples where Condition 2 is not met and, therefore, Manning's Equation requires a variable n value to match the results of the experimental data. While Manning's Equation (Equation 7-4) improves upon the Chezy Equation (Equation 7-2)—that is, the difference between the maximum and minimum n_{eq} values decreases from 0.0124 (n_c curve) to 0.008 (n curve)—the roughness coefficient is not constant unless x' of Equation 7-6 is optimized for these specific boundary roughness materials, as evidenced in the n_{opt} curve.

The results clearly indicate that either x' or the boundary roughness coefficient (n, f, or C) must vary to accurately describe the hydraulic behavior of the stage-discharge relationship as R_h varies. Although some research has suggested correcting Manning's Equation by changing x' (Blench, 1939), more recent research has focused on variable roughness coefficient predictive techniques (Limerinos, 1970; Bray, 1979; Griffiths, 1981; Bathurst et al., 1981; Jarret, 1984; Ugarte and Madrid, 1994; and Bathurst, 2002) for use in Equations 7-2, 7-3, and/or 7-4. Equation 7-9 shows that using the power law equation to determine a variable hydraulic roughness coefficient is basically the equivalent of changing the x' value of Equation 7-6 and applying a constant roughness coefficient.

These power law equations are generally developed for a specific boundary roughness type with the underlying assumption that the equation applies to a range of roughness element sizes (generally characterized by k). For example, Bray (1979) and Griffiths (1981) present equations developed for channels with rigid gravel beds; Bathurst (2002) presents an equation for mountain streams. Each of these equations uses a k value defined by gravel D_r. They assume that a single x' value may apply to a range of roughness element sizes that can be characterized by a common D_r value for a certain type of boundary roughness.

The r^2 value reported for the Bray (1979) and Griffiths (1981) equations are 0.355 and 0.591, respectively, suggesting that a considerable amount of scatter exists in the data. Griffiths (1981) attributes the scatter to inadequate descriptions of the channel reach and hydraulic variables, restrictions and errors in data collection procedures, irregularities in the alignments and channel cross-sections, and the rugged bed topography.

Bathurst (2002) found that if the data were divided into groupings based on channel similarities, the scatter decreased significantly (increased r^2 values). Dividing the data into two groups resulted in two equations with x' values of 1.047 and 1.43, respectively. The difference in these two x' values was attributed to differences in the channel slope: 1.047 for $S_e <$ 0.8% and 1.43 for $S_e >$ 0.8%.

The results from the current study (see Table 7-2) suggest that roughness element size may have a significant effect on the value of x'. The Bazin (1865) gravel data produced x' values equal to 0.721 and 0.822 for the small and large gravel tests. The block data, which are somewhat representative of a rigid gravel or small cobble bed (flow can pass over and around the projecting roughness elements), produced an x' value equal to 1.16, suggesting that x' increases with increasing gravel or roughness element size. The smoothest boundary materials (acrylic, pure cement, and cement-sand mix) produced the smallest and relatively constant x' values of 0.644, 0.676, and 0.684, respectively. The corrugated boundary roughness materials produced increasing x' values with increasing corrugation size ($x' = 0.732$ for Bazin's "laths of wood" and $x' =$ 0.968 for the relatively larger trapezoidal corrugations).

For the roughness materials evaluated in this study, channel slope was not a significant factor of the x' value (i.e., the data in Figure 7-1(C) fall on a single curve regardless of the channel slope). Although Bathurst (2002) points out differences between the channel geometries and typical boundary roughness materials used in flume studies and those found in natural mountain streams, both the Bathurst (2002) results and the current study indicate that x' is dependent on more than simply the roughness material type or channel geometry. Therefore, an equation in the form of Equation 7-6, with a constant hydraulic roughness coefficient, will not accurately describe the stage-discharge relationship for a general boundary type classification such as gravel channels. x' will vary with the size, density, spacing, and alignment of the boundary roughness elements.

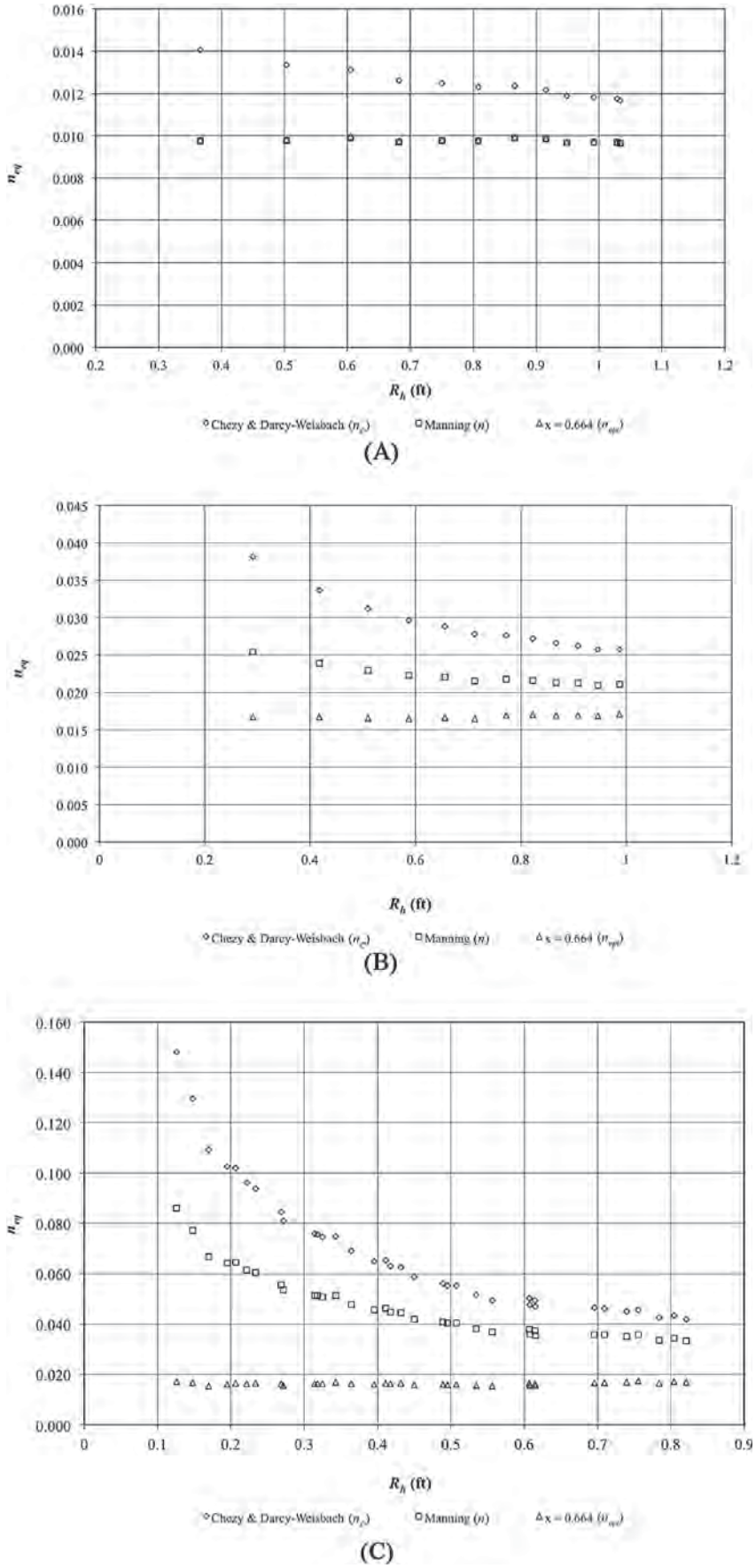

Figure 7-1. Equivalent Manning's* n *coefficients* (n_c, n, *and* n_{opt}) *for pure cement (data from Bazin, 1865) (A), large gravel (data from Bazin, 1865) (B), and block (C) roughness data.

The prospect of developing equations specific to the boundary roughness type as well as the size, density, and distribution of the individual roughness elements is a somewhat daunting task. Manning's (1889) original intent was a single simple equation that would produce "sufficiently accurate" results considering the information available. It is interesting that Manning's $x' = ⅔$ and his boundary-specific, constant n assumption have withstood the test of time for so long considering the resulting range of required x' values determined in this and other studies required to support a constant n value. A closer look at the data provides insight on the longevity and relative reliability of Manning's Equation.

The x' values reported in Table 7-2 represent the data with a single optimized head-discharge curve. Figure 7-2 presents $\log(V/S_e^{1/2})$ versus $\log(R_h)$ plots for the acrylic, metal lath, block, and trapezoidal corrugation channel lining material data in Figure 7-2 are better represented by two linear trend lines, each with a different slope (x'), as described by Equation 7-10. Consistent with Manning's Equation (Equation 7-4), the acrylic data correlated well with the $x' = ⅔$ trend line slope represented on the plot by a dashed line. The metal lath and the trapezoidal corrugation data sets both exhibit variable dependence on R_h as shown by the two distinct trend lines of differing slope corresponding to the "higher" and "lower" R_h data ranges. x' values for the higher R_h data ranges (metal lath and trapezoidal corrugation data) are reasonably represented by $x' = ⅔$ (Manning's Equation). The smaller R_h data ranges for both data sets require $x' > ⅔$ to match the experimental data (e.g., $x' = 0.9$ for the metal lath and $x' = 1.25$ for the trapezoidal corrugations are required to better match the larger R_h experimental data). The block data correspond to a single linear trend line with $x' = 1.2$. This result, however, may be due only to the fact that sufficiently high R_h values could not be achieved in the test facility to identify a range of R_h where the $x' = ⅔$ is appropriate. Note that the higher R_h block data (top 7-8 data points) are beginning to deviate from the trend line slightly. In summary, the acrylic boundary (over the full range of R_h) and the metal lath and trapezoidal corrugation channel lining materials at larger R_h values produced an $x' = ⅔$. For all other conditions, including the block channel lining material, alternate x' values were required in order to fit the data for each of the roughness materials.

These results suggest that Conditions 1 and 2 are met when either the roughness boundary itself is smooth (e.g., the acrylic and cement boundaries) or at higher R_h values for rougher boundaries. This finding is consistent with the *quasi-smooth* boundary condition theory discussed in Chapter 6, where stable eddies form between the roughness elements of the rougher boundaries, creating a *quasi-smooth* flow condition above the roughness elements. The acrylic and cement boundaries represent *smooth-flow* boundary conditions. When x' for the rougher boundary materials is equal to ⅔ (larger R_h values), the flow condition is consistent with the *quasi-smooth* boundary condition. When channels lined with rougher boundary materials operate outside of the *quasi-smooth* flow condition, then Conditions 1 and 2 are no longer met, $x' \neq ⅔$, and/or n cannot be considered constant. The longevity and relative reliability of the use of Manning's Equation (Equation 7-4) with boundary-specific constant n values suggests that many of the channels used in practice have relatively smooth flow boundaries (e.g., cement-lined channels) or that they may commonly operate in the *quasi-smooth* flow condition.

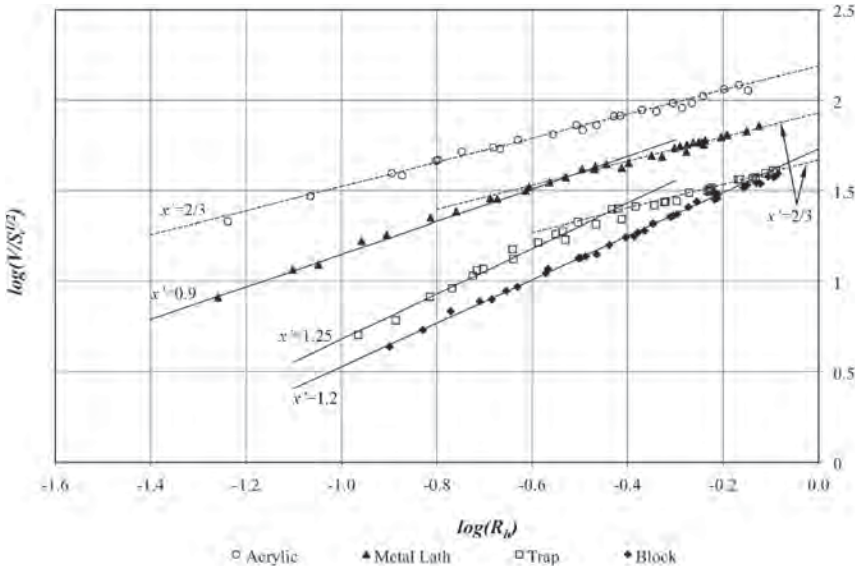

Figure 7-2. Plot of log(V/$S_e^{1/2}$) versus log(R_h) data for acrylic, metal lath, block, and trapezoidal corrugation boundary roughness materials.

7.6 Conclusions

When applying Manning's Equation, the assumption is often made that n is a constant value, independent of flow depth and discharge for a given channel lining material. An inspection of the experimental data from the current study and from Bazin's (1865) showed that the applicability of the constant n assumption diminishes as the roughness of the boundary increases. To produce a constant n value for a given boundary roughness material at all flow conditions, the mean velocity must be well represented by an equation in the form of Equation 7-6, and the representative x' coefficient must equal ⅔. This study evaluated these two conditions for a range of boundary roughness materials and produced the following conclusions:

1. The data showed that Equation 7-6 provided a relatively good overall fit to the data for each of the lining materials tested.
2. Only the smooth boundary materials (e.g., acrylic sheeting and pure cement) produced an $x' = ⅔$, based on the Equation 7-6 relationship for the entire range of R_h tested. x' was found to be a unique value for each boundary material tested, ranging from 0.644 (acrylic sheeting) to 1.16 (blocks), with the x' value increasing with increasing boundary roughness.
3. Relative to the other hydraulic roughness coefficients (C_c and f), Manning's n exhibited less variability with respect to changes in R_h (see Figure 7-1). As R_h increases, n approaches becoming or becomes constant. Based on the range of flow conditions tested (in a rectangular flume), the range of R_h values over which n is constant decreases as the roughness of the boundary material increases. For very smooth boundaries (e.g., acrylic sheeting), n was approximately constant over the entire range of R_h tested.
4. The value of x' that corresponds to Equation 7-6 varied with boundary roughness material type and R_h. The metal lath and trapezoidal corrugation data in Figure 7-2 show that two separate linear curves that correspond to different x' (Equation 7-6) values are required in order to match the experimental data. This means that over the range of R_h tested, a constant n value cannot be applied to these boundary roughness materials when using Manning's Equation (Equation 7-4) with $x' = ⅔$. Manning's Equation with a constant n value gives a good representation of the data at larger R_h values where *quasi-smooth*-type flow conditions exist. The block data also showed evidence that at larger R_h values there would be a shift in the x' value. Sufficiently high R_h data for the blocks were not obtainable with the experimental test setup to confirm the high R_h block x' value.
5. The results of this study show that Manning's n will not likely be a constant value for canals, streams, and rivers with rough boundaries such as large gravels and cobbles unless the R_h is sufficiently large. The limiting R_h above which *quasi-smooth* flow conditions exist and n becomes constant will be specific for each boundary roughness type and must be determined by testing.

CHAPTER 8

Open Channel Flow Resistance: Composite Roughness

8.1 Summary

Composite roughness in open channel flow describes a condition where different roughness materials line different parts of a channel cross-section. Some examples of composite roughness channels include concrete rectangular or trapezoidal channels where the channel invert has been covered with sand and/or gravel as a result of sediment transport; vegetation can also be present in the channel invert. Fish passage culverts, such as those discussed in Chapter 2, are another example of composite roughness channels. Most open channel flow problems are solved using Manning's Equation. Estimating the head-discharge relationship for composite roughness channels poses a unique challenge because Manning's Equation is a one-dimensional head-discharge relationship that is being applied to what are very likely three-dimensional flow problems. Ideally, a representative Manning's n hydraulic roughness coefficient would be defined that accounts for the three-dimensional nature of the composite roughness flow condition.

A literature search produced a list of 16 different relationships that have been proposed for estimating representative composite roughness n values, referred to as n_e, which are dependent upon the n values of the individual channel lining materials, referred to as n_i, that make up the composite roughness boundary geometry. The degree to which these relationships have been evaluated against experimental composite roughness data is limited. In this study, 12 different composite roughness channel configurations were tested in a rectangular laboratory flume, using combinations of the boundary roughness materials evaluated in Chapter 6 (acrylic sheeting, metal lath, blocks, and trapezoidal corrugations). The composite roughness configurations were categorized into three different channel types: Type I featured rougher walls and a smoother floor, Type II featured smoother walls and a rougher floor, and Type III featured rough walls and floor. The 16 different n_e relationships, which use a weighted average of the n_i values that is based on a corresponding flow subarea and/or wetted perimeter to each roughness material comprising the composite roughness boundary, were evaluated along with different methods for evaluating n_i. It was determined that for hydraulically rougher boundary roughness materials where n varies with flow conditions (e.g., n varied with R_h/K for all of the materials tested except for the smooth acrylic sheeting) the variation in n_i should be applied to the n_e relationships. In general, some of the relationships performed worse than the others, but no relationship proved to be more accurate than the other predictive relationships for all composite roughness configurations. The predictive error, which was represented by root-mean-square (*RMS*) values, ranged from approximately 5 to 90%, with the majority of the methods producing *RMS* values in the range of 5 to 20%.

Based on the fact that the more complicated n_e predictive methods didn't produce more accurate results than the simpler n_e predictive methods, the simpler n_e predictive methods are recommended, namely the Horton method, with the caveat that the level of uncertainty can still be significantly high. It should also be noted that even though the range of hydraulic roughness boundary materials (n_i) was broader, the number of composite roughness geometries tested (12) was larger, and the number of n_e relationships evaluated was significantly larger than in previous studies. The applicability of the test results to channels with cross-sections that are different than the one tested in this study, as well as applicability to composite roughness geometries that feature irregular roughness element patterns (the individual boundary roughness elements used in this study all feature uniform roughness element patterns) have not been determined. Until more accurate data are available, the results from this study are recommended as a first-order approximation for composite roughness problems in practice. The inclusion of a reasonable factor of safety is also recommended.

8.2 Introduction

It is not uncommon in open channel flow field applications for the wetted perimeter of a cross-section to be made up of more than one roughness material [e.g., concrete channels with the invert covered in sediment, gravel, and/or vegetation or buried-invert culverts (see Chapter 2)]. Yen (2002) refers to such channels as composite channels. The composite channel flow resistance will be a function of the combined effects of the individual flow boundary roughness materials. The most commonly used open channel flow equations (Manning, Chezy, Darcy-Weisbach), however, are one-dimensional and are limited to a single, representative hydraulic roughness coefficient. Yen (2002) published 16 different composite Manning's n (n_e) relationships (see Table 8-1) as possible candidates for use with Manning's Equation (Equation 8-1) to predict flow resistance in composite channels.

$$V = \frac{K_n}{n_e} R_h^{2/3} S_e^{1/2} \tag{8-1}$$

Table 8-1. Composite channel n_e relationships.

Name	n_e	Secondary Assumptions	Equation
Mean velocity assumption methods			
Horton	$= \left[\frac{\sum n_i^{3/2} P_i}{P}\right]^{2/3}$	$S_I = S_o$	Eqn. (8-2)
Colebatch	$= \left[\frac{\sum (n_i^{3/2} A_i)}{A}\right]^{2/3}$	Same as Horton but adjusted by a factor of $C = R_{wall}/R_{base}$	Eqn. (8-3)
Total force assumption methods			
Pavlovskii	$= \sqrt{\frac{\sum n_i^2 P_i}{P}}$	Yen (2002): $V_i/V = (R_i/R)^{1/6}$ or Flintham & Carling (1992): $V_i = V$ and $R_i = R$	Eqn. (8-4)
Total F2	$= \sqrt{\frac{n_i^2 A_i}{A}}$	$V_i/V = (R_{hi}/R_h)^{2/3}$	Eqn. (8-5)
Total F3	$= \sqrt{\frac{R_h^{1/3}}{P} \sum \frac{n_i^2 P_i}{R_{hi}^{1/3}}}$	$V_i = V$	Eqn. (8-6)
Total F4	$= \sqrt{\frac{\sum n_i^2 P_i R_{hi}^{2/3}}{P R_h^{2/3}}}$	$V_i/V = (R_{hi}/R_h)^{1/2}$	Eqn. (8-7)
Total discharge assumption methods			
Lotter	$= \frac{P R_h^{5/3}}{\sum (P_i R_{hi}^{5/3}/n_i)}$	$S_i = S_o$	Eqn. (8-8)
Lotter II	$= \frac{\sum P_i R_{hi}^{5/3}}{\sum (P_i R_{hi}^{5/3}/n_i)}$	–	Eqn. (8-9)
Total Q1	$= \frac{A}{\sum (A_i/n_i)}$	$S_i/S_o = (R_{hi}/R_h)^{4/3}$	Eqn. (8-10)
Total Q2	$= \frac{P}{\sum (P_i/n_i)}$	$S_i/S_o = (R_{hi}/R_h)^{10/3}$	Eqn. (8-11)
Total Q3	$= \frac{P R_h^{7/6}}{\sum (P_i R_{hi}^{7/6}/n_i)}$	$S_i/S_o = (R_{hi}/R_h)$	Eqn. (8-12)
Total shear velocity assumption methods			
LAD	$= \frac{\sum n_i A_i}{A}$	$V_i/V = (R_{hi}/R_h)^{7/6}$	Eqn. (8-13)
TexDOT	$= \frac{\sum n_i P_i}{P}$	$V_i/V = (R_{hi}/R_h)^{1/6}$	Eqn. (8-14)
Total U*1	$= \frac{\sum (n_i P_i / R_{hi}^{1/6})}{P/R_h^{1/6}}$	$V_i = V$	Eqn. (8-15)
Total U*2	$= \frac{\sum n_i P_i \sqrt{R_{hi}}}{P\sqrt{R_h}}$	$V_i/V = (R_{hi}/R_h)^{2/3}$	Eqn. (8-16)
Total U*3	$= \frac{\sum (n_i P_i R_{hi}^{1/3})}{P R_h^{1/3}}$	$V_i/V = (R_{hi}/R_h)^{1/2}$	Eqn. (8-17)

– indicates no secondary assumptions

In Equation 8-1, V is the mean velocity, K_n = 1.49 (1.0 SI units), R_h is the hydraulic radius [the ratio of the flow area (A) to the wetted perimeter (P)], and S_e is the friction slope, which at uniform depth is equal to the channel slope. The n_e relationships published by Yen (2002) are based on various techniques for weighting the resistance of the individual boundary roughness materials in the channel cross-section. This is accomplished by partitioning A and/or P (resulting in component A_i and/or P_i values) between the boundary roughness materials and applying the individual n values of the boundary roughness materials, referred to as component n values (n_i), to each partitioned section. The result is a single, representative n_e value that then is applied to Equation 8-1.

Previous studies compared relatively small subsets of the n_e relationships listed in Table 8-1 (Pillai, 1962; Cox, 1973; Flintham and Carling, 1992); in total, the performances of 5 of the 16 n_e relationships presented by Yen (2002) have been evaluated using experimental data. Yen (2002) states that the amount of published data available for composite channels is limited and therefore it is yet to be determined which of the 16 predictive n_e relationships is best suited for use. The current study provides an expanded experimental data set for evaluating the performance of the 16 n_e relationships using combinations of the four boundary roughness materials (acrylic sheeting, metal lath, trapezoidal corrugations, and blocks) discussed in Chapter 6.

The n_i values for the individual boundary roughness materials used in the current study ranged from n_i = 0.0096 for the smooth acrylic sheeting to n_i = 0.033 to 0.086 (R_h or R_h/k dependent) for the blocks. This range of n_i values exceeded the range of hydraulic roughness values evaluated in the previous studies (Pillai, 1962; Cox, 1973; Flintham and Carling, 1992). The composite channel flow resistance testing of the current study includes 12 different composite channel lining combinations of the individual lining materials.

According to Flintham and Carling (1992), the accuracy of n_e relationships should be dependent upon two factors: (1) the method used to partition the channel cross-sectional flow area into the subareas directly influenced by each roughness material lining the boundary and (2) an accurate determination of the n_i values. The influence of the flow area partitioning technique on n_e was found by Flintham and Carling (1992) to be relatively negligible when compared to the significance of the n_i values selected. This study examines the behavior of n_i (the dependence of n_i on R_h in a uniformly lined channel) and the influence of n_i on the n_e relationships.

8.3 Background

Component *n* values (n_i)

Chow (1959) states that the most difficult task in the use of Equation 8-1 is assigning a roughness coefficient (n) value and that the inexact methods for doing so range from guesswork to empirical relationships. Although the n_e relationships in Table 8-1 are fundamentally based on channel geometry and the distribution of hydraulic roughness boundary materials over the wetted perimeter, there remains a certain level of uncertainty in n_e due to the inherent uncertainty associated with specifying n_i. The relationship between n (or n_i) and Re, R_h/k, and other factors is discussed in Chapters 6 and 7.

Manning's objective in developing the one-dimensional, open channel flow equation (Equation 8-1) was to find a relationship where the hydraulic roughness coefficient (n) would be constant (dependent only on k and independent of the flow conditions). After evaluating Equation 8-1 (using the constant n assumption for boundary roughness) using numerous experimental data sets, Manning (1889) concluded that the equation was "sufficiently accurate." Chow (1959) states that, in general, n is not constant but decreases with increasing stage for most streams, a fact that was confirmed in Chapters 6 and 7. Other studies, meanwhile, have shown that n can vary with stage, discharge, and slope in certain uniformly lined channel applications (Limerinos, 1970; Bray, 1979; Bathurst et al., 1981); Yen (2002) recommends that n may be considered nearly a constant and almost independent of flow conditions. These apparent contradictions suggest that some level of uncertainty still exists regarding the appropriateness of the constant n assumption and Manning's Equation.

The n (or n_i) data for this study were determined in the rectangular test flume, uniformly lined with each boundary material separately. The n_i data, the constant and/or variable nature of which depends in part upon the boundary roughness (k) and R_h, are presented in Figure 8-1 for the smooth acrylic sheeting, metal lath sheeting, blocks, and trapezoidal corrugations.

The acrylic sheeting Manning's n data in Figure 8-1, which represents the smoothest boundary roughness material tested, remain relatively constant over the full range of R_h tested. The metal lath and trapezoidal corrugation n values vary with R_h over the lower 20 to 30% of the data range and are relatively constant above that limit. The block data varies over the full range of R_h tested; however, the fact that the block n data appears to be approaching a constant value suggests that the absence of a constant n range in the experimental data set is likely due more to flow capacity limitations than boundary roughness characteristics. These same boundary roughness materials were used to create the composite channel linings in the current study; the data in Figure 8-1 were used to generate the n_i values used in evaluating the n_e relationships in Table 8-1. The boundary roughness materials are identified in this chapter as follows: A (acrylic sheeting), B (metal lath), D (blocks), and E (trapezoidal corrugations). For all composite roughness test configurations, a common roughness material was used on the walls and a different roughness material was used on the floor.

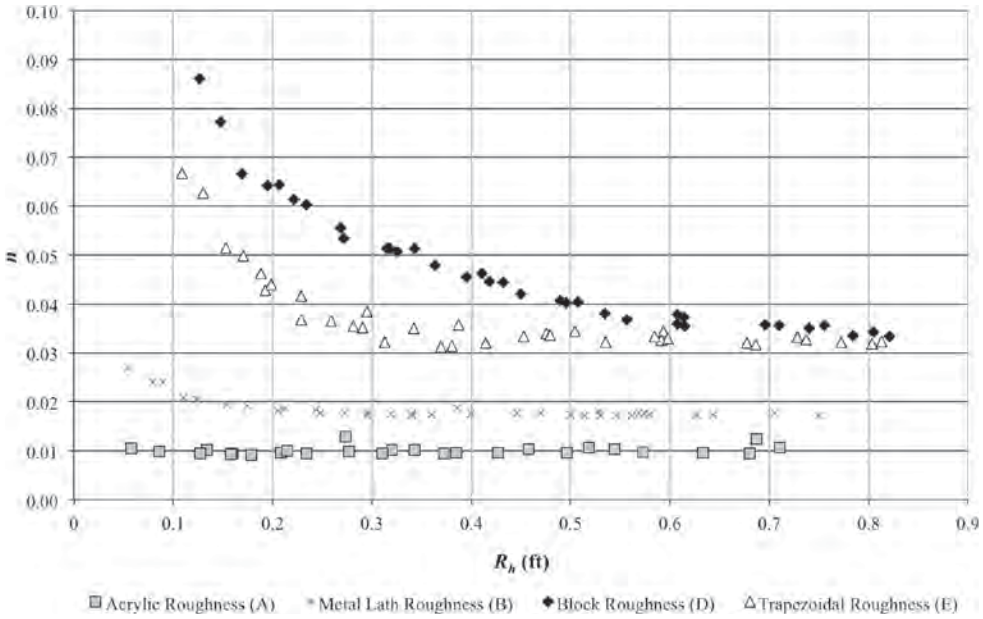

Figure 8-1. Manning's* n *data from channels with uniform roughness materials.

Composite Manning's *n* (n_e) Equations

The 16 n_e relationships listed in Table 8-1 are divided into four groups based on the main assumption used in their derivation. These assumptions are as follows:

- ***The Mean Velocity Assumption:*** The mean velocity in the cross-sectional flow subarea associated with each boundary roughness material is equal to the mean velocity of the entire channel cross-section.
- ***The Total Force Assumption:*** The sum of the forces resisting the flow in each subarea is equal to the total force resisting the flow in the channel.
- ***The Total Discharge Assumption:*** The sum of the subarea discharges is equal to the total channel discharge.
- ***The Total Shear Velocity (U*) Assumption:*** The weighted sum of the shear velocities of each subarea is equal to the total shear velocity of the channel.

Secondary assumptions are also typically required for the derivation of these equations. The secondary assumptions for each relationship, where applicable, are also listed in Table 8-1.

The n_e relationships shown in Table 8-1 are dependent on the way in which subareas of the channel cross-sectional flow area are apportioned to each boundary roughness material comprising the composite wetted perimeter. In Equations 8-2 through 8-17, R_{hi} is equal to the ratio of A_i to P_i ($R_{hi} = A_i/P_i$) and the subscript i denotes the different subareas of the channel cross-section associated with each of the roughness material components comprising the wetted perimeter. Two different subarea partitioning techniques are illustrated in Figure 8-2 (the 90° velocity contour bisecting method and the angle bisecting method for a rectangular channel cross-section).

Komora (1973) recommended that the cross-sectional flow area of a composite channel be subdivided by curves that intersect the cross-sectional velocity contours at right angles, as depicted in Figure 8-2. This requires detailed velocity data that are not likely to be available for most practical applications. To avoid this complication, Colebatch (1941) recommended using a straight line to bisect the angle at the point of the boundary roughness change (e.g., In Figure 8-2, the 45°-angled lines from the corner separate the flow subareas in the rectangular channel featuring different boundary roughness materials on the floor and walls). Flintham and Carling (1992) compared both methods to their data set and concluded that there were no obvious advantages with either subarea delineation method. For convenience, the angle bisection method was used throughout this study for the n_e equations.

Wherever the subarea dividing line is drawn, it is assumed that shear stress is equal to zero along that boundary (although not necessarily true). Consequently, only wetted perimeters corresponding to physical channel boundaries (P_i) are included in flow resistance calculations, as shown in Figure 8-2. Flow boundaries between adjacent subareas are not included as part of the P_i dimension (Yen, 2002).

Previous Studies

Three published studies were reviewed that evaluated the effectiveness of various subsets of the n_e relationships shown in Table 8-1. Each study featured a unique set of composite channel boundary roughness materials and configurations.

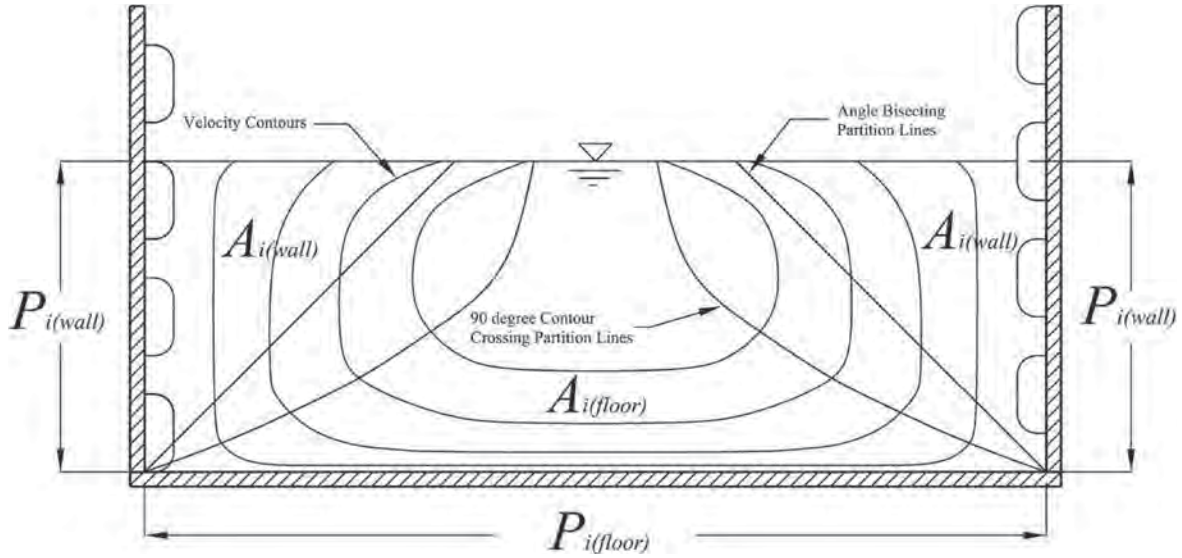

Figure 8-2. Cross-sectional area partitioning of subareas.

The experimental composite channel results were compared with the predictive n_e relationships.

Pillai (1962) studied composite roughness flow resistance in both rectangular and trapezoidal channels and evaluated the Horton (1933), Pavlovskii (1931), and Lotter (1933) n_e relationships using two different boundary roughness materials described as (1) smooth cement with fine sand and (2) cement plastered with gravel that passes a ½-in. sieve and was retained on a ¼-in. sieve. Pillai (1962) selected n_i as the average experimental n value ($n_{average}$) for each boundary roughness material, which values were reported as 0.009836 (cement and fine sand mix) and 0.0178 (cement and gravel). Of the three relationships evaluated by Pillai (1962), the Lotter relationship was the only one requiring subarea delineation. Lotter's relationship was only applied to the trapezoidal channel data where the subareas were divided using vertical lines originating at the corners of the channel cross-section. Pillai (1962) concluded that the Horton relationship performed the best and that the Lotter relationship gave inconsistent results.

Cox (1973) conducted composite roughness testing in a rectangular channel using the bisecting angle method for subarea delineation. Two roughness materials were tested, a plastic-coated plywood ($n = 0.0095$) and crushed limestone particles that passed a No. 4 sieve and were retained on a No. 8 sieve ($n_{average} = 0.0165$). Cox (1973) compared the Horton (1933), Colebatch (1941), and Los Angeles District (LAD) relationships and recommended the LAD and Colebatch relationships over the Horton.

Flintham and Carling (1992) studied composite roughness in a trapezoidal channel using the bisecting angle method for subarea delineation. Three roughness materials were tested: plywood, 0.24-in.-diameter gravel, and 0.55-in.-diameter gravel. The reported average Manning's n values for the 0.24-in. and 0.55-in. gravels were 0.019 and 0.022, respectively (the plywood n was not published). Flintham and Carling (1992) were the only ones to use n_i values that varied by boundary material in their analysis. They concluded that, with respect to the boundary roughness materials tested, using the varying n_i values improved the accuracy of the predictive relationships relative to using average n values. Their study was limited, however, to channel roughness configurations where the floor roughness exceeded the sidewall roughness. Flintham and Carling (1992) evaluated the Horton, Colebatch, Pavlovskii, and Lotter methods. They concluded that the Pavlovskii relationship was the most accurate, the Horton and Colebatch relationships were satisfactory, and the Lotter relationship performed poorly.

Four of the five relationships evaluated in the three different studies were identified at least once as a "best performer," but consensus was not achieved regarding an overall best method. The Lotter relationship, on the other hand, was singled out in each study as "not recommended for use." In the current study, all 16 predictive n_e relationships were evaluated against the experimental data set developed in the study. The number of boundary roughness materials tested in the current study (four), exceeded the number of roughness materials tested in any of the three previous studies. The diversity in composite roughness channel lining configurations and the hydraulic roughness characteristics of the boundary roughness materials used in the current study were also broader than those used in the previous studies.

8.4 Experimental Setup

All composite roughness testing was conducted in a 4-ft-wide by 3-ft-deep by 48-ft-long rectangular flume. Flow was supplied to the flume through either 8-in. or 20-in. diameter supply piping. Each supply pipe contained a calibrated orifice flow meter.

Four boundary roughness materials were used in this study:

- Acrylic flume walls and floor used as a smooth surface (see Figure 6-2),
- A commercially available metal lath sheeting material measuring ⅛-in. in height (see Figure 6-3),
- Wooden blocks that were 3.5 in. long (in the flow direction), 4.5 in. wide, and 1.5 in. tall, with a 1-in. radius rounded top edge (see Figures 6-4 and 6-5), and
- Trapezoidal corrugations that were 1.5 in. tall, 4.5 in. wide at the base, and 1.5 in. wide at the top (see Figures 6-6 and 6-7).

The blocks were attached to a plywood base in a staggered pattern with 1.83 in. between blocks, as shown in Figure 6-5. The trapezoidal strips were also attached to a plywood base and oriented perpendicular to the flow direction at a spacing of 1.5 in., as shown in Figure 6-7. The acrylic, metal lath, block, and trapezoidal corrugation roughness materials are hereafter identified as boundary roughness materials A, B, D, and E, respectively.

Manning's n data for each boundary roughness material were determined as described in Section 6-4. The n data for Material A were relatively constant ($n_{average}$=0.0096), as shown in Figure 8-1. The n data for materials B, D, and E varied with R_h (see Figure 8-1) and trend line functions were used to represent n_i in the n_e calculations.

Twelve different composite channel geometries were created through various combinations of the materials A, B, D, and E. In all cases, the channel sidewalls featured a common boundary roughness material while the floor featured another. The three-letter notation for the composite roughness configurations represents the sidewall, floor, and sidewall boundary roughness materials. The following combinations were tested: ABA, BAB, ADA, DAD, BDB, DBD, AEA, EAE, BEB, EBE, EDE, and DED. An example of the BDB composite roughness configuration (metal lath on the sidewalls and wooden blocks on the floor) is shown in Figure 8-3. The same procedure discussed in Section 6-4 to determine n_i for the uniform channel roughness lining tests was also used to determine the experimental composite n_e.

The composite roughness channel configurations were also categorized into three channel types. A Type I channel is one where the floor roughness exceeds the wall roughness (e.g., ABA, ADA, BDB, AEA, BEB); a Type II channel is one where the wall roughness exceeds the floor roughness (e.g., BAB, DAD, DBD, EAE, EBE); and a Type III channel is one where the walls and floor both feature "large roughness element" boundary materials of different types (e.g., EDE, DED).

8.5 Experimental Results

Optimization of the n_e Relationship

The results of the comparison between the experimental n_e data and the 16 n_e relationships shown in Table 8-1 were quantified using the *RMS* (Equations 8-18 and 8-19). Doubling the *RMS* represents a 95% confidence interval.

$$RMS = \sqrt{\frac{\Sigma PE^2}{samples}} \tag{8-18}$$

$$PE = \frac{predicted - measured}{measured} * 100 \tag{8-19}$$

In Equations 8-18 and 8-19, *PE* is the percent predictive error and *samples* represents the total number of data points sampled. The bias is the mean value of *PE*. *RMS* values of each equation were calculated for both the individual composite channel configurations (EAE, BDB, etc.) and each of the composite channel types (Types I, II, and III). The bias of each equation was also determined.

Flintham and Carling (1992) emphasized the sensitivity of the specific n_i values assigned to represent the individual roughness boundaries in a composite roughness channel when calculating n_e. Three different methods for determining n_i were used in the current study in an effort to investigate the influence of the R_h dependence of n_i on n_e. Method 1 assumed

Figure 8-3. Examples of composite roughness channel types: Type I (BDB) (A), Type II (DAD) (B), and Type III (EDE) (C).

a constant n_i value for each material that corresponds to the large-R_h constant n_i values shown in Figure 8-1 instead of the average n_i value as used by Flintham and Carling (1992). The constant n_i value for material D was estimated by extrapolating the experimental data trend to larger R_h values ($n_i = 0.0335$). Method 2 assumed that the $n_i = F(R_{hi})$ relationships for the composite roughness channel subareas are equal to the $n = F(R_h)$ relationships for the uniformly lined channel data (i.e., n_i for each subarea was calculated based on R_{hi} for that subarea). Method 3 is similar to Method 2 except that n_i for each subarea was calculated using R_h (the total channel hydraulic radius) rather than R_{hi} [i.e., $n_i = F(R_h)$]. The *RMS* values for the trend line functions used to predict n_i (using the n versus R_h data presented in Figure 8-1) for boundary roughness materials A, B, D, and E were 4.5%, 2.43%, 3.04%, and 4.29%, respectively.

The resulting total *RMS* values—based on a combined data set from all composite channel configurations (e.g., ADA, BEB, etc.) in each channel type (Types I, II, or III) of the individual relationships in Table 8-1—are presented in Table 8-2 according to channel type and method, or combination of methods, applied to determine n_i. Similar to the findings of previous studies, the Lotter (1933) relationship performed inconsistently with respect to its ability to match the experimental data from this study. The inconsistent results are shared by all the relationships within the total discharge assumption n_e group and, as a result, the outcome for the total discharge assumption relationships will be discussed separately from the other relationships.

It is clear that the predictive abilities of the n_e relationships are significantly improved by applying variable n_i (Method 2 or Method 3) where appropriate (see Table 8-2 and Figure 8-4 [A, B, and C]). This was a somewhat obvious or foregone conclusion, given the results of the analysis presented in Chapters 6 and 7. Not so obvious, however, were the results of the Type II channel, where the accuracy of the relationships decreased when accounting for n_i variability via Method 2 or Method 3 for the channel walls and the floor. Figure 8-4 (C) shows that at lower R_h values, too much emphasis is given to the channel wall roughness when calculating n_e. The reasons for this are likely related to the way the channel is divided into subsections (the values of P_i, A_i, and/or R_{hi}) and the net effect of the assigned subsection parameters, along with n_i, on predicting the contribution of the sidewall hydraulic roughness on the overall composite flow resistance of the channel. It is also possible that the hydraulic roughness characteristics of boundary roughness elements are location dependent. Even for a uniformly lined channel, the flow resistance associated with the walls may very well differ from the flow resistance produced by the channel floor.

It is important to note that, regardless of the technique used to estimate n_e based on n_i, an empirically based, one-dimensional equation [Manning's Equation (Equation 8-1)] is still being used in an attempt to solve a three-dimensional flow problem. As shown in Figure 8-4 (B), applying Method 1 to the floor and the walls of the channel under-predicted n_e values; applying either Method 2 or Method 3 to both the floor and the walls of the channel produced n_e values that over-predicted the measured values. As a result, the analysis was repeated with Method 1 applied to the channel walls and either Method 2 or 3 to the floor of the channel. Figure 8-4 (B) shows that, by applying Method 3 to the floor and Method 1 to the walls, the predicted n_e values more closely follow the trend of the experimental data over the range of R_h tested. They do not, however, provide a relatively good estimate of the measured n_e data. For some of the equations, the *RMS* values increased when using a combination-of-methods approach. For cases where the combination of methods resulted in an improvement (i.e., reduction in *RMS* values), the improvements were only modest [e.g., Type I and III channels as shown in Table 8-2 and Figure 8-4 (A and C)]. With respect to the Type II channel, the combination of methods provided an improvement only for the lowest R_h values tested, relative to Method 1. In general, it can be concluded that where data are available, a variable Manning's n should be applied to the n_i of the floor of the channel. A constant n_i may be applied to the walls of the channel with little change in predictive error; in fact, in most cases it improved n_e predictions.

Comparison of n_e Relationships

A comparison of the predictive accuracies of the various composite roughness n_e relationships listed in Table 8-2 shows that no single composite roughness n_e relationship performs appreciably better than the rest. Table 8-3 also shows that there is moderate scatter in the accuracy of each of the predictive n_e relationships over the range of composite roughness boundary configurations tested. For example, Colebatch (*RMS* = 3.3%) performs better than Horton (*RMS* = 6.0%) in the ADA composite channel; the opposite is true in the AEA composite channel where Horton (*RMS* = 5.9%) performs better than Colebatch (*RMS* = 8.80%). The *RMS* values based on the collective data of all the channel configurations ("Total *RMS*" reported in Table 8-3) show that, from a broad perspective, neither relationship (Horton nor Colebatch) is notably better than the other for any of the channel types (I, II, or III). The mean velocity assumption group has a slight advantage over the other groups based on consistency of predictive accuracy for the three different channel types. The total discharge assumption group gives inconsistent results. The results for the individual relationships fluctuate, to a certain extent, with both the channel configuration and channel type, as shown in Table 8-3.

Table 8-2. Summary of *RMS* values based on combined data sets for all 12 composite roughness test configurations.

n_i method*		Total *RMS* values for n_e equations															
		Mean Velocity		Total Force				Total Discharge					Total Shear Velocity				
Walls	Floor	Horton	Colebatch	Pavlovskii	Total F2	Total F3	Total F4	Lotter	Lotter II	Total Q	Total Q2	Total Q3	LAD	HDM	Total U*	Total U*2	Total U*3
CHANNEL TYPE I																	
1	1	25.6%	24.5%	24.8%	26.3%	25.2%	24.4%	25.5%	24.6%	27.9%	27.1%	29.1%	33.3%	28.7%	26.5%	25.6%	25.8%
2	2	7.8%	6.9%	7.3%	7.2%	7.6%	7.0%	13.6%	12.5%	16.3%	23.3%	15.5%	6.9%	9.2%	9.5%	7.9%	8.3%
1	2	7.9%	6.9%	7.3%	7.2%	7.6%	7.0%	13.7%	12.6%	16.5%	23.7%	15.7%	6.9%	9.2%	9.6%	7.9%	8.3%
3	3	6.5%	6.5%	6.3%	7.1%	6.4%	6.6%	12.4%	11.4%	15.3%	22.7%	14.4%	6.1%	7.5%	7.9%	6.5%	6.8%
1	3	6.5%	6.5%	6.3%	7.1%	6.4%	6.6%	12.5%	11.4%	15.4%	22.8%	14.5%	6.1%	7.5%	7.9%	6.5%	6.8%
CHANNEL TYPE II																	
1	1	13.0%	12.9%	14.4%	12.3%	15.9%	12.4%	18.7%	12.9%	22.3%	21.4%	20.3%	18.1%	20.8%	12.3%	13.2%	12.8%
2	2	52.0%	29.1%	88.0%	55.4%	102%	64.8%	20.7%	19.9%	18.6%	16.1%	19.1%	15.5%	27.1%	30.5%	19.6%	21.7%
1	2	11.9%	11.4%	15.1%	11.0%	18.2%	11.6%	21.2%	20.4%	19.2%	17.0%	19.7%	13.0%	11.0%	11.1%	11.8%	11.4%
3	3	32.3%	18.9%	53.6%	32.7%	62.9%	38.6%	20.9%	20.1%	18.9%	16.5%	19.4%	13.6%	18.6%	20.6%	14.9%	15.8%
1	3	11.9%	11.4%	15.1%	11.0%	18.2%	11.6%	21.1%	20.3%	19.2%	16.9%	19.6%	13.0%	11.0%	11.1%	11.8%	11.4%
CHANNEL TYPE III																	
1	1	24.3%	24.2%	24.2%	24.3%	24.3%	24.2%	24.1%	24.3%	25.1%	24.2%	24.2%	24.3%	24.4%	24.0%	24.5%	24.5%
2	2	7.5%	5.5%	8.3%	5.9%	9.8%	6.4%	6.3%	5.5%	5.4%	5.7%	5.5%	5.4%	6.8%	7.3%	5.8%	6.1%
1	2	6.9%	6.6%	6.8%	6.6%	6.7%	6.8%	7.7%	6.5%	6.7%	7.4%	6.9%	6.6%	6.9%	6.8%	7.0%	7.1%
3	3	5.3%	5.0%	5.4%	5.1%	5.9%	5.1%	5.5%	5.1%	4.9%	5.08%	5.0%	4.99%	5.19%	5.4%	4.99%	5.0%
1	3	5.5%	5.5%	5.5%	5.5%	5.3%	5.5%	6.1%	5.3%	5.3%	5.74%	5.4%	5.43%	5.45%	5.3%	5.58%	5.6%

* Method 1: n_i = constant, Method 2: $n_i = f(R_i)$, and Method 3: $n_i = f(R)$

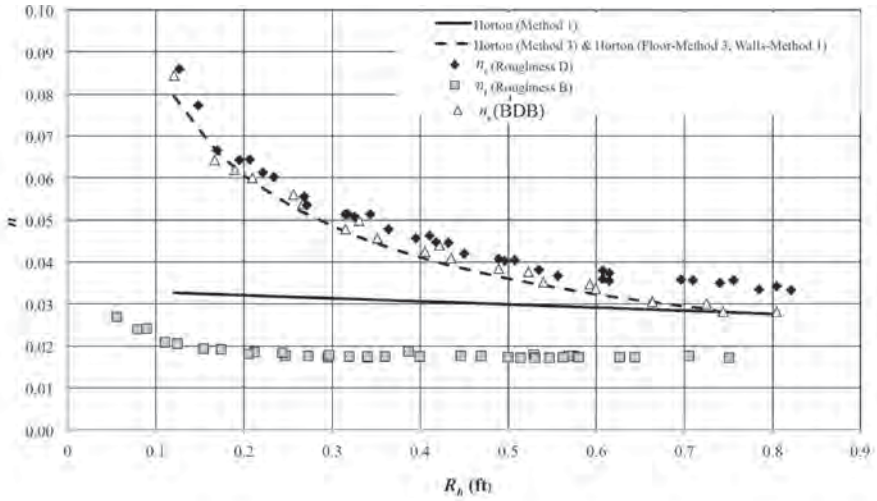

(A)

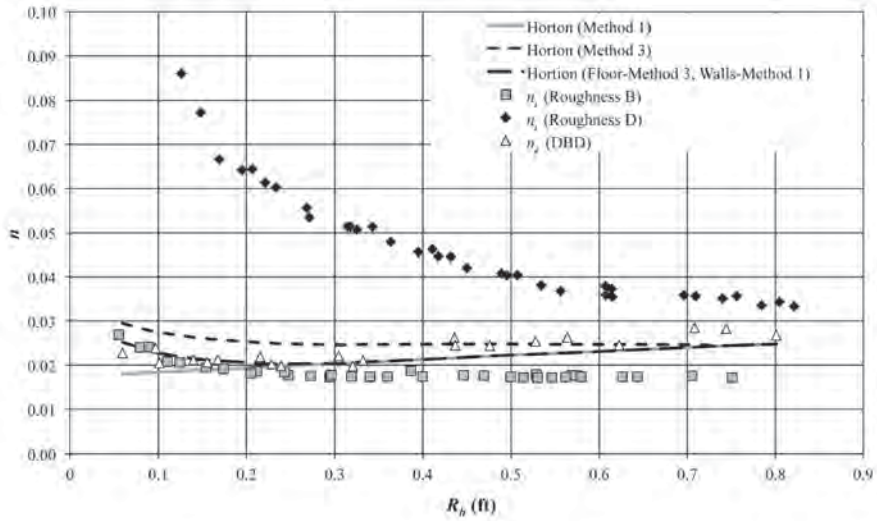

(B)

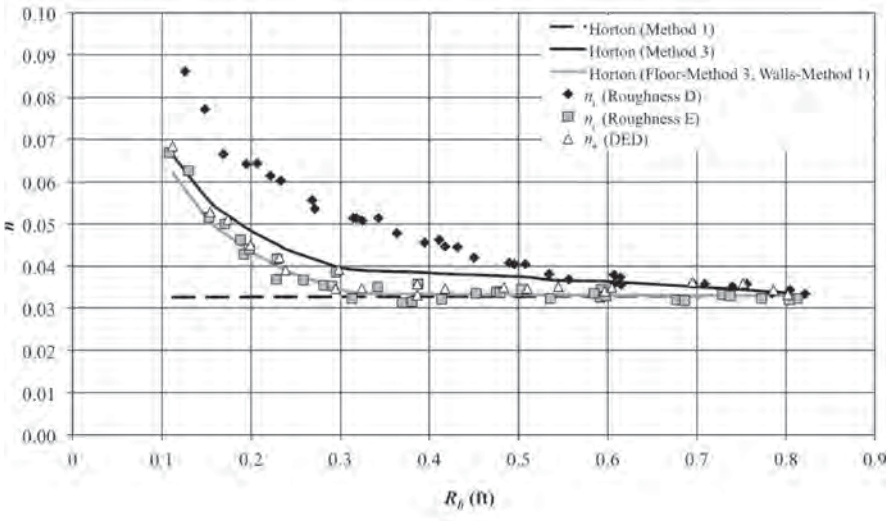

(C)

Figure 8-4. Examples of experimental and Horton relationship n_e versus R_h data for Type I, II, and III composite roughness channels along with the corresponding experimental n_i versus R_h data: (A) Type I (DBD), (B) Type II (DBD), (C) Type III (DED).

Table 8-3. Total *RMS* and bias for n_e relationships using Method 3 on the walls and Method 1 on the floor.

Config.		Horton	Colebatch	Pavlovskii	Total F2	Total F3	Total F4	Lotter	Lotter II	Total Q	Total Q2	Total Q3	LAD	HDM	Total U*1	Total U*2	Total U*3
CHANNEL TYPE I																	
ABA	*Bias*	-7.6%	-5.1%	-6.9%	-4.6%	-7.5%	-5.4%	-8.4%	-7.0%	-9.0%	-13.0%	-8.7%	-5.7%	-8.4%	-8.7%	-7.3%	-7.7%
	RMS	8.2%	6.0%	7.5%	5.6%	8.1%	6.3%	9.0%	7.7%	9.6%	13.5%	9.3%	6.5%	9.0%	9.3%	7.9%	8.3%
ADA	*Bias*	-4.9%	-0.2%	-2.3%	1.6%	-3.6%	0.2%	-20.7%	-19.3%	-26.0%	-37.0%	-24.5%	-2.7%	-8.5%	-9.3%	-5.8%	-6.7%
	RMS	6.0%	3.3%	3.9%	3.6%	4.7%	3.1%	21.3%	20.0%	26.4%	37.1%	25.0%	4.5%	9.4%	10.2%	6.9%	7.7%
BDB	*Bias*	-3.4%	0.4%	-1.9%	1.5%	-2.9%	0.3%	-7.9%	-6.3%	-10.4%	-17.8%	-9.6%	-0.9%	-5.3%	-5.9%	-3.4%	-4.1%
	RMS	4.6%	3.0%	3.6%	3.4%	4.2%	3.0%	8.4%	6.9%	10.8%	18.1%	10.0%	3.1%	6.2%	6.7%	4.5%	5.1%
AEA	*Bias*	0.6%	5.2%	3.0%	6.9%	1.8%	5.5%	-10.2%	-8.8%	-14.5%	-24.4%	-13.2%	3.1%	-2.4%	-3.2%	0.1%	-0.8%
	RMS	5.9%	8.8%	7.4%	10.5%	6.6%	9.3%	11.2%	9.9%	15.1%	24.6%	13.9%	6.9%	5.5%	5.8%	5.5%	5.3%
BEB	*Bias*	0.6%	3.8%	1.6%	4.6%	0.8%	3.5%	-1.2%	0.4%	-2.5%	-8.0%	-2.0%	2.9%	-0.7%	-1.1%	0.8%	0.3%
	RMS	7.1%	8.7%	7.6%	9.3%	7.2%	8.6%	6.7%	6.9%	7.0%	10.1%	6.9%	8.0%	6.8%	6.8%	7.1%	7.0%
Total	*Bias*	-3.0%	0.8%	-1.3%	2.0%	-2.3%	0.8%	-9.7%	-8.2%	-12.5%	-20.0%	-11.6%	-0.7%	-5.1%	-5.6%	-3.1%	-3.8%
	RMS	6.5%	6.5%	6.3%	7.1%	6.4%	6.6%	12.5%	11.4%	15.4%	22.8%	14.5%	6.1%	7.5%	7.9%	6.5%	6.8%
CHANNEL TYPE II																	
BAB	*Bias*	4.8%	0.7%	6.3%	1.7%	8.6%	2.9%	-5.3%	-4.0%	-3.0%	-0.6%	-3.5%	-0.3%	3.5%	4.6%	1.0%	1.7%
	RMS	6.5%	5.2%	7.6%	5.2%	9.6%	5.5%	9.3%	8.3%	7.4%	5.9%	7.8%	5.5%	5.8%	6.4%	5.2%	5.2%
DAD	*Bias*	2.4%	-7.3%	10.0%	-1.5%	15.1%	1.8%	-23.8%	-22.9%	-21.7%	-18.8%	-22.2%	-12.0%	-4.2%	-2.3%	-8.8%	-7.4%
	RMS	17.9%	19.7%	20.5%	17.5%	24.0%	17.4%	34.2%	33.5%	32.3%	29.8%	32.7%	23.0%	18.9%	18.4%	20.9%	20.2%
DBD	*Bias*	-4.5%	-8.7%	-2.8%	-7.3%	-0.6%	-6.1%	-15.8%	-14.6%	-13.4%	-10.9%	-14.0%	-9.9%	-6.0%	-5.0%	-8.5%	-7.8%
	RMS	9.1%	12.5%	7.9%	11.2%	7.2%	10.1%	19.9%	18.9%	17.7%	15.2%	18.2%	13.8%	10.4%	9.7%	12.5%	11.8%
EAE	*Bias*	14.1%	3.0%	22.6%	9.5%	28.3%	13.2%	-16.2%	-15.2%	-13.7%	-10.2%	-14.3%	-2.4%	6.7%	9.0%	1.4%	3.0%
	RMS	15.4%	7.5%	23.6%	11.3%	29.4%	14.6%	21.8%	20.9%	19.3%	16.0%	19.9%	8.6%	9.5%	11.1%	7.5%	7.7%
EBE	*Bias*	3.1%	-1.4%	4.8%	-0.1%	7.1%	1.2%	-8.9%	-7.5%	-6.2%	-3.5%	-6.9%	-2.6%	1.5%	2.7%	-1.1%	-0.4%
	RMS	5.2%	4.3%	6.7%	4.3%	8.7%	4.6%	10.3%	8.9%	7.6%	5.1%	8.2%	4.7%	4.1%	4.7%	4.0%	3.9%
Total	*Bias*	4.0%	-2.8%	8.2%	0.5%	11.7%	2.6%	-14.0%	-12.9%	-11.6%	-8.8%	-12.2%	-5.4%	0.3%	1.8%	-3.2%	-2.2%
	RMS	11.9%	11.4%	15.1%	11.0%	18.2%	11.6%	21.1%	20.3%	19.2%	16.9%	19.6%	13.0%	11.0%	11.1%	11.8%	11.4%
CHANNEL TYPE III																	
EDE	*Bias*	-1.2%	0.4%	-0.9%	0.6%	-1.1%	0.02%	-1.5%	0.07%	-1.1%	-3.6%	-1.1%	0.2%	-1.6%	-1.6%	-1.0%	-1.3%
	RMS	5.2%	5.5%	5.3%	5.6%	5.2%	5.4%	5.2%	5.0%	4.8%	5.3%	4.9%	5.4%	5.1%	5.1%	5.2%	5.2%
DED	*Bias*	-4.7%	-4.5%	-4.7%	-4.5%	-4.4%	-4.7%	-6.0%	-4.5%	-4.7%	-5.1%	-4.9%	-4.5%	-4.8%	-4.5%	-5.0%	-5.0%
	RMS	5.7%	5.5%	5.7%	5.5%	5.5%	5.6%	6.8%	5.6%	5.7%	6.1%	5.9%	5.5%	5.8%	5.6%	5.9%	5.9%
Total	*Bias*	-3.0%	-2.0%	-2.8%	-1.9%	-2.8%	-2.3%	-3.8%	-2.2%	-2.9%	-4.3%	-3.0%	-2.2%	-3.2%	-3.1%	-3.0%	-3.2%
	RMS	5.5%	5.5%	5.5%	5.5%	5.3%	5.5%	6.1%	5.3%	5.3%	5.7%	5.4%	5.4%	5.5%	5.3%	5.6%	5.6%

Based on the total *RMS* values for Channel Type I, on average the LAD, Horton, Colebatch, Pavlovskii, Total F3, Total F4, Total U*2, and Total U*3 predictive relationships performed the best (all within 1% of one another), with the LAD relationship producing a slightly smaller *RMS* value than the others. For the Type II channel, the Total F2, Horton, Colebatch, Total F4, HDM, Total U*1, Total U*2 and Total U*3 predictive relationships performed the best (all within 1.0% of one another), with Total F2 being slightly better than the others. For the Type III channel, all of the predictive n_e relationships performed essentially the same, with the total discharge relationships producing a slightly smaller *RMS* than the other relationships.

The results of the data presented in Table 8-3 show that no obvious advantage exists in using the more complicated subarea-dividing-based n_e relationships over the simpler-to-use relationships that only use P_i as the weighting parameter for the n_i in the channel. There is no need to divide the cross-section of the channel into subareas because (1) P_i is the sole weighting parameter in these relationships and (2) Method 3, which uses the total hydraulic radius (R_h) of the channel instead of R_{hi}, has been shown to work as well as or better than the other methods. There is one such equation per assumption group: the Horton relationship (mean velocity assumption group), Pavlovskii's relationship (total force assumption group), total Q2 (total discharge assumption group), and the HDM relationship (total shear velocity assumption group). Of those relationships, Horton is the most consistent when considering all three channel types (I, II, and III).

It is important to remember that the data in this study were collected in a channel with a simple and uniform cross-section (rectangular). In addition, although the range or boundary roughness materials varied appreciably in this study, it should be noted that a high level of roughness element uniformity existed for each composite roughness boundary material (no random roughness elements within a given boundary roughness material) in relation to itself. The extent to which these results can be applied to other types of composite roughness channels that feature different channel cross-sections and variation in the degree of component boundary roughness element uniformity (e.g., a buried-invert fish passage culvert, as shown in Figure 2-1) has yet to be determined. In the absence of better information, however, the data from this study can be used as a first-order approximation for other composite roughness channel applications. It is also important to note that, based on the variability in the *RMS* values in Table 8-3 for the individual composite roughness geometries (e.g., ADA, etc.), the predictive n_e values associated with any of the relationships listed in Table 8-2 should be considered approximate. This is especially true when looking at the "Total *RMS*" (presented in Tables 8-2 and 8-3), which is based on a compilation of all of the data from composite channel configurations in a single channel type (I, II, or III).

8.6 Conclusions

The conclusions associated with composite roughness open channel flow resistance in a rectangular flume that result from this study include the following:

1. It is important to note that, regardless of the technique used to estimate n_e based on n_i, in general, composite roughness open channel flow conditions are three-dimensional flow problems that researchers have attempted to solve with the empirically based one-dimensional, Manning's Equation (Equation 8-1). The likelihood of finding a robust n_e prediction method that will work with Equation 8-1 for solving a wide range of composite roughness channel configurations is low due to the complex nature of the problem.
2. Where data are available, a variable Manning's n (the appropriate n value for a given flow condition) should be used on the channel floor. A constant n_i may be applied to the walls of the channel with little negative impact to the predictive error; in fact, in most cases in this study, it improved n_e predictions.
3. The mean velocity assumption relationships, as a group, performed more consistently than the other groups as a whole; however, there are only two equations in the mean velocity group compared to the four or five equations of the others. The total discharge assumption relationships, as a group, performed inconsistently relative to the other relationships.
4. Based on the data obtained for this study, there is no evidence that a single n_e equation has a clear advantage over the rest. Taking into consideration the results from all three channel types, the most consistent equations (those which were within 1% of the lowest *RMS* of each channel type) were Horton, Colebatch, Total F4, Total U*2, and Total U*3.
5. Of these equations, there is no conclusive evidence that the more complex n_e equations will produce better results than the simplest equation (Horton's Equation, Horton 1933).
6. Due to the inconsistent results of the ability of the n_e equations to predict n_e for channels where the wall is relatively rough in comparison to the floor of the channel (Type II channels), it is recommended that further study be conducted to examine the difference between the resistance provided by a specific roughness material, whether it be on the wall of the channel or on the floor of the channel. For example, Christensen (1992) proposed an alternate definition of R_h, relative to the traditional A/P, rather than adjusting the hydraulic resistance coefficient to account for the variation in shear stress values along the wetted perimeter of the channel walls. Future works should include channels with cross-sectional shapes different than the rectangular shape tested in this study.

References

Allen, T. G., *The Behavior of Manning's n in Channels of Uniform and Composite Roughness.* Dissertation, Utah State University, Logan, UT (2012).

Anderson, D. S., *Inlet Loss Coefficients and Inlet Control Head-Discharge Relationships for Buried-Invert Culverts and Slip-Lined Culverts.* Thesis, Utah State University, Logan, UT (2006) 113 pp.

Anderson D. S. and B. P. Tullis, "Experimentally Determined Inlet Loss Coefficients for Buried-Invert, Circular Culverts." Proc. ASCE-EWRI Omaha, May 2006.

Ballinger, C. A., and P. G. Drake, *Culvert Repair Practices Manual: Volume I,* Rep. No. FHWA-RD-94-096. Federal Highway Administration, McLean, VA (1995a) 265 pp.

Ballinger, C. A., and P. G. Drake, *Culvert Repair Practices Manual: Volume II,* Rep. No. FHWA-RD-95-089. Federal Highway Administration (FHWA), McLean, VA (1995b) 354 pp.

Bates, K., B. Barnard, B. Heiner, J. P. Klavas, and P. D. Powers, *Design of Road Culverts for Fish Passage.* Washington Department of Fish and Wildlife, Olympia, WA (2003) 111 pp.

Bathurst, J. C., R. M. Li, and D. B. Simons, "Resistance Equation for Large Scale Roughness." *J. Hydr. Div.,* Vol. 107(HY12) (1981) pp. 1593–1613.

Bathurst, J. C., "At-a-Site Variation and Minimum Flow Resistance for Rivers." *J. Hydr. Div.,* Vol. 269 (2002) pp. 11–26.

Bazin, H., "Recherches Experimentales sur l'ecoulement de l'eau dans les canaux decouverts." *Memoires presentes par divers savants a l' Academie des sciences,* Vol 19 (1865) pp. 1-494.

Blaisdell, F. W., "Hydraulic Efficiency in Culvert Design." *J. of the Highway Division (ASCE),* Vol. 92(HW1) (1966) pp. 11–23.

Blench, T., "A New Theory of Turbulent Flow in Liquids of Small Viscosity." *J. Inst. of Civil Eng.,* Vol. 11, No. 6 (1939) pp. 611–612.

Bray, D. I., "Estimating Average Velocity in Gravel-Bed Rivers." *Proc. Am. Soc. Civ. Engrs, J. Hydraul. Div.,* Vol. 105 (HY9) (1979) pp. 1103–1122.

Brunner, G., *HEC-RAS, River Analysis System Hydraulic Reference Manual.* U.S. Army Corps of Eng, Davis, CA (2002) 411 pp.

Charbeneau R. J., A. D. Henderson, and L. C. Sherman, "Hydraulic Performance Curves for Highway Culverts." *J. of Hydraulic Engineering,* Vol. 132, No. 5 (2006) pp. 474–481.

Charbeneau R. J., A. D. Henderson, R. C. Murdock, and L. C. Sherman, *Hydraulics of Channel Expansions Leading to Low-Head Culverts.* Center for Transportation Research, University of Texas at Austin, Austin, TX (2002) 114 pp.

Chow, V. T., *Open-Channel Hydraulics.* McGraw-Hill, New York (1959) 680 pp.

Christensen, B. A., "Replacing Hydraulic Radius in Manning's Formula in Open Channel." In *Channel Flow Resistance: Centennial of Manning's Formula,* B. C. Yen, ed., Water Resources Publications, Littleton, CO (1992) 271–286 pp.

Colebatch, G. T., "Model Tests on the Lawrence Canal Roughness Coefficients." *J. Inst. Civil Eng. (Australia),* Vol. 13, No. 2 (1941) pp. 27–32.

Colebrook, F., "Turbulent Flow in Pipes with Particular Reference to the Transition Region between the Smooth and Rough Pipe Laws." *J. Inst. Civ. Eng.,* Vol. 11 (1939) pp. 133–156.

Cox, R. G., *Effective Hydraulic Roughness for Channels Having Bed Roughness Different from Bank Roughness,* Misc. Paper H-73-2. U.S. Army Corps of Engineers Waterways Experiment Station, Vicksburg, MS (1973) 64 pp.

Crowe, C. T., D. F. Elger, and J. A. Roberson, *Engineering Fluid Mechanics, 7th ed.* Wiley, New York (2001) 768 pp.

Flammer, G. H., R. W. Jeppson, and H. F. Keedy, *Fundamental Principles and Applications of Fluid Mechanics.* Utah State University, Logan, UT, Nashville, Tennessee: Vanderbilt University, Nashville, TN (1986) 356 pp.

Flintham, T. P., and Carling, P. A., "Manning's *n* of Composite Roughness in Channels of Simple Cross Section." In *Channel Flow Resistance: Centennial of Manning's formula,* B. C. Yen, ed., Water Resource Publications, Highlands Ranch, CO (1992) pp. 328–341.

Formica, G., "Experienze preliminari sulle predite de carico nei canale dovute a cambiamento di sezione." *L'Energia Elettrica, Milan,* Vol. 32, No. 7 (1955) pp.554–567.

French, J. L., *First Progress Report on Hydraulics of Culverts: Hydraulic Characteristics of Commonly Used Pipe Entrances,* NBS Report 4444. National Bureau of Standards, Washington, D.C. (1955) 74 pp.

French, J. L., *Second Progress Report on Hydraulics of Culverts: Pressure and Resistance Characteristics of a Model Pipe Culvert,* NBS Report 4911. National Bureau of Standards, Washington, D.C. (1956) 35 pp.

French, J. L., *Third Progress Report on Hydraulics of Culverts: Effects of Approach Channel Characteristics on Model Pipe Culvert Operation,* NBS Report 5306. National Bureau of Standards, Washington, D.C. (1957).

French, J. L., *Fourth Progress Report on Hydraulics of Culverts: Hydraulics of Improved Inlet Structures for Pipe Culverts,* NBS Report 7178. National Bureau of Standards, Washington, D.C. (1961) 132 pp.

French, J. L., *Fifth Progress Report on Hydraulics of Culverts: Non-Enlarged Box Culvert Inlets,* NBS Report 9327. National Bureau of Standards, Washington, D.C. (1966a).

French, J. L., *Sixth Progress Report on Hydraulics of Culverts: Tapered Box Culvert Inlets,* NBS Report 9355. National Bureau of Standards, Washington, D.C. (1966b).

French, J. L., *Seventh Progress Report on Hydraulics of Culverts: Tapered Box Inlets with Fall Concentration in the Inlet Structure,* NBS Report 9355. National Bureau of Standards, Washington, D.C. (1967).

Griffiths, G. A., "Flow Resistance in Coarse Gravel Bed Rivers" *Proc. Am. Soc. Civ. Engrs, J. Hydraul. Div.,* Vol. 107 (HY7) (1981) pp. 899–918.

Haderlie, G. M., *Inlet Control Hydraulics for Multiple Circular Culverts.* Thesis, Utah State University, Logan, UT (2007) 137 pp.

Haderlie, G. M. and B. P. Tullis, "Multi-Barrel Culvert Hydraulics Under Inlet Control." *J. Irrig. Drain. Eng.,* Vol. 134, No. 4 (2008), pp. 507–514.

Henderson, F. M., *Open Channel Flow.* Macmillan, New York (1966) 522 pp.

Hinds, J., "The Hydraulic Design of Flume and Siphon Transitions." *Transactions, ASCE,* Vol. 92 (1928) p. 1423.

Horton, R. E., "Separate Roughness Coefficients for Channel Bottom and Sides." *Engineering New-Record,* Vol. 111, No. 22, (1933) pp. 652–653.

Jarret, R. D. 1984. "Hydraulics of High Gradient Streams." *J. Hydr. Eng. Div.,* Vol. 101, No. 11 (1984) pp. 1519–1593.

Johnson, P. A., and E. R. Brown, "Stream Assessment for Multicell Culvert Use." *J. of Hydraulic Engineering,* Vol. 126, No. 5 (2000) pp. 381–386.

Jones, J. S., K. Kerenyi, and S. Stein, *Effects of Inlet Geometry on Hydraulic Performance of Box Culverts,* Publication No. FHWA-HRT-06-138. Federal Highway Administration, Washington, D.C. (2006) 158 pp.

Jordan, M. C., and R. F. Carlson, *Design of Depressed Invert Culverts.* Water Research Center, University of Alaska, Fairbanks, AK (1987) 64 pp.

Komora, J., "Hydraulic Resistance to Flow in Channels." 15th Congress of IAHR, Istanbul, *Proceedings* Vol. 1 (1973) pp. 195–202.

Korr, M. H., and L. A. Clayton, *Model Studies of Inlet Designs for Pipe Culverts on Steep Grades,* Bulletin No. 35. Engineering Experiment Station, Oregon State College, Corvallis, OR (1954) 39 pp.

Limerinos, J. T., "Determination of the Manning Coefficient from Measured Bed Roughness in Natural Channels," *U.S. Geological Survey Water Supply Paper,* 1898-B:47 (1970) 78 pp.

Lotter, G. K., "Soobrazheniia k Gidravlicheskomu Raschetu Rusel s Razlichnoi Sherokhovatostiiu Stenok." (Considerations on Hydraulic Design of Channels with Different Roughness of Walls.), *Izvestiia Vsesohuznogo nauchno-Issledovatel'skogo Instituta Gidrotechniki* (Trans. All-Union Sci. Res. Inst. Hydraulic Eng.), Leningrad, Vol. 9 (1933) pp. 238–241.

Maine Department of Transportation, *Fish Passage Policy and Design Guide.* Augusta, ME (2004) 84 pp.

Manning, R., "On the Flow of Water in Open Channels and Pipes." *Trans. Inst. Civil Eng.,* Vol. 20 (1889) pp. 161–207.

Mathaei, H. and S. Lewin, *Ensanches bruscos y paulatinos en canales.* Thesis, Univ. of Chile (1932).

Montes, S., *Hydraulics of Open Channel Flow.* ASCE Press, Reston, VA (1998) 697 pp.

Morris, H. M., "A New Concept of Flow in Rough Conduits." *Transactions,* American Society of Civil Engineers, Vol. 120 (1955) pp. 373–398.

Nikuradse, J., "Strömungsgesetze in rauhen Rohren." *VDI-Forschungsh.,* No. 361 (1933).

Normann, J. M., R. J. Houghtalen, and W. J. Johnston, *Hydraulic Design Series Number 5 (HDS-5), Hydraulic Design of Highway Culverts.* Federal Highway Administration (FHWA), Washington, D.C. (2001) 254 pp.

Pavlovskii, N. N., "K Voporosu o Raschetnoi dlia Ravnomernogo Dvizheniia v Vodotokahk s Neodnorodnymi Stenkami." (On a Design Formula for Uniform Flow in Channels with Nonhomogeneous Walls.) *Izvestiia Vsesoiuznogo Nauchno-Issledovatel'skogo Instituta Gidrotekhniki* (Trans. All-Union Sci. Res. Inst. Hydraulic Eng.), Leningrad, Vol. 3 (1931) pp. 157–164.

Pillai, C. R. S., "Composite Rugosity Coefficient in Open Channel Flow." *Irrigation and Power, J. Central Board of Irrigation and Power,* New Delhi, India, Vol. 19, No. 3 (1962) pp. 174–189.

Plastics Pipe Institute, "Chapter 11—Pipeline Rehabilitation by Slip-lining with Polyethylene Pipe." In *Handbook of PE Pipe,* The Society of the Plastics Industry, Inc., Washington, D.C. (1993) pp. 389–412.

Robinson, R. C. and B. P. Tullis, "Quantifying Culvert Exit Loss." Proc. Transportation Research Board Conference, Washington D.C., Jan. 2005.

Robinson, S. C., *Hydraulic Characteristics of a Buried Invert Elliptical Culvert Inlet and Quantification of Culvert Exit Loss.* MS Thesis, Utah State University (2005) 73 pp.

Rouse, J. and Ince, S., *History of Hydraulics.* Iowa Institute of Hydraulic Research, University of Iowa (1957).

Schiller, R. E., "Tests on Circular-Pipe Culvert Inlets." *Highway Research Board Bulletin 126,* Washington, D. C. (1956) pp. 11–23.

Streeter, V. L. and E. B. Wylie, *Fluid Mechanics, 7th ed.* McGraw-Hill Book Company, New York (1979) 562 pp.

Thompson, P. L. and R. T. Kilgore, *HEC-14, Hydraulic Design of Energy Dissipaters for Culverts and Channels: Hydraulic Engineering Circular 14, 3rd ed.,* FHWA-NHI-06-086. Federal Highway Administration (FHWA), Washington, D.C. (2006) 286 pp. http://www.fhwa.dot.gov/engineering/hydraulics/library_listing.cfm

Tullis, B. P. and D. S. Anderson, "Slip-Lined Culvert Inlet End Treatment Hydraulics." *J. Irrig. Drain. Eng.,* Vol. 136, No. 1 (2010) pp. 31–36.

Tullis, B. P., D. S. Anderson, and S.C. Robinson, "Entrance Loss Coefficients and Inlet Control Head-Discharge Relationships for Buried-Invert Culverts." *J. Irrig. Drain. Eng.,* Vol. 134, No. 6 (2008) pp. 831–839.

Tullis, B. P. and S. C. Robinson, "Quantifying Culvert Exit Loss." *J. Irrig. Drain. Eng,* Vol. 134, No. 2 (2008) pp. 263–266.

Tullis B. P, S. C. Robinson, and J. C. Young, "The Hydraulic Characteristics of Buried-Invert, Elliptical Culverts," Proc. Transportation Research Board Conference, Washington D.C. Jan 2005.

Tullis, J. P., *Hydraulics of Pipelines: Pumps, Valves, Cavitation, Transients.* John Wiley and Sons, New York (1989) 288 pp.

Ugarte, A. and M. Madrid, "Roughness Coefficient in Mountain Rivers." *ASCE Proc. Hydr. Engrg.* (1994) pp. 652–656.

Vennard, J. K., *Elementary Fluid Mechanics.* Wiley, New York (1940) 368 pp.

Wargo, R. S. and R. N. Weisman, "A Comparison of Single-Cell and Multicell Culverts for Stream Crossings." *J. of the American Water Resour. Assoc.,* Vol. 42, No. 4 (2006) pp. 989–995.

Yen, B. C., "Open Channel Flow Resistance." *Journal of Hydraulic Engineering,* Vol. 128 (2002) pp. 20–37.

Yen, B. C., "On Establishing Uniform Channel Flow with Tail Gate." *Water & Maritime Engineering,* Vol. 156, Issue WM3 (2003) pp. 281–283.

Notation

a = empirical coefficient to power law relationship
A = sectional flow area of culvert barrel or channel [L^2]
A_1 = control volume cross-sectional flow area at location 1 (see Figure 4-1) [L^2]
A_2 = control volume cross-sectional flow area at location 2 (see Figure 4-1) [L^2]
A_{ch} = channel cross-sectional flow area downstream of culvert outlet [L^2]
A_{flow} = average culvert flow cross-sectional area (equals A for full-pipe flow) [L^2]
A_i = component flow area resulting from the partitioning of a composite-channel into subareas between the boundary roughness materials [L^2]
A_p = culvert cross-sectional flow area [L^2]
b = empirical coefficient to power law relationship
c = coefficient for submerged inlet control head-discharge equation
C = boundary roughness coefficient
C_c = boundary roughness coefficient (Chezy's Equation)
C_d = discharge coefficient
D = interior height of culvert barrel for embedded culverts; culvert diameter for circular culverts [L]
D_h = maximum horizontal culvert span (diameter for circular culverts) [L]
D_r = representative particle diameter [L]
f = hydraulic roughness coefficient (Darcy-Weisbach Equation)
F = function of
Fr = Froude number
F_x = force acting in horizontal (x) direction [F]
g = acceleration due to gravity [L/t^2]
h = flow depth [L]
$h_{measured}$ = measured flow depth [L]
$h_{calculated}$ = calculated flow depth with GVF profile calculation [L]
$h_{average}$ = average of measured flow depth ($y_{measured}$) [L]
H = total head upstream of the flow measurement V-notched weir
H_c = total head at critical depth ($d_c+V_c^2/2g$) [L]
H_e = culvert entrance head loss [L]
H_o = culvert exit loss, energy per unit volume [L]
Hw = total energy upstream of a culvert relative to the culvert invert (or streambed for a buried-invert culvert) at the inlet [L]

Hw_i = headwater depth upstream of a culvert relative to the culvert invert (or streambed for a buried-invert culvert) at the inlet [L]
k = equivalent roughness height [L]
k_e = entrance loss coefficient
k_o = exit loss coefficient
k_s = pipe wall roughness height [L]
K = coefficient for unsubmerged inlet control equations
K_n = 1 for SI units and = $3.281^{(1-x)}$ (=1.49 when $x' = ⅔$) for ES units
K_u = unit conversion constant for inlet control equations 1.0, ES (1.811, SI)
L = length
m = side wall slope (horizontal to vertical) of trapezoidal channel cross-section
M = exponent in unsubmerged inlet control equations
n = Manning's n hydraulic roughness coefficient
n = boundary roughness coefficient (Manning's Equation)
$n_{average}$ = average n from experimental data
n_c = equivalent n value for Chezy and Darcy-Weisbach equations
n_e = composite Manning's n
n_{eq} = boundary roughness coefficient (dependent on x in Eqn. (6))
n_i = component n values of individual boundary roughness materials
n_{opt} = equivalent n value where x of Equation 6 is optimized
samples = number of data points sampled which contribute to the *RMS*
P = wetted perimeter [L]
P_i = component wetted perimeter resulting from the partitioning of a composite-channel into subareas between the boundary roughness materials [L]
P_1 = hydrostatic pressure at location 1 (see Figure 4-2) [F/L^2]
P_2 = hydrostatic pressure at location 2 (see Figure 4-2) [F/L^2]
PE = predictive error [%]
Q = volumetric flow rate [L^3/t]
r^2 = coefficient of determination
Re = Reynolds number
R_h = hydraulic radius (A_{flow}/P) [L]
R_{hi} = component hydraulic radius (A_i/P_i) [L]
RMS = Root Mean Square [%]
S_o = slope of culvert barrel [L/L]
S_e = the energy grade line slope (friction slope)
t = time
T = width of trapezoidal channel at water surface [L]
Tw = tailwater depth, measured relative to culvert outlet invert [L]
U^* = shear velocity
V = mean velocity of flow [L/t]
V = mean channel velocity [L/t]
V^* = shear velocity = $(gR_hS)^{1/2}$ [L/t]
V_{ch} = average channel flow velocity downstream of a culvert outlet [L/t]
V_p = average culvert flow velocity [L/t]
x = primary flow direction coordinate

x' = exponent applied to R_h in basic uniform-flow equation
y = flow depth
y' = exponent applied to S in basic uniform-flow equation
$y_{average}$ = average channel profile flow depth [L]
$y_{calculated}$ = flow depth calculated by the GVF computer program
$y_{measured}$ = measured flow depth
y_n = normal depth [L]
Y = constant for submerged inlet control equation
Δz = elevation difference between the inverts of the culvert outlet and channel [L]
γ = fluid specific weight [F/L^3]
θ = angle of the V-notch
ρ = fluid density [m/L^3]
ν = kinematic viscosity [L^2/t]

APPENDIX A

Buried-Invert Culvert Outlet Control Experimental Data Set (Tabular Support Data for Chapter 2)

Table A-1. Circular culvert, 20% buried-invert, outlet control performance data: thin-wall projecting end.

Run	Entrance	Approach	Control	S_o [%]	Q [cfs]	Re []	Hw/D []	k_e []
1	Projecting	Ponded	Outlet	-0.03	2.33	144,080	1.39	1.01
2	Projecting	Ponded	Outlet	-0.03	2.94	186,528	2.87	1.00
3	Projecting	Ponded	Outlet	-0.03	2.91	184,649	3.30	1.02
4	Projecting	Ponded	Outlet	-0.03	2.03	128,463	0.67	0.89
5	Projecting	Ponded	Outlet	-0.03	1.61	124,011	0.54	0.74
6	Projecting	Ponded	Outlet	-0.03	2.37	146,466	1.20	1.01
7	Projecting	Ponded	Outlet	-0.03	2.37	146,945	1.59	0.99
8	Projecting	Ponded	Outlet	-0.03	2.59	161,546	2.04	1.03
9	Projecting	Ponded	Outlet	-0.03	2.57	161,275	2.22	0.97
10	Projecting	Ponded	Outlet	-0.03	3.56	227,285	3.07	1.01
11	Projecting	Ponded	Outlet	-0.03	3.29	199,634	2.73	1.00
12	Projecting	Ponded	Outlet	-0.03	2.97	178,177	1.91	1.02
13	Projecting	Ponded	Outlet	-0.03	2.42	135,796	1.05	1.00
14	Projecting	Channelized	Outlet	-0.03	3.04	184,238	3.29	0.93
15	Projecting	Channelized	Outlet	-0.03	3.05	184,172	3.03	0.94
16	Projecting	Channelized	Outlet	-0.03	2.80	168,712	2.03	0.88
17	Projecting	Channelized	Outlet	-0.03	2.81	169,699	1.63	0.88
18	Projecting	Channelized	Outlet	-0.03	2.35	133,975	1.02	0.74
19	Projecting	Channelized	Outlet	-0.03	2.36	126,624	0.87	0.69
20	Projecting	Channelized	Outlet	-0.03	1.66	125,411	0.54	0.59
21	Projecting	Channelized	Outlet	-0.03	2.37	142,136	1.34	0.82
22	Projecting	Channelized	Outlet	-0.03	2.57	152,428	2.31	0.91

Table A-2. Circular culvert, 20% buried-invert, outlet control performance data: mitered to 1.5H:1V fill slope with flush headwall.

Run	Entrance	Approach	Control	S_o [%]	Q [cfs]	Re []	Hw/D []	k_e []
23	Mitered	Ponded	Outlet	-0.07	3.23	211,524	3.31	0.84
24	Mitered	Ponded	Outlet	-0.07	3.25	213,910	3.00	0.84
25	Mitered	Ponded	Outlet	-0.07	3.08	202,913	2.69	0.82
26	Mitered	Ponded	Outlet	-0.07	3.10	204,305	2.28	0.84
27	Mitered	Ponded	Outlet	-0.07	2.83	186,925	2.03	0.83
28	Mitered	Ponded	Outlet	-0.07	2.84	187,430	1.66	0.84
29	Mitered	Ponded	Outlet	-0.07	2.66	168,026	1.33	0.69
30	Mitered	Ponded	Outlet	-0.07	2.66	168,827	1.08	0.47
31	Mitered	Ponded	Outlet	-0.07	2.50	138,596	0.85	0.45
32	Mitered	Ponded	Outlet	-0.07	2.92	179,408	1.84	0.80
33	Mitered	Ponded	Outlet	-0.07	2.80	171,968	1.67	0.80
34	Mitered	Ponded	Outlet	-0.07	2.68	164,688	1.53	0.80
35	Mitered	Ponded	Outlet	-0.07	2.68	165,504	1.25	0.61
36	Mitered	Ponded	Outlet	-0.07	2.49	143,846	0.74	0.45
37	Mitered	Ponded	Outlet	-0.07	1.72	129,697	0.54	0.42
38	Mitered	Channelized	Outlet	-0.07	3.22	206,689	3.34	0.86
39	Mitered	Channelized	Outlet	-0.07	3.26	209,054	2.88	0.87
40	Mitered	Channelized	Outlet	-0.07	3.10	199,373	2.50	0.84
41	Mitered	Channelized	Outlet	-0.07	2.90	187,377	1.95	0.80
42	Mitered	Channelized	Outlet	-0.07	2.84	170,919	1.59	0.81
43	Mitered	Channelized	Outlet	-0.07	2.85	171,379	1.41	0.71
44	Mitered	Channelized	Outlet	-0.07	2.65	140,381	0.97	0.48
45	Mitered	Channelized	Outlet	-0.07	2.22	127,767	0.70	0.46
46	Mitered	Channelized	Outlet	-0.07	2.47	150,241	1.17	0.55

Table A-3. Circular culvert, 20% buried-invert, outlet control performance data: square-edged entrance with vertical headwall.

Run	Entrance	Approach	Control	S_o [%]	Q [cfs]	Re []	Hw/D []	k_e []
47	Square	Ponded	Outlet	-0.03	1.79	131,963	0.54	0.37
48	Square	Ponded	Outlet	-0.03	1.79	98,569	0.77	0.45
49	Square	Ponded	Outlet	-0.03	2.10	114,775	0.87	0.47
50	Square	Ponded	Outlet	-0.03	2.10	122,389	1.00	0.48
51	Square	Ponded	Outlet	-0.03	2.10	134,065	1.42	0.60
52	Square	Ponded	Outlet	-0.03	2.41	154,476	1.70	0.59
53	Square	Ponded	Outlet	-0.03	2.60	167,238	2.01	0.53
54	Square	Ponded	Outlet	-0.03	2.59	167,217	2.30	0.58
55	Square	Ponded	Outlet	-0.03	2.87	185,191	2.61	0.52
56	Square	Ponded	Outlet	-0.03	3.07	198,401	2.97	0.50
57	Square	Ponded	Outlet	-0.03	3.06	196,876	3.27	0.59
58	Square	Ponded	Outlet	-0.03	2.40	154,375	1.20	0.52
59	Square	Ponded	Outlet	-0.03	1.96	120,571	0.66	0.44

Table A-4. Circular culvert, 20% buried-invert, outlet control performance data: 45° beveled entrance with vertical headwall.

Run	Entrance	Approach	Control	S_o [%]	Q [cfs]	Re []	Hw/D []	k_e []
60	Beveled	Ponded	Outlet	-0.03	1.70	118,102	0.52	0.28
61	Beveled	Ponded	Outlet	-0.03	1.80	101,398	0.63	0.29
62	Beveled	Ponded	Outlet	-0.03	2.07	106,079	0.77	0.29
63	Beveled	Ponded	Outlet	-0.03	2.57	131,142	0.98	0.32
64	Beveled	Ponded	Outlet	-0.03	2.57	147,883	1.26	0.33
65	Beveled	Ponded	Outlet	-0.03	2.74	159,107	1.57	0.38
66	Beveled	Ponded	Outlet	-0.03	3.29	191,477	1.99	0.29
67	Beveled	Ponded	Outlet	-0.03	3.28	191,383	2.34	0.33
68	Beveled	Ponded	Outlet	-0.03	3.38	207,491	2.62	0.29
69	Beveled	Ponded	Outlet	-0.03	3.37	206,504	2.95	0.32
70	Beveled	Ponded	Outlet	-0.03	3.36	207,609	3.27	0.36
71	Beveled	Channelized	Outlet	-0.03	1.71	124,950	0.52	0.30
72	Beveled	Channelized	Outlet	-0.03	2.41	127,787	0.89	0.27
73	Beveled	Channelized	Outlet	-0.03	2.56	157,588	1.38	0.31
74	Beveled	Channelized	Outlet	-0.03	2.55	158,094	1.80	0.35
75	Beveled	Channelized	Outlet	-0.03	3.09	192,936	2.50	0.36
76	Beveled	Channelized	Outlet	-0.03	3.30	207,178	3.09	0.31
77	Beveled	Channelized	Outlet	-0.03	1.71	130,181	0.52	0.29

Table A-5. Circular culvert, 40% buried-invert, outlet control performance data: thin-wall projecting end.

Run	Entrance	Approach	Control	S_o [%]	Q [cfs]	Re []	Hw/D []	k_e []
78	Projecting	Ponded	Outlet	0.06	3.35	266,792	4.45	0.98
79	Projecting	Ponded	Outlet	0.06	3.37	269,706	3.99	0.98
80	Projecting	Ponded	Outlet	0.06	2.88	238,967	2.91	0.97
81	Projecting	Ponded	Outlet	0.06	2.91	242,960	2.37	0.98
82	Projecting	Ponded	Outlet	0.06	2.69	225,463	1.85	0.96
83	Projecting	Ponded	Outlet	0.06	2.69	227,136	1.37	0.99
84	Projecting	Ponded	Outlet	0.06	0.49	69,263	0.31	0.70
85	Projecting	Ponded	Outlet	0.06	1.18	108,025	0.56	0.72
86	Projecting	Ponded	Outlet	0.06	1.18	82,591	0.79	0.95
87	Projecting	Ponded	Outlet	0.06	1.14	83,355	0.68	0.92
88	Projecting	Ponded	Outlet	0.06	1.14	90,978	0.61	0.85
89	Projecting	Ponded	Outlet	0.06	1.54	117,490	1.02	0.98
90	Projecting	Ponded	Outlet	0.06	2.57	210,282	3.41	0.94
91	Projecting	Channelized	Outlet	0.06	0.59	83,795	0.34	0.69
92	Projecting	Channelized	Outlet	0.06	1.11	96,301	0.60	0.75
93	Projecting	Channelized	Outlet	0.06	1.16	89,061	0.73	0.82
94	Projecting	Channelized	Outlet	0.06	1.23	91,047	0.92	0.81
95	Projecting	Channelized	Outlet	0.06	3.01	249,375	4.33	0.89
96	Projecting	Channelized	Outlet	0.06	3.03	248,722	3.69	0.91
97	Projecting	Channelized	Outlet	0.06	2.90	236,952	3.11	0.93
98	Projecting	Channelized	Outlet	0.06	2.88	235,721	2.56	0.89
99	Projecting	Channelized	Outlet	0.06	2.66	217,423	2.13	0.88
100	Projecting	Channelized	Outlet	0.06	2.43	196,101	1.65	0.86
101	Projecting	Channelized	Outlet	0.06	2.19	177,788	1.29	0.84

Table A-6. Circular culvert, 40% buried-invert, outlet control performance data: mitered to 1.5H:1V fill slope with flush headwall.

Run	Entrance	Approach	Control	S_o [%]	Q [cfs]	Re []	Hw/D []	k_e []
102	Mitered	Ponded	Outlet	0.13	3.09	258,396	4.24	0.92
103	Mitered	Ponded	Outlet	0.13	2.90	239,491	3.64	0.88
104	Mitered	Ponded	Outlet	0.13	2.91	241,037	3.11	0.89
105	Mitered	Ponded	Outlet	0.13	2.59	215,596	2.55	0.92
106	Mitered	Ponded	Outlet	0.13	2.45	203,797	1.98	0.88
107	Mitered	Ponded	Outlet	0.13	2.19	185,037	1.46	0.78
108	Mitered	Ponded	Outlet	0.13	2.02	170,710	1.11	0.65
109	Mitered	Ponded	Outlet	0.13	1.77	138,340	0.74	0.50
110	Mitered	Ponded	Outlet	0.13	0.84	101,894	0.42	0.48
111	Mitered	Channelized	Outlet	0.13	0.85	103,010	0.42	0.49
112	Mitered	Channelized	Outlet	0.13	1.79	135,485	0.80	0.56
113	Mitered	Channelized	Outlet	0.13	3.10	268,043	4.13	0.93
114	Mitered	Channelized	Outlet	0.13	2.97	257,098	3.44	0.91
115	Mitered	Channelized	Outlet	0.13	2.70	234,841	2.88	0.88
116	Mitered	Channelized	Outlet	0.13	2.49	216,664	2.25	0.89
117	Mitered	Channelized	Outlet	0.13	2.23	194,298	1.76	0.82
118	Mitered	Channelized	Outlet	0.13	1.65	143,644	1.29	0.74

Table A-7. Circular culvert, 40% buried-invert, outlet control performance data: square-edged entrance with vertical headwall.

Run	Entrance	Approach	Control	S_o [%]	Q [cfs]	Re []	Hw/D []	k_e []
119	Square	Ponded	Outlet	0.06	2.91	230,837	3.92	0.54
120	Square	Ponded	Outlet	0.06	2.84	225,447	3.14	0.54
121	Square	Ponded	Outlet	0.06	2.71	215,903	2.20	0.57
122	Square	Ponded	Outlet	0.06	2.25	180,232	1.44	0.56
123	Square	Ponded	Outlet	0.06	2.04	144,055	1.00	0.48
124	Square	Ponded	Outlet	0.06	0.90	96,160	0.44	0.42
125	Square	Channelized	Outlet	0.06	0.59	85,726	0.33	0.37
126	Square	Channelized	Outlet	0.06	0.93	79,957	0.56	0.44
127	Square	Channelized	Outlet	0.06	1.18	91,253	0.74	0.46
128	Square	Channelized	Outlet	0.06	1.23	92,643	0.93	0.46
129	Square	Channelized	Outlet	0.06	3.06	253,831	4.30	0.52
130	Square	Channelized	Outlet	0.06	2.92	238,786	3.75	0.53
131	Square	Channelized	Outlet	0.06	2.79	226,093	3.25	0.58
132	Square	Channelized	Outlet	0.06	2.71	220,042	2.78	0.56
133	Square	Channelized	Outlet	0.06	2.60	209,429	2.37	0.53
134	Square	Channelized	Outlet	0.06	2.19	176,261	1.78	0.52
135	Square	Channelized	Outlet	0.06	2.19	176,261	1.41	0.50
136	Square	Channelized	Outlet	0.06	2.08	167,677	1.22	0.53

Table A-8. Circular culvert, 40% buried-invert, outlet control performance data: 45° beveled entrance with vertical headwall.

Run	Entrance	Approach	Control	S_o [%]	Q [cfs]	Re []	Hw/D []	k_e []
137	Beveled	Ponded	Outlet	0.06	3.09	247,643	3.94	0.36
138	Beveled	Ponded	Outlet	0.06	2.68	214,681	2.80	0.34
139	Beveled	Ponded	Outlet	0.06	2.43	196,463	2.03	0.36
140	Beveled	Ponded	Outlet	0.06	2.00	162,025	1.18	0.34
141	Beveled	Ponded	Outlet	0.06	1.11	89,990	0.58	0.29
142	Beveled	Channelized	Outlet	0.06	0.54	80,205	0.30	0.28
143	Beveled	Channelized	Outlet	0.06	0.96	79,175	0.60	0.33
144	Beveled	Channelized	Outlet	0.06	1.22	93,759	0.92	0.31
145	Beveled	Channelized	Outlet	0.06	3.08	254,821	4.28	0.34
146	Beveled	Channelized	Outlet	0.06	2.95	244,404	3.62	0.34
147	Beveled	Channelized	Outlet	0.06	2.82	234,228	3.04	0.34
148	Beveled	Channelized	Outlet	0.06	2.57	214,781	2.43	0.34
149	Beveled	Channelized	Outlet	0.06	2.34	195,939	1.92	0.35
150	Beveled	Channelized	Outlet	0.06	2.81	240,975	3.12	0.34
151	Beveled	Channelized	Outlet	0.06	2.09	177,425	1.49	0.33
152	Beveled	Channelized	Outlet	0.06	1.86	158,831	1.22	0.36

Table A-9. Circular culvert, 50% buried-invert, outlet control performance data: thin-wall projecting end.

Run	Entrance	Approach	Control	S_o [%]	Q [cfs]	Re []	Hw/D []	k_e []
153	Projecting	Ponded	Outlet	-0.05	2.82	290,162	5.21	0.93
154	Projecting	Ponded	Outlet	-0.05	2.43	241,114	2.72	0.94
155	Projecting	Ponded	Outlet	-0.05	2.13	212,309	1.83	1.02
156	Projecting	Ponded	Outlet	-0.05	1.90	187,794	1.41	0.97
157	Projecting	Ponded	Outlet	-0.05	1.71	143,237	1.01	0.86
158	Projecting	Ponded	Outlet	-0.05	0.93	86,638	0.67	0.82
159	Projecting	Ponded	Outlet	-0.05	0.50	74,117	0.39	0.59
160	Projecting	Ponded	Outlet	-0.05	2.17	212,436	2.52	0.95
161	Projecting	Ponded	Outlet	-0.05	3.04	295,473	2.69	0.94
162	Projecting	Ponded	Outlet	-0.05	3.00	291,625	3.59	0.95
163	Projecting	Ponded	Outlet	-0.05	2.89	302,711	5.14	0.94
164	Projecting	Channelized	Outlet	-0.05	2.88	292,982	5.13	0.93
165	Projecting	Channelized	Outlet	-0.05	2.63	268,134	4.23	0.93
166	Projecting	Channelized	Outlet	-0.05	2.51	259,473	3.22	0.97
167	Projecting	Channelized	Outlet	-0.05	2.24	232,673	2.54	0.89
168	Projecting	Channelized	Outlet	-0.05	1.98	205,514	1.88	0.84
169	Projecting	Channelized	Outlet	-0.05	1.87	194,929	1.39	0.78
170	Projecting	Channelized	Outlet	-0.05	1.71	151,952	0.99	0.67
171	Projecting	Channelized	Outlet	-0.05	1.10	106,431	0.71	0.61
172	Projecting	Channelized	Outlet	-0.05	0.57	99,448	0.42	0.57

Table A-10. Circular culvert, 50% buried-invert, outlet control performance data: mitered to 1.5H:1V fill slope with flush headwall.

Run	Entrance	Approach	Control	S_o [%]	Q [cfs]	Re []	Hw/D []	k_e []
173	Mitered	Ponded	Outlet	-0.002	3.04	242,818	5.36	0.87
174	Mitered	Ponded	Outlet	-0.002	2.88	226,352	4.56	0.88
175	Mitered	Ponded	Outlet	-0.002	2.72	213,581	3.84	0.89
176	Mitered	Ponded	Outlet	-0.002	2.53	198,654	3.10	0.90
177	Mitered	Ponded	Outlet	-0.002	2.32	182,518	2.44	0.92
178	Mitered	Ponded	Outlet	-0.002	2.33	182,501	2.04	0.88
179	Mitered	Ponded	Outlet	-0.002	2.07	164,743	1.60	0.83
180	Mitered	Ponded	Outlet	-0.002	1.98	146,411	1.15	0.58
181	Mitered	Ponded	Outlet	-0.002	2.41	193,048	1.32	0.66
182	Mitered	Ponded	Outlet	-0.002	2.47	198,664	1.50	0.76
183	Mitered	Ponded	Outlet	-0.002	2.04	141,679	1.01	0.48
184	Mitered	Ponded	Outlet	-0.002	1.47	116,003	0.75	0.43
185	Mitered	Ponded	Outlet	-0.002	1.78	133,178	0.86	0.44
186	Mitered	Ponded	Outlet	-0.002	1.07	93,341	0.61	0.47
187	Mitered	Ponded	Outlet	-0.002	0.61	67,981	0.42	0.54
188	Mitered	Channelized	Outlet	-0.002	3.06	244,526	5.22	0.89
189	Mitered	Channelized	Outlet	-0.002	2.72	217,068	4.29	0.89
190	Mitered	Channelized	Outlet	-0.002	2.74	218,091	3.52	0.87
191	Mitered	Channelized	Outlet	-0.002	2.53	200,746	2.75	0.87
192	Mitered	Channelized	Outlet	-0.002	2.31	183,993	1.76	0.75
193	Mitered	Channelized	Outlet	-0.002	2.20	175,889	1.24	0.66
194	Mitered	Channelized	Outlet	-0.002	1.51	114,907	0.78	0.49
195	Mitered	Channelized	Outlet	-0.002	2.31	184,737	1.78	0.78
196	Mitered	Channelized	Outlet	-0.002	0.60	66,599	0.42	0.57

Table A-11. Circular culvert, 50% buried-invert, outlet control performance data: square-edged entrance with vertical headwall.

Run	Entrance	Approach	Control	S_o [%]	Q [cfs]	Re []	Hw/D []	k_e []
197	Square	Ponded	Outlet	-0.05	3.04	305,469	5.28	0.55
198	Square	Ponded	Outlet	-0.05	2.83	279,609	4.05	0.55
199	Square	Ponded	Outlet	-0.05	2.63	258,347	3.08	0.55
200	Square	Ponded	Outlet	-0.05	2.40	235,837	2.08	0.57
201	Square	Ponded	Outlet	-0.05	2.13	210,717	1.51	0.54
202	Square	Ponded	Outlet	-0.05	1.94	192,266	1.23	0.51
203	Square	Ponded	Outlet	-0.05	1.09	97,380	0.75	0.38
204	Square	Channelized	Outlet	-0.05	0.78	95,564	0.49	0.30
205	Square	Channelized	Outlet	-0.05	1.18	100,378	0.88	0.38
206	Square	Channelized	Outlet	-0.05	2.86	282,632	4.72	0.53
207	Square	Channelized	Outlet	-0.05	2.55	254,699	3.62	0.54
208	Square	Channelized	Outlet	-0.05	2.25	226,178	2.59	0.53
209	Square	Channelized	Outlet	-0.05	1.96	198,590	1.73	0.52
210	Square	Channelized	Outlet	-0.05	1.65	168,536	1.24	0.49

Table A-12. Circular culvert, 50% buried-invert, outlet control performance data: 45° beveled entrance with vertical headwall.

Run	Entrance	Approach	Control	S_o [%]	Q [cfs]	Re []	Hw/D []	k_e []
211	Beveled	Ponded	Outlet	-0.05	2.91	278,577	4.60	0.32
212	Beveled	Ponded	Outlet	-0.05	2.38	227,166	3.16	0.32
213	Beveled	Ponded	Outlet	-0.05	2.07	200,429	1.75	0.32
214	Beveled	Ponded	Outlet	-0.05	1.63	136,677	1.00	0.28
215	Beveled	Channelized	Outlet	-0.05	1.19	109,573	0.72	0.23
216	Beveled	Channelized	Outlet	-0.05	0.87	100,060	0.53	0.23
217	Beveled	Channelized	Outlet	-0.05	0.65	86,985	0.43	0.22
218	Beveled	Channelized	Outlet	-0.05	2.95	292,240	4.96	0.31
219	Beveled	Channelized	Outlet	-0.05	2.97	285,311	4.23	0.31
220	Beveled	Channelized	Outlet	-0.05	2.80	267,199	3.52	0.32
221	Beveled	Channelized	Outlet	-0.05	2.57	245,232	2.77	0.33
222	Beveled	Channelized	Outlet	-0.05	2.40	229,340	2.07	0.33
223	Beveled	Channelized	Outlet	-0.05	1.94	185,837	1.45	0.33
224	Beveled	Channelized	Outlet	-0.05	1.55	126,729	0.98	0.28

Table A-13. Elliptical culvert, 50% buried-invert, outlet control performance data: thin-wall projecting end.

Run	Entrance	Approach	Control	S_o [%]	Q [cfs]	Re []	Hw/D []	k_e []
225	Projecting	ponded	Outlet	-0.10	0.76	75,563	0.46	0.88
226	Projecting	Ponded	Outlet	-0.10	1.00	81,463	0.55	0.92
227	Projecting	Ponded	Outlet	-0.10	1.12	83,073	1.42	1.17
228	Projecting	Ponded	Outlet	-0.10	1.26	90,761	0.67	0.86
229	Projecting	Ponded	Outlet	-0.10	1.26	81,181	1.00	1.07
230	Projecting	Ponded	Outlet	-0.10	1.26	76,031	0.85	0.88
231	Projecting	Ponded	Outlet	-0.10	2.08	158,758	3.81	1.06
232	Projecting	Ponded	Outlet	-0.10	2.10	160,346	3.19	1.11
233	Projecting	Ponded	Outlet	-0.10	2.10	160,991	1.44	1.13
234	Projecting	Ponded	Outlet	-0.10	2.16	166,013	2.31	1.13
235	Projecting	Ponded	Outlet	-0.10	4.16	317,434	3.07	1.14
236	Projecting	Ponded	Outlet	-0.10	4.16	317,434	4.06	1.09
237	Projecting	Ponded	Outlet	-0.10	4.20	320,793	2.09	1.11
238	Projecting	Channelized	Outlet	-0.10	0.81	76,905	0.47	0.53
239	Projecting	Channelized	Outlet	-0.10	1.15	86,739	1.44	0.90
240	Projecting	Channelized	Outlet	-0.10	1.23	86,606	0.65	0.56
241	Projecting	Channelized	Outlet	-0.10	1.26	74,669	0.91	0.67
242	Projecting	Channelized	Outlet	-0.10	2.14	153,170	1.27	0.82
243	Projecting	Channelized	Outlet	-0.10	2.24	164,813	3.56	1.00
244	Projecting	Channelized	Outlet	-0.10	2.27	162,675	1.81	0.88
245	Projecting	Channelized	Outlet	-0.10	2.28	166,933	3.03	0.99
246	Projecting	Channelized	Outlet	-0.10	2.29	167,630	2.54	0.88
247	Projecting	Channelized	Outlet	-0.10	4.13	308,724	4.05	1.04
248	Projecting	Channelized	Outlet	-0.10	4.37	326,472	3.08	1.05

Table A-14. Elliptical culvert, 50% buried-invert, outlet control performance data: mitered to 1.5H:1V fill slope with flush headwall.

Run	Entrance	Approach	Control	S_o [%]	Q [cfs]	Re []	Hw/D []	k_e []
249	Mitered	Ponded	Outlet	-0.08	0.76	93,677	0.44	0.53
250	Mitered	Ponded	Outlet	-0.08	1.11	89,648	0.66	0.55
251	Mitered	Ponded	Outlet	-0.08	1.16	84,743	0.75	0.43
252	Mitered	Ponded	Outlet	-0.08	1.47	103,778	0.86	0.40
253	Mitered	Ponded	Outlet	-0.08	1.53	116,969	0.99	0.48
254	Mitered	Ponded	Outlet	-0.08	1.53	135,452	1.23	0.70
255	Mitered	Ponded	Outlet	-0.08	1.54	136,668	1.82	0.77
256	Mitered	Ponded	Outlet	-0.08	1.54	136,894	1.52	0.76
257	Mitered	Ponded	Outlet	-0.08	1.54	138,246	2.24	0.84
258	Mitered	Ponded	Outlet	-0.08	1.54	138,696	2.72	0.93
259	Mitered	Ponded	Outlet	-0.08	2.06	176,340	3.40	0.89
260	Mitered	Ponded	Outlet	-0.08	2.82	241,278	4.85	0.87
261	Mitered	Channelized	Outlet	-0.08	0.90	108,368	0.49	0.55
262	Mitered	Channelized	Outlet	-0.08	1.16	97,738	0.67	0.56
263	Mitered	Channelized	Outlet	-0.08	1.86	135,285	0.90	0.49
264	Mitered	Channelized	Outlet	-0.08	2.39	217,185	1.68	0.73
265	Mitered	Channelized	Outlet	-0.08	2.39	200,197	1.14	0.51
266	Mitered	Channelized	Outlet	-0.08	3.06	264,096	4.50	0.93
267	Mitered	Channelized	Outlet	-0.08	3.08	275,319	3.57	0.93
268	Mitered	Channelized	Outlet	-0.08	3.09	277,915	3.08	0.92
269	Mitered	Channelized	Outlet	-0.08	3.12	281,639	2.04	0.82

Table A-15. Elliptical culvert, 50% buried-invert, outlet control performance data: square-edged entrance with vertical headwall.

Run	Entrance	Approach	Control	S_o [%]	Q [cfs]	Re []	Hw/D []	k_e []
270	Square	ponded	Outlet	-0.10	0.67	83,222	0.42	0.51
271	Square	ponded	Outlet	-0.10	0.94	81,360	1.46	0.62
272	Square	ponded	Outlet	-0.10	1.13	82,260	0.78	0.41
273	Square	ponded	Outlet	-0.10	1.15	83,106	0.90	0.48
274	Square	ponded	Outlet	-0.10	1.89	162,909	2.25	0.65
275	Square	ponded	Outlet	-0.10	2.01	164,137	0.81	0.43
276	Square	ponded	Outlet	-0.10	2.10	160,991	4.11	0.55
277	Square	ponded	Outlet	-0.10	2.15	163,586	2.77	0.61
278	Square	ponded	Outlet	-0.10	2.16	163,305	1.40	0.60
279	Square	ponded	Outlet	-0.10	3.68	317,283	2.87	0.63
280	Square	ponded	Outlet	-0.10	3.95	298,202	2.98	0.60
281	Square	ponded	Outlet	-0.10	4.22	318,557	4.67	0.59
282	Square	ponded	Outlet	-0.10	4.28	322,636	3.94	0.61
283	Square	ponded	Outlet	-0.10	4.32	327,195	2.23	0.60
284	Square	channelized	Outlet	-0.10	0.69	80,245	0.42	0.51
285	Square	channelized	Outlet	-0.10	1.01	83,402	0.62	0.46
286	Square	channelized	Outlet	-0.10	1.05	88,154	1.14	0.44
287	Square	channelized	Outlet	-0.10	1.05	88,205	1.71	0.61
288	Square	channelized	Outlet	-0.10	1.10	79,699	0.77	0.41
289	Square	channelized	Outlet	-0.10	1.14	82,359	0.92	0.43
290	Square	channelized	Outlet	-0.10	2.08	160,991	4.12	0.62
291	Square	channelized	Outlet	-0.10	2.10	163,295	1.23	0.57
292	Square	channelized	Outlet	-0.10	2.11	164,445	1.97	0.59
293	Square	channelized	Outlet	-0.10	4.09	317,972	3.41	0.61
294	Square	channelized	Outlet	-0.10	4.16	323,170	2.51	0.56

Table A-16. Elliptical culvert, 50% buried-invert, outlet control performance data: 45° beveled entrance with vertical headwall.

Run	Entrance	Approach	Control	S_o [%]	Q [cfs]	Re []	Hw/D []	k_e []
295	Square	ponded	Outlet	-0.10	2.07	165,222	4.37	0.31
296	Square	ponded	Outlet	-0.10	2.09	165,305	3.05	0.33
297	Square	ponded	Outlet	-0.10	2.10	166,534	1.85	0.32
298	Square	ponded	Outlet	-0.10	2.04	161,140	1.19	0.34
299	Square	ponded	Outlet	-0.10	2.18	154,966	0.84	0.23
300	Square	ponded	Outlet	-0.10	4.13	327,122	4.60	0.28
301	Square	ponded	Outlet	-0.10	4.16	330,139	2.54	0.31
302	Square	ponded	Outlet	-0.10	0.67	77,117	0.41	0.32
303	Square	ponded	Outlet	-0.10	1.16	81,312	0.74	0.24
304	Square	ponded	Outlet	-0.10	1.00	81,215	1.29	0.32
305	Square	channelized	Outlet	-0.10	1.03	79,781	1.75	0.37
306	Square	channelized	Outlet	-0.10	1.06	80,856	1.06	0.31
307	Square	channelized	Outlet	-0.10	1.22	78,644	0.90	0.32
308	Square	channelized	Outlet	-0.10	1.00	76,366	0.61	0.29
309	Square	channelized	Outlet	-0.10	2.56	172,361	1.11	0.30
310	Square	channelized	Outlet	-0.10	2.08	159,797	1.78	0.35
311	Square	channelized	Outlet	-0.10	2.11	161,526	2.68	0.36
312	Square	channelized	Outlet	-0.10	4.32	329,855	3.88	0.30
313	Square	channelized	Outlet	-0.10	4.46	340,253	2.20	0.32

APPENDIX B

Buried-Invert Culvert Inlet Control Experimental Data Set (Tabular Support Data for Chapter 2)

Table B-1. Circular culvert, 20% buried-invert, inlet control performance data: thin-wall projecting end.

Run	Entrance	Approach	Control	S_o [%]	Q [cfs]	Re []	Hw/D []	$Q/AD^{0.5}$ [$ft^{0.5}/s$]	$Hw/D-H_c/D+0.5S_o$ []	$(Q/AD^{0.5})^2$ [ft/s^2]
1	Projecting	Ponded	Inlet	2.69	1.54	202,516	0.51	1.34	0.09	1.79
2	Projecting	Ponded	Inlet	2.69	2.39	227,475	0.68	2.07	0.12	4.30
3	Projecting	Ponded	Inlet	2.69	2.85	248,769	0.77	2.48	0.14	6.14
4	Projecting	Ponded	Inlet	2.69	3.31	267,984	0.85	2.88	0.16	8.31
5	Projecting	Ponded	Inlet	2.69	3.62	285,502	0.91	3.15	0.18	9.93
6	Projecting	Ponded	Inlet	2.69	1.95	206,668	0.60	1.70	0.11	2.89
7	Projecting	Ponded	Inlet	2.69	1.16	171,834	0.43	1.01	0.08	1.02
8	Projecting	Ponded	Inlet	2.69	0.89	146,129	0.36	0.78	0.07	0.61
9	Projecting	Ponded	Inlet	2.69	0.69	125,044	0.31	0.60	0.07	0.36
10	Projecting	Ponded	Inlet	2.69	0.49	107,448	0.25	0.42	0.06	0.18
11	Projecting	Ponded	Inlet	2.69	4.00	301,003	0.97	3.48	0.19	12.09
12	Projecting	Ponded	Inlet	2.69	4.36	318,809	1.04	3.79	0.21	14.38
13	Projecting	Ponded	Inlet	2.69	4.74	341,348	1.12	4.12	0.25	16.95
14	Projecting	Ponded	Inlet	2.69	5.11	358,875	1.20	4.44	0.28	19.73
15	Projecting	Ponded	Inlet	2.69	5.52	378,291	1.29	4.80	0.32	23.06
16	Projecting	Ponded	Inlet	2.69	6.02	404,296	1.40	5.23	0.37	27.37
17	Projecting	Ponded	Inlet	2.69	6.54	432,938	1.55	5.68	0.46	32.30
18	Projecting	Ponded	Inlet	2.69	7.00	462,562	1.69	6.09	0.54	37.10
19	Projecting	Ponded	Inlet	2.69	7.49	484,423	1.85	6.51	0.64	42.38
20	Projecting	Ponded	Inlet	2.69	8.04	519,831	2.04	6.99	0.76	48.91
21	Projecting	Ponded	Inlet	2.69	8.23	534,625	2.12	7.16	0.82	51.27
22	Projecting	Ponded	Inlet	2.69	9.07	593,004	2.46	7.89	1.05	62.25
23	Projecting	Ponded	Inlet	2.69	10.15	648,922	2.93	8.83	1.39	77.95
24	Projecting	Ponded	Inlet	2.69	7.04	468,348	1.70	6.12	0.54	37.51
25	Projecting	Channelized	Inlet	2.69	0.51	118,531	0.25	0.45	0.05	0.20
26	Projecting	Channelized	Inlet	2.69	1.02	146,338	0.38	0.89	0.07	0.79
27	Projecting	Channelized	Inlet	2.69	1.52	197,956	0.49	1.33	0.08	1.76
28	Projecting	Channelized	Inlet	2.69	2.18	221,978	0.62	1.90	0.10	3.60
29	Projecting	Channelized	Inlet	2.69	3.06	258,123	0.77	2.66	0.12	7.08
30	Projecting	Channelized	Inlet	2.69	3.75	289,019	0.88	3.26	0.13	10.64
31	Projecting	Channelized	Inlet	2.69	2.64	240,641	0.70	2.29	0.11	5.25
32	Projecting	Channelized	Inlet	2.69	4.52	323,037	1.00	3.93	0.16	15.42
33	Projecting	Channelized	Inlet	2.69	5.26	359,001	1.14	4.57	0.21	20.91
34	Projecting	Channelized	Inlet	2.69	7.57	465,529	1.68	6.58	0.47	43.28
35	Projecting	Channelized	Inlet	2.69	7.00	447,821	1.55	6.09	0.40	37.10
36	Projecting	Channelized	Inlet	2.69	8.27	499,738	1.88	7.19	0.58	51.76
37	Projecting	Channelized	Inlet	2.69	9.01	540,599	2.14	7.84	0.75	61.41
38	Projecting	Channelized	Inlet	2.69	10.03	604,914	2.54	8.72	1.02	76.07
39	Projecting	Channelized	Inlet	2.69	6.73	423,942	1.49	5.85	0.37	34.25
40	Projecting	Channelized	Inlet	2.69	6.01	390,524	1.31	5.23	0.28	27.30
41	Projecting	Channelized	Inlet	2.69	6.25	403,247	1.37	5.43	0.31	29.52
42	Projecting	Channelized	Inlet	2.69	5.65	371,447	1.21	4.91	0.22	24.11
43	Projecting	Channelized	Inlet	2.69	4.74	333,373	1.04	4.12	0.17	16.95

Table B-2. Circular culvert, 20% buried-invert, inlet control performance data: mitered to 1.5H:1V fill slope with flush headwall.

Run	Entrance	Approach	Control	S_o [%]	Q [cfs]	Re []	Hw/D []	$Q/AD^{0.5}$ [$ft^{0.5}/s$]	$Hw/D\text{-}H_c/D+0.5S_o$ []	$(Q/AD^{0.5})^2$ [ft/s^2]
44	Mitered	Ponded	Inlet	2.76	9.46	608,858	2.28	8.22	0.82	67.55
45	Mitered	Ponded	Inlet	2.76	8.49	557,497	1.97	7.38	0.63	54.50
46	Mitered	Ponded	Inlet	2.76	7.49	505,180	1.67	6.51	0.45	42.35
47	Mitered	Ponded	Inlet	2.76	6.80	457,097	1.49	5.91	0.35	34.92
48	Mitered	Ponded	Inlet	2.76	5.95	402,784	1.24	5.17	0.21	26.73
49	Mitered	Ponded	Inlet	2.76	4.07	316,087	0.90	3.54	0.10	12.50
50	Mitered	Ponded	Inlet	2.76	3.37	289,464	0.79	2.93	0.08	8.56
51	Mitered	Ponded	Inlet	2.76	2.64	254,420	0.67	2.29	0.06	5.25
52	Mitered	Ponded	Inlet	2.76	1.93	221,181	0.55	1.67	0.05	2.81
53	Mitered	Ponded	Inlet	2.76	1.23	192,704	0.42	1.07	0.04	1.14
54	Mitered	Ponded	Inlet	2.76	0.72	140,902	0.30	0.63	0.04	0.40
55	Mitered	Channelized	Inlet	2.76	9.96	594,301	2.34	8.66	0.81	74.98
56	Mitered	Channelized	Inlet	2.76	8.95	536,568	2.00	7.78	0.60	60.54
57	Mitered	Channelized	Inlet	2.76	7.99	490,632	1.72	6.95	0.44	48.25
58	Mitered	Channelized	Inlet	2.76	6.88	436,544	1.45	5.98	0.30	35.75
59	Mitered	Channelized	Inlet	2.76	6.01	396,458	1.24	5.22	0.20	27.28
60	Mitered	Channelized	Inlet	2.76	4.54	331,988	0.97	3.94	0.11	15.55
61	Mitered	Channelized	Inlet	2.76	3.71	306,348	0.84	3.23	0.09	10.41
62	Mitered	Channelized	Inlet	2.76	3.01	270,579	0.73	2.62	0.07	6.84
63	Mitered	Channelized	Inlet	2.76	2.28	234,941	0.61	1.98	0.06	3.94
64	Mitered	Channelized	Inlet	2.76	1.56	212,773	0.48	1.36	0.05	1.84
65	Mitered	Channelized	Inlet	2.76	1.00	166,124	0.37	0.87	0.04	0.75

Table B-3. Circular culvert, 20% buried-invert, inlet control performance data: square-edged entrance with vertical headwall.

Run	Entrance	Approach	Control	S_o [%]	Q [cfs]	Re []	Hw/D []	$Q/AD^{0.5}$ [$ft^{0.5}/s$]	$Hw/D\text{-}H_c/D+0.5S_o$ []	$(Q/AD^{0.5})^2$ [ft/s^2]
66	Square	Ponded	Inlet	2.69	10.01	591,305	2.19	8.70	0.66	75.74
67	Square	Ponded	Inlet	2.69	9.06	542,858	1.92	7.88	0.52	62.07
68	Square	Ponded	Inlet	2.69	7.99	485,039	1.64	6.95	0.37	48.25
69	Square	Ponded	Inlet	2.69	6.99	434,912	1.41	6.07	0.26	36.87
70	Square	Ponded	Inlet	2.69	5.99	390,031	1.21	5.21	0.19	27.15
71	Square	Ponded	Inlet	2.69	4.97	346,352	1.04	4.32	0.14	18.68
72	Square	Ponded	Inlet	2.69	4.23	316,082	0.93	3.68	0.12	13.54
73	Square	Ponded	Inlet	2.69	3.47	285,392	0.80	3.02	0.09	9.11
74	Square	Ponded	Inlet	2.69	2.82	255,539	0.70	2.45	0.08	6.02
75	Square	Ponded	Inlet	2.69	2.16	228,772	0.59	1.88	0.07	3.53
76	Square	Ponded	Inlet	2.69	1.53	203,663	0.47	1.33	0.06	1.77
77	Square	Ponded	Inlet	2.69	1.01	156,573	0.37	0.88	0.05	0.77
78	Square	Ponded	Inlet	2.69	0.51	113,021	0.24	0.45	0.04	0.20
79	Square	Channelized	Inlet	2.69	0.72	125,755	0.30	0.62	0.05	0.39
80	Square	Channelized	Inlet	2.69	2.47	239,319	0.64	2.14	0.08	4.59
81	Square	Channelized	Inlet	2.69	3.89	298,640	0.88	3.38	0.11	11.46
82	Square	Channelized	Inlet	2.69	6.61	414,580	1.33	5.75	0.23	33.05
83	Square	Channelized	Inlet	2.69	8.26	493,991	1.69	7.18	0.39	51.58
84	Square	Channelized	Inlet	2.69	9.60	559,016	2.04	8.34	0.57	69.64

Table B-4. Circular culvert, 20% buried-invert, inlet control performance data: 45° beveled entrance with vertical headwall.

Run	Entrance	Approach	Control	S_o [%]	Q [cfs]	Re []	Hw/D []	$Q/AD^{0.5}$ [$ft^{0.5}/s$]	Hw/D-H_c/D+0.5S_o []	$(Q/AD^{0.5})^2$ [ft/s^2]
85	Beveled	Ponded	Inlet	2.69	9.85	588,591	1.89	8.56	0.38	73.31
86	Beveled	Ponded	Inlet	2.69	8.94	537,641	1.68	7.77	0.29	60.33
87	Beveled	Ponded	Inlet	2.69	4.52	331,097	0.93	3.93	0.07	15.41
88	Beveled	Ponded	Inlet	2.69	3.79	301,731	0.82	3.29	0.05	10.83
89	Beveled	Ponded	Inlet	2.69	3.03	270,044	0.71	2.63	0.05	6.92
90	Beveled	Ponded	Inlet	2.69	2.23	238,513	0.59	1.94	0.04	3.77
91	Beveled	Ponded	Inlet	2.69	1.52	202,014	0.46	1.32	0.03	1.74
92	Beveled	Ponded	Inlet	2.69	1.00	156,032	0.36	0.87	0.03	0.75
93	Beveled	Ponded	Inlet	2.69	0.52	115,054	0.23	0.45	0.02	0.20
94	Beveled	Ponded	Inlet	2.69	6.75	426,059	1.27	5.87	0.14	34.44
95	Beveled	Ponded	Inlet	2.69	7.47	463,830	1.39	6.49	0.17	42.14
96	Beveled	Ponded	Inlet	2.69	8.59	514,589	1.61	7.47	0.26	55.75
97	Beveled	Channelized	Inlet	2.69	0.42	164,978	0.20	0.36	0.02	0.13
98	Beveled	Channelized	Inlet	2.69	1.20	189,693	0.40	1.05	0.03	1.09
99	Beveled	Channelized	Inlet	2.69	2.11	251,543	0.56	1.84	0.03	3.38
100	Beveled	Channelized	Inlet	2.69	2.82	267,184	0.68	2.45	0.05	6.00
101	Beveled	Channelized	Inlet	2.69	4.04	312,630	0.87	3.52	0.07	12.36
102	Beveled	Channelized	Inlet	2.69	6.82	428,769	1.29	5.93	0.15	35.13
103	Beveled	Channelized	Inlet	2.69	7.03	541,752	1.33	6.11	0.16	37.35
104	Beveled	Channelized	Inlet	2.69	7.47	458,173	1.40	6.50	0.18	42.21
105	Beveled	Channelized	Inlet	2.69	8.49	507,700	1.60	7.38	0.26	54.50
106	Beveled	Channelized	Inlet	2.69	9.54	559,223	1.82	8.29	0.34	68.73

Table B-5. Circular culvert, 40% buried-invert, inlet control performance data: thin-wall projecting end.

Run	Entrance	Approach	Control	S_o [%]	Q [cfs]	Re []	Hw/D []	$Q/AD^{0.5}$ [$ft^{0.5}/s$]	Hw/D-H_c/D+0.5S_o []	$(Q/AD^{0.5})^2$ [ft/s^2]
107	Projecting	Ponded	Inlet	2.97	2.74	321,704	1.01	2.98	0.20	8.85
108	Projecting	Ponded	Inlet	2.97	2.32	290,974	0.89	2.51	0.17	6.32
109	Projecting	Ponded	Inlet	2.97	1.90	256,427	0.77	2.07	0.14	4.27
110	Projecting	Ponded	Inlet	2.97	1.48	221,454	0.65	1.61	0.12	2.58
111	Projecting	Ponded	Inlet	2.97	1.01	186,804	0.50	1.09	0.09	1.19
112	Projecting	Ponded	Inlet	2.97	0.58	151,625	0.34	0.63	0.06	0.39
113	Projecting	Ponded	Inlet	2.97	7.64	638,034	3.79	8.30	1.98	68.85
114	Projecting	Ponded	Inlet	2.97	8.74	729,316	4.68	9.48	2.59	89.96
115	Projecting	Ponded	Inlet	2.97	8.23	686,333	4.31	8.94	2.35	79.89
116	Projecting	Ponded	Inlet	2.97	6.96	593,143	3.36	7.55	1.70	57.05
117	Projecting	Ponded	Inlet	2.97	6.18	547,038	2.75	6.70	1.26	44.93
118	Projecting	Ponded	Inlet	2.97	5.30	465,686	2.16	5.76	0.84	33.13
119	Projecting	Ponded	Inlet	2.97	4.37	407,579	1.64	4.75	0.51	22.52
120	Projecting	Channelized	Inlet	2.97	6.37	540,855	2.59	6.92	1.06	47.85
121	Projecting	Channelized	Inlet	2.97	5.57	477,584	2.11	6.05	0.74	36.59
122	Projecting	Channelized	Inlet	2.97	4.88	427,389	1.75	5.30	0.52	28.04
123	Projecting	Channelized	Inlet	2.97	4.25	384,901	1.47	4.62	0.36	21.33
124	Projecting	Channelized	Inlet	2.97	2.74	294,500	0.99	2.98	0.18	8.85
125	Projecting	Channelized	Inlet	2.97	2.30	272,094	0.88	2.50	0.16	6.24
126	Projecting	Channelized	Inlet	2.97	1.92	245,519	0.77	2.09	0.14	4.35
127	Projecting	Channelized	Inlet	2.97	1.70	229,676	0.71	1.84	0.13	3.40
128	Projecting	Channelized	Inlet	2.97	1.22	199,701	0.57	1.32	0.11	1.75
129	Projecting	Channelized	Inlet	2.97	0.80	167,467	0.44	0.87	0.09	0.76
130	Projecting	Channelized	Inlet	2.97	0.53	142,346	0.34	0.57	0.07	0.33
131	Projecting	Channelized	Inlet	2.97	7.73	644,061	3.60	8.39	1.76	70.47
132	Projecting	Channelized	Inlet	2.97	8.34	689,946	4.14	9.05	2.16	81.95

Table B-6. Circular culvert, 40% buried-invert, inlet control performance data: mitered to 1.5H:1V fill slope with flush headwall.

Run	Entrance	Approach	Control	S_o [%]	Q [cfs]	Re []	Hw/D []	$Q/AD^{0.5}$ [$ft^{0.5}/s$]	$Hw/D-H_c/D+0.5S_o$ []	$(Q/AD^{0.5})^2$ [ft/s^2]
133	Mitered	Ponded	Inlet	3.53	3.06	322,440	0.96	3.32	0.08	11.05
134	Mitered	Ponded	Inlet	3.53	2.35	278,471	0.79	2.55	0.06	6.50
135	Mitered	Ponded	Inlet	3.53	1.79	243,576	0.65	1.95	0.05	3.79
136	Mitered	Ponded	Inlet	3.53	2.71	298,087	0.88	2.94	0.07	8.62
137	Mitered	Ponded	Inlet	3.53	1.18	206,032	0.50	1.28	0.04	1.64
138	Mitered	Ponded	Inlet	3.53	0.81	177,102	0.39	0.88	0.03	0.77
139	Mitered	Ponded	Inlet	3.53	4.64	417,863	1.56	5.03	0.38	25.33
140	Mitered	Ponded	Inlet	3.53	5.39	461,500	1.91	5.85	0.57	34.21
141	Mitered	Ponded	Inlet	3.53	7.06	568,161	2.86	7.66	1.18	58.73
142	Mitered	Ponded	Inlet	3.53	6.46	527,251	2.50	7.01	0.94	49.15
143	Mitered	Ponded	Inlet	3.53	6.16	508,429	2.33	6.69	0.84	44.71
144	Mitered	Ponded	Inlet	3.53	5.73	477,097	2.09	6.22	0.69	38.65
145	Mitered	Ponded	Inlet	3.53	5.07	434,405	1.75	5.51	0.48	30.31
146	Mitered	Channelized	Inlet	3.53	3.10	321,897	0.97	3.36	0.09	11.31
147	Mitered	Channelized	Inlet	3.53	2.22	272,460	0.76	2.41	0.06	5.81
148	Mitered	Channelized	Inlet	3.53	1.48	222,025	0.57	1.61	0.04	2.58
149	Mitered	Channelized	Inlet	3.53	5.60	465,824	1.91	6.08	0.54	36.91
150	Mitered	Channelized	Inlet	3.53	6.52	523,872	2.35	7.07	0.79	50.01
151	Mitered	Channelized	Inlet	3.53	4.98	429,938	1.67	5.41	0.42	29.23
152	Mitered	Channelized	Inlet	3.53	5.91	483,426	2.05	6.41	0.61	41.14
153	Mitered	Channelized	Inlet	3.53	7.04	563,809	2.65	7.64	0.97	58.35

Table B-7. Circular culvert, 40% buried-invert, inlet control performance data: square-edged entrance with vertical headwall.

Run	Entrance	Approach	Control	S_o [%]	Q [cfs]	Re []	Hw/D []	$Q/AD^{0.5}$ [$ft^{0.5}/s$]	$Hw/D-H_c/D+0.5S_o$ []	$(Q/AD^{0.5})^2$ [ft/s^2]
154	Square	Ponded	Inlet	2.97	0.64	160,059	0.34	0.70	0.04	0.49
155	Square	Ponded	Inlet	2.97	1.14	204,831	0.50	1.23	0.05	1.52
156	Square	Ponded	Inlet	2.97	0.88	181,961	0.42	0.95	0.05	0.91
157	Square	Ponded	Inlet	2.97	1.83	247,890	0.69	1.98	0.08	3.94
158	Square	Ponded	Inlet	2.97	2.56	284,717	0.87	2.77	0.10	7.70
159	Square	Ponded	Inlet	2.97	8.87	731,734	3.73	9.63	1.61	92.67
160	Square	Ponded	Inlet	2.97	8.01	669,530	3.20	8.69	1.29	75.56
161	Square	Ponded	Inlet	2.97	6.76	570,482	2.46	7.34	0.84	53.86
162	Square	Ponded	Inlet	2.97	4.99	444,948	1.62	5.42	0.37	29.34
163	Square	Channelized	Inlet	2.97	9.71	771,295	4.34	10.54	1.99	111.07
164	Square	Channelized	Inlet	2.97	8.73	700,778	3.60	9.47	1.51	89.74
165	Square	Channelized	Inlet	2.97	7.57	618,201	2.87	8.21	1.07	67.44
166	Square	Channelized	Inlet	2.97	6.23	518,883	2.17	6.77	0.66	45.79
167	Square	Channelized	Inlet	2.97	5.49	469,885	1.82	5.96	0.47	35.51
168	Square	Channelized	Inlet	2.97	4.72	418,080	1.52	5.12	0.32	26.20
169	Square	Channelized	Inlet	2.97	2.91	304,020	0.96	3.16	0.12	10.00
170	Square	Channelized	Inlet	2.97	2.21	261,347	0.79	2.39	0.09	5.73
171	Square	Channelized	Inlet	2.97	1.52	227,277	0.61	1.65	0.07	2.74

Table B-8. Circular culvert, 40% buried-invert, inlet control performance data: 45° Beveled Entrance with vertical headwall.

Run	Entrance	Approach	Control	S_o [%]	Q [cfs]	Re []	Hw/D []	$Q/AD^{0.5}$ [$ft^{0.5}/s$]	$Hw/D-H_c/D+0.5S_o$ []	$(Q/AD^{0.5})^2$ [ft/s^2]
172	Beveled	Ponded	Inlet	2.97	1.23	203,519	0.51	1.33	0.04	1.78
173	Beveled	Ponded	Inlet	2.97	0.63	149,090	0.33	0.69	0.03	0.47
174	Beveled	Ponded	Inlet	2.97	9.19	688,155	3.17	9.98	0.96	99.59
175	Beveled	Ponded	Inlet	2.97	8.05	616,696	2.61	8.74	0.69	76.43
176	Beveled	Ponded	Inlet	2.97	6.99	545,534	2.13	7.59	0.46	57.59
177	Beveled	Ponded	Inlet	2.97	5.53	449,643	1.59	6.00	0.23	36.05
178	Beveled	Ponded	Inlet	2.97	2.59	284,369	0.84	2.82	0.06	7.93
179	Beveled	Ponded	Inlet	2.97	1.85	250,231	0.67	2.01	0.05	4.04
180	Beveled	Channelized	Inlet	2.97	9.58	696,663	3.36	10.40	1.04	108.15
181	Beveled	Channelized	Inlet	2.97	8.65	630,693	2.91	9.39	0.85	88.23
182	Beveled	Channelized	Inlet	2.97	7.71	567,924	2.47	8.37	0.64	70.04
183	Beveled	Channelized	Inlet	2.97	6.84	514,237	2.10	7.42	0.46	55.10
184	Beveled	Channelized	Inlet	2.97	6.08	463,971	1.81	6.60	0.34	43.52
185	Beveled	Channelized	Inlet	2.97	5.18	409,214	1.53	5.62	0.24	31.61
186	Beveled	Channelized	Inlet	2.97	3.07	293,845	0.97	3.33	0.09	11.10
187	Beveled	Channelized	Inlet	2.97	2.23	250,139	0.77	2.42	0.07	5.83

Table B-9. Circular culvert, 50% buried-invert, inlet control performance data: thin-wall projecting end.

Run	Entrance	Approach	Control	S_o [%]	Q [cfs]	Re []	Hw/D []	$Q/AD^{0.5}$ [$ft^{0.5}/s$]	$Hw/D-H_c/D+0.5S_o$ []	$(Q/AD^{0.5})^2$ [ft/s^2]
188	Projecting	Ponded	Inlet	3.20	1.76	262,268	0.91	2.33	0.20	5.43
189	Projecting	Ponded	Inlet	3.20	1.50	241,099	0.80	1.98	0.17	3.91
190	Projecting	Ponded	Inlet	3.20	1.21	218,878	0.69	1.61	0.14	2.58
191	Projecting	Ponded	Inlet	3.20	0.89	183,704	0.55	1.18	0.12	1.40
192	Projecting	Ponded	Inlet	3.20	0.64	160,288	0.44	0.85	0.09	0.72
193	Projecting	Ponded	Inlet	3.20	0.40	128,467	0.32	0.53	0.07	0.28
194	Projecting	Ponded	Inlet	3.20	2.58	318,583	1.26	3.41	0.32	11.66
195	Projecting	Ponded	Inlet	3.20	3.55	400,661	1.84	4.70	0.64	22.10
196	Projecting	Ponded	Inlet	3.20	4.52	478,432	2.69	5.97	1.21	35.68
197	Projecting	Ponded	Inlet	3.20	5.71	597,661	3.98	7.55	2.13	57.05
198	Projecting	Ponded	Inlet	3.20	6.39	677,697	4.86	8.45	2.78	71.35
199	Projecting	Ponded	Inlet	3.20	5.12	551,307	3.30	6.77	1.64	45.80
200	Projecting	Ponded	Inlet	3.20	4.42	482,984	2.61	5.85	1.16	34.23
201	Projecting	Ponded	Inlet	3.20	3.18	377,673	1.59	4.20	0.49	17.68
202	Projecting	Channelized	Inlet	3.20	3.51	403,781	1.65	4.64	0.46	21.49
203	Projecting	Channelized	Inlet	3.20	2.62	323,523	1.22	3.47	0.26	12.04
204	Projecting	Channelized	Inlet	3.20	1.83	271,799	0.92	2.43	0.18	5.89
205	Projecting	Channelized	Inlet	3.20	1.60	248,241	0.83	2.12	0.16	4.48
206	Projecting	Channelized	Inlet	3.20	1.35	228,492	0.74	1.79	0.15	3.19
207	Projecting	Channelized	Inlet	3.20	1.07	204,676	0.62	1.41	0.13	1.99
208	Projecting	Channelized	Inlet	3.20	0.82	176,360	0.52	1.08	0.11	1.16
209	Projecting	Channelized	Inlet	3.20	0.61	161,316	0.43	0.81	0.09	0.66
210	Projecting	Channelized	Inlet	3.20	0.41	130,570	0.33	0.55	0.08	0.30
211	Projecting	Channelized	Inlet	3.20	6.54	663,724	4.74	8.64	2.60	74.73
212	Projecting	Channelized	Inlet	3.20	5.78	585,635	3.83	7.65	1.95	58.50
213	Projecting	Channelized	Inlet	3.20	5.10	527,528	3.05	6.75	1.40	45.56
214	Projecting	Channelized	Inlet	3.20	4.27	438,391	2.24	5.65	0.84	31.90

Table B-10. Circular culvert, 50% buried-invert, inlet control performance data: mitered to 1.5H:1V fill slope with flush headwall.

Run	Entrance	Approach	Control	S_o [%]	Q [cfs]	Re []	Hw/D []	$Q/AD^{0.5}$ [$ft^{0.5}/s$]	$Hw/D-H_c/D+0.5S_o$ []	$(Q/AD^{0.5})^2$ [ft/s^2]
215	Mitered	Ponded	Inlet	4.31	3.68	354,325	1.69	4.87	0.43	23.73
216	Mitered	Ponded	Inlet	4.31	3.02	305,558	1.27	3.99	0.20	15.91
217	Mitered	Ponded	Inlet	4.31	2.49	271,644	1.01	3.29	0.08	10.82
218	Mitered	Ponded	Inlet	4.31	2.18	255,954	0.92	2.88	0.07	8.32
219	Mitered	Ponded	Inlet	4.31	1.86	238,250	0.82	2.46	0.06	6.08
220	Mitered	Ponded	Inlet	4.31	1.52	220,872	0.71	2.01	0.05	4.03
221	Mitered	Ponded	Inlet	4.31	1.12	196,618	0.57	1.48	0.04	2.18
222	Mitered	Ponded	Inlet	4.31	0.87	177,030	0.48	1.15	0.04	1.33
223	Mitered	Ponded	Inlet	4.31	0.63	159,089	0.39	0.83	0.03	0.69
224	Mitered	Ponded	Inlet	4.31	0.45	146,570	0.31	0.59	0.03	0.35
225	Mitered	Ponded	Inlet	4.31	4.03	369,366	1.98	5.33	0.63	28.44
226	Mitered	Ponded	Inlet	4.31	4.49	398,066	2.31	5.93	0.82	35.19
227	Mitered	Ponded	Inlet	4.31	5.03	430,473	2.77	6.65	1.12	44.19
228	Mitered	Ponded	Inlet	4.31	5.54	481,070	3.26	7.33	1.45	53.68
229	Mitered	Ponded	Inlet	4.31	6.00	504,594	3.66	7.94	1.70	63.00
230	Mitered	Ponded	Inlet	4.31	6.58	544,853	4.31	8.70	2.14	75.61
231	Mitered	Channelized	Inlet	4.31	3.66	346,078	1.61	4.84	0.36	23.43
232	Mitered	Channelized	Inlet	4.31	3.00	302,110	1.25	3.97	0.18	15.72
233	Mitered	Channelized	Inlet	4.31	5.50	457,423	2.95	7.27	1.16	52.87
234	Mitered	Channelized	Inlet	4.31	4.71	408,527	2.33	6.22	0.78	38.73

Table B-11. Circular culvert, 50% buried-invert, inlet control performance data: square-edged entrance with vertical headwall.

Run	Entrance	Approach	Control	S_o [%]	Q [cfs]	Re []	Hw/D []	$Q/AD^{0.5}$ [$ft^{0.5}/s$]	$Hw/D-H_c/D+0.5S_o$ []	$(Q/AD^{0.5})^2$ [ft/s^2]
235	Square	Ponded	Inlet	3.20	3.66	399,214	1.59	4.84	0.35	23.47
236	Square	Ponded	Inlet	3.20	3.11	346,691	1.31	4.12	0.23	16.94
237	Square	Ponded	Inlet	3.20	2.62	315,024	1.11	3.46	0.16	11.96
238	Square	Ponded	Inlet	3.20	2.00	277,968	0.89	2.64	0.11	6.99
239	Square	Ponded	Inlet	3.20	1.57	254,413	0.75	2.08	0.09	4.33
240	Square	Ponded	Inlet	3.20	1.11	216,509	0.58	1.47	0.07	2.17
241	Square	Ponded	Inlet	3.20	0.77	187,486	0.45	1.01	0.06	1.03
242	Square	Ponded	Inlet	3.20	0.42	143,036	0.30	0.55	0.04	0.30
243	Square	Ponded	Inlet	3.20	7.47	698,041	4.58	9.88	2.08	97.55
244	Square	Ponded	Inlet	3.20	6.34	609,869	3.49	8.39	1.43	70.39
245	Square	Ponded	Inlet	3.20	5.46	522,781	2.74	7.23	0.97	52.23
246	Square	Ponded	Inlet	3.20	4.57	448,402	2.09	6.04	0.60	36.48
247	Square	Channelized	Inlet	3.20	7.00	652,751	4.01	9.26	1.70	85.66
248	Square	Channelized	Inlet	3.20	5.08	485,817	2.43	6.72	0.78	45.16
249	Square	Channelized	Inlet	3.20	2.89	321,056	1.22	3.82	0.20	14.62
250	Square	Channelized	Inlet	3.20	1.85	256,174	0.84	2.45	0.10	6.00
251	Square	Channelized	Inlet	3.20	1.22	217,737	0.62	1.61	0.08	2.59

Table B-12. Circular culvert, 50% buried-invert, inlet control performance data: 45° beveled entrance with vertical headwall.

Run	Entrance	Approach	Control	S_o [%]	Q [cfs]	Re []	Hw/D []	$Q/AD^{0.5}$ [$ft^{0.5}/s$]	$Hw/D-H_c/D+0.5S_o$ []	$(Q/AD^{0.5})^2$ [ft/s^2]
252	Beveled	Ponded	Inlet	3.20	3.67	367,773	1.40	4.85	0.16	23.54
253	Beveled	Ponded	Inlet	3.20	3.09	325,851	1.19	4.09	0.11	16.75
254	Beveled	Ponded	Inlet	3.20	2.09	273,556	0.87	2.76	0.07	7.61
255	Beveled	Ponded	Inlet	3.20	1.63	248,951	0.73	2.15	0.06	4.63
256	Beveled	Ponded	Inlet	3.20	1.18	216,155	0.59	1.57	0.05	2.45
257	Beveled	Ponded	Inlet	3.20	0.86	186,282	0.48	1.14	0.05	1.30
258	Beveled	Ponded	Inlet	3.20	0.50	145,382	0.33	0.66	0.04	0.43
259	Beveled	Ponded	Inlet	3.20	7.61	678,148	3.94	10.07	1.38	101.40
260	Beveled	Ponded	Inlet	3.20	6.56	590,093	3.12	8.68	0.98	75.37
261	Beveled	Ponded	Inlet	3.20	5.51	503,569	2.38	7.28	0.60	53.03
262	Beveled	Ponded	Inlet	3.20	4.57	431,546	1.84	6.04	0.35	36.48
263	Beveled	Channelized	Inlet	3.20	7.00	620,413	3.41	9.26	1.10	85.66
264	Beveled	Channelized	Inlet	3.20	1.85	256,839	0.82	2.45	0.08	6.00
265	Beveled	Channelized	Inlet	3.20	1.21	215,286	0.62	1.61	0.07	2.58
266	Beveled	Channelized	Inlet	3.20	4.13	398,934	1.65	5.47	0.28	29.89

Table B-13. Elliptical culvert, 50% buried-invert, inlet control performance data: thin-wall projecting end.

Run	Entrance	Approach	Control	S_o [%]	Q [cfs]	Re []	Hw/D []	$Q/AD^{0.5}$ [$ft^{0.5}/s$]	$Hw/D-H_c/D+0.5S_o$ []	$(Q/AD^{0.5})^2$ [ft/s^2]
267	Projecting	Ponded	Inlet	0.61	0.46	125,885	0.33	0.48	0.09	0.23
268	Projecting	Ponded	Inlet	0.61	0.60	138,496	0.39	0.62	0.10	0.39
269	Projecting	Ponded	Inlet	0.61	0.91	169,594	0.50	0.95	0.12	0.90
270	Projecting	Ponded	Inlet	0.61	1.29	200,735	0.63	1.34	0.13	1.81
271	Projecting	Ponded	Inlet	3.23	1.54	346,952	0.70	1.60	0.15	2.56
272	Projecting	Ponded	Inlet	0.61	1.85	237,446	0.81	1.93	0.17	3.71
273	Projecting	Ponded	Inlet	0.61	2.34	278,855	0.96	2.43	0.21	5.92
274	Projecting	Ponded	Inlet	0.61	3.02	311,212	1.19	3.14	0.29	9.84
275	Projecting	Ponded	Inlet	0.61	4.32	413,625	1.79	4.49	0.61	20.18
276	Projecting	Ponded	Inlet	3.23	5.22	556,421	2.29	5.42	0.93	29.42
277	Projecting	Ponded	Inlet	0.61	5.52	542,101	2.61	5.74	1.16	33.00
278	Projecting	Ponded	Inlet	0.61	6.50	619,028	3.38	6.76	1.71	45.67
279	Projecting	Ponded	Inlet	3.23	6.83	717,662	3.67	7.11	1.92	50.50
280	Projecting	Ponded	Inlet	0.61	7.23	764,909	4.18	7.52	2.31	56.51
281	Projecting	Ponded	Inlet	0.61	7.97	843,913	5.17	8.29	3.11	68.79
282	Projecting	Ponded	Inlet	3.23	9.06	924,542	6.08	9.42	3.71	88.76
283	Projecting	Channelized	Inlet	0.61	0.63	141,287	0.38	0.66	0.08	0.43
284	Projecting	Channelized	Inlet	3.23	1.23	281,440	0.56	1.28	0.10	1.64
285	Projecting	Channelized	Inlet	0.61	2.06	243,737	0.83	2.14	0.14	4.58
286	Projecting	Channelized	Inlet	0.61	2.74	284,114	1.01	2.85	0.17	8.15
287	Projecting	Channelized	Inlet	3.23	3.15	426,641	1.09	3.28	0.17	10.74
288	Projecting	Channelized	Inlet	3.23	4.16	472,607	1.45	4.32	0.32	18.69
289	Projecting	Channelized	Inlet	3.23	5.05	512,759	1.87	5.26	0.55	27.63
290	Projecting	Channelized	Inlet	3.23	5.37	564,082	2.08	5.59	0.68	31.21
291	Projecting	Channelized	Inlet	3.23	5.93	592,706	2.58	6.17	1.05	38.07
292	Projecting	Channelized	Inlet	3.23	6.29	635,484	2.89	6.55	1.27	42.84
293	Projecting	Channelized	Inlet	3.23	6.64	656,666	3.17	6.91	1.47	47.71
294	Projecting	Channelized	Inlet	3.23	6.91	725,904	3.37	7.19	1.60	51.69
295	Projecting	Channelized	Inlet	3.23	7.24	737,338	3.78	7.53	1.92	56.76
296	Projecting	Channelized	Inlet	3.23	7.85	828,123	4.45	8.17	2.43	66.70
297	Projecting	Channelized	Inlet	3.23	8.99	864,751	5.85	9.35	3.50	87.47

Table B-14. Elliptical culvert, 50% buried-invert, inlet control performance data: mitered to 1.5H:1V fill slope with flush headwall.

Run	Entrance	Approach	Control	S_o [%]	Q [cfs]	Re []	Hw/D []	$Q/AD^{0.5}$ [$ft^{0.5}/s$]	$Hw/D-H_c/D+0.5S_o$ []	$(Q/AD^{0.5})^2$ [ft/s^2]
298	Mitered	Ponded	Inlet	1.90	0.49	51,818	0.31	0.04	0.51	0.26
299	Mitered	Ponded	Inlet	1.90	2.04	242,078	0.79	0.09	2.12	4.49
300	Mitered	Ponded	Inlet	1.90	3.46	319,015	1.15	0.14	3.60	12.94
301	Mitered	Ponded	Inlet	1.90	2.87	287,194	1.00	0.12	2.99	8.91
302	Mitered	Ponded	Inlet	1.90	4.21	399,506	1.57	0.40	4.38	19.18
303	Mitered	Ponded	Inlet	1.90	2.40	265,172	0.86	0.08	2.49	6.22
304	Mitered	Ponded	Inlet	1.90	1.62	210,532	0.68	0.08	1.69	2.84
305	Mitered	Ponded	Inlet	1.90	1.16	196,612	0.54	0.06	1.21	1.46
306	Mitered	Ponded	Inlet	1.90	0.81	178,245	0.43	0.05	0.84	0.71
307	Mitered	Ponded	Inlet	1.90	5.03	437,454	2.03	0.68	5.23	27.34
308	Mitered	Ponded	Inlet	1.90	5.97	527,103	2.64	1.07	6.21	38.57
309	Mitered	Ponded	Inlet	1.90	6.93	602,246	3.43	1.63	7.20	51.89
310	Mitered	Ponded	Inlet	1.90	7.93	675,183	4.29	2.22	8.25	68.09
311	Mitered	Channelized	Inlet	1.90	8.04	650,637	4.20	2.10	8.36	69.88
312	Mitered	Channelized	Inlet	1.90	6.36	536,256	2.75	1.09	6.61	43.74
313	Mitered	Channelized	Inlet	1.90	4.63	413,529	1.73	0.47	4.81	23.16
314	Mitered	Channelized	Inlet	1.90	3.04	294,503	1.05	0.13	3.17	10.03
315	Mitered	Channelized	Inlet	1.90	2.03	227,380	0.78	0.09	2.11	4.44
316	Mitered	Channelized	Inlet	1.90	1.01	187,549	0.52	0.09	1.05	1.10

Table B-15. Elliptical culvert, 50% buried-invert, inlet control performance data: square-edged entrance with vertical headwall.

Run	Entrance	Approach	Control	S_o [%]	Q [cfs]	Re []	Hw/D []	$Q/AD^{0.5}$ [$ft^{0.5}/s$]	$Hw/D-H_c/D+0.5S_o$ []	$(Q/AD^{0.5})^2$ [ft/s^2]
317	Square	Ponded	Inlet	0.60	0.61	158,620	0.37	0.64	0.07	0.41
318	Square	Ponded	Inlet	0.60	1.19	197,698	0.56	1.24	0.09	1.54
319	Square	Ponded	Inlet	0.60	1.76	237,406	0.72	1.83	0.10	3.36
320	Square	Ponded	Inlet	0.60	2.55	290,037	0.93	2.65	0.13	7.05
321	Square	Ponded	Inlet	0.60	3.67	359,398	1.25	3.82	0.21	14.56
322	Square	Ponded	Inlet	0.60	4.79	473,840	1.69	4.98	0.41	24.85
323	Square	Ponded	Inlet	0.60	5.89	555,960	2.21	6.12	0.68	37.47
324	Square	Ponded	Inlet	0.60	6.78	640,075	2.73	7.05	0.98	49.70
325	Square	Ponded	Inlet	0.60	7.58	721,157	3.29	7.89	1.33	62.22
326	Square	Ponded	Inlet	0.60	9.02	860,351	4.40	9.38	2.03	87.97
327	Square	Channelized	Inlet	0.60	0.60	156,885	0.36	0.63	0.07	0.40
328	Square	Channelized	Inlet	0.60	1.76	245,523	0.71	1.83	0.10	3.34
329	Square	Channelized	Inlet	1.14	2.09	285,313	0.79	2.17	0.10	4.72
330	Square	Channelized	Inlet	0.60	2.32	285,978	0.86	2.41	0.12	5.80
331	Square	Channelized	Inlet	0.60	3.03	331,627	1.05	3.15	0.15	9.91
332	Square	Channelized	Inlet	0.60	4.75	482,369	1.67	4.94	0.40	24.45
333	Square	Channelized	Inlet	1.14	5.22	511,726	1.87	5.43	0.49	29.52
334	Square	Channelized	Inlet	0.60	6.32	604,672	2.46	6.57	0.83	43.14
335	Square	Channelized	Inlet	0.60	7.82	763,615	3.47	8.13	1.45	66.10
336	Square	Channelized	Inlet	1.14	8.04	770,092	3.60	8.37	1.52	69.98
337	Square	Channelized	Inlet	0.60	9.20	901,043	4.58	9.57	2.15	91.55

Table B-16. Elliptical culvert, 50% buried-invert, inlet control performance data: 45° beveled entrance with vertical headwall.

Run	Entrance	Approach	Control	S_o [%]	Q [cfs]	Re []	Hw/D []	$Q/AD^{0.5}$ [$ft^{0.5}/s$]	$Hw/D-H_c/D+0.5S_o$ []	$(Q/AD^{0.5})^2$ [ft/s^2]
338	Beveled	Ponded	Inlet	1.14	1.01	229,364	0.33	1.05	0.06	1.09
339	Beveled	Ponded	Inlet	1.14	2.02	285,345	0.52	2.10	0.08	4.39
340	Beveled	Ponded	Inlet	3.23	4.16	449,703	0.88	4.32	0.14	18.69
341	Beveled	Ponded	Inlet	1.14	6.04	522,787	1.35	6.28	0.38	39.46
342	Beveled	Ponded	Inlet	3.23	7.57	659,902	1.82	7.87	0.68	61.93
343	Beveled	Ponded	Inlet	1.14	9.00	744,069	2.41	9.36	1.11	87.67
344	Beveled	Channelized	Inlet	1.14	1.22	237,764	3.23	1.27	0.06	1.62
345	Beveled	Channelized	Inlet	1.14	2.49	311,209	3.23	2.59	0.09	6.69
346	Beveled	Channelized	Inlet	1.14	2.00	320,043	3.23	2.08	0.07	4.32
347	Beveled	Channelized	Inlet	1.14	3.52	371,728	3.23	3.66	0.12	13.41
348	Beveled	Channelized	Inlet	1.14	4.51	427,053	3.23	4.69	0.18	21.97
349	Beveled	Channelized	Inlet	3.23	5.41	491,441	3.23	5.63	0.27	31.71
350	Beveled	Channelized	Inlet	1.14	5.52	492,620	3.23	5.74	0.28	32.90
351	Beveled	Channelized	Inlet	1.14	6.49	564,834	3.23	6.75	0.44	45.62
352	Beveled	Channelized	Inlet	1.14	7.04	612,232	3.23	7.32	0.54	53.58
353	Beveled	Channelized	Inlet	3.23	7.51	652,925	3.23	7.81	0.65	61.03
354	Beveled	Channelized	Inlet	3.23	7.97	686,516	3.23	8.29	0.77	68.69
355	Beveled	Channelized	Inlet	3.23	8.07	697,711	3.23	8.39	0.82	70.47
356	Beveled	Channelized	Inlet	3.23	8.86	753,902	3.23	9.21	1.04	84.85
357	Beveled	Channelized	Inlet	3.23	9.96	849,414	3.23	10.36	1.32	107.35
358	Beveled	Channelized	Inlet	3.23	11.02	930,144	3.23	11.46	1.89	131.44

APPENDIX C

Outlet Control Experimental Data Set for Traditional Projecting and Slip-Lined Inlet End Treatments (Tabular Support Data for Chapter 3)

Table C-1. Circular culvert outlet control performance data: thin-wall projecting end.

Run	Entrance	Approach	Control	S_o [%]	Q [cfs]	Re []	Hw/D []	k_e []
1	projecting	ponded	outlet	0.07	2.88	207,576	3.82	0.79
2	projecting	ponded	outlet	0.07	2.66	189,737	3.17	0.78
3	projecting	ponded	outlet	0.07	1.20	86,589	1.26	0.83
4	projecting	ponded	outlet	0.07	1.19	70,578	0.95	0.75
5	projecting	ponded	outlet	-0.06	3.08	238,220	3.89	0.79
6	projecting	ponded	outlet	-0.06	2.18	169,241	1.90	0.82
7	projecting	ponded	outlet	-0.06	2.26	175,716	2.43	0.80
8	projecting	ponded	outlet	-0.06	2.92	228,997	3.40	0.78
9	projecting	ponded	outlet	-0.06	0.90	69,761	0.67	0.71
10	projecting	ponded	outlet	-0.06	0.56	56,334	0.52	0.75

Table C-2. Slip-lined circular culvert outlet control performance data: 2-inch projecting end.

Run	Entrance	Approach	Control	S_o [%]	Q [cfs]	Re []	Hw/D []	k_e []
11	2-inch projecting	ponded	outlet	-0.06	2.87	225,178	3.65	0.75
12	2-inch projecting	ponded	outlet	-0.06	2.83	232,482	3.06	0.77
13	2-inch projecting	ponded	outlet	-0.06	2.65	218,633	2.50	0.76
14	2-inch projecting	ponded	outlet	-0.06	2.40	198,100	1.94	0.78
15	2-inch projecting	ponded	outlet	-0.06	2.13	175,176	1.49	0.78
16	2-inch projecting	ponded	outlet	-0.06	1.59	100,877	1.01	0.71
17	2-inch projecting	ponded	outlet	-0.06	1.17	80,539	0.79	0.66
18	2-inch projecting	ponded	outlet	-0.06	0.53	56,514	0.50	0.68

Table C-3. Slip-lined circular culvert outlet control performance data: 4-inch projecting end.

Run	Entrance	Approach	Control	S_o [%]	Q [cfs]	Re []	Hw/D []	k_e []
19	4-inch projecting	ponded	outlet	0.03	2.34	168,709	2.37	0.77
20	4-inch projecting	ponded	outlet	0.03	2.18	157,278	1.77	0.79
21	4-inch projecting	ponded	outlet	0.03	1.89	136,830	1.32	0.80
22	4-inch projecting	ponded	outlet	0.03	1.65	97,989	1.02	0.77
23	4-inch projecting	ponded	outlet	0.03	2.86	205,944	4.19	0.76
24	4-inch projecting	ponded	outlet	0.03	2.69	193,137	3.42	0.76
25	4-inch projecting	ponded	outlet	0.03	2.51	180,313	2.77	0.78
26	4-inch projecting	ponded	outlet	0.03	1.19	72,470	0.85	0.73
27	4-inch projecting	ponded	outlet	0.03	0.92	68,119	0.66	0.66
28	4-inch projecting	ponded	outlet	0.03	0.44	41,620	0.45	0.69

Table C-4. Slip-lined circular culvert outlet control performance data: 2-inch tapered, projecting end.

Run	Entrance	Approach	Control	S_o [%]	Q [cfs]	Re []	Hw/D []	k_e []
29	2-inch tapered proj.	ponded	outlet	-0.06	3.08	241,753	3.94	0.70
30	2-inch tapered proj.	ponded	outlet	-0.06	2.80	216,816	3.02	0.69
31	2-inch tapered proj.	ponded	outlet	-0.06	2.60	200,177	2.46	0.69
32	2-inch tapered proj.	ponded	outlet	-0.06	2.39	185,157	1.96	0.72
33	2-inch tapered proj.	ponded	outlet	-0.06	1.20	85,493	0.80	0.71
34	2-inch tapered proj.	ponded	outlet	-0.06	0.54	56,958	0.50	0.68
35	2-inch tapered proj.	ponded	outlet	-0.06	1.19	98,551	1.39	0.73

Table C-5. Slip-lined circular culvert outlet control performance data: 4-inch tapered projecting end.

Run	Entrance	Approach	Control	S_o [%]	Q [cfs]	Re []	Hw/D []	k_e []
36	4-inch tapered proj.	ponded	outlet	0.03	3.00	225,301	4.27	0.68
37	4-inch tapered proj.	ponded	outlet	0.03	2.86	217,791	3.57	0.68
38	4-inch tapered proj.	ponded	outlet	0.03	2.59	196,854	2.76	0.70
39	4-inch tapered proj.	ponded	outlet	0.03	2.43	189,391	1.95	0.71
40	4-inch tapered proj.	ponded	outlet	0.03	2.27	172,335	1.39	0.71
41	4-inch tapered proj.	ponded	outlet	0.03	1.14	75,812	0.77	0.62
42	4-inch tapered proj.	ponded	outlet	0.03	0.81	64,326	0.61	0.61
43	4-inch tapered proj.	ponded	outlet	0.03	0.48	45,319	0.46	0.62
44	4-inch tapered proj.	ponded	outlet	0.03	1.94	122,401	1.12	0.68

APPENDIX D

Inlet Control Experimental Data Set for Traditional Projecting and Slip-Lined Inlet End Treatments (Tabular Support Data for Chapter 3)

Table D-1. Circular culvert inlet control performance data: thin-wall projecting end.

Run	Entrance	Approach	Control	S_o [%]	Q [cfs]	Re []	Hw/D []	$Q/AD^{0.5}$. [ft0.5/s]	Hw/D-H_c/D+0.5S_o []	$(Q/AD^{0.5})^2$ [ft/s2]
1	projecting	ponded	Inlet	4.43	2.92	239,772	1.46	3.92	0.36	15.33
2	projecting	ponded	Inlet	4.43	1.80	178,144	0.98	2.41	0.17	5.83
3	projecting	ponded	Inlet	4.43	1.47	158,271	0.86	1.97	0.14	3.87
4	projecting	ponded	Inlet	4.43	1.10	138,046	0.72	1.47	0.11	2.17
5	projecting	ponded	Inlet	4.43	0.80	118,510	0.60	1.07	0.09	1.15
6	projecting	ponded	Inlet	4.43	0.42	86,009	0.42	0.56	0.07	0.32
7	projecting	ponded	Inlet	4.43	5.99	428,268	3.97	8.03	2.00	64.55
8	projecting	ponded	Inlet	4.43	5.22	376,172	3.25	7.01	1.53	49.15
9	projecting	ponded	Inlet	4.43	4.50	323,758	2.58	6.03	1.08	36.41
10	projecting	ponded	Inlet	4.43	3.93	288,584	2.11	5.27	0.76	27.80
11	projecting	channel	Inlet	4.43	4.61	333,894	2.57	6.18	1.03	38.23
12	projecting	channel	Inlet	4.43	4.97	354,449	2.86	6.67	1.22	44.52
13	projecting	channel	Inlet	4.43	4.22	303,589	2.26	5.67	0.83	32.11
14	projecting	channel	Inlet	4.43	3.61	259,735	1.85	4.85	0.57	23.50
15	projecting	channel	Inlet	4.43	1.80	171,846	0.97	2.41	0.16	5.83
16	projecting	channel	Inlet	4.43	1.21	139,890	0.76	1.62	0.12	2.64
17	projecting	channel	Inlet	4.43	0.92	121,081	0.65	1.23	0.11	1.51
18	projecting	channel	Inlet	4.43	0.61	101,109	0.52	0.82	0.08	0.67

Table D-2. Slip-lined circular culvert inlet control performance data: 2-inch projecting end.

Run	Entrance	Approach	Control	S_o [%]	Q [cfs]	Re []	Hw/D []	$Q/AD^{0.5}$. [ft0.5/s]	Hw/D-H_c/D+0.5S_o []	$(Q/AD^{0.5})^2$ [ft/s2]
19	2-inch Proj.	ponded	inlet	4.43	5.62	423,261	3.60	7.55	1.75	56.93
20	2-inch Proj.	ponded	inlet	4.43	4.56	348,540	2.60	6.12	1.07	37.40
21	2-inch Proj.	ponded	inlet	4.43	3.50	276,822	1.78	4.69	0.54	22.01
22	2-inch Proj.	ponded	inlet	4.43	1.63	173,016	0.91	2.18	0.15	4.77
23	2-inch Proj.	ponded	inlet	4.43	1.08	136,948	0.72	1.45	0.12	2.09
24	2-inch Proj.	ponded	inlet	4.43	0.57	97,069	0.50	0.77	0.08	0.59
25	2-inch Proj.	channel	inlet	4.43	5.49	397,849	3.24	7.37	1.44	54.28
26	2-inch Proj.	channel	inlet	4.43	4.85	354,602	2.67	6.51	1.06	42.37
27	2-inch Proj.	channel	inlet	4.43	4.16	306,171	2.11	5.58	0.69	31.11
28	2-inch Proj.	channel	inlet	4.43	3.33	254,471	1.58	4.48	0.38	20.03
29	2-inch Proj.	channel	inlet	4.43	1.77	178,133	0.93	2.37	0.13	5.63
30	2-inch Proj.	channel	inlet	4.43	1.43	156,309	0.82	1.92	0.12	3.68
31	2-inch Proj.	channel	inlet	4.43	1.07	133,346	0.70	1.44	0.10	2.08
32	2-inch Proj.	channel	inlet	4.43	0.63	101,021	0.52	0.84	0.08	0.71

Table D-3. Slip-lined circular culvert inlet control performance data: 4-inch projecting end.

Run	Entrance	Approach	Control	S_o [%]	Q [cfs]	Re []	Hw/D []	$Q/AD^{0.5}$. [ft0.5/s]	Hw/D-H_c/D+0.5S_o []	$(Q/AD^{0.5})^2$ [ft/s2]
33	4-inch proj.	ponded	inlet	4.43	5.70	418,664	3.69	7.64	1.82	58.42
34	4-inch proj.	ponded	inlet	4.43	4.60	343,226	2.66	6.17	1.12	38.07
35	4-inch proj.	ponded	inlet	4.43	3.26	259,799	1.64	4.37	0.46	19.12
36	4-inch proj.	ponded	inlet	4.43	1.61	168,325	0.90	2.16	0.15	4.65
37	4-inch proj.	ponded	inlet	4.43	1.02	134,286	0.69	1.37	0.11	1.87
38	4-inch proj.	ponded	inlet	4.43	0.50	92,768	0.47	0.68	0.08	0.46
39	4-inch proj.	channel	inlet	4.43	4.85	354,914	2.69	6.52	1.08	42.45
40	4-inch proj.	channel	inlet	4.43	3.51	267,138	1.70	4.71	0.46	22.18
41	4-inch proj.	channel	inlet	4.43	1.61	164,624	0.88	2.16	0.13	4.65
42	4-inch proj.	channel	inlet	4.43	1.03	134,152	0.68	1.39	0.10	1.92
43	4-inch proj.	channel	inlet	4.43	0.59	99,171	0.50	0.79	0.08	0.62

Table D-4. Slip-lined circular culvert inlet control performance data: 2-inch tapered projecting end.

Run	Entrance	Approach	Control	S_o [%]	Q [cfs]	Re []	Hw/D []	$Q/AD^{0.5}$ [ft0.5/s]	$Hw/D-H_c/D+0.5S_o$ []	$(Q/AD^{0.5})^2$ [ft/s2]
44	2-inch taprd. proj.	ponded	inlet	4.43	5.70	409,409	3.41	7.65	1.54	58.59
45	2-inch taprd. proj.	ponded	inlet	4.43	5.06	367,437	2.87	6.80	1.20	46.18
46	2-inch taprd. proj.	ponded	inlet	4.43	4.39	322,477	2.32	5.90	0.85	34.76
47	2-inch taprd. proj.	ponded	inlet	4.43	3.71	278,244	1.85	4.98	0.55	24.83
48	2-inch taprd. proj.	ponded	inlet	4.43	3.09	241,059	1.49	4.15	0.35	17.21
49	2-inch taprd. proj.	ponded	inlet	4.43	1.89	175,559	0.99	2.54	0.16	6.45
50	2-inch taprd. proj.	ponded	inlet	4.43	1.50	153,720	0.86	2.01	0.13	4.03
51	2-inch taprd. proj.	ponded	inlet	4.43	1.18	136,263	0.75	1.59	0.11	2.52
52	2-inch taprd. proj.	ponded	inlet	4.43	0.91	118,450	0.64	1.22	0.10	1.48
53	2-inch taprd. proj.	ponded	inlet	4.43	0.69	104,168	0.55	0.92	0.09	0.86
54	2-inch taprd. proj.	ponded	inlet	4.43	0.41	80,213	0.42	0.55	0.07	0.30
55	2-inch taprd. proj.	channel	inlet	4.43	5.53	385,563	3.15	7.42	1.33	55.11
56	2-inch taprd. proj.	channel	inlet	4.43	5.07	356,186	2.76	6.81	1.08	46.34
57	2-inch taprd. proj.	channel	inlet	4.43	4.57	326,548	2.34	6.13	0.82	37.57
58	2-inch taprd. proj.	channel	inlet	4.43	3.91	284,003	1.90	5.24	0.55	27.47
59	2-inch taprd. proj.	channel	inlet	4.43	3.05	234,033	1.44	4.09	0.31	16.72
60	2-inch taprd. proj.	channel	inlet	4.43	1.79	168,259	0.93	2.41	0.13	5.79
61	2-inch taprd. proj.	channel	inlet	4.43	1.47	150,706	0.83	1.97	0.12	3.87
62	2-inch taprd. proj.	channel	inlet	4.43	1.10	129,470	0.70	1.48	0.10	2.20
63	2-inch taprd. proj.	channel	inlet	4.43	0.81	111,604	0.59	1.08	0.08	1.17
64	2-inch taprd. proj.	channel	inlet	4.43	0.53	89,975	0.47	0.72	0.07	0.51

Table D-5. Slip-lined circular culvert inlet control performance data: 2-inch tapered projecting end.

Run	Entrance	Approach	Control	S_o [%]	Q [cfs]	Re []	Hw/D []	$Q/AD^{0.5}$ [ft0.5/s]	$Hw/D-H_c/D+0.5S_o$ []	$(Q/AD^{0.5})^2$ [ft/s2]
65	4-inch taprd. proj.	ponded	inlet	4.43	6.10	404,475	3.85	8.19	1.84	67.03
66	4-inch taprd. proj.	ponded	inlet	4.43	5.36	357,594	3.07	7.20	1.31	51.80
67	4-inch taprd. proj.	ponded	inlet	4.43	4.55	313,312	2.40	6.10	0.88	37.24
68	4-inch taprd. proj.	ponded	inlet	4.43	3.76	267,805	1.86	5.05	0.55	25.49
69	4-inch taprd. proj.	ponded	inlet	4.43	3.11	228,138	1.49	4.17	0.35	17.38
70	4-inch taprd. proj.	ponded	inlet	4.43	1.42	146,700	0.82	1.91	0.12	3.64
71	4-inch taprd. proj.	ponded	inlet	4.43	1.09	129,668	0.70	1.46	0.10	2.12
72	4-inch taprd. proj.	ponded	inlet	4.43	0.81	111,941	0.60	1.09	0.09	1.19
73	4-inch taprd. proj.	ponded	inlet	4.43	0.57	93,802	0.49	0.76	0.07	0.58
74	4-inch taprd. proj.	channel	inlet	4.43	5.53	409,409	3.41	7.42	1.33	55.11
75	4-inch taprd. proj.	channel	inlet	4.43	5.07	367,437	2.87	6.81	1.08	46.34
76	4-inch taprd. proj.	channel	inlet	4.43	4.57	322,477	2.32	6.13	0.82	37.57
77	4-inch taprd. proj.	channel	inlet	4.43	3.91	278,244	1.85	5.24	0.55	27.47
78	4-inch taprd. proj.	channel	inlet	4.43	3.05	241,059	1.49	4.09	0.31	16.72
79	4-inch taprd. proj.	channel	inlet	4.43	1.79	175,559	0.99	2.41	0.13	5.79
80	4-inch taprd. proj.	channel	inlet	4.43	1.47	153,720	0.86	1.97	0.12	3.87
81	4-inch taprd. proj.	channel	inlet	4.43	1.10	136,263	0.75	1.48	0.10	2.20
82	4-inch taprd. proj.	channel	inlet	4.43	0.81	118,450	0.64	1.08	0.08	1.17
83	4-inch taprd. proj.	channel	inlet	4.43	0.53	104,168	0.55	0.72	0.07	0.51

APPENDIX E

Single and Multibarrel Culvert Experimental Data Sets (Tabular Support Data for Chapter 5)

Table E-1. Single-barrel culvert experimental data.

Run [ ]	Barrel Spacing [ ]	Approach Condition [ ]	Barrel [ ]	Q total [cfs]	Q Left [cfs]	Q Middle [cfs]	Q Right [cfs]	S_o [%]	Hw/D Left [ ]	Hw/D Middle [ ]	Hw/D Right [ ]	$Q/AD^{0.5}$ [$ft^{0.5}/s$]	$Hw/D-H_c/D+.5S_o$ [ ]	$(Q/AD^{0.5})^2$ [ft/s^2]	$Hw/D+.5S_o$ [ ]
1	3D	Reservoir	Right	0.08	N/A	N/A	0.08	2.750	N/A	N/A	0.304	0.314	0.042	0.098	0.318
2	3D	Reservoir	Right	0.54	N/A	N/A	0.55	2.750	N/A	N/A	0.856	2.044	0.116	4.178	0.870
3	3D	Reservoir	Right	0.39	N/A	N/A	0.39	2.750	N/A	N/A	0.715	1.467	0.104	2.152	0.729
4	3D	Reservoir	Right	0.76	N/A	N/A	0.76	2.750	N/A	N/A	1.086	2.852	0.183	8.135	1.100
5	3D	Reservoir	Right	1.10	N/A	N/A	1.09	2.750	N/A	N/A	1.501	4.092	0.364	16.747	1.515
6	3D	Reservoir	Right	1.26	N/A	N/A	1.26	2.750	N/A	N/A	1.742	4.696	0.491	22.053	1.756
7	3D	Reservoir	Right	1.57	N/A	N/A	1.57	2.750	N/A	N/A	2.312	5.860	0.831	34.341	2.325
8	3D	Reservoir	Right	1.86	N/A	N/A	1.87	2.750	N/A	N/A	3.074	7.003	1.347	49.044	3.088
9	3D	Reservoir	Right	2.23	N/A	N/A	2.22	2.750	N/A	N/A	4.147	8.292	-	68.749	4.161
10	3D	Reservoir	Left	0.08	N/A	0.08	N/A	2.494	N/A	0.315	N/A	0.309	0.055	0.096	0.328
11	3D	Reservoir	Left	0.39	N/A	0.39	N/A	2.494	N/A	0.719	N/A	1.459	0.108	2.129	0.732
12	3D	Reservoir	Left	0.54	N/A	0.55	N/A	2.494	N/A	0.867	N/A	2.044	0.125	4.177	0.879
13	3D	Reservoir	Left	0.76	N/A	0.77	N/A	2.494	N/A	1.090	N/A	2.869	0.182	8.229	1.102
14	3D	Reservoir	Left	1.10	N/A	1.11	N/A	2.494	N/A	1.527	N/A	4.163	0.375	17.331	1.539
15	3D	Reservoir	Left	1.26	N/A	1.28	N/A	2.494	N/A	1.785	N/A	4.779	0.516	22.836	1.797
16	3D	Reservoir	Left	1.57	N/A	1.60	N/A	2.494	N/A	2.386	N/A	5.964	0.883	35.573	2.398
17	3D	Reservoir	Left	1.87	N/A	1.88	N/A	2.494	N/A	3.131	N/A	7.030	1.396	49.423	3.143
18	3D	Reservoir	Left	2.23	N/A	2.22	N/A	2.494	N/A	4.169	N/A	8.283	-	68.616	4.182
19	3D	Reservoir	Left	0.08	0.08	N/A	N/A	2.224	0.3244	N/A	N/A	0.313	0.061	0.098	0.336
20	3D	Reservoir	Left	0.54	0.55	N/A	N/A	2.224	0.8911	N/A	N/A	2.059	0.145	4.237	0.902
21	3D	Reservoir	Left	0.39	0.39	N/A	N/A	2.224	0.7398	N/A	N/A	1.465	0.126	2.147	0.751
22	3D	Reservoir	Left	0.76	0.76	N/A	N/A	2.224	1.1027	N/A	N/A	2.843	0.199	8.080	1.114
23	3D	Reservoir	Left	1.10	1.10	N/A	N/A	2.224	1.5515	N/A	N/A	4.126	0.405	17.026	1.563
24	3D	Reservoir	Left	1.26	1.26	N/A	N/A	2.224	1.8233	N/A	N/A	4.721	0.564	22.287	1.834
25	3D	Reservoir	Left	1.57	1.57	N/A	N/A	2.224	2.3926	N/A	N/A	5.857	0.910	34.310	2.404
26	3D	Reservoir	Left	1.90	1.90	N/A	N/A	2.224	3.2068	N/A	N/A	7.117	1.450	50.646	3.218
27	3D	Reservoir	Left	2.29	2.27	N/A	N/A	2.224	4.3095	N/A	N/A	8.482	-	71.936	4.321
28	1.5D	Reservoir	Right	0.08	N/A	N/A	0.08	2.511	N/A	N/A	0.299	0.306	0.040	0.093	0.311
29	1.5D	Reservoir	Right	0.26	N/A	N/A	0.26	2.511	N/A	N/A	0.571	0.986	0.080	0.972	0.583
30	1.5D	Reservoir	Right	0.40	N/A	N/A	0.39	2.511	N/A	N/A	0.718	1.462	0.106	2.138	0.731
31	1.5D	Reservoir	Right	0.56	N/A	N/A	0.56	2.511	N/A	N/A	0.888	2.080	0.139	4.327	0.901
32	1.5D	Reservoir	Right	0.76	N/A	N/A	0.75	2.511	N/A	N/A	1.087	2.793	0.194	7.804	1.100
33	1.5D	Reservoir	Right	1.10	N/A	N/A	1.10	2.511	N/A	N/A	1.506	4.111	0.364	16.899	1.519
34	1.5D	Reservoir	Right	1.26	N/A	N/A	1.25	2.511	N/A	N/A	1.741	4.686	0.490	21.958	1.754
35	1.5D	Reservoir	Right	1.41	N/A	N/A	1.40	2.511	N/A	N/A	2.001	5.246	0.643	27.517	2.014
36	1.5D	Reservoir	Right	1.57	N/A	N/A	1.57	2.511	N/A	N/A	2.353	5.860	0.871	34.341	2.365
37	1.5D	Reservoir	Right	1.94	N/A	N/A	1.91	2.511	N/A	N/A	3.233	7.151	1.471	51.135	3.246
38	1.5D	Reservoir	Left	0.08	N/A	0.08	N/A	2.525	N/A	0.308	N/A	0.313	0.045	0.098	0.320
39	1.5D	Reservoir	Left	0.26	N/A	0.26	N/A	2.525	N/A	0.577	N/A	0.987	0.086	0.974	0.590
40	1.5D	Reservoir	Left	0.40	N/A	0.39	N/A	2.525	N/A	0.718	N/A	1.454	0.108	2.115	0.731
41	1.5D	Reservoir	Left	0.56	N/A	0.56	N/A	2.525	N/A	0.887	N/A	2.087	0.137	4.354	0.900
42	1.5D	Reservoir	Left	0.76	N/A	0.75	N/A	2.525	N/A	1.085	N/A	2.816	0.188	7.930	1.097
43	1.5D	Reservoir	Left	1.10	N/A	1.10	N/A	2.525	N/A	1.519	N/A	4.125	0.375	17.012	1.532
44	1.5D	Reservoir	Left	1.26	N/A	1.25	N/A	2.525	N/A	1.772	N/A	4.684	0.522	21.942	1.784

(continued on next page)

Table E-1. (Continued).

Run [ ]	Barrel Spacing [ ]	Approach Condition [ ]	Barrel [ ]	Q total [cfs]	Q Left [cfs]	Q Middle [cfs]	Q Right [cfs]	S_o [%]	Hw/D Left [ ]	Hw/D Middle [ ]	Hw/D Right [ ]	$Q/AD^{0.5}$ [$ft^{0.5}/s$]	$Hw/D-H_c/D+.5S_o$ [ ]	$(Q/AD^{0.5})^2$ [ft/s^2]	$Hw/D+.5S_o$ [ ]
45	1.5D	Reservoir	Left	1.41	N/A	1.40	N/A	2.525	N/A	2.019	N/A	5.225	0.665	27.300	2.032
46	1.5D	Reservoir	Left	1.57	N/A	1.56	N/A	2.525	N/A	2.372	N/A	5.818	0.899	33.853	2.384
47	1.5D	Reservoir	Left	1.94	N/A	1.92	N/A	2.525	N/A	3.254	N/A	7.182	1.484	51.588	3.266
48	1.5D	Reservoir	Left	0.08	0.08	N/A	N/A	2.470	0.3052	N/A	N/A	0.305	0.046	0.093	0.318
49	1.5D	Reservoir	Left	0.40	0.40	N/A	N/A	2.470	0.7232	N/A	N/A	1.500	0.102	2.249	0.736
50	1.5D	Reservoir	Left	0.56	0.57	N/A	N/A	2.470	0.8963	N/A	N/A	2.137	0.135	4.569	0.909
51	1.5D	Reservoir	Left	0.76	0.76	N/A	N/A	2.470	1.0912	N/A	N/A	2.857	0.186	8.163	1.104
52	1.5D	Reservoir	Left	0.26	0.27	N/A	N/A	2.470	0.5821	N/A	N/A	1.019	0.082	1.039	0.594
53	1.5D	Reservoir	Left	1.10	1.11	N/A	N/A	2.470	1.5233	N/A	N/A	4.163	0.371	17.331	1.536
54	1.5D	Reservoir	Left	1.26	1.26	N/A	N/A	2.470	1.7707	N/A	N/A	4.711	0.515	22.192	1.783
55	1.5D	Reservoir	Left	1.57	1.58	N/A	N/A	2.470	2.3798	N/A	N/A	5.892	0.891	34.715	2.392
56	1.5D	Reservoir	Left	1.92	1.95	N/A	N/A	2.470	3.2658	N/A	N/A	7.274	1.474	52.907	3.278
57	1.5D	Reservoir	Left	1.41	1.41	N/A	N/A	2.470	2.0208	N/A	N/A	5.280	0.655	27.883	2.033
58	2D, 1.5D Dep.	Trapezoid	Right	0.09	N/A	N/A	0.08	2.886	N/A	N/A	0.296	0.294	0.044	0.087	0.311
59	2D, 1.5D Dep.	Trapezoid	Left	0.09	N/A	0.08	N/A	2.544	N/A	0.295	N/A	0.302	0.038	0.091	0.308
60	2D, 1.5D Dep.	Trapezoid	Left	0.26	N/A	0.26	N/A	2.544	N/A	0.560	N/A	0.975	0.072	0.951	0.573
61	2D, 1.5D Dep.	Trapezoid	Left	0.40	N/A	0.41	N/A	2.544	N/A	0.708	N/A	1.519	0.083	2.308	0.720
62	2D, 1.5D Dep.	Trapezoid	Left	0.58	N/A	0.57	N/A	2.544	N/A	0.872	N/A	2.149	0.109	4.619	0.885
63	2D, 1.5D Dep.	Trapezoid	Left	0.76	N/A	0.77	N/A	2.544	N/A	1.044	N/A	2.884	0.133	8.316	1.056
64	2D, 1.5D Dep.	Trapezoid	Left	1.11	N/A	1.13	N/A	2.544	N/A	1.454	N/A	4.241	0.288	17.982	1.467
65	2D, 1.5D Dep.	Trapezoid	Left	1.26	N/A	1.28	N/A	2.544	N/A	1.673	N/A	4.789	0.403	22.937	1.686
66	2D, 1.5D Dep.	Trapezoid	Left	1.42	N/A	1.46	N/A	2.544	N/A	1.977	N/A	5.476	0.573	29.982	1.990
67	2D, 1.5D Dep.	Trapezoid	Left	1.59	N/A	1.61	N/A	2.544	N/A	2.297	N/A	6.026	0.782	36.311	2.310
68	2D, 1.5D Dep.	Trapezoid	Left	1.94	N/A	1.94	N/A	2.544	N/A	3.223	N/A	7.267	1.434	52.803	3.236
69	2D, 1.5D Dep.	Trapezoid	Left	0.09	0.08	N/A	N/A	2.625	0.3026	N/A	N/A	0.309	0.043	0.095	0.316
70	2D, 1.5D Dep.	Trapezoid	Left	0.27	0.27	N/A	N/A	2.625	0.5655	N/A	N/A	1.004	0.070	1.007	0.579
71	2D, 1.5D Dep.	Trapezoid	Left	0.40	0.40	N/A	N/A	2.625	0.7155	N/A	N/A	1.500	0.095	2.249	0.729
72	2D, 1.5D Dep.	Trapezoid	Left	0.56	0.56	N/A	N/A	2.625	0.8719	N/A	N/A	2.101	0.119	4.413	0.885
73	2D, 1.5D Dep.	Trapezoid	Left	0.76	0.77	N/A	N/A	2.625	1.0719	N/A	N/A	2.872	0.164	8.247	1.085
74	2D, 1.5D Dep.	Trapezoid	Left	1.11	1.11	N/A	N/A	2.625	1.4810	N/A	N/A	4.163	0.329	17.331	1.494
75	2D, 1.5D Dep.	Trapezoid	Left	1.24	1.24	N/A	N/A	2.625	1.6797	N/A	N/A	4.641	0.438	21.542	1.693
76	2D, 1.5D Dep.	Trapezoid	Left	1.43	1.42	N/A	N/A	2.625	2.0067	N/A	N/A	5.324	0.633	28.340	2.020
77	2D, 1.5D Dep.	Trapezoid	Left	1.59	1.62	N/A	N/A	2.625	2.3388	N/A	N/A	6.043	0.820	36.515	2.352
78	2D, 1.5D Dep.	Trapezoid	Left	1.94	1.94	N/A	N/A	2.625	3.2414	N/A	N/A	7.261	1.453	52.716	3.255
79	3D, 1.5D Dep.	Trapezoid	Left	1.41	N/A	1.44	N/A	2.444	N/A	1.972	N/A	5.384	0.586	28.982	1.984
80	3D, 1.5D Dep.	Trapezoid	Left	1.25	N/A	1.29	N/A	2.444	N/A	1.685	N/A	4.810	0.410	23.140	1.697
81	3D, 1.5D Dep.	Trapezoid	Left	1.41	1.40	N/A	N/A	2.440	2.0336	N/A	N/A	5.227	0.678	27.321	2.046

Table E-2. Double-barrel culvert experimental data.

	Barrel	Approach		Q	Q	Q	Q	S_o	S_o	S_o	Hw/D	Hw/D	Hw/D	Left-Barrel Data				Middle-Barrel Data				Right-Barrel Data			
Run [ ]	Spacing [ ]	Condition [ ]	Barrels []	total [cfs]	Left [cfs]	Mid. [cfs]	Right [cfs]	Left [%]	Mid. [%]	Right [%]	Left [ ]	Mid. [ ]	Right [ ]	$Q/AD^{0.5}$ [$ft^{0.5}/s$]	$Hw/D-H_c/D+.5S_o$ [ ]	$(Q/AD^{0.5})^2$ [ft/s^2]	$Hw/D+.5S_o$ [ ]	$Q/AD^{0.5}$ [$ft^{0.5}/s$]	$Hw/D-H_c/D+.5S_o$ [ ]	$(Q/AD^{0.5})^2$ [ft/s^2]	$Hw/D+.5S_o$ [ ]	$Q/AD^{0.5}$ [$ft^{0.5}/s$]	$Hw/D-H_c/D+.5S_o$ [ ]	$(Q/AD^{0.5})^2$ [ft/s^2]	$Hw/D+.5S_o$ [ ]
82	1.5D	Reservoir	Left, Mid.	0.18	N/A	0.09	0.08	N/A	2.53	2.51	N/A	0.322	0.305	N/A	N/A	N/A	N/A	0.340	0.047	0.116	0.334	0.311	0.044	0.096	0.318
83	1.5D	Reservoir	Left, Mid.	0.53	N/A	0.26	0.25	N/A	2.53	2.51	N/A	0.581	0.564	N/A	N/A	N/A	N/A	0.976	0.093	0.953	0.593	0.951	0.083	0.904	0.577
84	1.5D	Reservoir	Left, Mid.	0.80	N/A	0.40	0.39	N/A	2.53	2.51	N/A	0.736	0.719	N/A	N/A	N/A	N/A	1.482	0.119	2.196	0.749	1.470	0.105	2.162	0.732
85	1.5D	Reservoir	Left, Mid.	1.15	N/A	0.56	0.57	N/A	2.53	2.51	N/A	0.906	0.890	N/A	N/A	N/A	N/A	2.087	0.156	4.357	0.919	2.115	0.133	4.474	0.902
86	1.5D	Reservoir	Left, Mid.	1.61	N/A	0.77	0.82	N/A	2.53	2.51	N/A	1.147	1.131	N/A	N/A	N/A	N/A	2.860	0.242	8.181	1.160	3.067	0.185	9.406	1.143
87	1.5D	Reservoir	Mid., Right	2.21	1.04	1.11	N/A	2.47	2.53	N/A	1.509	1.514	N/A	3.873	0.411	15.003	1.522	4.146	0.365	17.189	1.527	N/A	N/A	N/A	N/A
88	1.5D	Reservoir	Mid., Right	2.21	1.08	1.09	N/A	2.47	2.53	N/A	1.517	1.522	N/A	4.053	0.385	16.425	1.529	4.089	0.384	16.717	1.534	N/A	N/A	N/A	N/A
89	1.5D	Reservoir	Left, Mid.	2.21	N/A	1.06	1.14	N/A	2.53	2.51	N/A	1.519	1.503	N/A	N/A	N/A	N/A	3.948	0.408	15.584	1.532	4.244	0.335	18.011	1.515
90	1.5D	Reservoir	Left, Mid.	2.52	N/A	1.23	1.29	N/A	2.53	2.51	N/A	1.774	1.758	N/A	N/A	N/A	N/A	4.594	0.541	21.103	1.787	4.811	0.483	23.145	1.770
91	1.5D	Reservoir	Left, Mid.	2.82	N/A	1.35	1.47	N/A	2.53	2.51	N/A	2.036	2.019	N/A	N/A	N/A	N/A	5.063	0.713	25.636	2.049	5.483	0.614	30.060	2.032
92	1.5D	Reservoir	Mid., Right	2.82	1.40	1.40	N/A	2.47	2.53	N/A	2.035	2.040	N/A	5.217	0.682	27.220	2.047	5.242	0.682	27.478	2.052	N/A	N/A	N/A	N/A
93	1.5D	Reservoir	Left, Mid.	3.12	N/A	1.54	1.60	N/A	2.53	2.51	N/A	2.345	2.328	N/A	N/A	N/A	N/A	5.756	0.885	33.137	2.357	5.980	0.822	35.757	2.341
94	1.5D	Reservoir	Mid., Right	3.81	1.92	1.87	N/A	2.47	2.53	N/A	3.152	3.156	N/A	7.173	1.383	51.451	3.164	7.004	1.428	49.049	3.169	N/A	N/A	N/A	N/A
95	1.5D	Reservoir	Left, Mid.	3.78	N/A	1.88	1.91	N/A	2.53	2.51	N/A	3.153	3.136	N/A	N/A	N/A	N/A	7.017	1.421	49.245	3.165	7.144	1.375	51.043	3.148
96	1.5D	Reservoir	Left, Mid.	3.76	N/A	1.88	1.96	N/A	2.53	2.51	N/A	3.229	3.213	N/A	N/A	N/A	N/A	7.031	1.495	49.441	3.242	7.310	1.413	53.443	3.225
97	3D	Reservoir	Mid., Right	2.54	1.25	1.27	N/A	2.44	2.44	N/A	1.775	1.783	N/A	4.661	0.528	21.728	1.787	4.761	0.518	22.666	1.796	N/A	N/A	N/A	N/A
98	3D	Reservoir	Mid., Right	3.51	1.74	1.74	N/A	2.44	2.44	N/A	2.785	2.794	N/A	6.489	1.170	42.101	2.797	6.489	1.179	42.103	2.806	N/A	N/A	N/A	N/A
99	3D	Reservoir	Mid., Right	2.84	1.42	1.42	N/A	2.44	2.44	N/A	2.058	2.067	N/A	5.314	0.686	28.237	2.070	5.299	0.698	28.076	2.079	N/A	N/A	N/A	N/A
100	3D	Reservoir	Left, Mid.	0.15	N/A	0.08	0.08	N/A	2.44	2.43	N/A	0.308	0.291	N/A	N/A	N/A	N/A	0.288	0.057	0.083	0.320	0.286	0.041	0.082	0.303
101	3D	Reservoir	Left, Mid.	0.53	N/A	0.26	0.27	N/A	2.44	2.43	N/A	0.588	0.572	N/A	N/A	N/A	N/A	0.961	0.104	0.924	0.601	0.994	0.078	0.987	0.584
102	3D	Reservoir	Left, Mid.	0.80	N/A	0.39	0.41	N/A	2.44	2.43	N/A	0.741	0.724	N/A	N/A	N/A	N/A	1.467	0.128	2.153	0.753	1.516	0.100	2.297	0.737
103	3D	Reservoir	Left, Mid.	1.14	N/A	0.55	0.58	N/A	2.44	2.43	N/A	0.913	0.896	N/A	N/A	N/A	N/A	2.057	0.168	4.231	0.925	2.172	0.128	4.717	0.908
104	3D	Reservoir	Left, Mid.	1.65	N/A	0.80	0.83	N/A	2.44	2.43	N/A	1.167	1.150	N/A	N/A	N/A	N/A	3.005	0.233	9.029	1.179	3.099	0.198	9.602	1.162
105	3D	Reservoir	Left, Mid.	2.20	N/A	1.08	1.12	N/A	2.44	2.43	N/A	1.517	1.500	N/A	N/A	N/A	N/A	4.051	0.385	16.408	1.529	4.196	0.342	17.602	1.512
106	3D	Reservoir	Left, Mid.	2.54	N/A	1.24	1.33	N/A	2.44	2.43	N/A	1.795	1.778	N/A	N/A	N/A	N/A	4.646	0.552	21.581	1.807	4.971	0.473	24.709	1.790
107	3D	Reservoir	Left, Mid.	3.79	N/A	1.86	1.92	N/A	2.44	2.43	N/A	3.181	3.164	N/A	N/A	N/A	N/A	6.934	1.468	48.082	3.193	7.158	1.399	51.239	3.176
108	3D	Reservoir	Left, Mid.	3.11	N/A	1.55	1.58	N/A	2.44	2.43	N/A	2.324	2.308	N/A	N/A	N/A	N/A	5.781	0.859	33.416	2.337	5.895	0.819	34.749	2.320
110	2D	Reservoir	Left, Mid.	2.81	N/A	1.39	1.45	N/A	2.52	2.28	N/A	2.003	2.012	N/A	N/A	N/A	N/A	5.208	0.652	27.125	2.015	5.437	0.614	29.560	2.023
111	2D	Reservoir	Mid., Right	0.16	0.08	0.08	N/A	2.42	2.52	N/A	0.306	0.297	N/A	0.310	0.045	0.096	0.319	0.305	0.039	0.093	0.310	N/A	N/A	N/A	N/A
112	2D	Reservoir	Mid., Right	0.52	0.26	0.26	N/A	2.42	2.52	N/A	0.574	0.565	N/A	0.988	0.082	0.976	0.587	0.965	0.080	0.931	0.578	N/A	N/A	N/A	N/A
113	2D	Reservoir	Mid., Right	0.81	0.40	0.40	N/A	2.42	2.52	N/A	0.731	0.722	N/A	1.494	0.111	2.232	0.743	1.507	0.099	2.270	0.734	N/A	N/A	N/A	N/A
114	2D	Reservoir	Mid., Right	1.14	0.56	0.57	N/A	2.42	2.52	N/A	0.900	0.891	N/A	2.100	0.146	4.409	0.912	2.124	0.133	4.512	0.904	N/A	N/A	N/A	N/A
115	2D	Reservoir	Mid., Right	1.63	0.78	0.83	N/A	2.42	2.52	N/A	1.149	1.140	N/A	2.930	0.229	8.584	1.161	3.099	0.188	9.601	1.152	N/A	N/A	N/A	N/A
116	2D	Reservoir	Mid., Right	2.18	1.08	1.11	N/A	2.42	2.52	N/A	1.492	1.483	N/A	4.026	0.366	16.205	1.505	4.146	0.335	17.189	1.496	N/A	N/A	N/A	N/A
117	2D	Reservoir	Mid., Right	2.57	1.27	1.30	N/A	2.42	2.52	N/A	1.796	1.787	N/A	4.731	0.536	22.384	1.808	4.867	0.502	23.691	1.800	N/A	N/A	N/A	N/A
118	2D	Reservoir	Mid., Right	2.81	1.38	1.42	N/A	2.42	2.52	N/A	2.028	2.019	N/A	5.175	0.683	26.778	2.041	5.299	0.651	28.076	2.032	N/A	N/A	N/A	N/A
119	2D	Reservoir	Mid., Right	3.18	1.57	1.63	N/A	2.42	2.52	N/A	2.427	2.418	N/A	5.882	0.941	34.603	2.439	6.102	0.887	37.235	2.431	N/A	N/A	N/A	N/A
120	2D	Reservoir	Mid., Right	3.52	1.77	1.77	N/A	2.42	2.52	N/A	2.881	2.872	N/A	6.624	1.237	43.882	2.893	6.608	1.232	43.666	2.884	N/A	N/A	N/A	N/A
121	2D	Reservoir	Mid., Right	3.76	1.87	1.88	N/A	2.42	2.52	N/A	3.194	3.185	N/A	7.004	1.464	49.057	3.206	7.031	1.450	49.441	3.197	N/A	N/A	N/A	N/A
122	2D, 1.5D Dep	Reservoir	Mid., Right	0.65	0.09	0.55	N/A	2.63	2.54	N/A	0.341	0.859	N/A	0.328	0.073	0.107	0.354	2.069	0.112	4.281	0.872	N/A	N/A	N/A	N/A
123	2D, 1.5D Dep	Reservoir	Mid., Right	1.02	0.24	0.78	N/A	2.63	2.54	N/A	0.549	1.067	N/A	0.912	0.079	0.832	0.562	2.905	0.152	8.441	1.079	N/A	N/A	N/A	N/A
124	2D, 1.5D Dep	Reservoir	Mid., Right	1.32	0.39	0.94	N/A	2.63	2.54	N/A	0.728	1.246	N/A	1.450	0.120	2.102	0.741	3.502	0.218	12.261	1.259	N/A	N/A	N/A	N/A
125	2D, 1.5D Dep	Reservoir	Mid., Right	1.60	0.56	1.04	N/A	2.63	2.54	N/A	0.863	1.381	N/A	2.075	0.115	4.308	0.876	3.901	0.278	15.221	1.393	N/A	N/A	N/A	N/A
126	2D, 1.5D Dep	Reservoir	Mid., Right	1.97	0.79	1.19	N/A	2.63	2.54	N/A	1.059	1.577	N/A	2.945	0.137	8.672	1.072	4.461	0.369	19.902	1.590	N/A	N/A	N/A	N/A
127	2D, 1.5D Dep	Reservoir	Mid., Right	2.56	1.11	1.44	N/A	2.63	2.54	N/A	1.475	1.992	N/A	4.154	0.325	17.252	1.488	5.379	0.608	28.933	2.005	N/A	N/A	N/A	N/A
128	2D, 1.5D Dep	Reservoir	Mid., Right	2.76	1.34	1.61	N/A	2.63	2.54	N/A	1.810	2.328	N/A	5.007	0.499	25.068	1.824	6.002	0.818	36.022	2.341	N/A	N/A	N/A	N/A
129	2D, 1.5D Dep	Reservoir	Mid., Right	3.19	1.47	1.69	N/A	2.63	2.54	N/A	2.050	2.568	N/A	5.499	0.642	30.242	2.063	6.332	0.988	40.094	2.581	N/A	N/A	N/A	N/A
130	2D, 1.5D Dep	Reservoir	Mid., Right	3.47	1.62	1.84	N/A	2.63	2.54	N/A	2.387	2.905	N/A	6.045	0.868	36.542	2.401	6.865	1.208	47.132	2.918	N/A	N/A	N/A	N/A

Table E-3. Three-barrel culvert experimental data set.

Run	Barrel Spacing	Approach Condition	Q	Q			S_o			Re	Hw/D			$Q/AD^{0.5}$			$Hw/D\text{-}H_c/D\text{+}.5S_o$			$(Q/AD^{0.5})^2$			$Hw/D\text{+}.5S_o$		
[ ]	[ ]	[ ]	total [cfs]	Left [cfs]	Middle [cfs]	Right [cfs]	Left [%]	Middle [%]	Right [%]	[]	Left [ ]	Middle [ ]	Right [ ]	Left [$ft^{0.5}/s$]	Middle [$ft^{0.5}/s$]	Right [$ft^{0.5}/s$]	Left [ ]	Middle [ ]	Right [ ]	Left [ft/s^2]	Middle [ft/s^2]	Right [ft/s^2]	Left [ ]	Middle [ ]	Right [ ]
131	3D	Rect. chnl	4.46	1.48	1.50	1.48	2.92	2.92	2.56	183106	1.986	1.981	1.981	5.545	5.589	5.541	0.571	0.556	0.564	30.750	31.237	30.700	2.001	1.995	1.994
132	3D	Rect. chnl	4.20	1.40	1.41	1.40	2.92	2.92	2.56	173222	1.827	1.822	1.822	5.230	5.287	5.226	0.474	0.457	0.467	27.349	27.956	27.315	1.842	1.836	1.835
133	3D	Rect. chnl	3.46	1.13	1.19	1.17	2.92	2.92	2.56	149645	1.459	1.454	1.454	4.239	4.431	4.355	0.295	0.254	0.266	17.966	19.633	18.964	1.474	1.468	1.467
134	3D	Rect. chnl	2.83	0.95	0.98	0.95	2.92	2.92	2.56	122264	1.231	1.226	1.226	3.547	3.658	3.567	0.196	0.170	0.186	12.584	13.381	12.724	1.246	1.240	1.238
135	3D	Rect. chnl	1.65	0.55	0.56	0.56	2.92	2.92	2.56	81570	0.853	0.847	0.847	2.070	2.087	2.079	0.108	0.099	0.099	4.285	4.357	4.321	0.867	0.862	0.860
136	3D	Rect. chnl	1.16	0.39	0.39	0.39	2.92	2.92	2.56	67509	0.691	0.686	0.686	1.450	1.472	1.464	0.084	0.074	0.074	2.103	2.167	2.143	0.706	0.700	0.699
137	3D	Rect. chnl	0.72	0.24	0.24	0.24	2.92	2.92	2.56	48023	0.526	0.521	0.521	0.891	0.909	0.901	0.064	0.054	0.054	0.793	0.827	0.812	0.541	0.536	0.534
138	3D	Rect. chnl	0.35	0.12	0.12	0.12	2.92	2.92	2.56	39814	0.358	0.353	0.353	0.435	0.446	0.440	0.046	0.036	0.037	0.190	0.199	0.193	0.372	0.367	0.365
139	3D 40° Skew	Rect. chnl	2.88	0.95	0.97	0.95	2.70	2.82	2.83	117999	1.227	1.221	1.221	3.547	3.623	3.567	0.191	0.171	0.182	12.584	13.125	12.724	1.241	1.235	1.235
140	3D 40° Skew	Rect. chnl	1.82	0.62	0.62	0.60	2.70	2.82	2.83	86671	0.916	0.909	0.909	2.307	2.328	2.241	0.121	0.110	0.128	5.321	5.418	5.022	0.929	0.923	0.923
141	3D 40° Skew	Rect. chnl	1.37	0.46	0.46	0.45	2.70	2.82	2.83	72175	0.767	0.760	0.760	1.738	1.730	1.679	0.093	0.088	0.100	3.021	2.993	2.819	0.780	0.774	0.774
142	3D 40° Skew	Rect. chnl	0.85	0.29	0.29	0.28	2.70	2.82	2.83	58355	0.596	0.590	0.590	1.084	1.095	1.038	0.080	0.071	0.086	1.174	1.199	1.078	0.610	0.604	0.604
143	3D 40° Skew	Rect. chnl	0.50	0.16	0.18	0.16	2.70	2.82	2.83	45200	0.492	0.486	0.486	0.610	0.669	0.608	0.116	0.091	0.111	0.372	0.447	0.369	0.506	0.500	0.500
144	3D 40° Skew	Rect. chnl	1.82	0.62	0.62	0.60	2.70	2.82	2.83	88982	0.917	0.910	0.910	2.307	2.328	2.241	0.122	0.112	0.129	5.321	5.418	5.022	0.930	0.924	0.924
145	3D 40° Skew	Rect. chnl	0.86	0.29	0.30	0.28	2.70	2.82	2.83	43657	0.603	0.596	0.596	1.100	1.120	1.046	0.082	0.071	0.090	1.210	1.254	1.095	0.616	0.610	0.610
146	3D 40° Skew	Rect. chnl	1.72	0.59	0.59	0.54	3.04	2.91	2.83	91620	0.904	0.912	0.872	2.194	2.193	2.032	0.134	0.141	0.135	4.813	4.811	4.129	0.919	0.926	0.886
147	3D 40° Skew	Rect. chnl	6.16	2.06	2.06	2.04	3.04	2.91	2.83	255367	3.481	3.489	3.449	7.706	7.697	7.621	1.588	1.597	1.576	59.387	59.247	58.084	3.496	3.503	3.463
148	3D 40° Skew	Rect. chnl	5.22	1.76	1.76	1.72	3.04	2.91	2.83	212711	2.694	2.702	2.662	6.599	6.560	6.446	1.059	1.074	1.059	43.540	43.039	41.547	2.709	2.716	2.676
149	3D 40° Skew	Rect. chnl	4.72	1.58	1.60	1.56	3.04	2.91	2.83	190354	2.266	2.273	2.233	5.905	5.977	5.848	0.778	0.770	0.756	34.873	35.720	34.203	2.281	2.288	2.247
150	3D 40° Skew	Rect. chnl	3.53	1.20	1.20	1.16	3.04	2.91	2.83	148101	1.567	1.575	1.535	4.506	4.499	4.339	0.353	0.362	0.351	20.300	20.243	18.826	1.582	1.589	1.549
151	3D 40° Skew	Rect. chnl	6.85	2.30	2.30	2.27	3.04	2.91	2.83	288022	4.276	4.284	4.244	8.587	8.612	8.473	-	-	-	73.733	74.165	71.791	4.291	4.298	4.258
152	3D	Non-unif	5.23	1.69	1.88	1.69	2.22	2.49	2.75	219200	2.779	2.715	2.660	6.330	7.016	6.321	1.198	0.984	1.084	40.066	49.230	39.949	2.790	2.728	2.674
153	3D	Non-unif	4.75	1.55	1.69	1.56	2.22	2.49	2.75	196433	2.414	2.351	2.296	5.814	6.327	5.813	0.941	0.772	0.826	33.798	40.037	33.791	2.426	2.364	2.310
154	3D	Non-unif	4.10	1.36	1.46	1.33	2.22	2.49	2.75	171063	1.987	1.924	1.869	5.091	5.476	4.966	0.658	0.521	0.566	25.920	29.982	24.659	1.999	1.937	1.883
155	3D	Non-unif	3.46	1.13	1.25	1.09	2.22	2.49	2.75	149296	1.646	1.583	1.528	4.239	4.684	4.075	0.479	0.333	0.394	17.967	21.942	16.606	1.657	1.596	1.542
156	3D	Non-unif	2.79	0.96	1.03	0.90	2.22	2.49	2.75	127731	1.334	1.271	1.215	3.582	3.862	3.350	0.289	0.175	0.217	12.829	14.917	11.222	1.345	1.283	1.229
157	3D	Non-unif	1.85	0.62	0.63	0.57	2.22	2.49	2.75	91131	1.013	0.950	0.895	2.302	2.363	2.129	0.217	0.142	0.137	5.297	5.585	4.533	1.024	0.962	0.909
158	3D	Non-unif	2.38	0.79	0.82	0.78	2.22	2.49	2.75	110156	1.212	1.149	1.094	2.947	3.077	2.912	0.288	0.201	0.179	8.684	9.470	8.478	1.223	1.161	1.107
159	3D	Non-unif	1.35	0.47	0.47	0.41	2.22	2.49	2.75	78004	0.853	0.790	0.735	1.750	1.775	1.537	0.173	0.106	0.106	3.063	3.151	2.361	0.864	0.802	0.748
160	3D	Non-unif	0.87	0.31	0.30	0.25	2.22	2.49	2.75	59888	0.673	0.610	0.555	1.172	1.129	0.952	0.131	0.081	0.075	1.373	1.275	0.906	0.684	0.623	0.569
161	3D	Non-unif	0.52	0.20	0.18	0.14	2.22	2.49	2.75	45637	0.524	0.462	0.406	0.752	0.673	0.541	0.100	0.064	0.054	0.565	0.452	0.293	0.536	0.474	0.420
162	1.5D	Reservoir	2.07	0.64	0.74	0.68	2.47	2.53	2.51	103880	1.022	1.027	1.010	2.392	2.749	2.525	0.208	0.143	0.170	5.724	7.558	6.376	1.034	1.040	1.023
163	1.5D	Reservoir	0.34	0.11	0.12	0.11	2.47	2.53	2.51	39548	0.367	0.372	0.355	0.416	0.449	0.395	0.060	0.053	0.057	0.173	0.202	0.156	0.379	0.384	0.368
164	1.5D	Reservoir	0.56	0.19	0.20	0.18	2.47	2.53	2.51	52098	0.482	0.487	0.471	0.697	0.759	0.674	0.076	0.062	0.072	0.486	0.577	0.455	0.494	0.500	0.483
165	1.5D	Reservoir	1.03	0.33	0.37	0.33	2.47	2.53	2.51	69462	0.671	0.676	0.659	1.237	1.381	1.252	0.113	0.083	0.098	1.531	1.908	1.567	0.683	0.688	0.672
166	1.5D	Reservoir	1.24	0.40	0.45	0.40	2.47	2.53	2.51	76880	0.745	0.750	0.733	1.480	1.665	1.482	0.129	0.091	0.117	2.192	2.774	2.196	0.757	0.763	0.746
167	1.5D	Reservoir	1.55	0.49	0.56	0.48	2.47	2.53	2.51	96610	0.850	0.855	0.838	1.816	2.093	1.807	0.158	0.103	0.148	3.298	4.380	3.265	0.862	0.868	0.851
168	1.5D	Reservoir	2.06	0.64	0.74	0.68	2.47	2.53	2.51	126904	1.019	1.024	1.008	2.386	2.749	2.546	0.207	0.140	0.164	5.693	7.558	6.480	1.032	1.037	1.020
169	1.5D	Reservoir	2.56	0.79	0.92	0.86	2.47	2.53	2.51	121522	1.199	1.204	1.187	2.962	3.421	3.221	0.273	0.191	0.212	8.772	11.705	10.373	1.211	1.216	1.200
170	1.5D	Reservoir	3.53	1.17	1.21	1.18	2.47	2.53	2.51	151588	1.644	1.649	1.632	4.390	4.540	4.417	0.449	0.426	0.432	19.272	20.610	19.507	1.656	1.661	1.645
171	1.5D	Reservoir	4.16	1.42	1.43	1.37	2.47	2.53	2.51	178233	2.002	2.006	1.990	5.304	5.338	5.137	0.632	0.630	0.653	28.129	28.493	26.387	2.014	2.019	2.002
172	1.5D	Reservoir	4.74	1.53	1.69	1.59	2.47	2.53	2.51	204444	2.405	2.410	2.394	5.723	6.315	5.955	0.952	0.834	0.893	32.750	39.876	35.463	2.418	2.423	2.406
173	1.5D	Reservoir	5.30	1.75	1.81	1.76	2.47	2.53	2.51	222584	2.863	2.868	2.851	6.549	6.772	6.572	1.236	1.192	1.219	42.891	45.865	43.197	2.876	2.881	2.864
174	1.5D	Reservoir	6.06	2.08	2.00	1.99	2.47	2.53	2.51	280087	3.557	3.562	3.545	7.775	7.494	7.453	-	1.718	1.711	60.450	56.161	55.545	3.569	3.574	3.557
175	1.5D	Reservoir	6.06	2.06	1.98	2.01	2.47	2.53	2.51	276877	3.557	3.562	3.545	7.693	7.408	7.509	1.664	1.738	1.697	59.176	54.881	56.381	3.569	3.574	3.557

176	3D	Reservoir	0.33	0.11	0.11	0.11	2.44	2.44	2.43	39040	0.364	0.373	0.356	0.411	0.423	0.409	0.059	0.064	0.053	0.169	0.179	0.167	0.376	0.385	0.369
177	3D	Reservoir	0.58	0.19	0.20	0.19	2.44	2.44	2.43	52142	0.490	0.499	0.482	0.726	0.743	0.718	0.075	0.078	0.069	0.527	0.552	0.516	0.502	0.511	0.494
178	3D	Reservoir	1.02	0.34	0.35	0.33	2.44	2.44	2.43	68625	0.667	0.676	0.659	1.260	1.301	1.252	0.104	0.102	0.098	1.586	1.694	1.567	0.679	0.688	0.671
179	3D	Reservoir	1.22	0.40	0.41	0.40	2.44	2.44	2.43	76547	0.737	0.746	0.729	1.490	1.550	1.502	0.118	0.113	0.108	2.221	2.402	2.255	0.749	0.758	0.742
180	3D	Reservoir	1.56	0.51	0.53	0.51	2.44	2.44	2.43	87944	0.857	0.865	0.849	1.907	1.995	1.909	0.144	0.134	0.136	3.635	3.981	3.643	0.869	0.878	0.861
181	3D	Reservoir	1.96	0.63	0.68	0.65	2.44	2.44	2.43	101825	0.991	1.000	0.983	2.373	2.541	2.444	0.181	0.157	0.159	5.630	6.457	5.972	1.003	1.012	0.995
182	3D	Reservoir	2.56	0.83	0.88	0.87	2.44	2.44	2.43	119089	1.213	1.222	1.205	3.098	3.304	3.269	0.261	0.231	0.221	9.601	10.917	10.685	1.225	1.234	1.217
183	3D	Reservoir	3.59	1.19	1.24	1.20	2.44	2.44	2.43	157302	1.661	1.669	1.653	4.457	4.653	4.476	0.453	0.425	0.441	19.866	21.651	20.031	1.673	1.681	1.665
184	3D	Reservoir	3.30	1.10	1.15	1.10	2.44	2.44	2.43	144143	1.513	1.522	1.505	4.100	4.299	4.111	0.372	0.344	0.363	16.810	18.484	16.899	1.525	1.534	1.517
185	3D	Reservoir	4.17	1.39	1.44	1.39	2.44	2.44	2.43	175312	1.998	2.006	1.990	5.197	5.395	5.191	0.649	0.618	0.642	27.006	29.106	26.947	2.010	2.019	2.002
186	3D	Reservoir	4.72	1.58	1.64	1.59	2.44	2.44	2.43	209269	2.385	2.394	2.377	5.905	6.138	5.931	0.894	0.854	0.881	34.873	37.673	35.180	2.397	2.406	2.389
187	3D	Reservoir	5.28	1.75	1.79	1.77	2.44	2.44	2.43	229716	2.825	2.833	2.817	6.549	6.679	6.598	1.197	1.177	1.179	42.891	44.610	43.534	2.837	2.846	2.829
188	3D	Reservoir	6.05	2.04	2.01	1.96	2.44	2.44	2.43	282154	3.515	3.523	3.506	7.611	7.508	7.328	1.642	1.675	1.702	57.924	56.377	53.704	3.527	3.535	3.519
189	2D	Reservoir	0.34	0.11	0.12	0.11	2.42	2.52	2.28	41306	0.367	0.358	0.367	0.423	0.435	0.411	0.057	0.044	0.061	0.179	0.189	0.169	0.379	0.370	0.378
190	2D	Reservoir	0.57	0.19	0.20	0.18	2.42	2.52	2.28	53081	0.483	0.474	0.483	0.713	0.730	0.690	0.072	0.058	0.079	0.508	0.533	0.476	0.495	0.487	0.495
191	2D	Reservoir	1.02	0.33	0.36	0.33	2.42	2.52	2.28	69256	0.667	0.658	0.667	1.246	1.334	1.243	0.107	0.077	0.107	1.553	1.779	1.545	0.679	0.670	0.678
192	2D	Reservoir	1.25	0.40	0.43	0.41	2.42	2.52	2.28	78346	0.745	0.736	0.745	1.510	1.623	1.527	0.121	0.087	0.117	2.281	2.634	2.330	0.757	0.748	0.756
193	2D	Reservoir	1.55	0.48	0.54	0.52	2.42	2.52	2.28	88880	0.851	0.842	0.851	1.799	2.026	1.926	0.162	0.105	0.134	3.238	4.103	3.710	0.863	0.855	0.863
194	2D	Reservoir	1.98	0.63	0.69	0.65	2.42	2.52	2.28	102499	0.987	0.978	0.987	2.347	2.583	2.424	0.183	0.127	0.166	5.507	6.673	5.875	0.999	0.991	0.999
195	2D	Reservoir	2.56	0.81	0.90	0.86	2.42	2.52	2.28	121130	1.196	1.187	1.196	3.022	3.354	3.213	0.259	0.187	0.222	9.133	11.249	10.322	1.208	1.200	1.208
196	2D	Reservoir	3.30	1.10	1.15	1.09	2.42	2.52	2.28	150845	1.522	1.513	1.522	4.118	4.299	4.092	0.378	0.335	0.382	16.961	18.484	16.747	1.534	1.525	1.533
197	2D	Reservoir	4.16	1.39	1.44	1.38	2.42	2.52	2.28	181154	1.995	1.986	1.995	5.197	5.372	5.158	0.646	0.603	0.652	27.006	28.859	26.609	2.007	1.998	2.006
198	2D	Reservoir	4.72	1.56	1.63	1.57	2.42	2.52	2.28	209260	2.384	2.374	2.383	5.836	6.100	5.884	0.907	0.843	0.896	34.064	37.214	34.619	2.396	2.387	2.395
199	2D	Reservoir	5.27	1.76	1.78	1.79	2.42	2.52	2.28	241948	2.827	2.818	2.827	6.574	6.666	6.701	1.194	1.165	1.165	43.215	44.433	44.903	2.839	2.831	2.838
200	2D	Reservoir	6.06	2.04	2.03	2.04	2.42	2.52	2.28	308415	3.562	3.553	3.562	7.611	7.581	7.635	1.689	1.688	1.682	57.924	57.466	58.300	3.574	3.565	3.573
201	2D 1.5D Dep.	Trap. Channel	0.73	0.08	0.56	0.09	2.63	2.54	2.89	88377	0.337	0.855	0.326	0.299	2.093	0.329	0.082	0.104	0.058	0.090	4.380	0.109	0.350	0.868	0.340
202	2D 1.5D Dep.	Trap. Channel	1.29	0.22	0.81	0.26	2.63	2.54	2.89	110892	0.574	1.092	0.563	0.840	3.046	0.975	0.125	0.151	0.077	0.706	9.277	0.950	0.588	1.105	0.577
203	2D 1.5D Dep.	Trap. Channel	1.73	0.36	0.95	0.43	2.63	2.54	2.89	124053	0.732	1.250	0.721	1.328	3.559	1.598	0.153	0.211	0.079	1.763	12.664	2.553	0.745	1.263	0.735
204	2D 1.5D Dep.	Trap. Channel	2.17	0.50	1.09	0.58	2.63	2.54	2.89	135898	0.880	1.397	0.868	1.872	4.086	2.166	0.176	0.260	0.103	3.506	16.699	4.692	0.893	1.410	0.882
205	2D 1.5D Dep.	Trap. Channel	2.77	0.72	1.25	0.81	2.63	2.54	2.89	151105	1.095	1.613	1.083	2.686	4.684	3.025	0.224	0.363	0.148	7.212	21.942	9.152	1.108	1.626	1.098
206	2D 1.5D Dep.	Trap. Channel	3.68	1.10	1.52	1.10	2.63	2.54	2.89	184110	1.464	1.982	1.453	4.128	5.687	4.111	0.320	0.536	0.312	17.037	32.338	16.899	1.477	1.995	1.467
207	2D 1.5D Dep.	Trap. Channel	4.02	1.22	1.61	1.22	2.63	2.54	2.89	196548	1.630	2.147	1.618	4.545	6.026	4.565	0.407	0.632	0.392	20.653	36.311	20.839	1.643	2.160	1.632
208	2D 1.5D Dep.	Trap. Channel	4.53	1.41	1.75	1.41	2.63	2.54	2.89	211975	1.971	2.488	1.959	5.282	6.547	5.279	0.606	0.862	0.596	27.901	42.867	27.863	1.984	2.501	1.973
209	2D 1.5D Dep.	Trap. Channel	5.05	1.59	1.89	1.59	2.63	2.54	2.89	235658	2.308	2.826	2.296	5.940	7.058	5.943	0.811	1.085	0.800	35.284	49.811	35.321	2.321	2.838	2.311
210	2D 1.5D Dep.	Trap. Channel	0.73	0.09	0.53	0.10	2.44	2.44	2.49	89960	0.350	0.841	0.353	0.347	1.995	0.384	0.072	0.110	0.059	0.121	3.981	0.148	0.362	0.853	0.365
211	2D 1.5D Dep.	Trap. Channel	1.30	0.24	0.80	0.28	2.44	2.44	2.49	117985	0.587	1.078	0.590	0.898	2.999	1.053	0.121	0.145	0.080	0.806	8.994	1.109	0.599	1.090	0.602
212	2D 1.5D Dep.	Trap. Channel	1.74	0.36	0.95	0.45	2.44	2.44	2.49	131912	0.746	1.237	0.749	1.346	3.567	1.682	0.162	0.197	0.086	1.812	12.726	2.828	0.758	1.249	0.761
213	2D 1.5D Dep.	Trap. Channel	2.17	0.51	1.07	0.60	2.44	2.44	2.49	149449	0.899	1.390	0.901	1.918	3.992	2.242	0.184	0.269	0.119	3.679	15.936	5.024	0.911	1.402	0.914
214	2D 1.5D Dep.	Trap. Channel	2.77	0.73	1.23	0.83	2.44	2.44	2.49	157545	1.118	1.609	1.121	2.728	4.612	3.087	0.238	0.372	0.171	7.442	21.268	9.529	1.130	1.621	1.133
215	2D 1.5D Dep.	Trap. Channel	2.79	0.81	1.26	0.78	2.44	2.44	2.49	173117	1.139	1.629	1.141	3.037	4.695	2.912	0.198	0.377	0.225	9.225	22.040	8.478	1.151	1.642	1.153
216	2D 1.5D Dep.	Trap. Channel	2.48	0.69	1.16	0.66	2.44	2.44	2.49	161169	1.017	1.508	1.019	2.595	4.339	2.451	0.163	0.322	0.194	6.733	18.825	6.005	1.029	1.520	1.032

Abbreviations and acronyms used without definitions in TRB publications:

AAAE	American Association of Airport Executives
AASHO	American Association of State Highway Officials
AASHTO	American Association of State Highway and Transportation Officials
ACI–NA	Airports Council International–North America
ACRP	Airport Cooperative Research Program
ADA	Americans with Disabilities Act
APTA	American Public Transportation Association
ASCE	American Society of Civil Engineers
ASME	American Society of Mechanical Engineers
ASTM	American Society for Testing and Materials
ATA	American Trucking Associations
CTAA	Community Transportation Association of America
CTBSSP	Commercial Truck and Bus Safety Synthesis Program
DHS	Department of Homeland Security
DOE	Department of Energy
EPA	Environmental Protection Agency
FAA	Federal Aviation Administration
FHWA	Federal Highway Administration
FMCSA	Federal Motor Carrier Safety Administration
FRA	Federal Railroad Administration
FTA	Federal Transit Administration
HMCRP	Hazardous Materials Cooperative Research Program
IEEE	Institute of Electrical and Electronics Engineers
ISTEA	Intermodal Surface Transportation Efficiency Act of 1991
ITE	Institute of Transportation Engineers
NASA	National Aeronautics and Space Administration
NASAO	National Association of State Aviation Officials
NCFRP	National Cooperative Freight Research Program
NCHRP	National Cooperative Highway Research Program
NHTSA	National Highway Traffic Safety Administration
NTSB	National Transportation Safety Board
PHMSA	Pipeline and Hazardous Materials Safety Administration
RITA	Research and Innovative Technology Administration
SAE	Society of Automotive Engineers
SAFETEA-LU	Safe, Accountable, Flexible, Efficient Transportation Equity Act: A Legacy for Users (2005)
TCRP	Transit Cooperative Research Program
TEA-21	Transportation Equity Act for the 21st Century (1998)
TRB	Transportation Research Board
TSA	Transportation Security Administration
U.S.DOT	United States Department of Transportation